

AFFDL-TR-72-64

VOLUME III

DEVELOPMENT OF AN UNDERSTANDING OF THE FATIGUE PHENOMENA
OF BONDED AND BOLTED JOINTS
IN ADVANCED FILAMENTARY COMPOSITE MATERIALS

VOLUME III. FATIGUE ANALYSIS AND FATIGUE MODE STUDIES

A. C. Fehrle, J. R. Carroll, S. M. Freeman, et al.
Lockheed-Georgia Company
Marietta, Georgia

TECHNICAL REPORT AFFDL-TR-72-64, VOLUME III

June 1972

Approved for public release; distribution unlimited

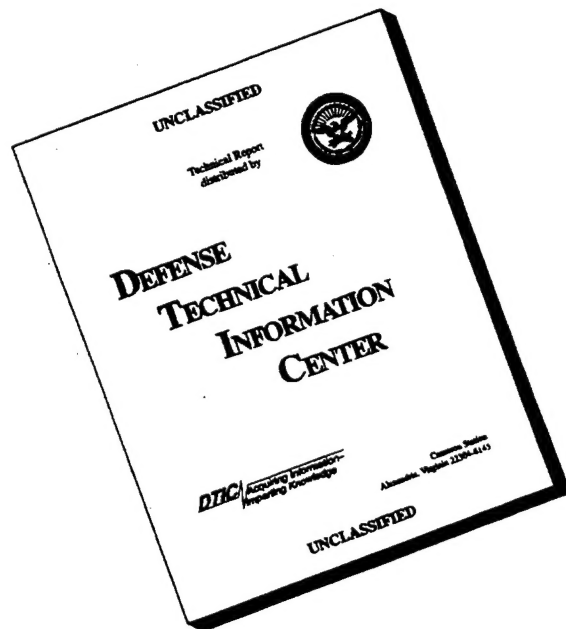
AIR FORCE FLIGHT DYNAMICS LABORATORY
AIR FORCE SYSTEMS COMMAND
WRIGHT-PATTERSON AIR FORCE BASE, OHIO

DTIC QUALITY INSPECTED 1

19960424 063

PLASTIC
17459

DISCLAIMER NOTICE



THIS DOCUMENT IS BEST QUALITY AVAILABLE. THE COPY FURNISHED TO DTIC CONTAINED A SIGNIFICANT NUMBER OF PAGES WHICH DO NOT REPRODUCE LEGIBLY.

NOTICE

When Government drawings, specifications, or other data are used for any purpose other than in connection with a definitely related Government procurement operation, the United States Government thereby incurs no responsibility nor any obligation whatsoever; and the fact that the Government may have formulated, furnished, or in any way supplied the said drawings, specifications, or other data, is not to be regarded by implication or otherwise as in any manner licensing the holder or any other person or corporation, or conveying any rights or permission to manufacture, use, or sell any patented invention that may in any way be related thereto.

Copies of this report should not be returned unless return is required by security considerations, contractual obligations, or notice on a specific document.

DEVELOPMENT OF AN UNDERSTANDING OF THE FATIGUE PHENOMENA
OF BONDED AND BOLTED JOINTS
IN ADVANCED FILAMENTARY COMPOSITE MATERIALS
VOLUME III. FATIGUE ANALYSIS AND FATIGUE MODE STUDIES

A. C. Fehrle, J. R. Carroll, S. M. Freeman, et al.
Lockheed-Georgia Company
Marietta, Georgia

Approved for public release; distribution unlimited

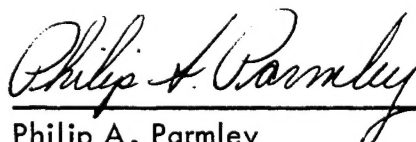
FOREWORD

This report summarizes the work accomplished under Contract F33615-70-C-1302, "Development of an Understanding of the Fatigue Phenomena of Bonded and Bolted Joints in Advanced Filamentary Composite Materials", and was prepared by the Lockheed-Georgia Company, a Division of Lockheed Aircraft Corporation. The work reported herein was sponsored by the Advanced Composite Branch, Air Force Flight Dynamics Laboratory, Air Force Systems Command, Wright-Patterson Air Force Base, Ohio 45433. Mr. Rodman Joblove, FBC, was the Air Force Project Engineer and Mr. A. C. Fehrle was the Lockheed-Georgia Program Manager.

The authors of Volume III are Mr. J. R. Carroll, Mr. A. C. Fehrle, Mr. S. M. Freeman and Mr. R. M. Gray. Mr. J. R. Carroll was responsible for conducting the fatigue analysis and cumulative damage studies. Mr. J. R. Carroll and Mr. A. C. Fehrle conducted the evaluation of specimen variables as they related to static and fatigue strength and joint efficiency. Mr. S. M. Freeman and Mr. R. M. Gray were jointly responsible for conducting the failure mode studies and relating failure modes to specimen configuration and loading conditions.

This technical report has been reviewed and is approved.

For internal control purposes, this report has been assigned Lockheed-Georgia Company Report Number ER-11319.



Philip A. Parmley
Chief, Advanced Composite Branch
Structures Division
Air Force Flight Dynamics Laboratory

ABSTRACT

This report presents the results of the empirical program undertaken to increase the basic understanding of the fatigue phenomena of advanced composites joints. Four basic design concepts have been evaluated and include both bonded and mechanically fastened joints. A broad spectrum of joint geometry variations and loading conditions are included to identify the significant parameters affecting the fatigue endurance of composite joints. Test data and analyses are included for constant amplitude testing and program fatigue loading. Realistic spectrum and block spectrum data are evaluated using Miners Cumulative Damage Theory.

In conjunction with other analyses and evaluations, failure mode studies were conducted on the fracture surface of failed specimens. Scanning electron microscope (SEM) photomicrographs were used for this failure study. Specific failure modes related to specimen configuration, loading conditions, and fatigue history were defined. Failure modes that have been identified and related to loading conditions include; shear in the resin versus load direction and stress ratio (R); peel in the laminate due to a cleavage load; peel or tension fracture due to tension-tension fatigue. Some specimens subjected to complex loading exhibited multiple failure modes.

TABLE OF CONTENTS

<u>Section</u>	<u>Title</u>	<u>Page</u>
I	INTRODUCTION	1
II	FATIGUE STUDIES	4
	2.1 GENERAL CONSIDERATIONS	4
	2.2 PROGRAM APPROACH	5
	2.3 TEST SPECTRUM DEVELOPMENT	10
	2.3.1 Realistic Spectrum Development	10
	2.3.2 Block Spectrum Development	13
	2.4 DATA PRESENTATION AND ANALYSIS	37
	2.4.1 Test Specimen Definition	39
	2.4.2 Constant Amplitude Tests	39
	2.4.3 Cumulative Damage Analysis	143
	2.5 FATIGUE ANALYSIS	157
	2.5.1 Constant Amplitude Design Data	157
	2.5.2 Cumulative Damage Design Data	164
	2.6 CONCLUSIONS	169
III	FAILURE MODE STUDIES	171
	3.1 GENERAL	171
	3.2 DETERMINATION OF SHEAR AND PEEL FAILURE MODES	172
	3.3 INITIAL JOINT FAILURE STUDIES	178
	3.4 CONFIGURATION A STUDIES	181
	3.4.1 Specimen IA111A03	182
	3.4.2 Specimen IA111D01	186
	3.4.3 Specimen IA111D09	190
	3.4.4 Specimen IA113A01	196
	3.4.5 Specimen IA113D03	204
	3.4.6 Specimen IIA11C03	212

TABLE OF CONTENTS (Cont'd)

<u>Section</u>	<u>Title</u>	<u>Page</u>
3.5	CONFIGURATION B STUDIES	217
3.5.1	Specimen IB111C01	218
3.5.2	Specimen IIB31A05	220
3.6	CONFIGURATION C STUDIES	224
3.6.1	Specimen IC111A01	225
3.6.2	Specimen IC111A02	228
3.6.3	Specimen IC111D03	231
3.7	CONCLUSION OF FAILURE MODE STUDIES	233
	REFERENCES	241

LIST OF FIGURES

<u>Figure</u>	<u>Title</u>	<u>Page</u>
1	Cumulative Occurrences (Original Data)	26
2	MIL-A-8866 Cumulative Negative Nz Curve	27
3	Cumulative Occurrences (Modified)	28
4	Close Support Mission	29
5	Interdiction Mission	30
6	Training Mission	31
7	Peacetime Mission	32
8	Close Support (Modified)	33
9	Interdiction (Modified)	34
10	Training (Modified)	35
11	Peacetime (Modified)	36
12	Bonded Joint Evaluation Phase I, Configuration A, Small Scale Specimens	53
13	Bonded Joint Evaluation Phase I, Configuration B, Small Scale Specimens	55
14	Bonded Joint Evaluation Phase I, Configuration C, Small Scale Specimens	57
15	Bonded Joint Evaluation Phase I, Configuration D, Small Scale Specimens	59
16	Bolted Joint Evaluation Phase I, Configuration E, Small Scale Specimens	61
17	Bolted Joint Evaluation Phase I, Configuration F, Small Scale Specimens	65
18	Constant Life Diagram - Phase I Configuration A Specimens	67
19	Constant Life Diagram - Phase I Configuration E Specimens	68
20	Fatigue Data for Single Butt Joint Adhesive Evaluation	69
21	S-N Curve - Specimen IA111A, Baseline Data	87
22	S-N Curve - Specimen IA111B, Baseline Data	88
23	S-N Curve - Specimen IA111C, Baseline Data	89
24	S-N Curve - Specimen IA113A, Baseline Data	90
25	S-N Curve - Specimen IA112A, Baseline Data	91

LIST OF FIGURES (Cont'd)

<u>Figure</u>	<u>Title</u>	<u>Page</u>
26	S-N Curve - Specimen IB111A, Baseline Data	92
27	S-N Curve - Specimen IB111C, Baseline Data	93
28	S-N Curve - Specimen IB112A, Baseline Data	94
29	S-N Curve - Specimen IB121A, Baseline Data	95
30	S-N Curve - Specimen ID111A, Baseline Data	96
31	S-N Curve - Specimen ID114A, Baseline Data	97
32	S-N Curve - Specimen IA211A, Ply Stacking	98
33	S-N Curve - Specimen IA213A, Ply Stacking	99
34	S-N Curve - Specimen IB211A, Ply Stacking	100
35	S-N Curve - Specimen IA311A, Short Lap Effects	101
36	S-N Curve - Specimen IA312A, Short Lap Effects	102
37	S-N Curve - Specimen IA313A, Short Lap Effects	103
38	S-N Curve - Specimen IB311A, Short Lap Effects	104
39	S-N Curve - Specimen IA911A, Long Lap Effects	105
40	S-N Curve - Specimen IA911C, Long Lap Effects	106
41	S-N Curve - Specimen IA411A, Thickness Effects	107
42	S-N Curve - Specimen IA613A, Second Adhesive	108
43	S-N Curve - Specimen IA811A, Preload/Low Cycle Data	109
44	S-N Curve - Specimen E1A, Graphite-Epoxy Evaluation	110
45	S-N Curve - Specimen E2A, S Glass-Epoxy Evaluation	111
46	S-N Curve - Specimen IC111A, Baseline Data	112
47	S-N Curve - Specimen IIA11A, Baseline Data	113
48	S-N Curve - Specimen IIA11C, Baseline Data	114
49	S-N Curve - Specimen IIB11A, Baseline Data	115
50	S-N Curve - Specimen IIB11C, Baseline Data	116
51	S-N Curve - Specimen IIA12A, Baseline Data	117
52	S-N Curve - Specimen IIB12A, Baseline Data	118
53	S-N Curve - Specimen IIA91A, Long Lap Effects	119
54	S-N Curve - Specimen IIA91C, Long Lap Effects	120

LIST OF FIGURES (Cont'd)

<u>Figure</u>	<u>Title</u>	<u>Page</u>
55	S-N Curve - Specimen IIB31A, Short Lap Effects	121
56	S-N Curve - Specimen IE111A, Baseline Data	129
57	S-N Curve - Specimen IE111B, Baseline Data	130
58	S-N Curve - Specimen IE112A, Baseline Data	131
59	S-N Curve - Specimen IE122A, Baseline Data	132
60	S-N Curve - Specimen IE211A, Stacking Order Evaluation	133
61	S-N Curve - Specimen IE211B, Stacking Order Evaluation	134
62	S-N Curve - Specimen IE311A, Edge Distance Evaluation	135
63	S-N Curve - Specimen IE321A, Edge Distance Evaluation	136
64	S-N Curve - Specimen IE411A & IE421A, Thickness Effects	137
65	S-N Curve - Specimen IE511A, Preload/Low Cycle Data	138
66	S-N Curve - Specimen IE721A, IE711A, and IE731A, Pinned Joints	139
67	S-N Curve - Specimen IF113A, Baseline Data	140
68	S-N Curve - Specimen IF413A, Thickness Effects	141
69	S-N Curve - Specimen IIE111A, Baseline Data	142
70	Typical Strip-Chart Recording of Individual Load Levels in Each Mission, Realistic Load Spectrum	153
71	Average Realistic Spectrum Missions 1 and 4	154
72	RMS Fatigue Curve - Bonded Joints	155
73	RMS Fatigue Curve - Mechanical Joints	156
74	Boron Flexure Specimen - Horizontal Shear Failure	173
75	Boron Flexure Specimen Peeled Apart	174
76	Facing Fracture Surfaces - Flexure Specimen	175
77	Facing Fracture Surfaces - Shear Mode Flexure Specimen	176
78	Facing Fracture Surfaces - Peel Mode Flexure Specimen	177
79	Typical View of Fracture Surface - Fatigue Specimen R = -1.0	179
80	Typical View of Fracture Surface - Fatigue Specimen R = +10.0	180

LIST OF FIGURES (Cont'd)

<u>Figure</u>	<u>Title</u>	<u>Page</u>
81	IA111A03 - Failure Surface A	183
82	IA111A03 - Failure Surface B	184
83	IA111A03 - Failure Surface A 200X Magnification	185
84	IA111A03 - Failure Surface B 100X Magnification	185
85	IA111D01 - Failure Surface A	187
86	IA111D01 - Failure Surface B	188
87	IA111D01 - Failure Surface B 100X Magnification	189
88	IA111D09 - Failure Surface A Titanium Splice Plate	191
89	IA111D09 - Failure Surface B Boron Adherend	192
90	IA111D09 - Failure Surface B Map SEM 40X Magnification	193
91	IA111D09 - Surface B SEM 48X Magnification	194
92	IA111D09 - Surface B SEM 51X Magnification	194
93	IA111D09 - Surface B SEM 100X Magnification	195
94	IA113A01 - Failure Surface A Boron Splice Plate	197
95	IA113A01 - Failure Surface B Loaded Boron Adherend	198
96	IA113A01 - Failure Surface A Map SEM 40X Magnification	199
97	IA113A01 - Failure Surface A SEM 53X Magnification	200
98	IA113A01 - Failure Surface A SEM 117X and 235X Magnification	202
99	IA113A01 - Failure Surface B Map SEM 40X Magnification	203
100	IA113A01 - Failure Surface B SEM 98X Magnification	205
101	IA113A01 - Failure Surface B SEM 110X Magnification	205
102	IA113D03 - Failure Surface A, Boron Splice Plate	206
103	IA113D03 - Failure Surface B, Boron Adherend	207
104	IA113D03 - Failure Surface A, 40X Magnification	208
105	IA113D03 - Failure Surface B, 40X Magnification	209
106	Enlargement of Figure 104, Lower Left Hand Corner, 122X Magnification	210
107	Enlargement of Figure 104, Upper Center, 100X Magnification	210

LIST OF FIGURES (Cont'd)

<u>Figure</u>	<u>Title</u>	<u>Page</u>
108	Enlargement of Figure 105, Just Below Center, 117X Magnification	211
109	Enlargement of Figure 105, Near Center, 110X Magnification	211
110	Specimen IIA11C03 - Overall View - Magnification 2X	213
111	Specimen IIA12A01 - Overall View - Magnification 1/3X	215
112	SEM Photomicrograph of -1 Square in Figure 111, Surface B, 20X Magnification	216
113	SEM Photomicrograph of -2 Square in Figure 111, Surface B, 20K Magnification	216
114	Specimen IB111C01 - Surface A - Magnification 4X	219
115	Specimen IIB31A05 - Overall View - Magnification 2X	221
116	Specimen IIB31A05 - Surface B - Magnification 6X	222
117	SEM Photomicrograph of -1 Square in Figure 116	223
118	SEM Photomicrograph of -2 Square in Figure 116	223
119	Specimen IC111A01 - Overall View	226
120	Specimen IC111A01 - Surface B - Magnification 4X	226
121	SEM Photomicrograph of Area Outlined in Figure 120	227
122	SEM Photomicrograph of Area Outlined in Figure 121	227
123	Specimen IC111A02 - Overall View	229
124	Specimen IC111A02 - Surface B, Magnification 4X	229
125	SEM Photomicrograph of Section from Area Designated by Square in Figure 124	230
126	Specimen IC111D03 - Overall View	232
127	Specimen IC111D03 - Surface B - Magnification 4X	232
128	Shear Failure in Matrix Subjected to a Stress Ratio of $R = -1.0$	234
129	Shear Failure in Matrix Subjected to Tension-Tension Fatigue, $R = +0.1$	235
130	Shear Failure in Matrix Subjected to Compression-Compression Fatigue, $R = +10.0$	236
131	Shear Failure in Matrix Subjected to Static Compression	237

LIST OF FIGURES (Cont'd)

<u>Figure</u>	<u>Title</u>	<u>Page</u>
132	Cohesive Shear in the Adhesive as Illustrated in Section 2.	238
133	Spalling of Boron Fibers in 45° Plies Subjected to a Tension-Tension Fatigue Load Applied at 0°	239
134	Peel Failure in Matrix Subjected to Static Tension	240
135	Shear and Flatwise Tension or Peel in a Tee Joint	240

LIST OF TABLES

<u>Table</u>	<u>Title</u>	<u>Page</u>
I	Single Flight Loading Chart - Close Support Mission	15
II	Single Flight Loading Chart - Interdiction Mission	16
III	Single Flight Loading Chart - Training Mission	17
IV	Single Flight Loading Chart - Peacetime Mission	18
V	Additional Loadings	19
VI	Flight Sequence (400 Flight Random Schedule)	20
VII	Test Sequence (400 Flight Random Schedule)	22
VIII	Block Loading Spectrum	24
IX	Truncated Block Loading Spectrum	25
X	Alternate Adherend Materials Evaluation	41
XI	Material Verification and Checkout Tests	41
XII	Bonded Joints Evaluation, Phase I - Small Scale Specimens	43
XIII	Bonded Joints Evaluation, Phase II - Medium Scale Specimens	45
XIV	Bonded Joints Evaluation, Phase III - Large Scale Specimens	47
XV	Mechanical Joints Evaluation, Small and Medium Scale Specimens	49
XVI	Index of Bonded Joint Fatigue Data	51
XVII	Index of Mechanical Joint Fatigue Data	52
XVIII	Degradation of Bonded Joints, One-Inch Width, Stiffness and Ultimate Loads Data	82
XIX	Post Fatigue Data, One-Inch Specimens, Stiffness and Ultimate Loads Data	84
XX	Degradation of Bonded Joints, Three-Inch Width, Stiffness and Ultimate Loads Data	85
XXI	Post Fatigue Data, IIB11A Specimens	80
XXII	Configuration IIIA and IIIB Test Data	86
XXIII	Cumulative Damage Test Specimens	145
XXIV	Block Loading Cumulative Damage Summary	150

LIST OF TABLES (Cont'd)

<u>Table</u>	<u>Title</u>	<u>Page</u>
XXV	RMS Loads Data	151
XXVI	Damage Summary - Realistic Spectrum Tests	152
XXVII	Joint Static Strength Versus Fatigue Endurance	168
XXVIII	Actual Versus Predicted Fatigue Endurance	166

I. INTRODUCTION

This program was undertaken to develop an understanding of the fatigue phenomena of structural joints in advanced filamentary composite materials and to develop analytical and testing methods to support proper fatigue design of advanced composite structural joints. The program included the evaluation of both bonded and bolted joints. Primary emphasis was placed on joints in boron-epoxy; however, a limited evaluation of bonded joints in graphite-epoxy and glass-epoxy were included. Although the sizes of the joints for this investigation were small (one to ten inches in width), all configurations evaluated are representative of typical structural joints currently utilized in advanced filamentary composite structures.

The program consisted of three major areas of investigation:

- o Analysis Methods
- o Fabrication, Inspection and Testing
- o Fatigue Analysis and Failure Mode Studies

Analytical methods for determining joint stresses were divided into two major tasks; (1) analysis of bonded joints and (2) analysis of bolted joints. Primary emphasis was placed on the development of a closed form elastic analysis procedure for bonded joints. This analysis was used to evaluate a number of joint variables. A "plastic zone" approach was used to extend the closed form analysis procedure to include joints with inelastic adhesive stress-strain behavior. The results of the elastic closed form solution were verified with finite element analyses, photoelastic analysis, and strain gage data. Finite element analyses were used to evaluate the step lap bonded joints and bolted joints.

The experimental program consisted of fabrication, inspection, and testing of a large quantity of joint specimens. Fabrication and inspection methods were established which resulted in specimens being fabricated to close tolerances and of uniform high quality. This provided specimens that would consistently develop stresses that were predicted

by the analytical methods. Developing testing techniques and actual specimen testing was a major portion of the program. Establishing proper specimen support was essential to obtaining repeatable joint strengths within a specimen configuration. Equally important was determining the proper cyclic rate for the different stress ratios and specimen configurations to preclude specimen heating and erratic and unreliable fatigue lives.

Evaluation of the experimental results was divided into two separate but related tasks. These tasks were failure mode studies and fatigue analysis. The failure mode studies mentioned were photomicrographic analyses of the failure surfaces. This failure mode analysis does not replace but augments the gross failure modes generally defined within the experimental phases of a program. The photomicrographic analysis conducted within this program established failure modes related to specific joint designs, joint loading, and fatigue history. The fatigue analysis established relationships between specimen configurations, joint variables, material combinations, loading conditions, and stress ratio effects for constant amplitude loading. The relationship between constant amplitude fatigue and spectrum fatigue (block and realistic) was also evaluated for specific joint configurations.

This report is divided into three separate volumes each containing the developments accomplished within a major area of investigation. Each volume is a self-contained document, complementing the other two volumes but not dependent upon them for coherence or continuity. The titles of the three volumes are:

- Volume I - Analysis Methods
- Volume II - Fabrication, Inspection and Testing
- Volume III - Fatigue Analysis and Failure Mode Studies

Volume III contains two areas of investigation; Fatigue Studies and Failure Mode Studies. The fatigue studies included the evaluation of a broad spectrum of joint geometry variations and loading conditions. Constant amplitude S-N curves are presented for all joint parameters included in the program and spectrum fatigue evaluation was conducted

on the basic joint configurations. A number of design parameters were defined for improving fatigue capability of structural joints in advanced composites. The failure mode studies consisted of photomicrographic evaluation of the fractured surfaces. Included herein are photomicrographs depicting specific failure modes as they relate to specimen configurations and loading conditions. Failure modes defined in this study are applicable to failure investigations on full size structural components.

II. FATIGUE STUDIES

2.1 GENERAL CONSIDERATIONS

In any air vehicle design and development program, structural fatigue is one of several design criteria that must be considered both from an analytical and empirical standpoint. Increasing demands for structural reliability have directed more and more attention to advances in materials development as one step toward improving fatigue endurance. Advanced composite structures, boron-epoxy and graphite-epoxy, hold great promise in providing strength, stiffness, and weight savings and it is prudent that detailed investigations be conducted to develop fatigue design criteria for realistic structural applications of these composites. As a part of this objective, this program has been conducted to develop an understanding of the fatigue phenomena of advanced composites joints.

This has been accomplished, not by developing a large statistical fatigue data sample, but through a systematic, parametric study of important factors which effect the fatigue endurance of composite joints. The program includes realistic joint concepts common in air vehicle structures and consists of both bonded and mechanically fastened joints. Basically, the tests conducted are considered in two phases; (1) constant amplitude fatigue data to investigate the parameters which effect fatigue of the joints and develop design guidelines and (2) program fatigue tests (block and realistic spectrum tests) to evaluate the effect of this type testing and to determine the applicability of existing cumulative damage theories for advanced composite structures.

Program details, test data presentation, and analysis is included in the following sections.

2.2 PROGRAM APPROACH

In the past decade there have been numerous research and production oriented programs to evaluate the fatigue phenomena of advanced composite materials, Reference 8. These investigations have been primarily concerned with the basic composite laminate, boron-epoxy and graphite-epoxy, and/or specific structural configurations for a particular design application. This program is, however, directed toward the systematic study of the overall understanding of the parameters involved in designing advanced composites joints for adequate fatigue endurance.

To accomplish these program goals, both bonded and mechanically fastened joints have been evaluated empirically. These tests have included a broad parametric study of joint geometric concepts and have included both constant amplitude and spectrum loadings. A survey of typical aircraft structural configurations has led to identification of four basic joint types which are included in the program; i.e.,

- Type 1 - Single splice butt joint - both bonded and mechanically fastened
- Type 2 - Stepped scarf joint - bonded only
- Type 3 - Surface to support structure attachment - both bonded and mechanically fastened
- Type 4 - Double splice butt joint - bonded only

Two joint concepts, Type 1 and Type 2 above, have received the most extensive evaluation while joint concepts, Type 3 and Type 4, have been considered on a more limited basis. The major emphasis, however, is on the single splice butt joint, both bonded and with mechanical fasteners, which is most commonly used in aircraft structures where a flush joint or attachment is specified for structural smoothness. By varying the splice plate geometry, primarily the thickness, this basic joint concept may be made representative of a skin, panel or plate splice joint over a part of the sub-structure. In order to evaluate the mechanically fastened joint concept more extensively, two variations are included, one containing metallic shims to improve fastener bearing strength and the second containing additional plies of $\pm 45^\circ$ boron to accomplish the same task.

The bonded scarf joint concept, Type 2, is the second most extensively investigated joint, but to a lesser extent than Type 1. The most significant difference in the two concepts is that the scarf joint provides an in-line path for load transfer and thereby reduces adherend bending and stress concentrations. Limited evaluation of Types 3 and 4 complements the basic program in depth and scope. The surface-to-support structure attachment joint (Type 3) is a modification of the single splice butt joint, and by applying load to the simulated support structure, normal to the sheet adherend, the condition of joint bending is included in the investigation. The double splice joint, represented by Type 4, provides an additional joint concept for investigation which differs from the previous concepts in practical application and method of analysis.

The four bonded joint concepts have been evaluated in three phases which are defined in terms of specimen geometry. These include one-inch wide specimens in Phase I and 3.0" and 10.0" wide specimens in Phases II and III respectively. The mechanically fastened joints are included in one-inch and two-inch widths only, Phases I and II. The major program effort has involved the Phase I specimens with the subsequent phases included to investigate the two-dimensional effects in the joints, such as Poisson's Ratio and variations in coefficients of thermal expansion.

The parameters that have been evaluated for the four basic joint configurations include the following:

Bonded Joint Parametric Studies

Bonded Joint - Type 1

- a. Three adherend combinations
- b. Two filament orientations and two stacking orders
- c. Two adherend thicknesses
- d. Three bondline lap lengths
- e. Two adhesive materials
- f. Three constant amplitude loading conditions with variations in loading and cycling rates for three individual stress ratios
- g. Strength and stiffness degradation

- h. Cumulative damage
- i. Preload and low cycle effects

Bonded Joint - Type 2

- a. Two adherend combinations
- b. Two filament orientations with one variation in stacking order
- c. Two bondline lap lengths
- d. Two constant amplitude loading conditions
- e. Strength and stiffness degradation
- f. Cumulative damage

Bonded Joint - Type 3

- a. One adherend combination
- b. One stress ratio with two stress levels
- c. Combined loading conditions, (axial and bending)

Bonded Joint - Type 4

- a. Two adherend combinations
- b. One stress ratio for each configuration with two stress levels each

Mechanical Joint Parametric Studies

Mechanical Joint - Type 1

- a. Two adherend combinations, composite-to-composite and composite-to-titanium
- b. Torqued fasteners and retention of torque during fatigue loading
(NOTE: A limited number of pin bearing specimens have been tested for comparative purposes.)
- c. Two filament orientations, 0° and $0^\circ/\pm 45^\circ$ and two stacking orders
- d. Two fastener edge distances, $e/D = 2$ and $e/D = 1.5$
- e. Two reinforcements in joint areas, titanium shims (0.012") and build-up of $\pm 45^\circ$ boron plies
- f. Uniaxial loading, tension-tension, tension-compression, and compression-compression at constant amplitude
- g. Cumulative damage effects - realistic and block spectrum loading

- h. Evaluation of width effects
- i. Two composite thicknesses
- j. Preload and low cycle fatigue evaluation

Mechanical Joint - Type 2

- a. One adherend combination with titanium shim build-up
- b. Evaluation of thickness effects
- c. Combined loading (axial and bending)

To establish a data base for both the bonded and mechanically fastened joints, it was necessary to characterize one configuration of each to a relatively broad extent. The one-inch wide, bonded single splice butt joint with $0^\circ/\pm 45^\circ$ fiber orientation and boron-titanium-boron adherend combination provides baseline data with which all subsequent bonded joint evaluations have been compared. For the mechanical joints, the narrow, single splice butt joint with titanium shims, $0^\circ/\pm 45^\circ$ fiber orientation, and fastener edge distance of 2.0 is the baseline configuration for comparison of the various parameters evaluated.

Constant amplitude fatigue tests have been completed and the resulting data were used as the basis for evaluating the effect of the various parameters, included in this program, on the fatigue endurance of composite joints. Also, the baseline data developed for the bonded and mechanically fastened joints have been utilized to construct constant life diagrams. These constant life diagrams have been used for cumulative damage analyses of the block and realistic spectrum loading test data.

To extend this fatigue evaluation from the constant amplitude testing to loadings more representative of the actual aircraft environment, selected configurations were subjected to block and "realistic" spectrum loading tests. These test spectra have been developed using a reasonably realistic fighter aircraft wing loading spectrum and the "realistic" spectrum includes frequency as well as amplitude variation. Test data have been evaluated to determine the adequacy of cumulative damage theories as applicable to advanced composite structures.

The test specimen details and parameters involved in this program are discussed in 2.4.1 and the constant amplitude test data is presented in 2.4.2. The test spectrum development for the realistic and block spectrum tests is discussed in 2.3 and test results are presented in 2.4.3. The analysis of test data and recommendations for fatigue of composite joints is included in 2.5.

2.3 TEST SPECTRUM DEVELOPMENT

2.3.1 Realistic Spectrum Development

Available unclassified reports containing data on the design loadings and actually experienced loadings for fighter aircraft were collected and studied. It was apparent that the major portion of fatigue damage was caused by loadings due to aircraft maneuvers. The maneuver load frequency spectrum of MIL-A-8866 (Ref. 1) was used as the basis for spectrum development. The g loading requirements of MIL-A-8861 (Ref. 2) and the service-life requirements of ASD-TR-66-57 (Ref. 3) were also used in establishing loadings. Limit load factors of +7.33 and -3.0 were selected for use in the spectrum development. From MIL-A-8866, the spectrum loading curves would then encompass from 35% to 125% of the +7.33g limit load (+2.56g to +9.16g), and from 0% to 110% of the -3.0g limit load (0g to -3.3g). The MIL-A-8866 occurrence table figures were summed to make the 4000 flight-hours cumulative curves shown in Figures 1 and 2. High-load cutoffs for testing were selected as +10g and -3.6g; low-load cutoffs used were +2.56g and 0g. Four fighter-type missions were selected from information sources to represent a realistic fighter aircraft usage. These are listed as:

- (1) Close Air-Support Mission from ASD-TR-68-65 (Ref. 4);
- (2) Interdiction Mission from ASD-TR-68-65;
- (3) Training Mission from GD/FW Report FW69-257 (Ref. 5);
- (4) Peacetime Mission from AFFDL-TR-67-107-2 (Ref. 6).

Cumulative occurrence +g curves for these missions as presented in the referenced reports or as modified for 4000 flight hours, are shown in Figure 1 along with the MIL-A-8866 curve. The summation of these four mission curves did not agree with the MIL-A-8866 total curve, so the mission curves were modified slightly so that, at all N_z values, the cumulative occurrence summation would equal the MIL-A-8866 curve. Figure 3 presents the resulting curves.

Each mission curve was divided into applicable flight segments in accordance with the information in the referenced reports from which the missions were obtained. These mission curves and segments are presented in Figures 4, 5, 6, and 7 for 4000 flight hours. Negative N_z data was apportioned to the missions and segments in the same proportion as the positive N_z loadings so that the distribution would be relatively even throughout the spectrum. For this apportionment, the relationship of positive N_z at +2.56g was used as a basis for distribution. The resulting curves are presented in Figures 8 through 11. This relationship at +2.56g was also used to establish the number of flights of each mission to be considered. It was assumed that the MIL-A-8866 total curve for 4000 flight hours applied to a total of 4000 flights so that the specified 4000 landings would be obtained. From these curves then, by knowing the total number of occurrences in each mission type for 4000 flight hours and the total number of flights for each mission type, the average number of occurrences per flight per mission and per mission segment were obtained. To account for ground-air-ground cycles, each flight was started and ended with -1.0g. The total flight breakdown per 4000 flight hours was calculated to be:

Close Support Mission	-	1108 flights
Interdiction Mission	-	284 flights
Training Mission	-	844 flights
Peacetime Mission	-	1764 flights

An attempt was made to utilize a realistic sequencing of the damage source segments in a typical single flight loading chart. This approach was abandoned for the following reasons. As shown in Figures 4 through 11, each mission is divided into specific flight segments such as air-to-ground combat, ascent, descent, and others. Each of these segments represents a specific damage source, but within each segment there are many loadings which cannot be applied to a single flight. For example, in the Interdiction Mission (Figure 5), a limit load factor of 7.33g occurs only once in 4000 flight hours during the "descent" segment. Attempts to account for this load in a typical single flight become meaningless, since this would require application of a fractional cycle of this load level in each loading spectrum. This problem is obviously greatly magnified by the large number of such less-than-full-cycle loadings in each segment of each flight. The situation is further complicated by any attempt to derive normal orderly sequencing of loading segments within a given flight.

While it is not beyond the realm of possibility to generate representative full cycles per flight for testing purposes, there would necessarily be many different flight spectra for each mission type, with the result that testing load inputs would greatly exceed the capability of existing test equipment. Under this plan it would have required 26 different flight spectra to cover the Interdiction Missions. Simplification of the program was therefore necessary, and it was decided to test in 400-flight spectrum blocks with the blocks repeated 10 times to obtain the 4000 flight lifetime. This action resulted in deletion of the identification of the damage source segment and the orderly sequence of flight events from the typical single-flight loading chart.

The change to a 400 flight spectrum block resulted in the following flight breakdown:

Close Support Mission	-	111 flights
Interdiction Mission	-	29 flights
Training Mission	-	84 flights
Peacetime Mission	-	176 flights

The single-flight loading charts for the 400 flight spectrum are presented in Tables I through IV. In order to account for the correct number of loadings required, per the occurrence curves, the loadings which occur in numbers which could not be evenly divided into the spectrum blocks are presented separately in Table V. These loadings will be applied as noted during the testing program. In the single-flight tables, some loadings occur each time a flight is made; others occur only during certain flights. The non-regular loadings are indicated by adding a fraction after the load level number. For example, the load "+5($\frac{1}{3}$)", indicates that this particular loading (+5g) occurs once per three flights of this mission.

The 400 flights of the realistic spectrum were assigned flight numbers: flights 1-111 for Close Support missions, flights 112-140 for Interdiction missions, flights 141-224 for Training missions, and flights 225-400 for Peacetime missions. These 400 numbers were randomized by means of a random number table. The resulting list of numbers-at-random was examined for instances where several flights of any one mission type were in

succession. An arbitrary limit of three flights of any one mission type in succession was applied and the list of random numbers was changed accordingly. This list of numbers was then established as the testing sequence. Table VI presents the Flight Sequence vs. Test Sequence with the flight numbers in numerical order; Table VII presents the same information with the test sequence in numerical order.

2.3.2 Block Spectrum Development

MIL-A-8866 maneuver occurrence loadings for 4000 flights plus 4000 occurrences of $-1.0g$ were combined and divided into 10 approximately equal blocks. These blocks were identical except for the occurrences which could not be evenly divided into 10 groups. The same g loadings used in the realistic spectrum were used in the block spectrum. The difference is that in the realistic spectrum, the loads are applied randomly and flight-by-flight, and in the block spectrum the loads are applied in sequence of ascending or descending magnitude with all cycles of the same magnitude being applied in a group. In the odd-numbered blocks, ascending order of magnitude is used; in even-numbered blocks, descending order of magnitude is used.

Due to the number of block loadings being too large for the capacity of the test equipment storage register, the 10 blocks were changed to two blocks which could be repeated five times to obtain the 4000 flight spectrum. The first block will be run in ascending order of g loadings and the second block will be run in descending order of g loadings. This loading scheme, when repeated five times will equate the 4000 flight spectrum. The block loadings for the bonded joint specimens are shown in Table VIII. Total test loadings in the two block spectrum sequence are essentially the same as those in the application of two 400-flight realistic spectrum blocks.

Some difficulty was encountered with the cumulative damage testing of the mechanical joint specimens. Repeated attempts to obtain acceptable fatigue failures using the original block loading spectrum were unsuccessful. It was decided therefore that the loading spectrum would have to be modified and the $1.0g$ load level increased. Various changes were made until satisfactory failures were obtained within an acceptable time

span. The spectrum that was finally adopted for both the Phase I and Phase II mechanical joint specimens is presented in Table IX. The value of the 1.0g load was selected to give a joint net section stress of approximately 39,000 psi at the 8.0g load level. Since most of the 1-inch wide specimens were used to establish the loading spectrum, it was necessary to test a few additional contingency specimens in order to obtain sufficient data points for spectrum evaluation. The Phases I and II realistic loading spectrum tests were conducted without any difficulties. In both cases the selection of the 1.0g load level was based on the results of the block spectrum testing.

TABLE II SINGLE FLIGHT LOADING CHART - (400-FLT. RANDOMIZED)

[illegible]

TABLE III
SINGLE FLIGHT LOADING CHART—(400-FLT. RANDOMIZED)

TRAINING MISSION (84 FLIGHTS)

[illegible]

TABLE V ADDITIONAL LOADINGS TO BE APPLIED WITH THE NOTED
400-FLIGHT SPECTRUM GROUP

	F	T	F	T	F	T	F	T	F	T	F	T	F	T	F	T
First 400																
Flt. Group	+1	+2.56	+1	-3.2	+1	+9	+1	-3.6	+1	-0.8	+1					
Second 400																
Flt. Group	+1	+2.56	+1	-3.2	+1	+8	+1	-0.8	+1	-3.2	+1	+2.56	+1			
Third 400																
Flt. Group	+1	+2.56	+1	-3.2	+1	+8	+1	-0.8	+1	-0.8	+1	+2.56	+1			
Fourth 400																
Flt. Group	+1	+2.56	+1	-3.2	+1	-3.6	+1	-0.8	+1	-0.8	+1					
Fifth 400																
Flt. Group	+1	+2.56	+1	-3.2	+1	+9	+1	+8	+1	-0.8	+1					
Sixth 400																
Flt. Group	+1	+2.56	+1	-3.2	+1	+9	+1	+8	+1	-0.8	+1					
Seventh 400																
Flt. Group	+1	+2.56	+1	-3.2	+1	-2.0	+1	-3.6	+1	-0.8	+1	-0.8	+1			
Eighth 400																
Flt. Group	+1	+2.56	+1	-3.2	+1	+8	+1	-0.8	+1	-0.8	+1	+2.56	+1			
Ninth 400																
Flt. Group	+1	+2.56	+1	-3.2	+1	+8	+1	-0.8	+1	-3.2	+1	+2.56	+1			
Tenth 400																
Flt. Group	+1	+2.56	+1	-3.2	+1	+9	+1	-3.6	+1	-0.8	+1					

TABLE VI FLIGHT SEQUENCE (400 FLT. RANDOM SCHEDULE)

[illegible]

TABLE VI FLIGHT SEQUENCE (400 FLT. RANDOM SCHEDULE) (CONT'D)

FLT. NO.	TEST SEQ.	FLT. NO.	TEST SEQ.	FLT. NO.	TEST SEQ.	FLT. NO.	TEST SEQ.	FLT. NO.	TEST SEQ.	FLT. NO.	TEST SEQ.	FLT. NO.	TEST SEQ.
211	47	241	215	271	373	301	270	331	139	361	115	391	280
212	17	242	31	272	224	302	171	332	353	362	30	392	152
213	316	243	264	273	352	303	244	333	292	363	348	393	184
214	260	244	298	274	194	304	69	334	335	364	195	394	314
215	153	245	283	275	309	305	83	335	188	365	331	395	141
216	278	246	293	276	114	306	321	336	154	366	226	396	168
217	101	247	199	277	72	307	38	337	339	367	243	397	357
218	363	248	40	278	43	308	343	338	315	368	217	398	390
219	388	249	295	279	208	309	205	339	82	369	97	399	381
220	192	250	79	280	34	310	241	340	383	370	160	400	212
221	150	251	360	281	26	311	22	341	376	371	385		
222	305	252	63	282	355	312	233	342	100	372	368		
223	286	253	124	283	190	313	94	343	389	373	253		
224	239	254	299	284	369	314	400	344	393	374	20		
225	211	255	147	285	322	315	87	345	365	375	157		
226	341	256	196	286	257	316	256	346	361	376	221		
227	379	257	273	287	223	317	330	347	300	377	118		
228	323	258	19	288	218	318	107	348	148	378	230		
229	57	259	53	289	142	319	274	349	238	379	65		
230	220	260	287	290	327	320	163	350	398	380	164		
231	136	261	349	291	307	321	12	351	99	381	228		
232	46	262	125	292	106	322	246	352	271	382	36		
233	5	263	183	293	28	323	45	353	11	383	259		
234	24	264	284	294	170	324	306	354	60	384	8		
235	302	265	15	295	92	325	366	355	359	385	80		
236	318	266	231	296	236	326	289	346	372	386	39		
237	362	267	77	297	74	327	209	357	137	387	51		
238	110	268	55	298	201	328	391	358	234	388	131		
239	27	269	129	299	181	329	200	359	134	389	371		
240	64	270	213	300	127	330	394	360	387	390	180		

TABLE VII TEST SEQUENCE (400 FLT. RANDOM SCHEDULE)

[illegible]

TABLE VII TEST SEQUENCE (400 FLT. RANDOM SCHEDULE) (CONT'D)

TEST SEQ.	FLT. NO.	TEST SEQ.	FLT. NO.	TEST SEQ.	FLT. NO.	TEST SEQ.	FLT. NO.	TEST SEQ.	FLT. NO.	TEST SEQ.	FLT. NO.	TEST SEQ.	FLT. NO.
211	225	241	310	271	352	301	164	331	365	361	346	391	328
212	400	242	131	272	114	302	235	332	148	362	237	392	187
213	270	243	367	273	257	303	199	333	83	363	218	393	344
214	161	244	303	274	319	304	58	334	205	364	109	394	330
215	241	245	111	275	107	305	222	335	334	365	345	395	4
216	12	246	322	276	196	306	324	336	104	366	325	396	120
217	368	247	47	277	40	307	291	337	207	367	22	397	89
218	288	248	185	278	216	308	76	338	135	368	372	398	350
219	29	249	91	279	11	309	275	339	337	369	284	399	23
220	230	250	115	280	391	310	138	340	169	370	59	400	314
221	376	251	144	281	203	311	31	341	226	371	389		
222	106	252	175	282	3	312	167	342	55	372	356		
223	287	253	373	283	245	313	206	343	308	373	271		
224	272	254	155	284	264	314	394	344	45	374	46		
225	125	255	101	285	127	315	338	345	108	375	201		
226	366	256	316	286	223	316	213	346	133	376	341		
227	15	257	286	287	260	317	168	347	42	377	119		
228	381	258	85	288	122	318	236	348	363	378	170		
229	61	259	383	289	326	319	159	349	261	379	227		
230	378	260	214	290	209	320	184	350	82	380	7		
231	266	261	186	291	96	321	306	351	124	381	399		
232	30	262	62	292	333	322	285	352	273	382	189		
233	312	263	14	293	246	323	228	353	332	383	340		
234	358	264	243	294	130	324	65	354	27	384	94		
235	117	265	98	295	249	325	140	355	282	385	371		
236	296	266	178	296	35	326	39	356	44	386	177		
237	145	267	118	297	66	327	290	357	397	387	360		
238	349	268	95	298	244	328	54	358	188	388	219		
239	224	269	36	299	254	329	152	359	355	389	343		
240	9	270	301	300	347	330	317	360	251	390	398		

TABLE VIII BLOCK SPECTRUM LOADINGS

Load in "g's"		Cycles of Load in Block Number:									
Min.	Max.	1	2	3	4	5	6	7	8	9	10
-3.6	+1	1	0								
-3.2	+1	1	1								
-2.8	+1	4	4								
-2.4	+1	8	8								
-2.0	+1	11	11								
-1.6	+1	15	15								
-1.2	+1	18	18								
-1.0	+1	400	400								
-0.8	+1	34	35	BLOCK 1	BLOCK 2	BLOCK 1	BLOCK 2	BLOCK 1	BLOCK 2	BLOCK 1	BLOCK 2
-0.4	+1	76	76	BLOCK 1	BLOCK 2	BLOCK 1	BLOCK 2	BLOCK 1	BLOCK 2	BLOCK 1	BLOCK 2
0	+1	233	234	BLOCK 1	BLOCK 2	BLOCK 1	BLOCK 2	BLOCK 1	BLOCK 2	BLOCK 1	BLOCK 2
+1	+2.56	3802	3803								
+1	+3	6500	6500								
+1	+4	3600	3600								
+1	+5	1800	1800	REPEAT	REPEAT	REPEAT	REPEAT	REPEAT	REPEAT	REPEAT	REPEAT
+1	+6	810	810	REPEAT	REPEAT	REPEAT	REPEAT	REPEAT	REPEAT	REPEAT	REPEAT
+1	+7	237	237	REPEAT	REPEAT	REPEAT	REPEAT	REPEAT	REPEAT	REPEAT	REPEAT
+1	+8	45	44	REPEAT	REPEAT	REPEAT	REPEAT	REPEAT	REPEAT	REPEAT	REPEAT
+1	+9	7	8								
+1	+10	1	1								

NOTE:

For IA Specimens 1.0g = 240 lbs

IIIA Specimens 1.0g = 1480 lbs

IIIB Specimens 1.0g = 2940 lbs

TABLE IX - TRUNCATED BLOCK SPECTRUM LOADINGS

Load in "g's"		Cycles of Load in Block Number:									
		1	2	3	4	5	6	7	8	9	10
Min.	Max.										
-3.6	+1	1	0								
-3.2	+1	1	1								
-2.8	+1	4	4								
-2.4	+1	8	8								
-2.0	+1	11	11								
+1	+4	3600	3600	REPEAT BLOCK 1	REPEAT BLOCK 2	REPEAT BLOCK 1	REPEAT BLOCK 2	REPEAT BLOCK 1	REPEAT BLOCK 2	REPEAT BLOCK 1	REPEAT BLOCK 2
+1	+5	1800	1800								
+1	+6	810	810								
+1	+7	237	237								
+1	+8	53	53								

NOTE:

For IE Specimens 1.0g = 360 lbs

III E Specimens 1.0g = 690 lbs

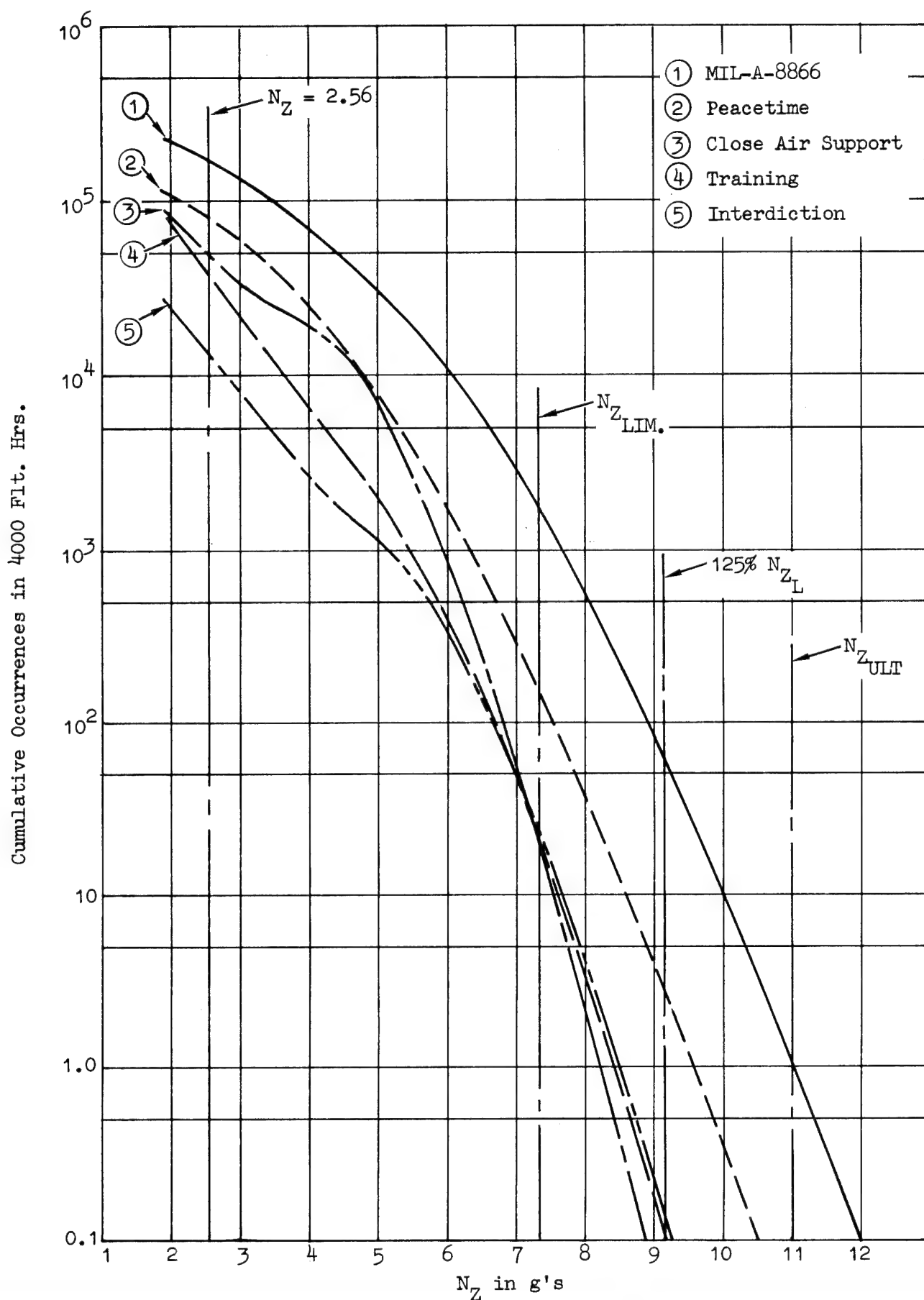


Figure 1 Cumulative Occurrences (Original Data)

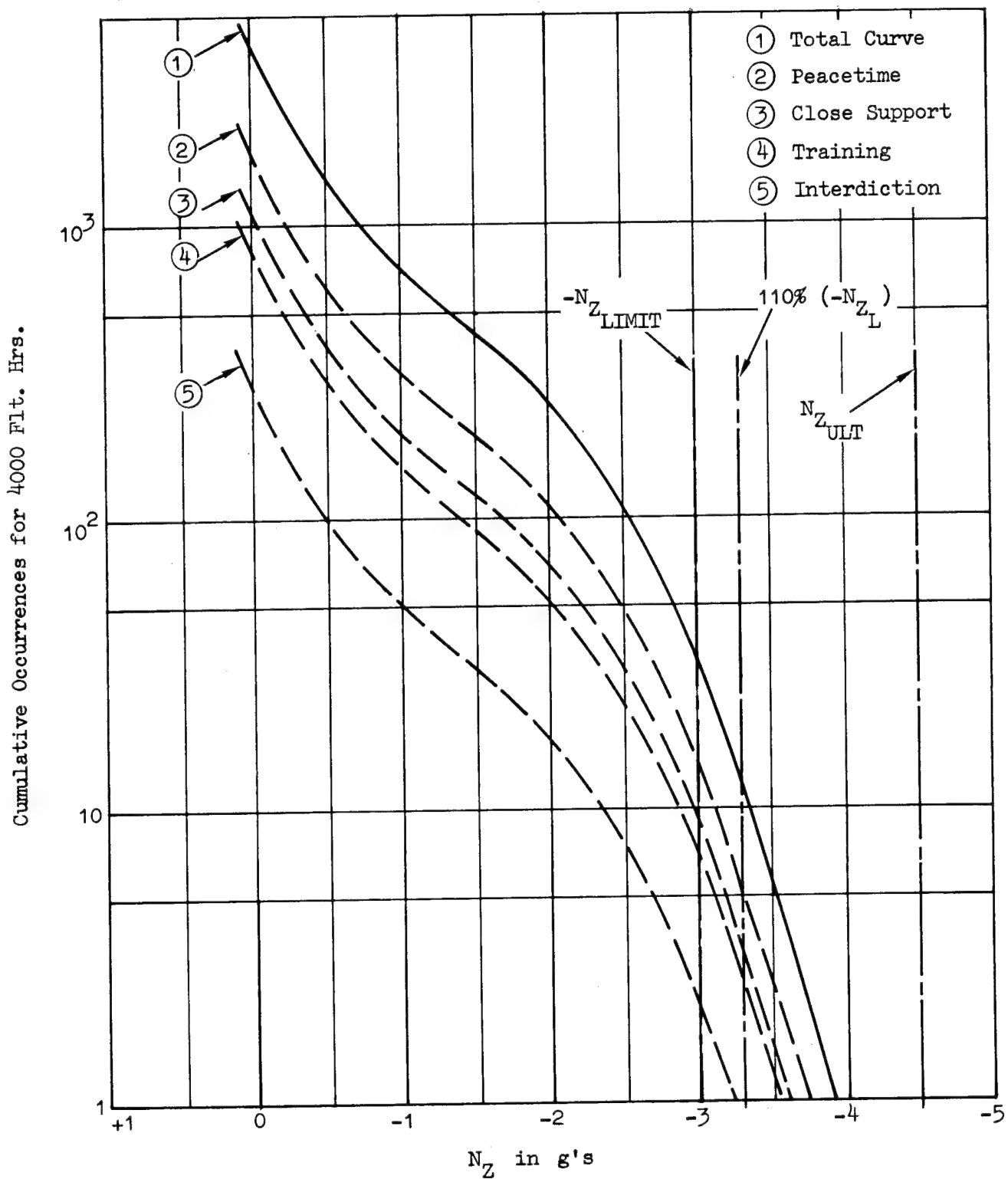


Figure 2 MIL-A-8866 Cumulative Negative N_Z Curve

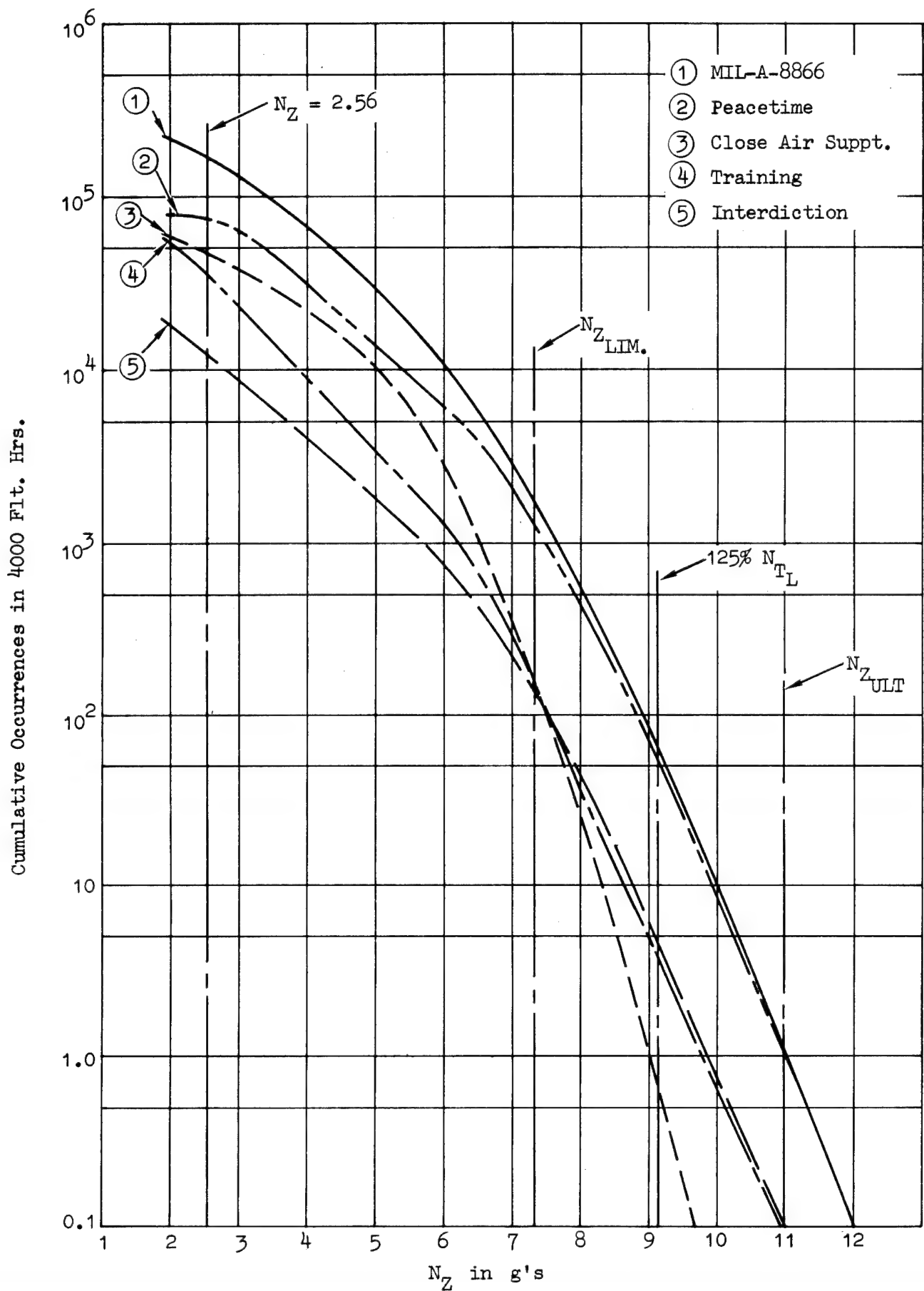


Figure 3 Cumulative Occurrences (Modified)

Cumulative Occurrences in 4000 Flt. Hrs.

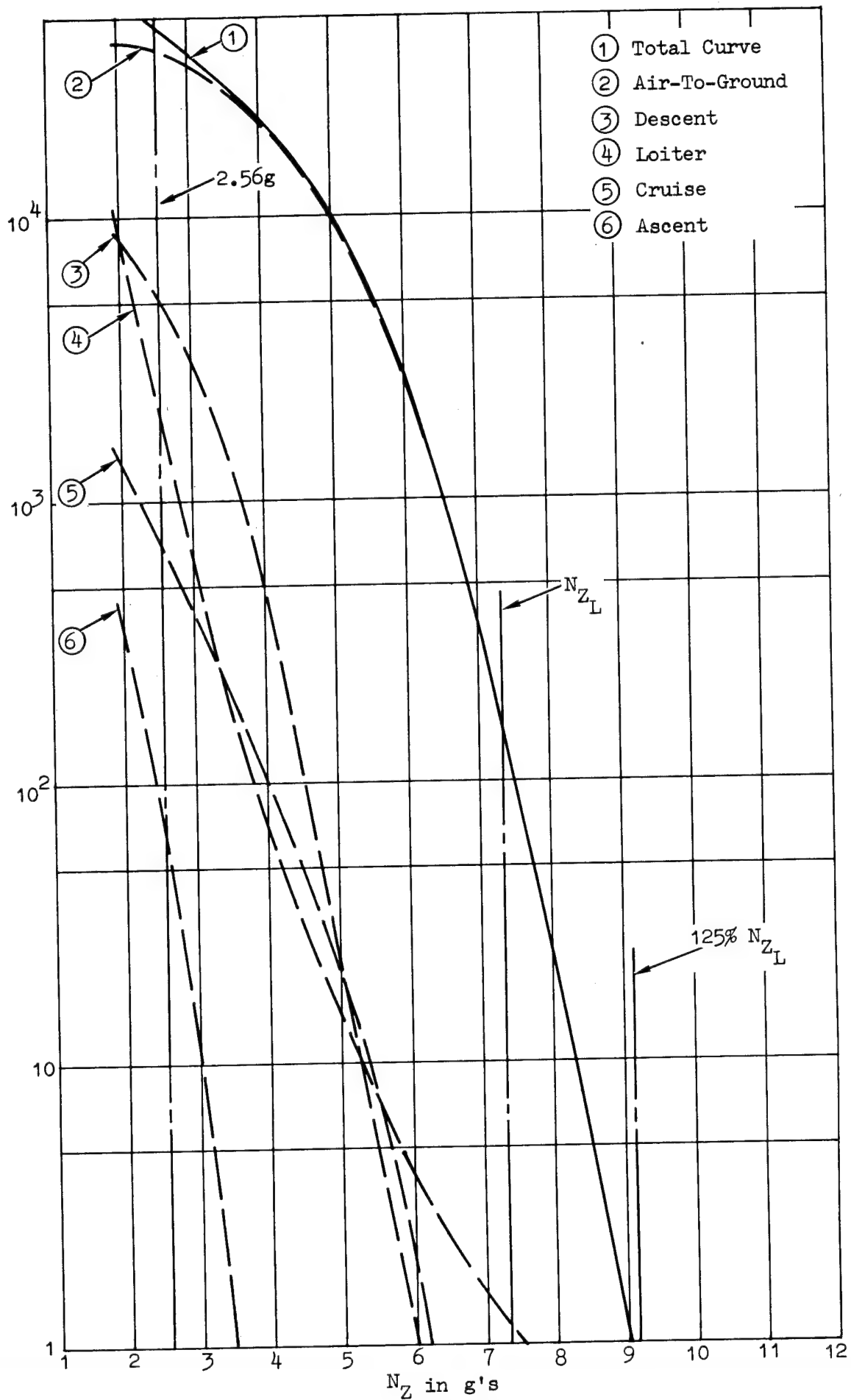


Figure 4 Close Support Mission

Cumulative Occurrences in 4000 Flt. Hrs.

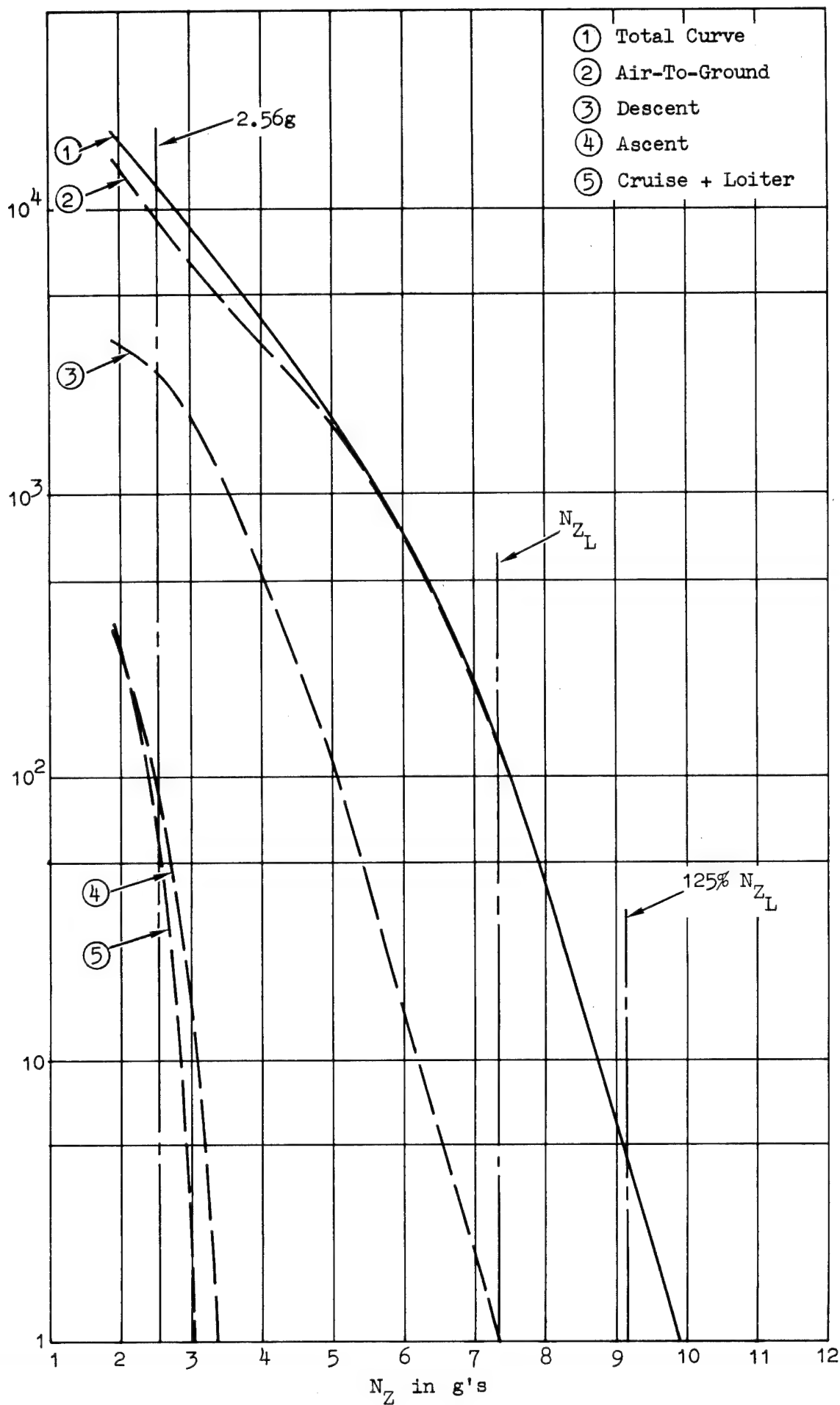


Figure 5 Interdiction Mission

Cumulative Occurrences in 4000 Flt. Hrs.

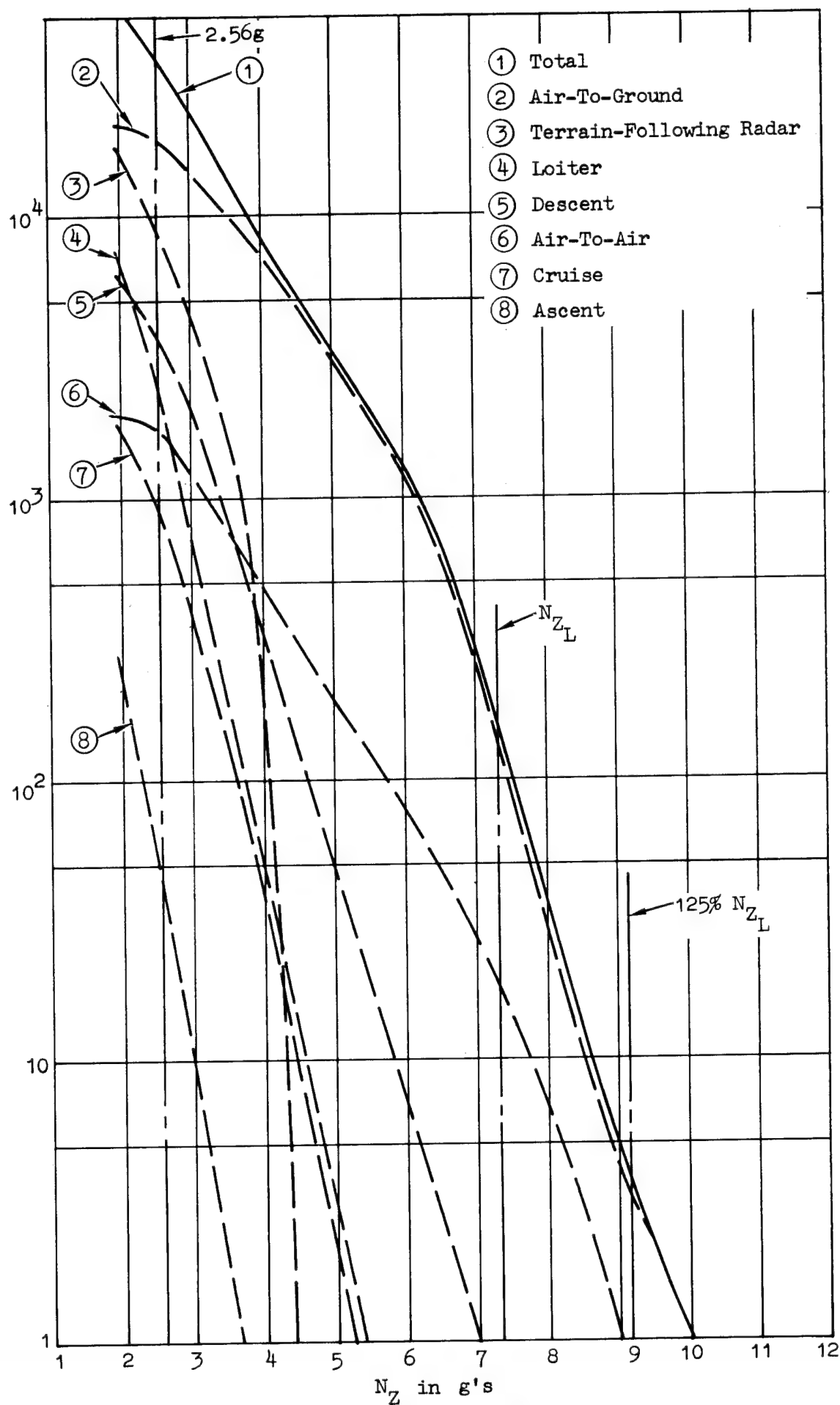


Figure 6 Training Mission

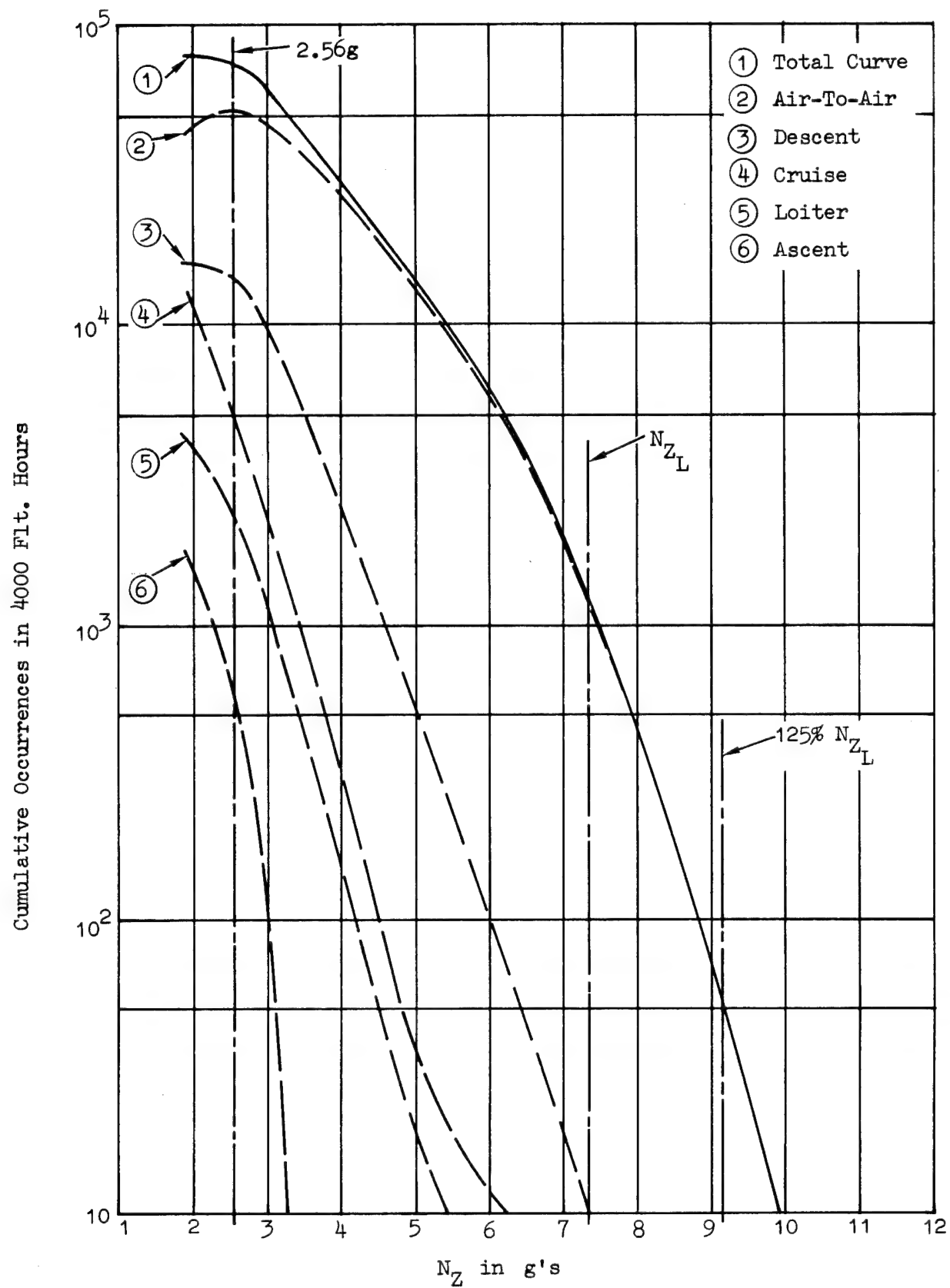


Figure 7 Peacetime Mission

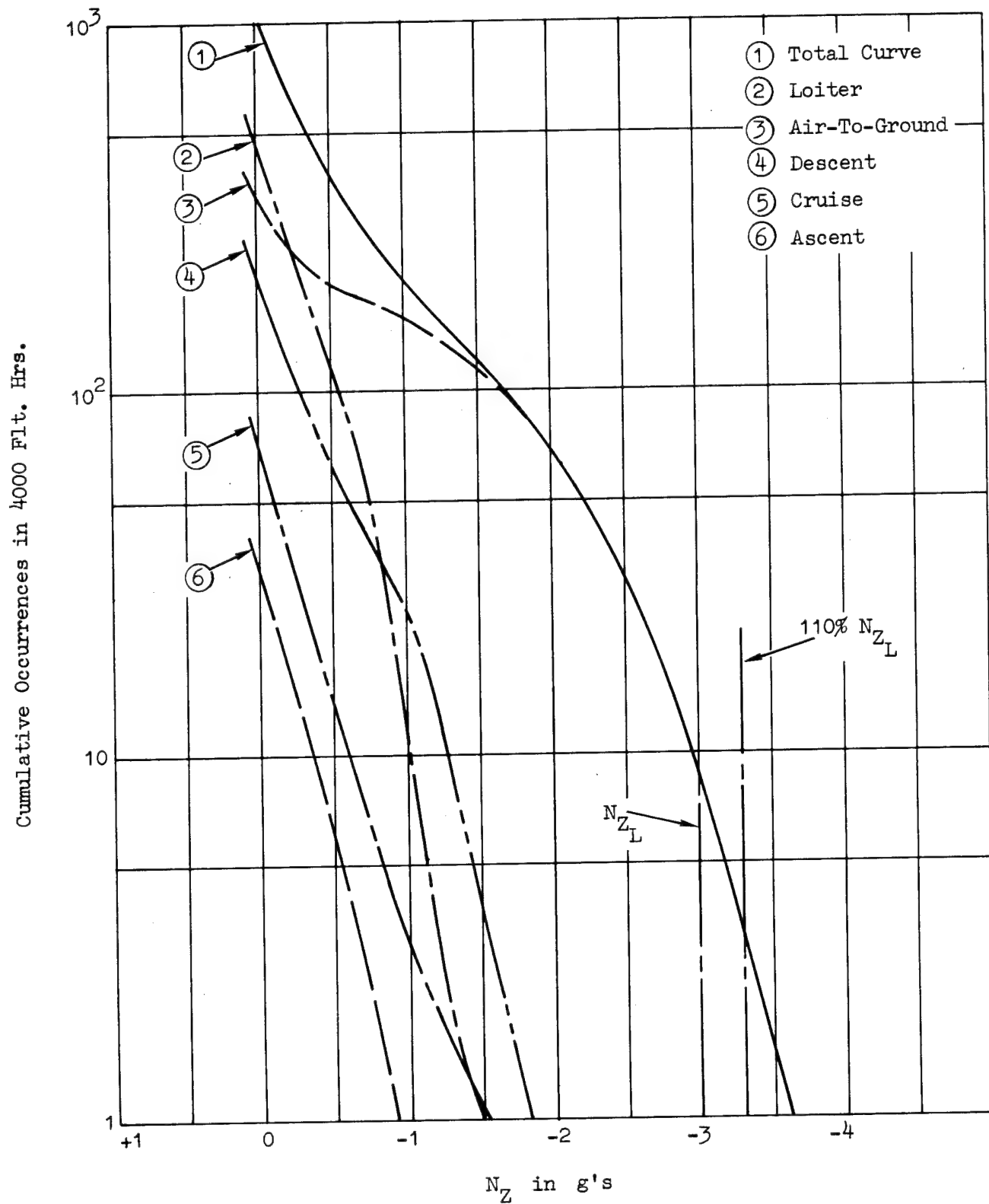


Figure 8 Close Support

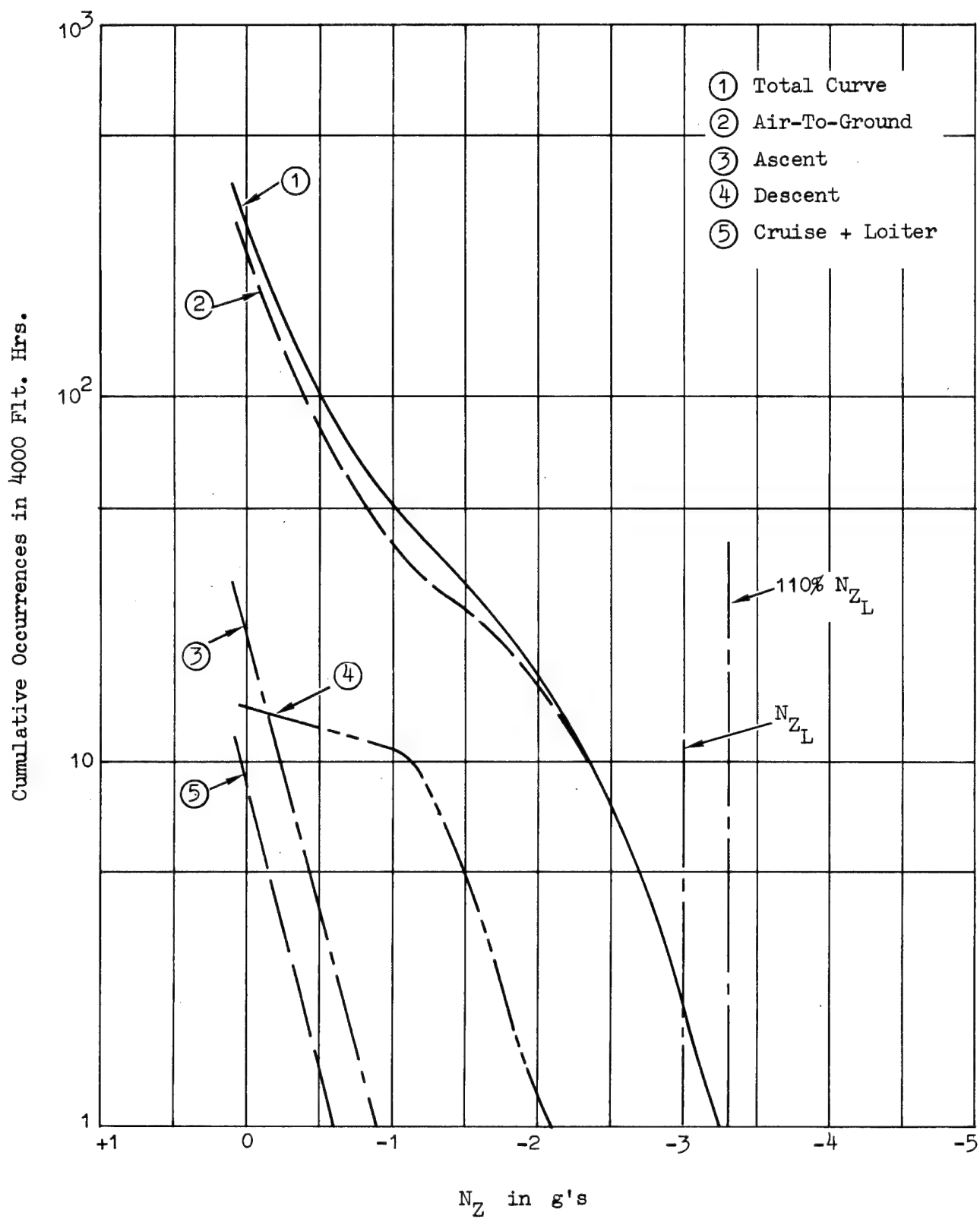


Figure 9 Interdiction

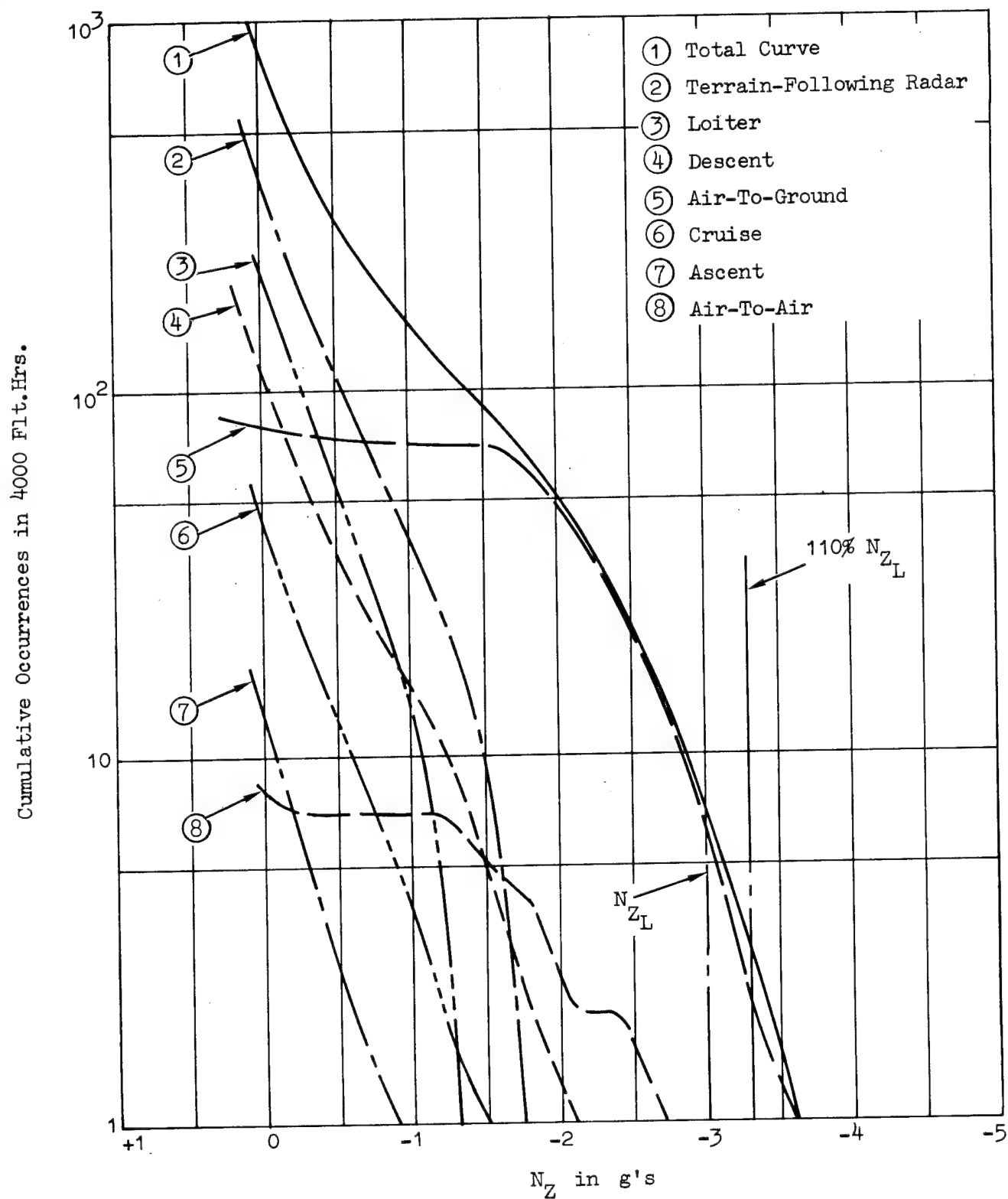


Figure 10 Training

Cumulative Occurrences in 4000 Flt. Hrs.

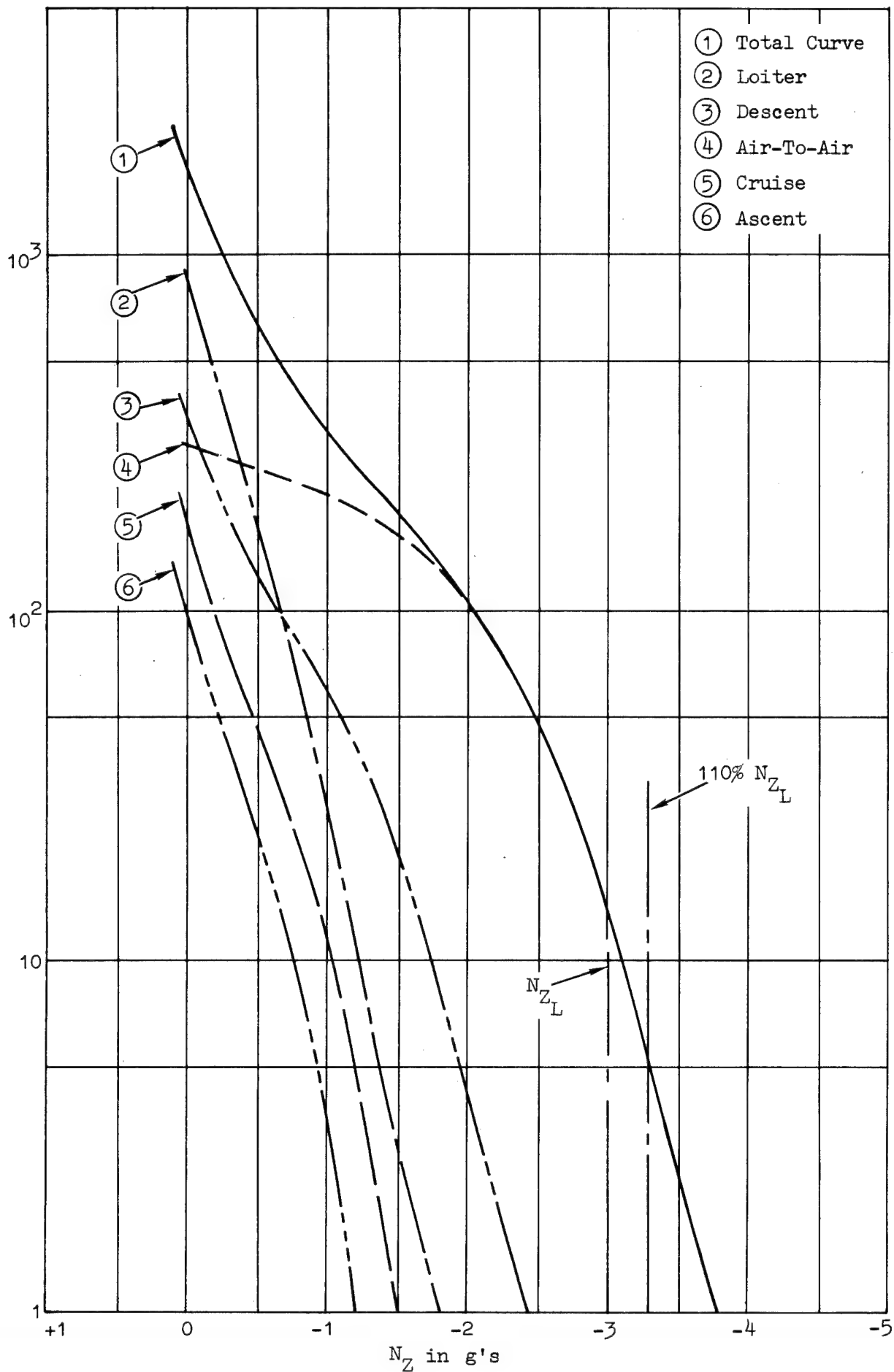


Figure 11 Peacetime

2.4 DATA PRESENTATION AND ANALYSIS

Constant amplitude and spectrum loading (both block and realistic spectrum testing) fatigue tests have been conducted on a wide variety of composite joint specimens to obtain S-N data to develop a better understanding of the fatigue phenomena of built-up composite structures. This program includes bonded and mechanically fastened joints with various parametric studies intended to cover a broad spectrum of possible joint geometric variables. The individual phases of the program are defined in terms of specimen geometry as follows:

- Phase I - Small scale specimens of one-inch width
- Phase II - Medium scale specimens of 2 to 3-inch width
- Phase III - Large scale specimens of ten-inch width

A detailed discussion and evaluation of the fatigue data developed in this program is included in paragraphs 2.4.2 Constant Amplitude Tests and 2.4.3 Spectrum Loading Tests. The test parameters and details of each test specimen configuration are included in 2.4.1. In paragraph 2.4.2 all fatigue data are plotted as stress versus cycles to failure and where sufficient test points exists, the logarithm mean value of N cycles for each test group (at a constant stress value) was calculated and the S-N curve drawn as nearly through these log-mean points as possible.

For those Phase I specimens considered as baseline, to which all other parametric tests are compared, sufficient data has been developed to establish S-N curves. These specimens are identified as Configuration IA111 (bonded joints) and IE111 (mechanically fastened joints), see Tables XII and XV, and S-N curves have been developed for $R = +0.10$ and $R = -1.0$ for each configuration and also $R = +10.0$ for IA111 specimens. In subsequent program tasks for evaluation of the various parameters (ply stacking, edge distance, etc.) data points for that task are plotted and the appropriate "baseline" curve is included on the plot for direct comparison. Also included on each data plot is the range and average of the static test results. These static test data are plotted at the $1/4$ -cycle abscissa location in each case.

In some instances in 2.4.2, the comparison between the baseline data and that developed in other tasks is made on the basis of percent of static allowables. In this report, the term allowables pertains to the average static strength determined from limited tests for the specific configuration. These static test data are not to be considered design allowables since there are not enough data available to statistically determine true design allowables. The comparison as a percent F_{su} or F_{tu} is made for the different sets of data at the same number of cycles and value of R and provides a good evaluation of the fatigue endurance or strength between two or more joint concepts. This can be used then in the parametric or preliminary design evaluation of various joint configurations to evaluate fatigue endurance on the basis of joint static strength.

In order to monitor and preclude specimen heating with repeated application of load, thermocouples were installed on each specimen and the maximum rate of cyclic load application was 1800 cpm. The maximum allowable temperature rise during any test was established at 10°F above ambient, and was maintained throughout the program.

One of the parameters for evaluation, in the Phase I bonded joint program, is fiber orientation and test plans included 0°/±45° as the baseline and 0°/90° for comparative evaluation. Static control tests on single splice butt joint specimens with 8-ply 0°/90° orientation yielded low laminate strengths. Investigation into the cause of the low strength exhibited by these specimens revealed that the low strength was induced by the use of peel plies on the bonding surfaces. Smooth surface specimens tested for comparative purposes developed predicted ultimate strength for the fiber orientation. The thicker (16-ply) 0°/90° specimens also exhibited low tensile strength; however, the strength of these laminates was sufficient to develop required load to evaluate the joint.

The test data developed from this comprehensive fatigue evaluation of bonded and mechanically fastened composite joints are presented in the following sections.

2.4.1 Test Specimen Definition

In this program four basic concepts of aircraft structural joints have been evaluated as discussed in paragraph 2.2. For identification, the bonded joints are designated as Configuration A through D and the mechanically fastened joints as Configurations E and F. Test specimen identification for all program phases is as shown in Tables X through XV. This includes a definition of the type of specimen, test parameters, and number of specimens required to accomplish the objectives of this program. Accompanying drawings for the small scale, Phase I specimen configurations are presented in Figures 12 through 17. The Phase II and III specimens are identical except for width.

2.4.2 Constant Amplitude Tests

To accomplish the overall goals of this program, two types of fatigue tests have been conducted; (1) Constant amplitude tests to develop basic S-N data for composite joints and (2) Spectrum loading tests - block and realistic spectrum testing, simulating fighter aircraft wing maneuver loads. The objectives of the constant amplitude test program are, to develop basic composite joints fatigue data in sufficient quantity for parametric studies, cumulative damage analyses, to aid in developing a better understanding of the basic fatigue phenomena of joints, and to develop design guidelines. The parameters that have been evaluated here for the four basic joint configurations include the following:

- o Adherend combinations
- o Filament orientation
- o Ply stacking
- o Lap-length - bonded joints
- o Strength and stiffness degradation
- o Adhesive systems
- o Low cycle fatigue
- o Preload
- o Rate of load application
- o Edge distance - mechanically fastened joints

- o Pinned joints
- o Fastener Torque
- o Joint Reinforcement
- o Width of specimen
- o Stress ratio, R

Baseline S-N data have been developed for both bonded and mechanically fastened joints at three stress range ratios, $R = +0.10$, -1.0 , and $+10$. Using these data, constant life diagrams have been constructed (Figures 18 and 19) and utilized as the basis for the cumulative damage analyses discussed in 2.4.3. These data also form the basis for evaluating the various parametric studies listed above. In addition to the bonded joint fatigue tests, both static and fatigue tests on the EPON EA 9601 adhesive have been conducted. Test results are presented on the Materials Verification and Checkout Data Forms and an S-N curve is shown in Figure 20. These test data show the ultimate shear strength to be high and a good fatigue life was obtained for the range of stress levels used.

The following sections present the test data for each of the four basic joint concepts included on this program. These four concepts are identified as bonded joint Configurations A through D and Configurations E and F for the mechanically fastened joints. For reference, Tables XVI and XVII list the phase task, specimen drawing number, and figure number for all the constant amplitude S-N data.

TABLE X

ALTERNATE ADHEREND MATERIALS EVALUATION
GRAPHITE EPOXY AND GLASS EPOXY COMPOSITES

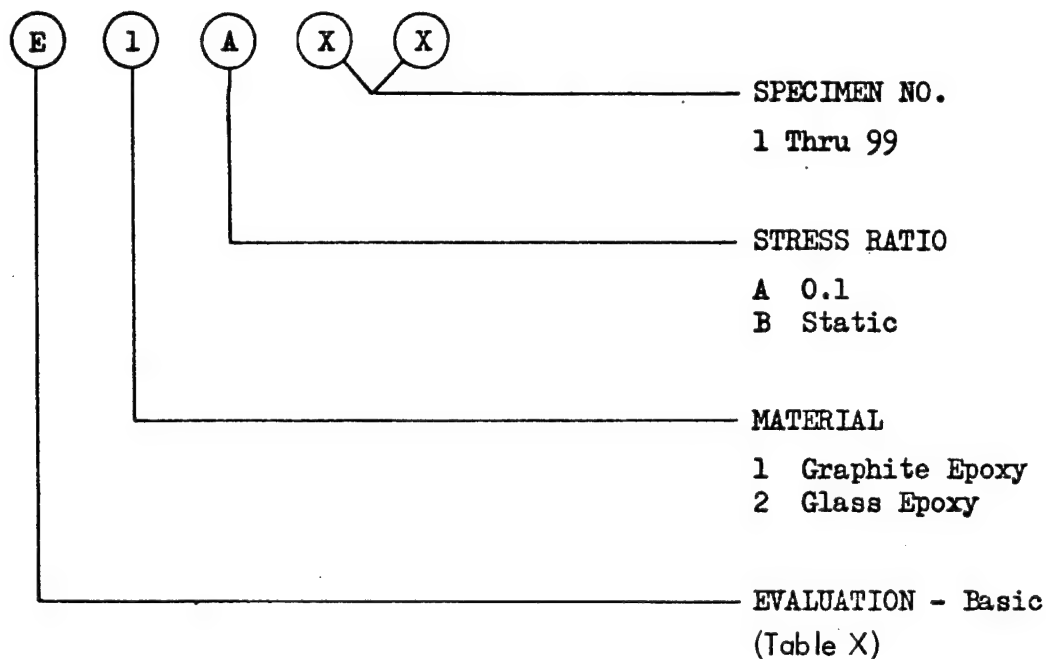
COMPOSITE MATERIAL	JOINT CONFIGURATION	FATIGUE TESTS AT R = 0.1	STATIC CONTROLS
Graphite Epoxy	"A"	10	3
Glass Epoxy	"A"	11	3
TOTALS		21	6

TABLE XI

MATERIAL VERIFICATION AND CHECKOUT TESTS

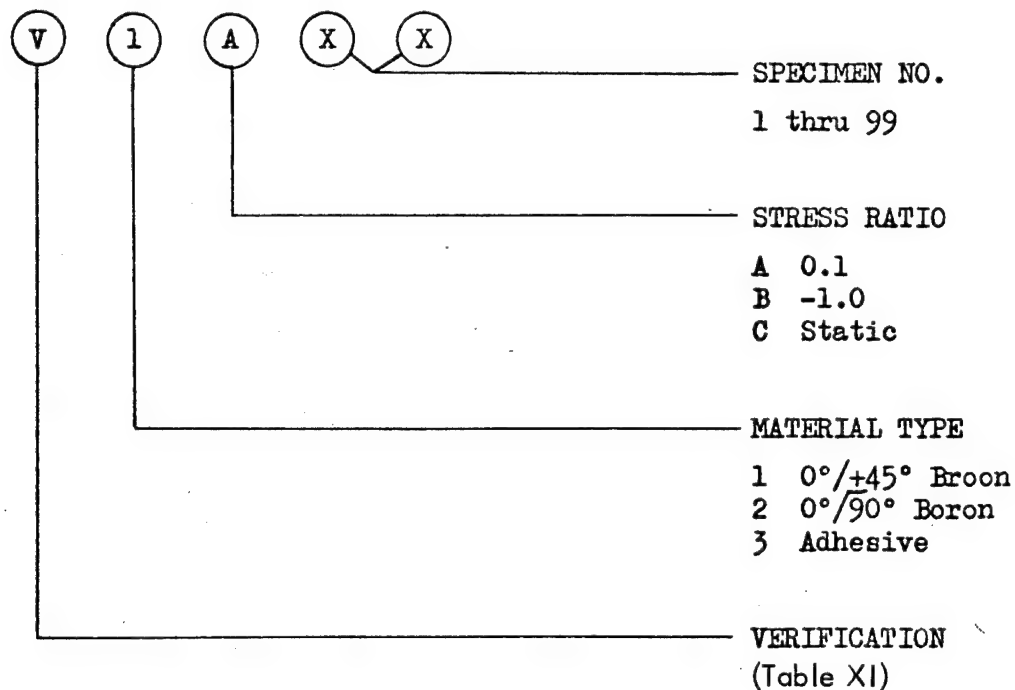
MATERIAL		FATIGUE TESTS		STATIC CONTROLS TENSILE STRENGTH
TYPE	SPECIMEN	R = 0.1	R = -1.0	
0°/±45° N 5505	Coupon	5	10	3
0°/90° N 5505	Coupon	5		3
Program Adhesives	Single Lap Joint	15		5
TOTALS		25	10	11

SPECIMEN IDENTIFICATION
EVALUATION - ALTERNATE ADHEREND MATERIALS



Specimen ElB01 identifies the number one static test specimen for basic evaluation of graphite epoxy.

SPECIMEN IDENTIFICATION
VERIFICATION OF MATERIALS



Specimen V1B04 identifies the number 4 fatigue specimen to be tested at a stress ratio of $R = -1.0$ for verification of material strength for a 0°/+45° boron laminate.

TABLE XII

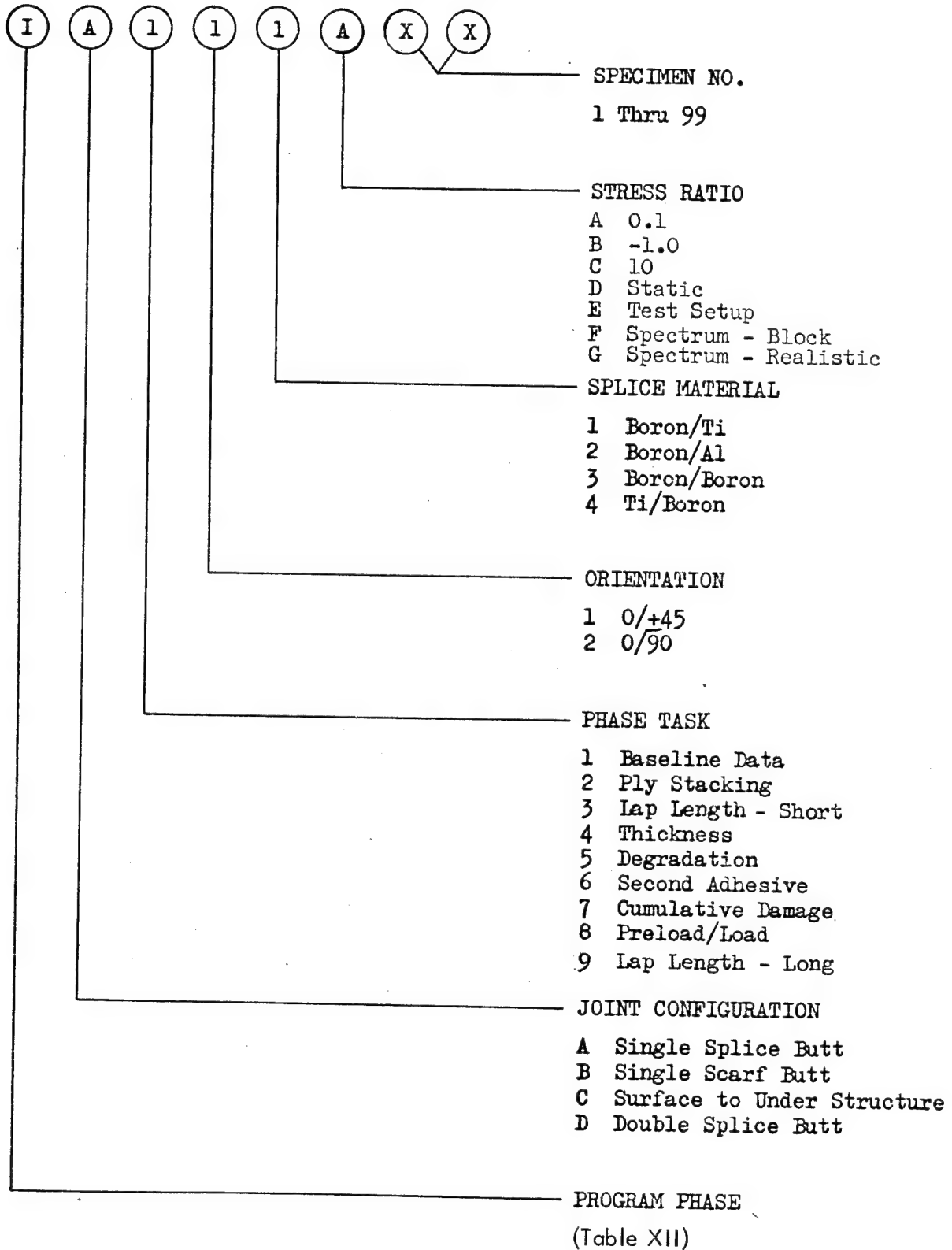
BONDED JOINTS EVALUATION

PHASE I - SMALL SCALE SPECIMENS

JOINT CONFIGURATION	"A"				"B"				"C"		"D"		TOTALS		
	Boron/Ti		Boron/Boron	Boron/Al	Boron/Ti		Boron/Al	Boron/Ti	Boron/Ti	Ti/Boron					
LOADING STRESS RATIO	0.1	-1.0	+10	(ST)	0.1	(ST)	0.1	(ST)	0.1	(ST)	0.1	(ST)	0.1	(ST)	
PROGRAM TASKS	NUMBER OF SPECIMENS														
BASELINE DATA	22	22	26	(14)	14	(4)	10	(3)	10	10	8	(3)	10	(3)	
	10			(6)	10	(3)									
	10				7	(3)	5	(3)	10	10					
	12		10	(9)											
LAP LENGTH EFFECTS	10														
	10			(3)											
THICKNESS EFFECTS	10			(3)											
	10			(4)											
DEGRADATION OF JOINT,	19		12	(9)											
	Not Done			(3)	10	(3)									
SECOND ADHESIVE															
CUMULATIVE DAMAGE STUDY															
	10														
	11														
PRELOAD/LOW CYCLE															
0°/±45°, Std	14														
TOTALS	TOTALS													375	109

SPECIMEN IDENTIFICATION

BONDED JOINTS - PHASE I



Specimen number IB121A08 identifies a specimen for Phase I with a single scarf butt configuration for generating base line data on 0°/90° specimen joined to titanium and tested at a stress ratio of R = +0.1. The specimen number within this set is number 8.

TABLE XIII

BONDED JOINTS EVALUATION
PHASE II - MEDIUM SCALE SPECIMENS

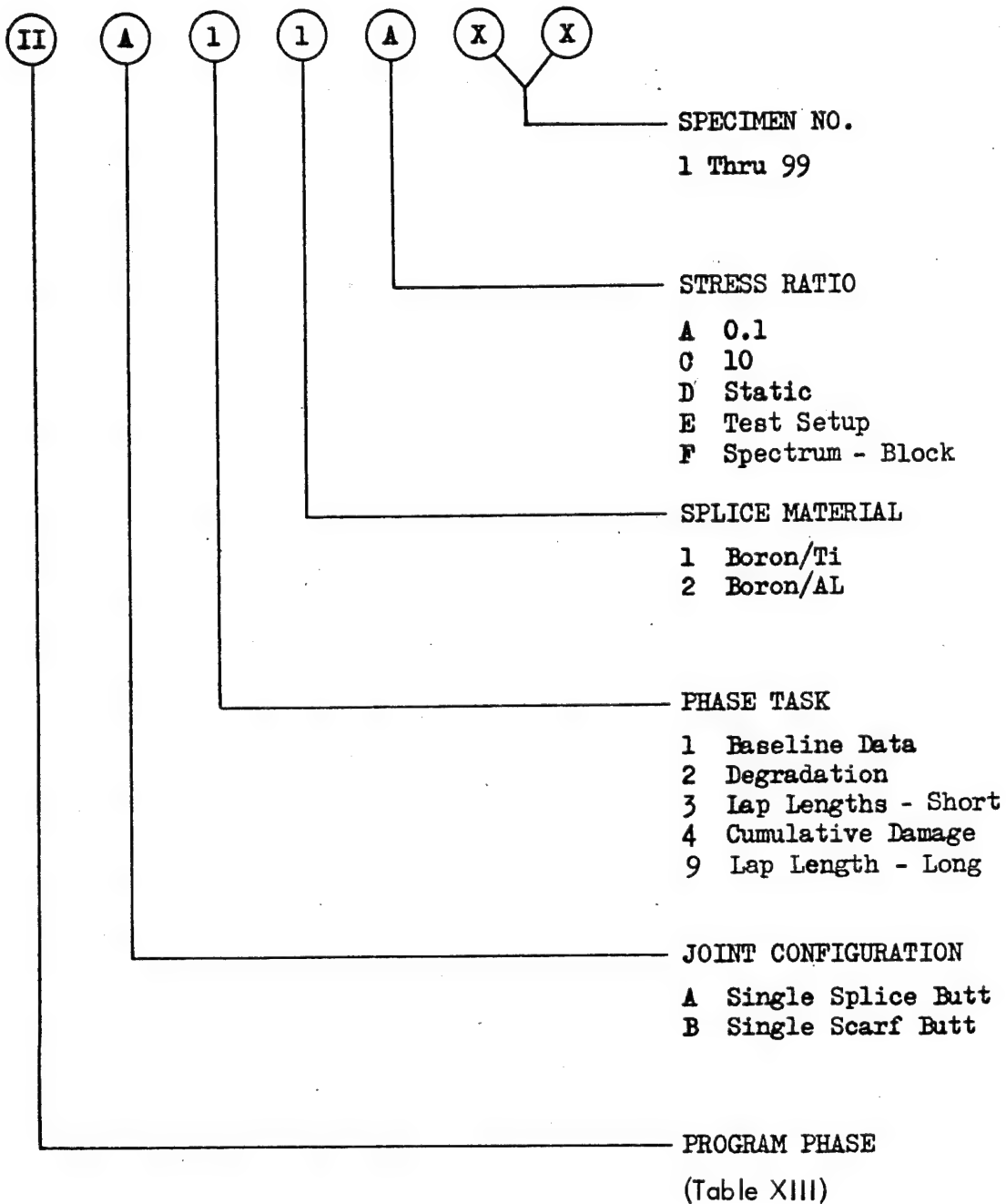
JOINT CONFIGURATION	"A"	"B"	TOTALS
ADHEREND COMBINATIONS	Boron/Ti (Al*)	Boron/Ti	
LOADING STRESS RATIO	0.1 10 (ST)	0.1 10 (ST)	
PROGRAM TASK	NUMBER OF SPECIMENS		FAT. (ST)
BASELINE DATA	15* 5 10**	10* 6 7**	36 (17)
DEGRADATION OF JOINT PROPERTIES	10*		10
LAP LENGTH EFFECTS 1. Short Lap 2. Long Lap	5 5 (6)	5 (3)	5 (3) 10 (6)
CUMULATIVE DAMAGE EVALUATION FOR BLOCK SPECTRUM LOADING	[5]		5
TOTALS			66 26

* Five (5) specimens from each of the indicated groups are to have boron composite - aluminum adherends.

** Three (3) specimens aluminum.

SPECIMEN IDENTIFICATION

BONDED JOINTS - PHASE II



Specimen number IIA32C02 identifies a specimen for Phase II with a single splice butt configuration for evaluation of overlap length with aluminum splice adherend tested as a stress ratio of $R = +10$. The specimen number within this set is number 2.

TABLE XIV

BONDED JOINTS EVALUATION
PHASE III - LARGE SCALE SPECIMENS

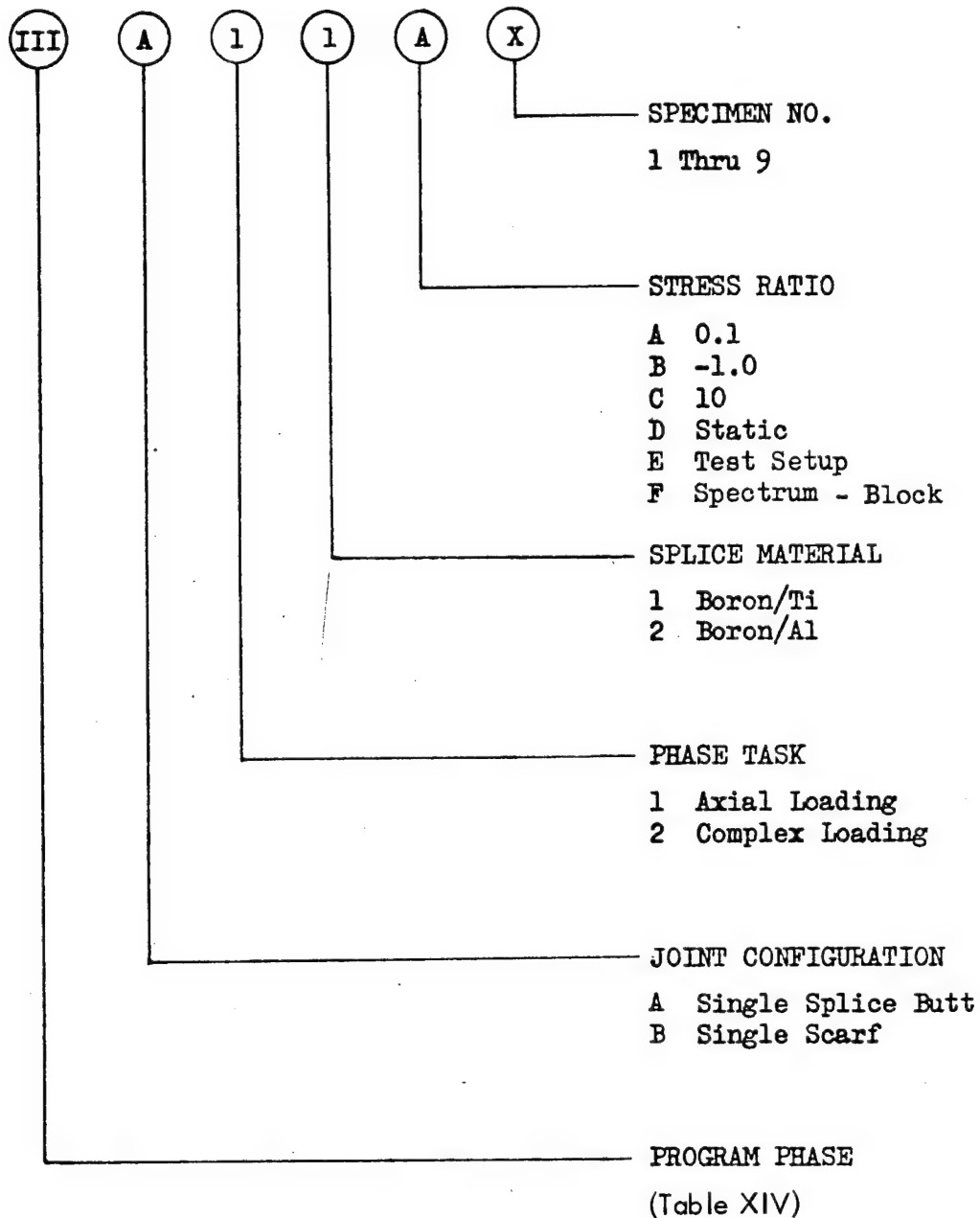
JOINT TYPE	"A"				"B"			TOTALS	
ADHERENDS	Boron/Ti (Al*)				Boron/Ti				
STRESS RATIO	0.1	-1.0	10	(ST)	0.1	-1.0	(ST)	FAT.	(ST.)
PROGRAM TASK	NUMBER OF SPECIMENS								
AXIAL LOADING FOR LARGE JOINTS	2*	2*	1	(2*) 8**	1	1	(3**)	7	13
COMPLEX LOAD EVALUATION FOR BLOCK SPECTRUM CYCLING	[1]				[1]			2	
	TOTALS							9	13

* One (1) specimen of each group indicated is to have boron composite
- aluminum adherends.

** 1" wide static specimens.

SPECIMEN IDENTIFICATION

BONDED JOINTS - PHASE III

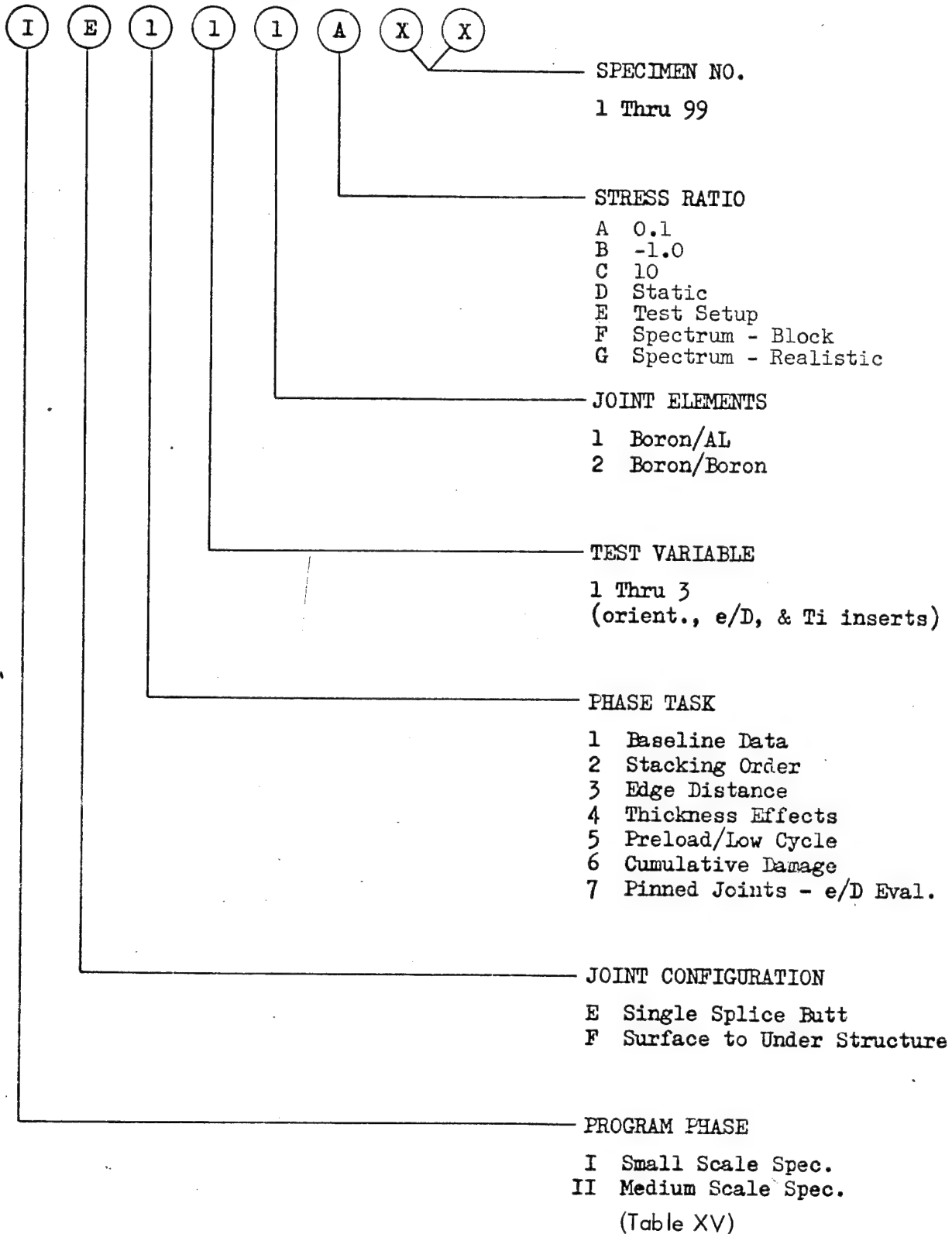


Specimen number IIIA11B2 identifies a specimen for Phase III with a single titanium splice plate butt joint configuration for evaluation of axial loading a stress ratio of $R = -1.0$. The specimen number within this set is number 2.

TABLE XV
MECHANICAL JOINTS EVALUATION
SMALL AND MEDIUM SCALE SPECIMENS

PROGRAM SECTION	PHASE I - SMALL SPECIMEN					PHASE II - MEDIUM SPECIMEN		TOTALS				
	"E"		"F"		"E"							
	Boron/Ti		Boron/Al		Boron/Ti							
LOADING STRESS RATIO	0.1	-1.0	10	(ST)	0.1	(ST)	0.1	10	(ST)	FAT	(ST.)	
NUMBER OF SPECIMENS												
BASELINE DATA 1. 0°/±45°, Ti Inserts 2. 0°, Ti Inserts	17	10	3	(5)	5 10	(3) (3)	11	(3)	10	(6)	56 10	17 (3)
	5	5		(3)							10	3
STACKING ORDER - 0°/±45°, ±45° Buildup	5			(3)							5	(3)
	6			(3)							6	(3)
EDGE DISTANCE 1. 0°/±45°, Ti Inserts 2. 0°/±45°, ±45° Buildup	5			(3)			5	(3)			10	(6)
	5			(3)							5	(3)
THICKNESS EFFECTS 1. 0°/±45°, Ti Inserts 2. 0°/±45°, ±45° Buildup	10										10	
PRELOAD/LOW CYCLE 0°/±45°, Ti Inserts	5								5		10	
	7										12	
CUMULATIVE DAMAGE 0°/±45°, Ti Inserts 1. Realistic Spectrum 2. Block Spectrum	5								5		10	
									5			
PINNED JOINTS/EDGE DISTANCE EVALUATION 1. (e/D) ₁ , Ti Inserts 2. (e/D) ₂ , Ti Inserts 3. (e/D) ₁ , ±45° Buildup	5			(3)							5	(3)
	5			(3)							5	(3)
	5			(3)							5	(3)
Sub Totals											149	47

SPECIMEN IDENTIFICATION
MECHANICAL JOINTS - PHASE I & II



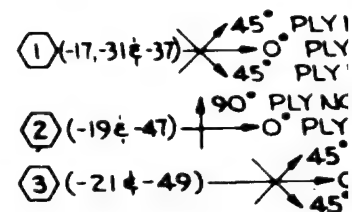
Specimen number IE311A03 identifies a specimen for Phase I with a single butt configuration for evaluation of fastener edge distance in a composite containing titanium skins joined to an aluminum splice plate. The specimen will be tested at a stress ratio of $R = +0.1$ and is specimen number 3 within the set of specimens.

TABLE XVI INDEX OF BONDED JOINT FATIGUE DATA

Specimen Code	Phase Task	Adherend Combinations	Drawing Number	S-N Curve Figure No.
IA111A	Baseline Data	Boron: Ti: Boron	7226-1302IA-1A	21
IA111B	Baseline Data	Boron: Ti: Boron	7226-1302IA-1A	22
IA111C	Baseline Data	Boron: Ti: Boron	7226-1302IA-1A	23
IA112A	Baseline Data	Boron: Al: Boron	7226-1302IA-1C	25
IA113A	Baseline Data	Boron: Boron: Boron	7226-1302IA-1B	24
IA211A	Ply-Stacking	Boron: Ti: Boron	7226-1302IA-5A	32
IA213A	Ply-Stacking	Boron: Boron: Boron	7226-1302IA-5B	33
IA311A	Short Lap Length	Boron: Ti: Boron	7226-1302IA-9A	35
IA312A	Short Lap Length	Boron: Al: Boron	7226-1302IA-9B	36
IA313A	Short Lap Length	Boron: Boron: Boron	7226-1302IA-9C	37
IA411A	Thickness Effects	Boron: Ti: Boron	7226-1302IA-13A	41
IA613A	Second Adhesive	Boron: Boron: Boron	7226-1302IA-1BX	42
IA811A	Preload/Low Cycle	Boron: Ti: Boron	7226-1302IA-1A	43
IA911A	Long Lap Length	Boron: Ti: Boron	7226-1302IA-11A	39
IA911C	Long Lap Length	Boron: Ti: Boron	7226-1302IA-11A	40
IB111A	Baseline Data	Boron: Titanium	7226-1302IB-1A	26
IB111C	Baseline Data	Boron: Titanium	7226-1302IB-1A	27
IB112A	Baseline Data	Boron: Aluminum	7226-1302IB-1B	28
IB121A	Baseline Data	Boron: Titanium	7226-1302IB-3A	29
IB211A	Ply Stacking	Boron: Titanium	7226-1302IB-5A	34
IB311A	Short Lap Length	Boron: Titanium	7226-1302IB-9A	38
IC111A	Baseline Data	Boron: Titanium	7226-1302IC-1A	46
ID111A	Baseline Data	Boron: Titanium	7226-1302ID-1A	30
ID114A	Baseline Data	Titanium: Boron	7226-1302ID-1B	31
IIA11A	Baseline Data	Boron: Ti: Boron	7226-1302IA-1A	47
IIA11C	Baseline Data	Boron: Ti: Boron	7226-1302IA-1A	48
IIA12A	Baseline Data	Boron: Al: Boron	7226-1302IA-1C	51
IIA91A	Long Lap Length	Boron: Ti: Boron	7226-1302IA-11A	53
IIA91C	Long Lap Length	Boron: Ti: Boron	7226-1302IA-11A	54
IIB11A	Baseline Data	Boron: Titanium	7226-1302IB-1A	49
IIB11C	Baseline Data	Boron: Titanium	7226-1302IB-1A	50
IIB12A	Baseline Data	Boron: Aluminum	7226-1302IB-1B	52
IIB31A	Short Lap Length	Boron: Titanium	7226-1302IB-9A	55
E1A	Baseline Data	Graphite: Ti: Graphite	7226-1302IB-1A	44
E2A	Baseline Data	S Glass: Ti: S Glass	7226-1302IB-1A	45
-	Adhesive Evaluation	Titanium	-	20

TABLE XVII INDEX OF MECHANICAL JOINT FATIGUE DATA

Specimen Code	Phase Task	Joint Elements	Drawing Number	S-N Curve Figure No.
IE111A	Baseline Data	Boron: Titanium	7226-1302IE-1A	56
IE111B	Baseline Data	Boron: Titanium	7226-1302IE-1A	57
IE112A	Baseline Data	Boron: Boron	7226-1302IE-1B	58
IE122A	Baseline Data	Boron: Boron	7226-1302IE-3B	59
IE211A	Stacking Order	Boron: Titanium	7226-1302IE-5A	60
IE211B	Stacking Order	Boron: Titanium	7226-1302IE-5A	61
IE311A	Edge Distance Effects	Boron: Titanium	7226-1302IE-7A	62
IE321A	Edge Distance Effects	Boron: Titanium	7226-1302IE-9A	63
IE411A	Thickness Effects	Boron: Titanium	7226-1302IE-11A	64
IE421A	Thickness Effects	Boron: Titanium	7226-1302IE-13A	64
IE511A	Preload/Low Cycle	Boron: Titanium	7226-1302IE-1A	65
IE711A	Pinned Joints	Boron: Titanium	7226-1302IE-15A	66
IE721A	Pinned Joints	Boron: Titanium	7226-1302IE-17A	66
IE731A	Pinned Joints	Boron: Titanium	7226-1302IE-19A	66
IE111A	Baseline Data	Boron: Titanium	7226-1302IE-1A	69
IF113A	Baseline Data	Boron: Aluminum	7226-1302IF-1A	67
IF413A	Thickness Effects	Boron: Aluminum	7226-1302IF-3A	68



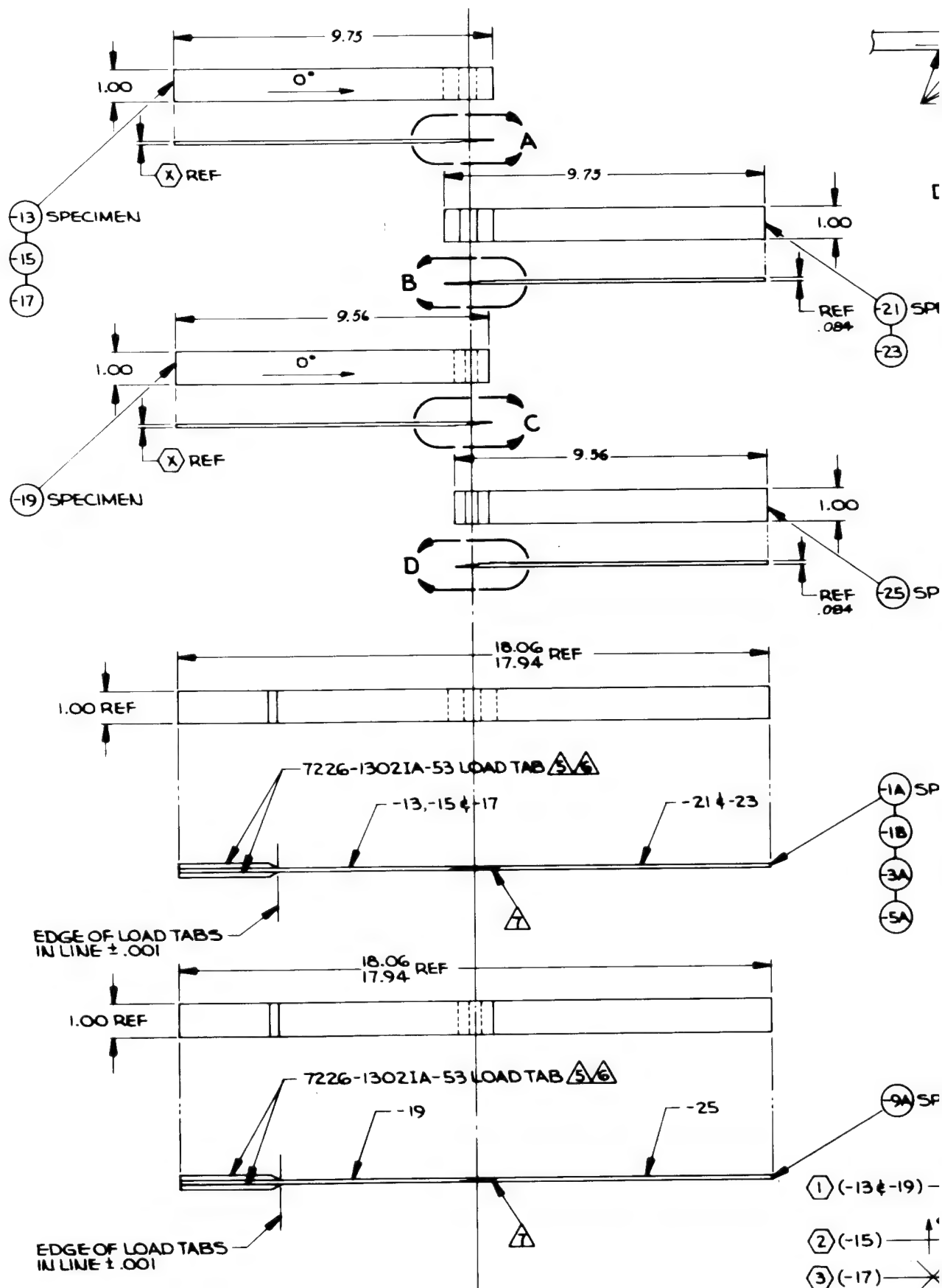
PART NO.	29	31	33	35	37	39
L	1.520			1.020		

- ⚠ FAB PER STP 60-202**
NOTE:

(4) (-23 & -51) ———— $\begin{array}{l} \uparrow 90^\circ \text{ PLY NO. 1, 3, 6 \& 8} \\ \rightarrow 0^\circ \text{ PLY NO. 2, 4, 5 \& 7} \end{array}$
 (5) (-25) ———— $\begin{array}{l} \nearrow 45^\circ \text{ PLY NO. 2, 7, 10 \& 15} \\ \rightarrow 0^\circ \text{ PLY NO. 1, 4, 5, 8, 9, 12, 13 \& 16} \\ \searrow 45^\circ \text{ PLY NO. 3, 6, 11 \& 14} \end{array}$
 (6) (-27) ———— $\begin{array}{l} \uparrow 90^\circ \text{ PLY NO. 2, 4, 6, 8, 9, 11, 13 \& 15} \\ \rightarrow 0^\circ \text{ PLY NO. 1, 3, 5, 7, 10, 12, 14 \& 16} \end{array}$

QTY

UNLESS OTHERWISE SPECIFIED DIMENSIONS ARE IN INCHES.			CONTRACT NO. F33615-70-C-1302		LOCKHEED-GEORGIA COMPANY A DIVISION OF LOCKHEED AIRCRAFT CORPORATION MARIETTA, GEORGIA	
TOLERANCES ON:			DFTMM TENDLER		5/4/70	
FRAC- TIONS	DECIMALS		CHK		BONDED JOINT EVALUATION, PHASE I, CONFIGURATION 'A' SMALL SCALE SPECIMENS	
	.X	.XX	MATL			
± 1/16	± .1	STRESS				
± .03	± .010	SUPV				
± .2°		PROJ				
REFERENCE					SIZE	CODE IDENT
ABBEVIATIONS - DIMS						NUMBER
FATIGUE TEST						DWG NO.
STATIC TEST						7226-1302IA
VAL ENGR			Figure 12		98997	
WT					SCALE NONE	53





- NOTE :**

QTY

LIST OF MATERIAL

TOLERANCES ON:

VAL	ENGR
WCT	

Figure

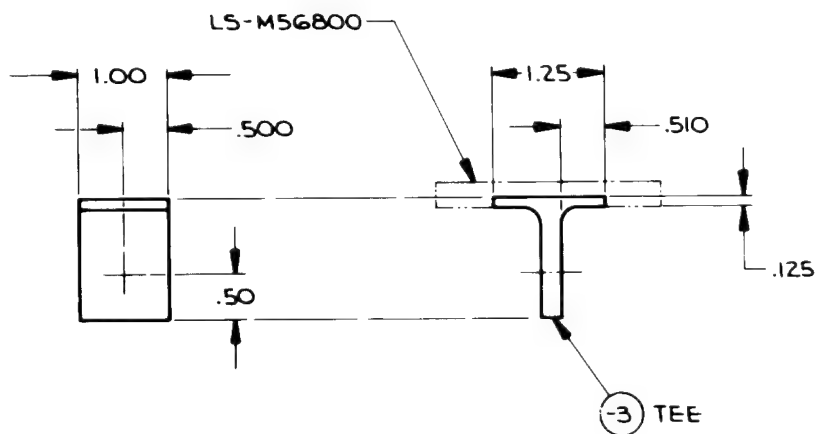
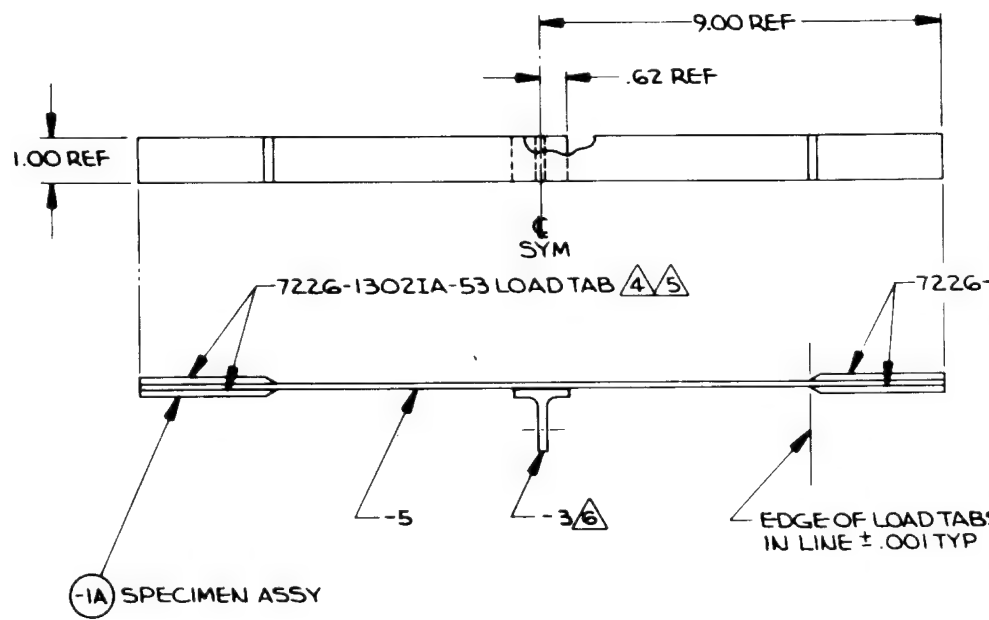
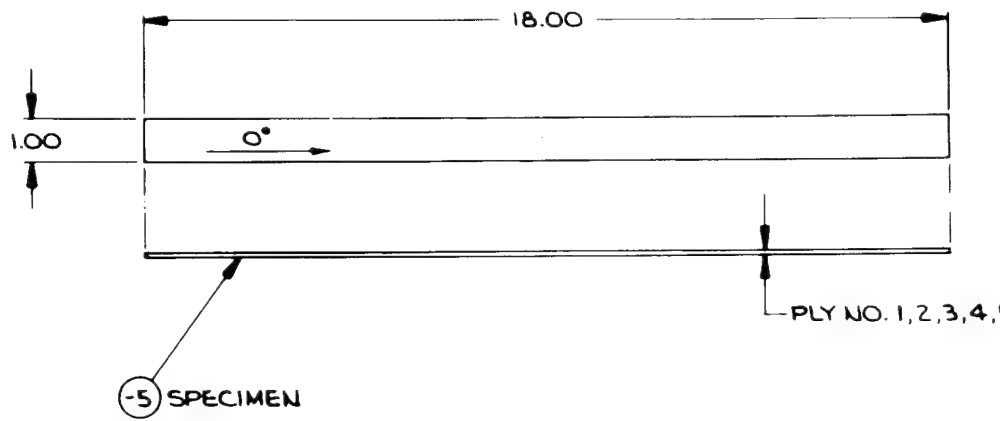
3

1	2	3	4	5	6	7	8	9	10	11	12	13	14	15	16	17	18	19	20	21	22	23	24	25	26	27	28	29	30	31	32	33	34	35	36	37	38	39	40	41	42	43	44	45	46	47	48	49	50	51	52	53	54	55	56	57	58	59	60	61	62	63	64	65	66	67	68	69	70	71	72	73	74	75	76	77	78	79	80	81	82	83	84	85	86	87	88	89	90	91	92	93	94	95	96	97	98	99	100
---	---	---	---	---	---	---	---	---	----	----	----	----	----	----	----	----	----	----	----	----	----	----	----	----	----	----	----	----	----	----	----	----	----	----	----	----	----	----	----	----	----	----	----	----	----	----	----	----	----	----	----	----	----	----	----	----	----	----	----	----	----	----	----	----	----	----	----	----	----	----	----	----	----	----	----	----	----	----	----	----	----	----	----	----	----	----	----	----	----	----	----	----	----	----	----	----	----	----	-----

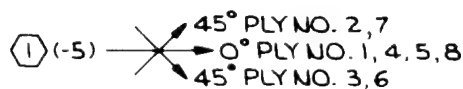
SCALE 1-100	DATE 1-10-1962
-------------	----------------

REAL HOME




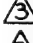

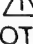
55



2,3,4,5,6,7,8 REF





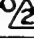



-7226-1302IA-53 LOAD TAB  

-  BOND USING STM 30-102 TYPE III .060 PSF - BOND LINE TOLERANCE $\pm .0015$
-  OUTER SURFACES SHALL BE FLAT AND PARALLEL WITHIN .002
-  BOND USING STM 30-102 TYPE III .045 PSF
-  NARMCO 5505 BORON FILAMENT
-  MACHINE PER DS 30003 125/ ALL MACHINED SURFACES
-  FAB PER STP 60-202

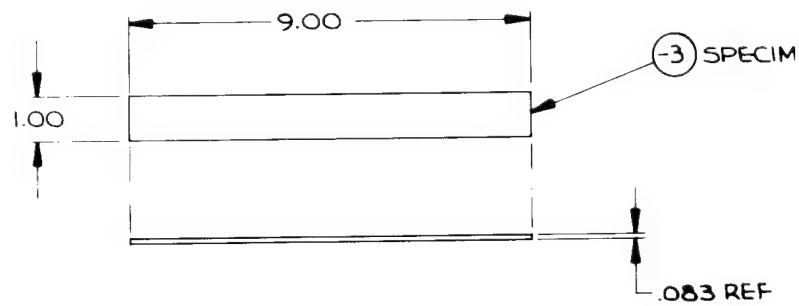
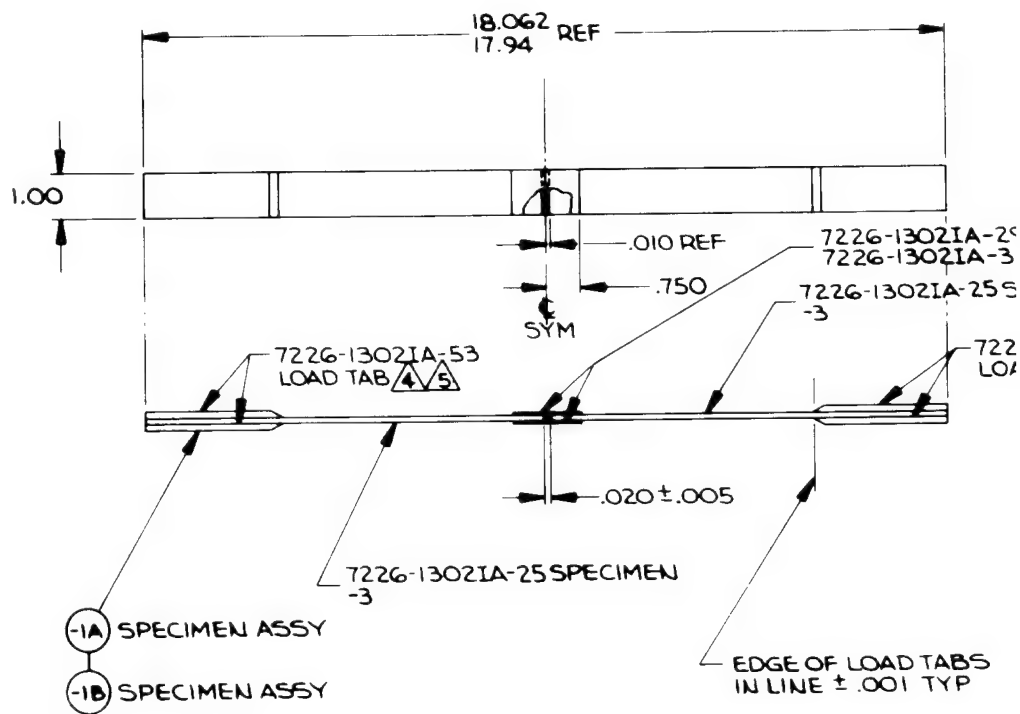
NOTE:

AD TABS
DITYP

4	7226-1302IA-53	LOAD TAB			
1	-5	SPECIMEN	 	 X1 X18	
1	-3	TEE	LS-M56800 (ALTER) 	1	STM 04-302
	-1A	SPECIMEN ASSY			
-1A	PART OR IDENTIFYING NO.	NOMENCLATURE OR DESCRIPTION	MATERIAL OR NOTE	MATL SIZE	MATL SPEC

QTY LIST OF MATERIAL			CONTRACT NO. F33615-70-C-1302		CODE		LOCKHEED-GEORGIA COMPANY A DIVISION OF LOCKHEED AIRCRAFT CORPORATION MARIETTA, GEORGIA	
UNLESS OTHERWISE SPECIFIED DIMENSIONS ARE IN INCHES.			DFTMM TENDLER		CHK <i>W. Ch...</i>		DATE <i>11/1/70</i>	
TOLERANCES ON:			MATT		STRESS		SAMP	
FRAC.	DECIMALS	ANGLES	PROJ <i>A. C. F...</i>		SIZE		CODE IDENT NUMBER	
± 1/16 ± .1 ± .03 ± .010 ± .2°	X XX XXX				DWG NO. 7226-1302IC		98897	
REFERENCE					SCALE NONE		SHEET 1 OF 1	
ABBREVIATIONS - D55025			Figure 14					
FATIGUE TEST								
STATIC TEST								
VAL ENGR								
WT								

2



21A-29 SPLICE $\triangle 6$
 21A-31 SPLICE $\triangle 6$
 A-25 SPECIMEN

7226-13021A-53
 LOAD TAB $\triangle 4 \triangle 5$

- $\triangle 6$ BOND USING STM 30-102 TYPE III .060 PSF - BOND LINE TOLERANCE $\pm .0015$
 - $\triangle 5$ OUTER SURFACES SHALL BE FLAT AND PARALLEL WITHIN .002
 - $\triangle 4$ BOND USING STM 30-102 TYPE III .045 PSF
 - $\triangle 3$ FAB PER STP 51-304
 - $\triangle 2$ CLOSE TOLERANCE PER DS 30009
 - $\triangle 1$ FAB PER STP 60-202
- NOTE:



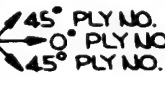
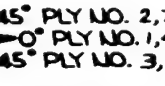
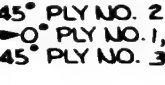
ABS
 YP

PECIMEN

4	4	7226-13021A-53	LOAD TAB			
2		7226-13021A-31	SPLICE			
	2	7226-13021A-29	SPLICE			
	2	7226-13021A-25	SPECIMEN			
2		-3	SPECIMEN	TI-6AL-4V ANNEALED $\triangle 2 \triangle 3$.083 X 1 X 9	STM07-306
-	-	-1A -1B	SPECIMEN ASSY	$\triangle 1$		
-1B -1A		PART OR IDENTIFYING NO.	NOMENCLATURE OR DESCRIPTION	MATERIAL OR NOTE	MATL SIZE	MATL SPEC

REF

QTY LIST OF MATERIAL			CONTRACT NO. F35615-70-C-1302		CODE 4/14/70
UNLESS OTHERWISE SPECIFIED DIMENSIONS ARE IN INCHES.			BFTMM TENDLER		
TOLERANCES ON:			CHK <i>R. H. Gordon</i>		4/14/70
PRAC.	DECIMALS	ANGLES	MATL		
THICKS	.X .XX .XXX		STRESS		
$\pm 1/16$	$\pm .1$	$\pm .001$	SUPV		
REFERENCE			PROJ <i>U.S. Table</i>		4/14/70
ABBREVIATIONS - 003825			Figure 15		
FATIGUE TEST			SIZE CODE RIGHT		
STATIC TEST			NUMBER		
VAL ENGR			98897		
WT			7226-13021D		
			SCALE NONE		
			SHEET 1 OF 1		

- ①(-21-41)  45° PLY NO. 2 & 7
0° PLY NO. 1, 4, 5 & 8
45° PLY NO. 3 & 6
- ②(-23-43)  0° PLY NO. 1 THRU 8
- ③(-25)  45° PLY NO. 2 & 7
0° PLY NO. 1, 4, 5 & 8
45° PLY NO. 3 & 6
- ④(-27)  45° PLY NO. 2, 7, 10 & 15
0° PLY NO. 1, 4, 5, 8, 9, 12, 13 & 16
45° PLY NO. 3, 6, 11 & 14
- ⑤(-29)  45° PLY NO. 2, 7, 10 & 15
0° PLY NO. 1, 4, 5, 8, 9, 12, 13 & 16
45° PLY NO. 3, 6, 11 & 14

△ HL 19 PB6 PIN & HL87-6 COLLAR

△ HL 18 PB6 PIN & HL87-6 COLLAR

△ TI-8AL-1V-1M DA STM07-306 FAB PER STP 51-304

△ TORQUE TO 30^{±1.5} IN. LBS.

△ FOR PIN BEARING TEST USE STSAF009DOGLN (HI-LOK) OR EQUIVALENT MANUFACTURED PIN HAVING .1895 DIA SHANK .1860

9. WET INSTALL FASTENERS PER STP 56-105

△ OUTER SURFACES SHALL BE FLAT AND PARALLEL WITHIN .002

△ BOND USING STM 30-102 TYPE III .045 PSF

△ NORMCO 5505 BORON FILAMENT

5. INSTALL FASTENERS PER DS 5055

△ FAB PER DS 30004

3. YBD = STSAE01SD + STSAE007

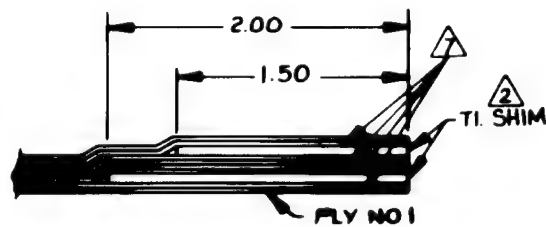
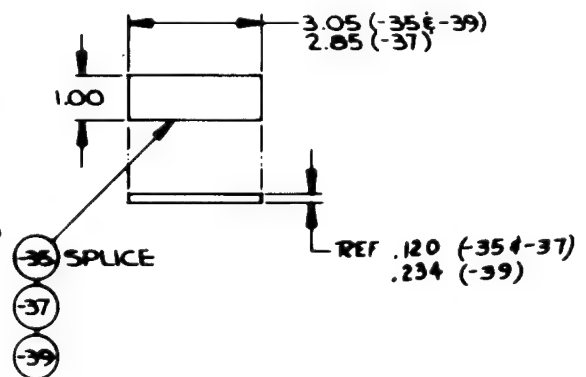
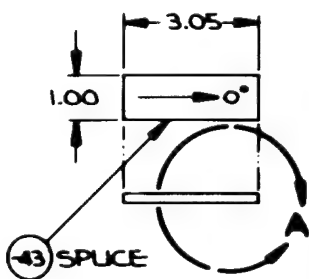
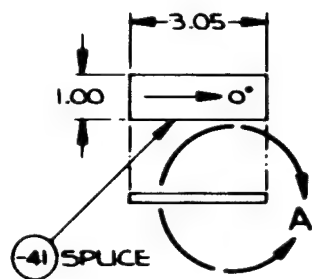
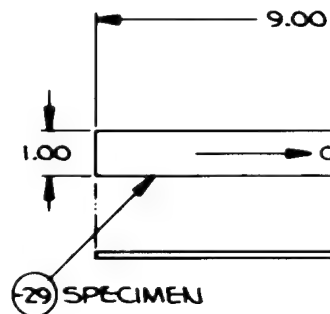
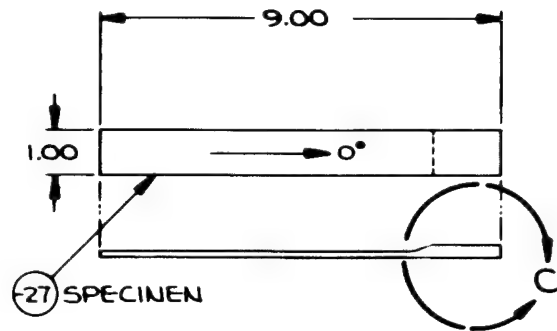
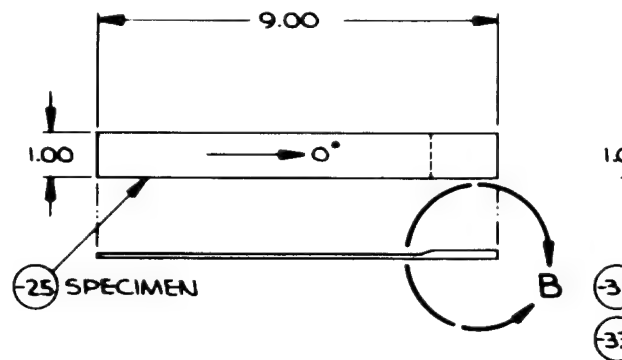
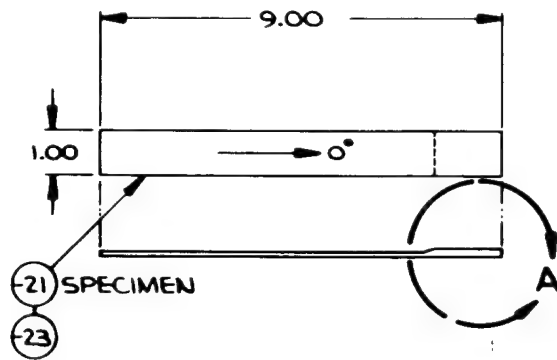
△ SHIMS - .012 TI-6AL-4V ANNEALED STM07-306 FAB PER STP 51-304

△ FAB PER STP 60-202

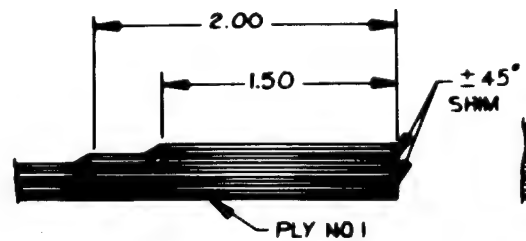
NOTE:

51

2



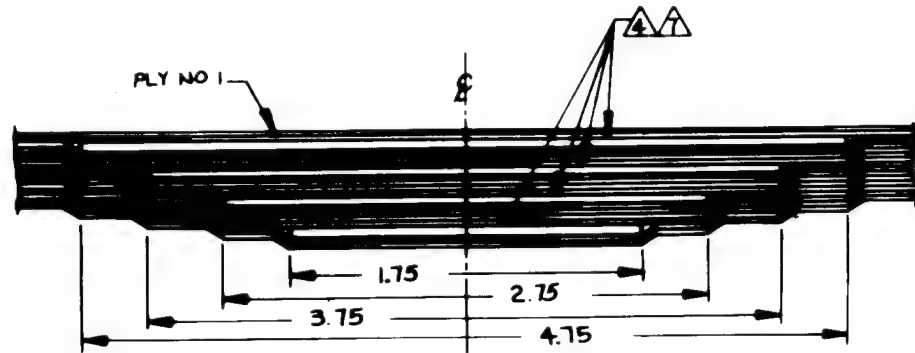
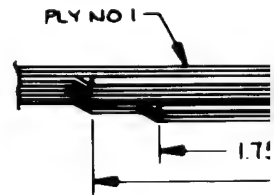
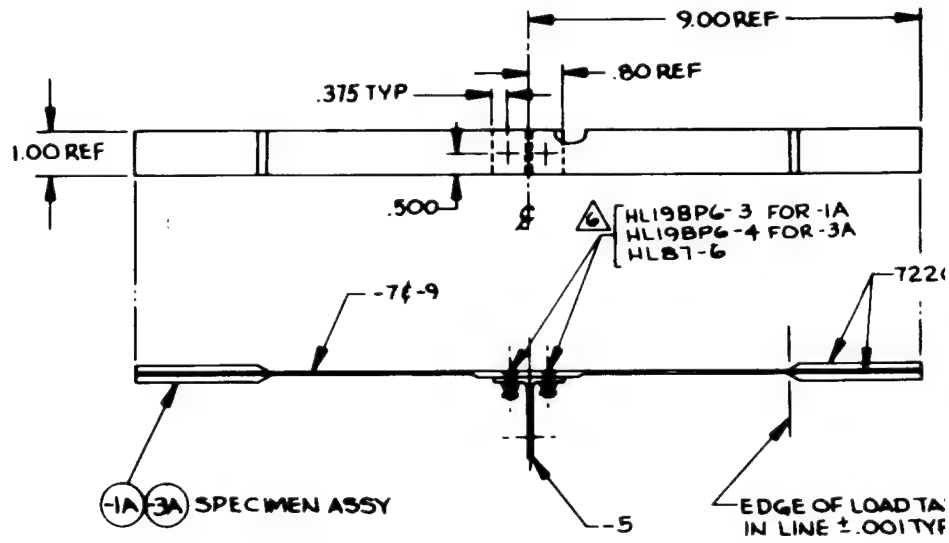
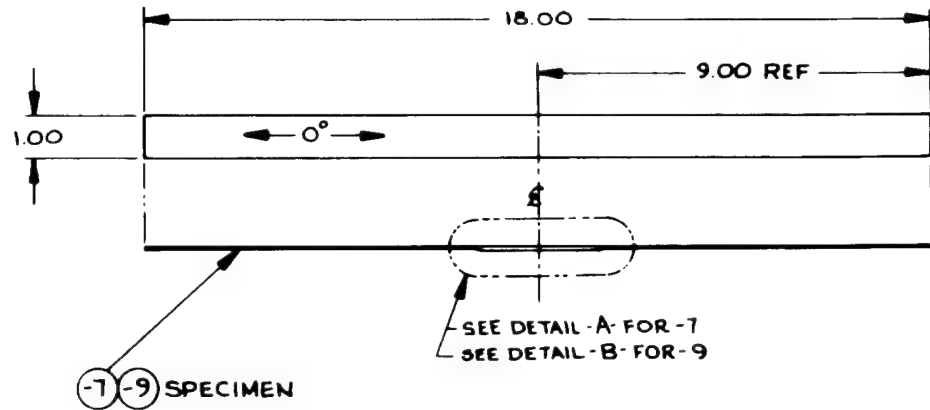
DETAIL A (FOR -21; 23; 41 & -43)



DETAIL B FOR -25



DE
DE

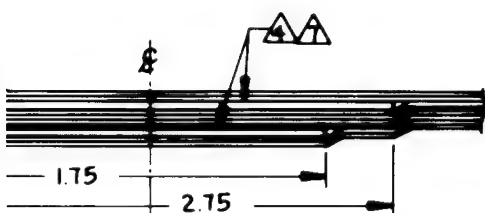


DETAIL-B- FOR -9



4 5









LOAD TABS
OO/TYP



DETAIL-A- FOR-7

- ② FOR-9
- 45° PLY NO 2, 7, 10 & 15
0° PLY NO 1, 4, 5, 8, 9, 12, 13 & 16
45° PLY NO 3, 6, 11 & 14
- ① FOR-7
- 45° PLY NO 2 & 7
0° PLY NO 1, 4, 5 & 8
45° PLY NO 3 & 6
8. INSTALL FASTENERS PER DS 5055 (NET INSTALL PER STP 56-107)
- ① SHIMS - .012 TI-6AL-4V ANNEALED STM07-306
FAB PER STP 51-304
- ⑥ TORQUE TO 30 ± 1.5 IN LBS.
- ③ OUTER SURFACES SHALL BE FLAT AND PARALLEL WITHIN .002
- ④ BOND USING STM 30-102 TYPE III .045 PSF
- ③ NARMCO 5505 BORON FILAMENT
- ② MACHINE PER DS 30003 125/ ALL MACHINED SURFACES
- ① FAB PER STP 60-202

NOTE :-

2	2	HL87-6	COLLAR			
2		HL19BP6-4	PIN			
	2	HL19BP6-3	PIN			
4	4	7226-13021A-53	LOAD TAB			
1		-9	SPECIMEN			
	1	-7	SPECIMEN			
1	1	-5	TEE	LS-M30057	100	7075 AL ALLOY
-		-3A	SPECIMEN ASSY			
	-	-1A	SPECIMEN ASSY			
-3A	-1A	PART OR IDENTIFYING NO.	NOMENCLATURE OR DESCRIPTION	MATERIAL OR NOTE	MATL SIZE	MATL SPEC

UNLESS OTHERWISE SPECIFIED DIMENSIONS ARE IN INCHES.			CONTRACT NO. F33615-70-C-1302		LOCKHEED-GEORGIA COMPANY A DIVISION OF LOCKHEED AIRCRAFT CORPORATION MARIETTA, GEORGIA	
TOLERANCES ON:			EFTMM COLEMAN		BOLTED JOINT EVALUATION PHASE I, CONFIGURATION 'F' SMALL SCALE SPECIMENS	
FRAC.	DECIMALS	ANGLES	CHK R.C. Felt			
XTIME	.X	.XX	MAYL			
± 1/16	± .001	± .005	STRSS			
REFERENCE			SUPV		SIZE <input type="checkbox"/> CODE IDENT NUMBER 98997 BSWG NO. 7226-1302IF SCALE NONE SHEET <input type="checkbox"/> OF <input type="checkbox"/>	
ABBREVIATIONS - D95825			PROJ O.C. Felt			
FATIGUE TEST			Figure 17			
STATIC TEST						
VAL ENGR						
WT						

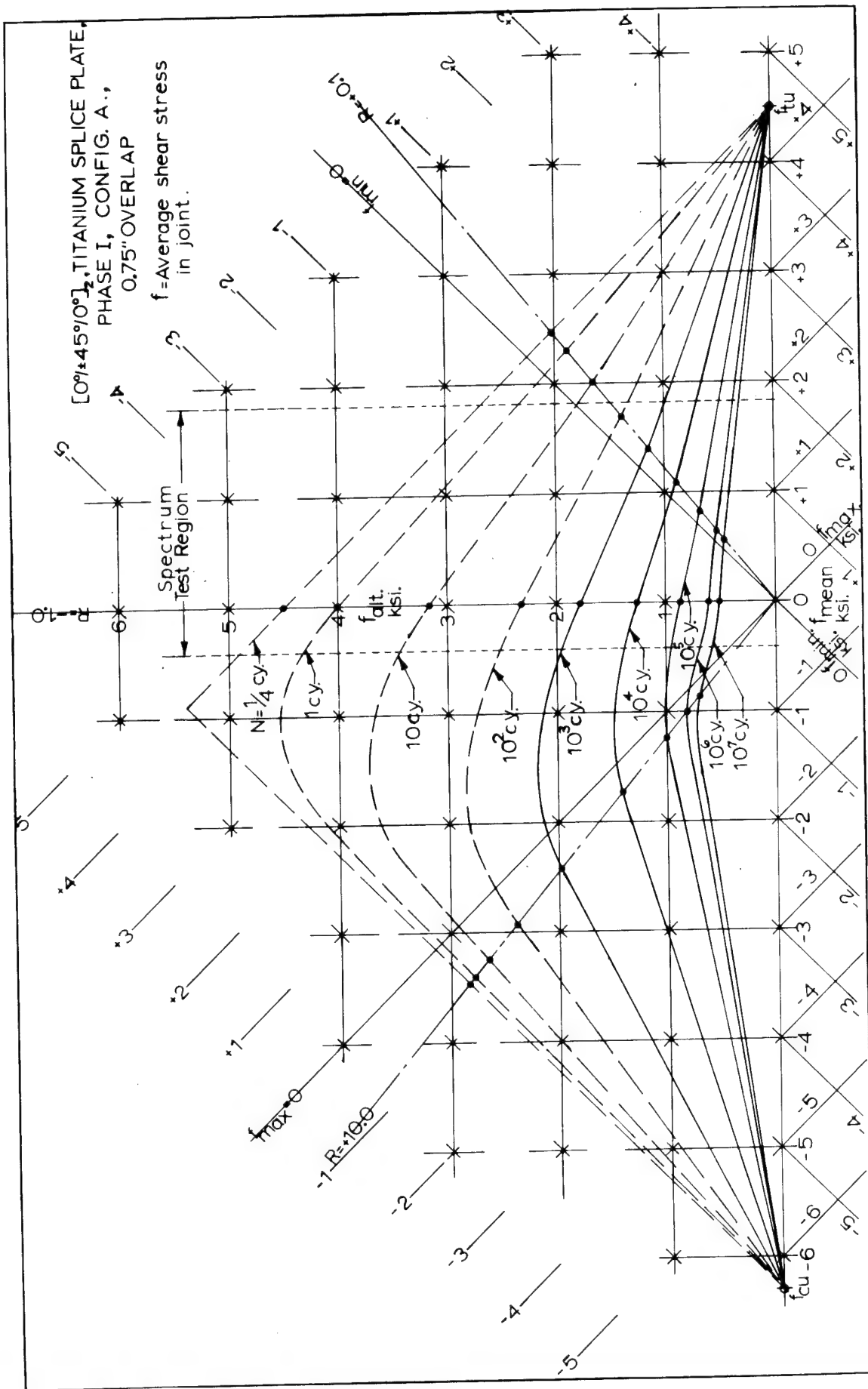
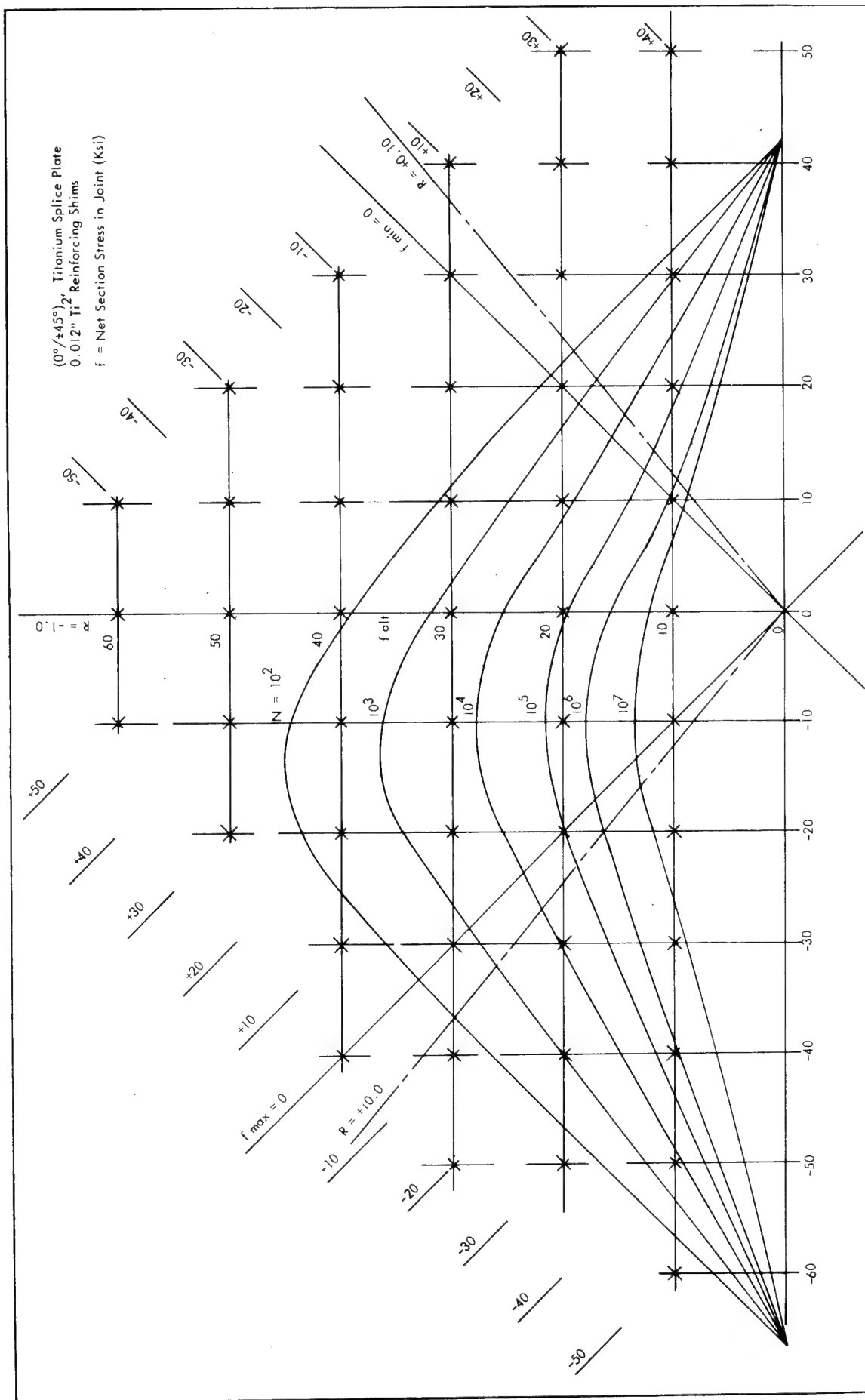


Figure 18. Constant Life Diagram, Phase I, Configuration A Specimens



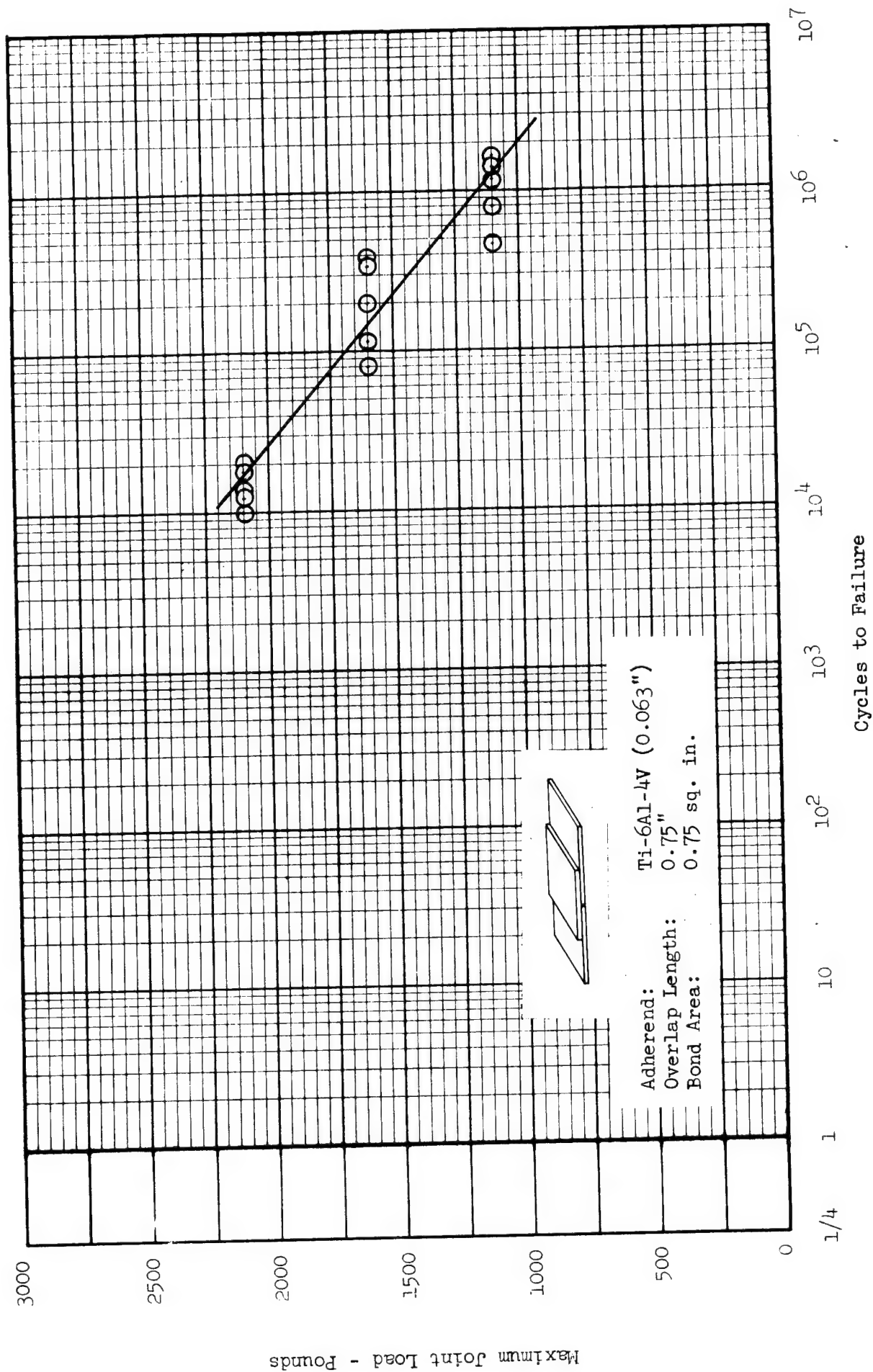


Figure 20 Fatigue Data for Single Butt Joint Adhesive Evaluation - EPON 9601 Configuration A, R = + 0.10

2.4.2.1 Phase I Bonded Joint Analysis

This phase of the overall program, as defined in Table XII, includes tests of 1.0" wide specimens of the four basic joint configurations. Adherend combinations, stacking order, thickness, lap length, etc. are evaluated and compared to the baseline data. Specific details, test data, and analysis for the various program tasks are included in the following sections.

2.4.2.1.1 Baseline Data - Fatigue data have been developed for three adherend combinations (Boron/Ti, Boron/Boron, and Boron/Al) for the four basic joint configurations (A, B, C, and D). To establish a data base, Configuration A with $0^\circ/\pm 45^\circ$ fiber orientation and the Boron/Ti adherend combination has been evaluated in detail and is the standard to which all Phase I bonded joint data is compared. These specimens are identified as IA111A, B, or C, see Table XII. Fatigue curves for these specimens are presented in Figures 21 through 23 and the constant life diagram developed from these data is shown in Figure 18. These S-N curves are presented as average joint shear stress versus cycles to failure. It should be noted that for $R = +10.0$, the value of $F_s \max.$ plotted is the most negative stress or F_{\min} in calculation of R and not F_{\max} . Generally the fatigue data are consistent in that scatter for any given set of data points rarely exceeds one decade.

As a part of the IA baseline testing, three adherend combinations have been evaluated. When compared to the Boron/Ti baseline, the Boron/Boron combination has approximately the same average fatigue life, but somewhat larger scatter, see Figure 24. The Boron/Al combination exhibits a shorter fatigue life than the baseline (Figure 25) due to the increase in peak stress resulting from the residual thermal stress, see Volume I on this report for stress analysis procedures. The Boron/Ti joint appears to have the best fatigue endurance for the single splice bonded butt joint; however, the final choice is dependent on specific design conditions as discussed in detail in 2.5, Fatigue Analysis.

Additional baseline tests were run with Configuration IB, a stepped scarf joint. For comparison with the baseline, tests have been run at $R = +0.10$ and $+10.0$ and include both Boron/Ti and Boron/Al adherend combinations. Figures 26 and 27 show the comparison between IA and IB at the two stress ratios considered. The IB data appear to show a somewhat shorter fatigue life; however, comparison between the two joints is good when based on the fatigue strength as a percentage of the static allowables. The S-N data for IB with the Boron/Al adherend combination, Figure 28, developed longer lives than anticipated as all specimens failed in the aluminum which is not unrealistic since the boron and aluminum are the same thickness. This is not a good illustration of the fatigue strength of the joint, however, but does allow increased confidence in this joint as compared to an all aluminum joint.

Test data for Configuration IB with $0^\circ/90^\circ$ orientation and boron adherends are shown in Figure 29. This fiber orientation results in improved fatigue strength as compared to the $0^\circ/\pm 45^\circ$, IB data. Also, the $0^\circ/90^\circ$ orientation in Configuration IB specimens gives approximately a 10% increase in fatigue strength over the IA baseline data, when compared on the basis of percent of static allowables.

The baseline data for the two variations of Configuration ID are shown in Figures 30 and 31. By comparison of these data with the baseline data for the Configuration A specimens, it can be seen that the static and fatigue strength of these two configurations are approximately equal. This close comparison was anticipated based on the symmetry and similarity of designs and the method of testing. Based on the analysis of this joint configuration, these data may be combined with those developed for the Configuration A specimens to better define the fatigue capability of the single overlap butt joint.

2.4.2.1.2 Ply Stacking - In order to evaluate ply stacking or sequence of fiber orientation, several Configuration IA and IB specimens have been tested with $\pm 45^\circ/0^\circ$ fiber orientation for comparison with the $0^\circ/\pm 45^\circ$ baseline test data. Boron/Ti and Boron/Boron adherend combinations have been evaluated. Comparison with the IA baseline data shows that the $\pm 45^\circ/0^\circ$ stacking has equivalent fatigue strength. Data for this evaluation are presented in Figures 32 through 34.

Data in Reference 7 show the $\pm 45^\circ/0^\circ$ fiber orientation with the Narmco 5505 boron-epoxy to have improved strength compared to the same material with the $0^\circ/\pm 45^\circ$ orientation. The static test results here do not support this trend, as evidenced by comparing the range of static test results for the IA211 specimens and the data from the IA111 configuration. The range of average joint shear stress for the $\pm 45^\circ/0^\circ$ specimens is 5300 to 5500 psi whereas the range for the $0^\circ/\pm 45^\circ$ specimens is 4200 to 6300 psi. The higher static test data for the $0^\circ/\pm 45^\circ$ orientation are from specimens identical to the baseline specimen (average static strength of 4500 psi) which were fabricated for the degradation of joint fatigue evaluation. It is concluded, then, that the two fiber orientations considered here have equivalent fatigue and static strength within the scatter of the data included. This is true for both the Boron/Ti and Boron/Boron adherend combinations considered.

2.4.2.1.3 Lap Length - For the bonded joint designs, the effect of lap length on fatigue endurance is an important parameter to consider. In this program both short and long lap length effects have been evaluated for comparison with the baseline data. Specimen Codes for these tests are IA3 and IB3 for short lap length and IA9 for the long lap length. Three adherend combinations (Boron/Ti, Boron/Boron, and Boron/Al) are considered and all fiber orientation is $0^\circ/\pm 45^\circ$.

The data presented in Figures 35 through 38 show the effect of the short overlap as compared to the standard 0.75" overlap for each of the three IA baseline adherend combinations. The fatigue endurance of the Boron/Ti and Boron/Boron specimens with this short overlap is equivalent to the standard overlap, baseline data; however, the Boron/Al combination shows a reduction in fatigue strength. This is in keeping with the test results for the standard 0.75" overlap with the aluminum adherend where it was concluded that the reduction in fatigue strength is due to increased peak stress in the joint resulting from induced thermal stresses.

The long lap length data (1.0" overlap) are presented in Figures 39 and 40 along with the baseline data for the 0.75" overlap. As noted, the longer overlap results in a reduced fatigue endurance either in a direct comparison or when compared on the basis of percent of the static allowables.

Based on these tests and subsequent Phase II and III data, the shorter lap lengths (0.50"-0.75") appear to approach an optimum design for both the butt splice and the stepped scarf joint. This of course is related to the joint L/t ratio and is further substantiated by test results from other program tasks. Specific conclusions and recommendations are discussed in 2.5, Fatigue Analysis.

2.4.2.1.4 Thickness Effects - To determine what effect varying adherend thickness has on the fatigue endurance of the bonded joints, ten (10) specimens identical to the Boron/Ti baseline (IA111) except for adherend thickness, were fabricated and tested. These specimens are identified as IA411 and have a 16-ply, $0^\circ/\pm 45^\circ$ Boron laminate in lieu of the 8-ply, $0^\circ/\pm 45^\circ$ baseline. Test data are presented in Figure 41. The increased thickness has no degradation on the fatigue endurance of the basic joint concept (the test data are within the scatter of the baseline data) and the results are comparable to that for the short overlap evaluation. This is as expected since the increased thickness with the standard lap length reduces the specimen L/t ratio.

2.4.2.1.5 Degradation of Joints - To evaluate the degradation of the bonded joints with cumulative fatigue cycles, Configuration IA and IB specimens have been tested at specific load levels for a predetermined number of cycles and then subjected to static failing loads. Joint stiffness (the slope of the load-deflection curve taken about the splice, over a two inch gage length) and static failing loads are used to measure any degradation of the joints. Data are presented in Table XVIII for Configuration IA at $R=+0.10$ and $+10.0$ and for Configuration IB at $R=+0.10$. In all instances, the joint stiffness and failing load before fatigue testing is the average of the static test results.

Analysis of the data in Table XVIII does show loss of joint stiffness for some of the IA511A specimens but these reduced values are considered to be within the scatter in the data. Overall, there is no apparent stiffness degradation in the joints evaluated. As expected, the IA511A and C specimens show a loss of strength after application of repeated cycles, with the $R=+0.10$ data showing the greatest loss. The IB stepped scarf joint shows practically no loss of strength compared to the average static test results.

Previous investigators have evaluated the residual strength of boron-epoxy laminates, Reference 8, by cycling test specimens to a prescribed percentage of its lifetime and then statically failing each specimen to evaluate residual strength. The specimens involved include the Narmco 5505 boron-epoxy with $0^\circ/\pm 45^\circ$ fiber orientation. These laminated specimens, $K_f = 1.0$, show the same trend as the joints evaluated in this program as regards residual strength. For a stress ratio of $+0.10$ there is no significant strength degradation, compared to the average static test results, at $N = 3 \times 10^5$ cycles. There is only a 15% reduction at 3×10^6 cycles. For the tension-tension fatigue tests of the bonded lap joints (IA511A), there is approximately a 15% reduction in strength at 2×10^6 cycles, when comparing average strength values. The compressive tests show approximately a 10% reduction in strength after the same number of cycles. The bonded scarf joint results show no decrease at $N = 2 \times 10^5$ cycles which is in keeping with the basic boron-epoxy laminate test results.

Post fatigue test data for several Phase I specimens that did not fail (run-out at approximately 10^7 cycles) during fatigue testing are included in Table XIX. These data further substantiate the trends discussed above.

2.4.2.1.6 Second Adhesive - The primary adhesive system for this program is EPON EA 9601, as discussed in Volume II, Specimen Fabrication; however, a second adhesive has been evaluated as one of the program tasks. This adhesive system is Metlbond 329, and tests were scheduled with Boron/Boron and Boron/Ti adherend combinations. Test data for the Boron/Boron combination with the Metlbond 329 adhesive are presented in Figure 42. Since static tests on Boron/Ti joints with this same adhesive yield low strengths, and the fatigue test data in Figure 42 are low, testing on the remainder of the specimens was suspended. For the IA joints evaluated in this program, the EPON EA 9601 adhesive system is superior to the Metlbond 329.

2.4.2.1.7 Preload/Low Cycle - Basic Boron/Ti adherend combinations with $0^\circ/\pm 45^\circ$ fiber orientation have been tested to evaluate the effect of static preload on the joint fatigue strength and to obtain low cycle S-N data. For the tests to evaluate effect of preload, each specimen was statically loaded to predetermined tension stresses in the

universal testing machines, then removed and reinstalled in the tuning-fork machines for fatigue tests. The static preloads were determined by taking 75 percent, 85 percent, and 90 percent of a predetermined static value representing 100 percent of design ultimate shear stress. This stress was 4000 psi and was determined by deducting one standard deviation from the mean value of all the tensile static ultimate values obtained for the boron/titanium standard joint specimens. The $R = +0.10$ fatigue tests were performed in the tuning-fork machines at a maximum stress level of 1400 psi. Figure 43 shows the preload fatigue data compared with the baseline fatigue data for a stress ratio of $R = +0.10$. It appears that preloads of 3000 psi, 3400 psi, and 3600 psi do not significantly affect the fatigue life of the joints (four of the six specimens fall within the baseline scatter band).

Low cycle fatigue data are also shown in Figure 43. These specimens were tested in an MTS electrohydraulic closed-loop servo controlled system at a cyclic rate of 5 cps. Attempts were made to obtain fatigue lives between 2500 and 5000 cycles, however, this proved difficult and the test data has a scatter band of approximately two decades. These low cycle test data have been included with the baseline data to extrapolate the S-N curves to the 1/4-cycle ultimate strength and as an aid in developing the constant life diagram for the IA configuration.

Additional baseline data tests at a stress ratio of $R = -1.0$ and at a cyclic rate of 1 cycle per second were also conducted to determine the influence of cyclic rate on fatigue life. These yielded the same results as tests conducted at 900 to 1800 cycles per minute, indicating that cyclic rate is not a prime factor if a constant specimen temperature is maintained during testing (no more than 10°F rise above room temperature). The specimens were tested at an average joint shear stress of 1400 psi and the test data exhibit very narrow scatter (2.2×10^3 to 4.4×10^3 cycles) and is coincident with the baseline data at 1400 psi, $R = -1.0$ in Figure 22.

2.4.2.1.8 Alternate Adherend Materials Evaluation - A quantity of graphite/epoxy and glass/epoxy Configuration A, 1-inch wide bonded joint specimens have been tested, Table X. Static tensile tests were conducted in a universal testing machine

and fatigue tests were conducted in Lockheed designed resonant frequency machines. Test methods were similar to those adopted for the Phase I Configuration A boron/epoxy bonded joint specimens and comparable stress levels were selected for the fatigue tests. Two stress levels were used for each material and a stress ratio of $R=+0.1$ was used for all fatigue tests. Five specimens were tested at 1400 psi and the other five were tested at approximately 2000 psi. The test results are presented as S-N curves in Figures 44 and 45. It can be seen that the static and fatigue capabilities of the two joints were quite different. The stiffness of the graphite/epoxy joint was obviously greater than the glass/epoxy joint but the static strength was considerably lower.

Both static and fatigue data for the glass/epoxy joint agrees well with the IA111 baseline specimen data. The graphite/epoxy data is in agreement with the baseline data at higher stress levels when the two are compared on the basis of percent of static strength; however, at higher cycles (10^6), the graphite exhibits higher fatigue strength, again compared as percent F_{su} . Where low load amplitude, high cumulative cycles are the joint design criteria, the trend from this limited data is that the graphite/epoxy joint is the more attractive for fatigue endurance.

2.4.2.1.9 Configuration IC Data - As one part of the Phase I bonded joint analyses, tests have been run on specimens representative of a surface panel to support structure attachment. The test specimen details are as shown in Figure 14. The applied loading for this series of tests was a combined axial load and sideload which induced bending in the basic laminate. Static sideloads were varied from 40 to 70 pounds. Test data are presented in Figure 46 and as noted there is a decrease in fatigue strength with increased sideloads.

2.4.2.2 Phase II Bonded Joint Analysis

In Phase II, the bonded joint specimen geometry is extended from the 1-inch wide Phase I specimen to a 3-inch width. This phase is restricted to the $0^\circ/\pm 45^\circ$ fiber orientation with some of the principal parameters from Phase I held for comparison. The three tasks included here to demonstrate the transition from the one-dimensional to the two-dimensional condition are:

- o Baseline data for direct comparison
- o Lap length effects
- o Degradation of bond strength

The Phase II program is directed primarily at the definition of difficulties which arise in the transition from narrow coupon specimens to those with sufficient width to impose Poisson and transverse thermal effects. The areas of investigation are therefore, in terms of specimen geometry, those for which these effects are most apparent. Table XIII defines the number of specimens, joint configurations, and program tasks for Phase II.

2.4.2.2.1 Baseline Data - The specimens utilized to develop baseline data for Phase II include the single splice butt joint and the stepped scarf joint configurations identical to the Phase I specimens except for the 3.0" width. Both the Boron/Ti and Boron/Al adherend combinations are included and tests have been conducted at stress range ratios of +0.10 and +10.0.

Data for the Boron/Ti, three-inch, single splice butt joint are shown in Figures 47 and 48 for $R = +0.10$ and $+10.0$. Comparing these data with the one-inch baseline test results shows that there is a loss of fatigue strength or endurance with the increased specimen width. Although there are limited test data here, it is theorized that the reduced fatigue strength is attributed to the Poisson effect and transverse, thermally induced residual shear stresses at the specimen edges. With the wider specimen, the transverse strains due to the Poisson effect may result in a plane strain state in the adhesive toward the central region of the specimen. This results in a stress condition, in this region, which approaches a hydrostatic stress state and causes the adhesive to behave locally in a very brittle manner and will not allow plastic deformation. As the adhesive approaches this plane strain state under load, brittle failures occur near the center of the wider specimens after fewer cycles of load application, hence the reduction in fatigue endurance compared to the one-inch baseline specimen. This theory is further substantiated with the ten-inch wide joints where two of the IIIA specimens failed at the center of the specimen, and at the completion of the fatigue test, the joint was still intact at one edge.

Similar fatigue data for the 3.0-inch stepped lap joint (IIB) is shown in Figure 49. These results are somewhat surprising in that the data are equivalent to the IA baseline which reverses the IIA data trend. When compared on the basis of percent of ultimate strength, the IIB data is approximately 20% higher than the baseline. Indications are that the 3-step lap joint results in a softer interface between the adherends (approaching a true scarf) and increases the fatigue endurance. This apparently offsets the Poisson effect that is evident in the IIA results.

Test data for Configuration IIB at $R = +10.0$ are presented in Figure 50. These specimens failed at lower stress levels than the one-inch wide specimens tested at the same stress range ratio, see Figure 23 for comparison. Static allowables for the IIB specimens are approximately 70% of the baseline allowables and this, combined with the Poisson effect and possibly residual thermal stresses, apparently leads to the reduction in fatigue strength.

Baseline data for the IIA and IIB specimens with Boron/Al adherends are presented in Figures 51 and 52. These 3-inch specimen tests resulted in data similar to the one-inch wide Boron/Al adherend data in that the fatigue endurance is somewhat less than the baseline data. This may be attributed to the residual thermal stress inherent with the Boron/Al combinations. It should be noted that all IIB12 failures are in the aluminum adherend which is not a true evaluation of the joint interface but does show that the strength of the adherends can be developed through the bonded joint. This allows a designer to use this joint design in a structural component with the same confidence with which aluminum is used for other applications.

2.4.2.2.2 Lap Length Effects - Both long and short lap length effects have been evaluated for the 3-inch wide specimens for comparison with baseline data. Figures 53 and 54 are long lap data for the single splice butt joint and Figure 55 presents the stepped scarf joint, short lap data. The IIA data trends are the same as those developed with the long lap one-inch specimens, that is, the increased L/t ratio results in a decreased fatigue life.

The IIB, short lap data shows an increased fatigue endurance with the smaller L/t as compared to the baseline data. These results substantiate the trends established with the IIB11A data, Figure 49, which shows the fatigue endurance is improved as the stepped interface approaches a true scarf.

2.4.2.2.3 Degradation of Joints - Degradation of the 3-inch bonded joints (Configurations IIA21 and IIA22) has been evaluated in the same manner as the 1.0" specimens. Typical specimens with Boron/Ti and Boron/Al adherends have been cycled at prescribed loadings for a specific number of cycles (approaching the joint endurance) without failure and then statically loaded to failure to measure joint degradation with the cumulative cycles. The extent of degradation is measured by comparing joint stiffness and failing load after cycling with average data from static tests. The data for these tests are presented in Table XX.

Generally the joint stiffness is not reduced below the average static test results in the cyclic range evaluated here. The residual strength or ultimate load capability after fatigue cycling does show a significant reduction compared to the average static strength for the single splice butt joint with the Boron/Ti adherend combination. The residual strength of these particular 3-inch specimens is approximately 70% of the static strength where the one-inch specimens had about a 15% strength reduction. The specimens evaluated with the Boron/Al joint were cycled for only 5000 cycles and show no loss of strength with cumulative cycles. This trend was discussed in 4.2.1.6 where previous data indicates no loss of strength at lifetimes less than 10^5 cycles.

Two of the 3-inch stepped scarf joint specimens (IIB11A) did not fail during the fatigue tests and were subsequently static loaded to failure. These post fatigue data are tabulated below.

TABLE XXI POST FATIGUE DATA, IIB11A SPECIMENS

<u>Specimen</u>	<u>Avg. Joint Stiffness</u>	<u>F_{s max}</u>	<u>N</u>	<u>Post Fatigue Stiffness</u>	<u>Avg. Static Strength</u>	<u>Residual Strength</u>
IIB11A01	1850	900	9×10^6	1980	17000	16500
IIB11A04	1850	900	9×10^6	2040	17000	17300

2.4.2.3 Phase III Bonded Joint Analysis

In addition to the one- and three-inch wide specimens discussed in 4.2.1 and 4.2.3, selected tests have been run with seven, 10-inch wide specimens. These tests include both Configuration A and B bonded joints, and the Phase III program details as defined in Table XIV. The boron/titanium and boron/aluminum (IIIA) specimens have been tested at stress ratios of $R=+0.1$ and $R=-1.0$. Where possible, the selected stress levels were the same as those used for the equivalent 3-inch wide specimens, but the fatigue lives were found to be generally lower. (See Table XXII.)

Since there were only seven specimens included in this program phase, the test data are tabulated along with applicable Phase I test results, for comparison. All the 10-inch wide single splice butt joint data exhibit substantially lower fatigue lives than comparable one-inch specimens. Again, this is attributed to the plane strain state in the adhesive toward the central region of the specimen which is non-existent in the 1.0" baseline specimens, as discussed in 4.2.2.1. The fatigue failures apparently occur in this brittle, central region of the joint and propagate toward the specimen edges. Two of the IIA specimens failed across the center section and then at one edge but had a narrow band, approximately 2.0" wide along one edge, that did not fail. This tends to substantiate the theory of failures originating at the central area where the adhesive is in a state of plane strain; however, further work is needed to evaluate the fatigue capabilities of the wider specimens.

Another interesting phenomena associated with the failure mode studies of these 10.0" wide specimens is the fracture surface condition at the specimen edges. Past experience has shown that residual transverse shear stresses exist at the specimen edges after assembly and these stresses combined with the axial stresses due to fatigue loading result in a combined stress state at the specimen edge of sufficient magnitude to produce cohesive failure in the adhesive. This is evidenced by a striation type fracture surface at the edges of the IIIA specimens. This combined stress state is apparently not as damaging as the Poisson effect in the center of the joint, however, since all failures appear to originate at the center and propagate outward.

The 10-inch wide Configuration B, $R = -1.0$, specimen was tested at a stress level of ± 800 psi. Since this stress level produced a failure in the 10-inch wide Configuration A specimen after 11,400 cycles, it was believed that the life of the Configuration B specimen would not exceed 10^5 cycles. However, failure had not occurred after 5×10^5 cycles, at which point fatigue testing was discontinued since it was felt that the fatigue capability of the joint had been proven. Testing of the $R = +0.10$ Configuration B, 10-inch wide specimen was temporarily halted due to a failure in the titanium adherend at the end fitting attachment holes. The specimen was repaired by bonding titanium tabs onto the failed end and the test was successfully completed. Failure occurred after 107,510 cycles at a stress level of 1400 psi. These data are included in Table XXII, also.

The IIIB configuration data shows a continuance of the IIB data trend; that is, these wider, stepped scarf joint specimens show improved fatigue endurance as compared to the IA or IB baseline data. This trend is associated with the lap geometry and should be pursued further.

TABLE XVIII DEGRADATION OF BONDED JOINTS, ONE-INCH WIDTH,
STIFFNESS AND ULTIMATE LOADS DATA

Specimen No.	Average Stiffness Static Tests Kips/In	Stiffness After 5x10 ³ Cycles Kips/In	Stiffness After 2x10 ⁶ Cycles Kips/In	Average Static Ult. Load Pounds	Ult Load After Applied Cycles Pounds
IA511A01	344	349		3410	2960
A02			337		2540
A03		272			2120
A04			323		2990
A05		299			2450
A07		320			2490
A14		339			2160
A15	344		351	3410	3210
IA511C01	325		381	-4385	-3600
C02		379			-4220
C03			373		-4260
C04		374			-3540
C05			354		-3580
C06		352			-4220
C07			356		-4280
C10		368			-3400
C11			335		-4280
C12	325	347		-4385	-4440

TABLE XVIII (Cont'd)

Specimen No.	Average Stiffness Static Tests Kips/In	Stiffness After 5×10^3 Cycles Kips/In	Stiffness After 2×10^6 Cycles Kips/In	Average Static Ult. Load Pounds	Ult Load After Applied Cycles Pounds
IB511A01	557	527		5600	5570
A02			570		5500
A03		570			6100
A04			572		5700
A05		570			6070
A06			576		5300
A07		590			5920
A08			610		5740
A09		561			5540
A10	557		563	5600	5820

NOTE: Average joint shear stresses for each of the tabulated cyclic loading conditions are:

Configuration	F_{smax}	N
IA511A	2000 psi	5×10^3
	1100	2×10^6
IA511C	-2700	5×10^3
	-1600	2×10^6
IB511A	1400	5×10^3
	800	2×10^5

TABLE XIX POST FATIGUE DATA, ONE-INCH SPECIMENS,
STIFFNESS AND ULTIMATE LOADS DATA

Specimen No.	Avg. Stiffness Static Tests Kips/In	Cyclic Stress psi	N Cycles	Stiffness After Cyclic Tests Kips/In	Static Ult. Load Pounds	Ult. Load After Cyclic Tests Pounds
IA111A14	331	1100	10^7	286	3440	2640
B03	331	1800	10^7	366	3330	2400
C12	-	-1400	10^7	352	-3150	-3120
C17	-	-1400	10^7	351	-3150	-3620
IA613A02	341	1100	10^7	352	3430	1990
A04	341	1000	5.3×10^6	333	3430	2060
IB311A01	605	500	10^7	634	4460	4920
A02	605	900	4.5×10^6	576	4460	3800

TABLE XX

DEGRADATION OF BONDED JOINTS, THREE-INCH WIDTH
STIFFNESS AND ULTIMATE LOADS DATA

Specimen No.	Average Stiffness Static Tests KIPS/IN	Stiffness After 2.0×10^5 Cycles KIPS/IN	Average Static Ult. Load Pounds	Ult. Load After Cycling Pounds
IIA21A01	992	968	10100	7800
A02		980		6040
IIA11A04		961		9060
A08	992	862	10100	5300

NOTE: $F_{S_{MAX}} = 1100$ psi for these tests

		Stiffness After 5.0×10^3 Cycles		
IIA22A01	914	915	6333	9420
A02		903		5420
A03		976		7540
A04		948		5920
A05	914	943	6333	7860

NOTE: $F_{S_{MAX}} = 1300$ psi for these tests

TABLE XXII
CONFIGURATION IIIA AND IIIB TEST DATA

<u>Spec. No.</u>	<u>Ave Static Fsu PSI</u>	<u>F_{MAX} PSI</u>	<u>Cyclic Rate CPM</u>	<u>Fatigue Life Cycles</u>	<u>Baseline Data</u> ⁽¹⁾	
					<u>Spec. No.</u>	<u>N Cycles</u>
IIIA11A1	4930	1100	300	1.96×10^5	IA111A	3×10^6
B1	4930	800	300	1.14×10^4	IA111B	1.3×10^5
C1	-4650	-160	480	1.09×10^6	IA111C	∞
IIIA12A1	5170	1300	300	9.2×10^3	IA112A	8.4×10^4
B1	5170	800	300	9.57×10^3	IA111B	1.3×10^5
IIIB11A1 ⁽²⁾	3700	1400	300-420	1.84×10^5	IB111A	4.5×10^4
B1	3700	800	180	5×10^5 (NF)	IA111B	1.3×10^5

- NOTE: (1) Fatigue life of one-inch specimen at same stress level as ten-inch wide specimens
- (2) Specimen failed at end fitting, repaired with bonded Ti tabs and testing continued to $N = 1.84 \times 10^5$

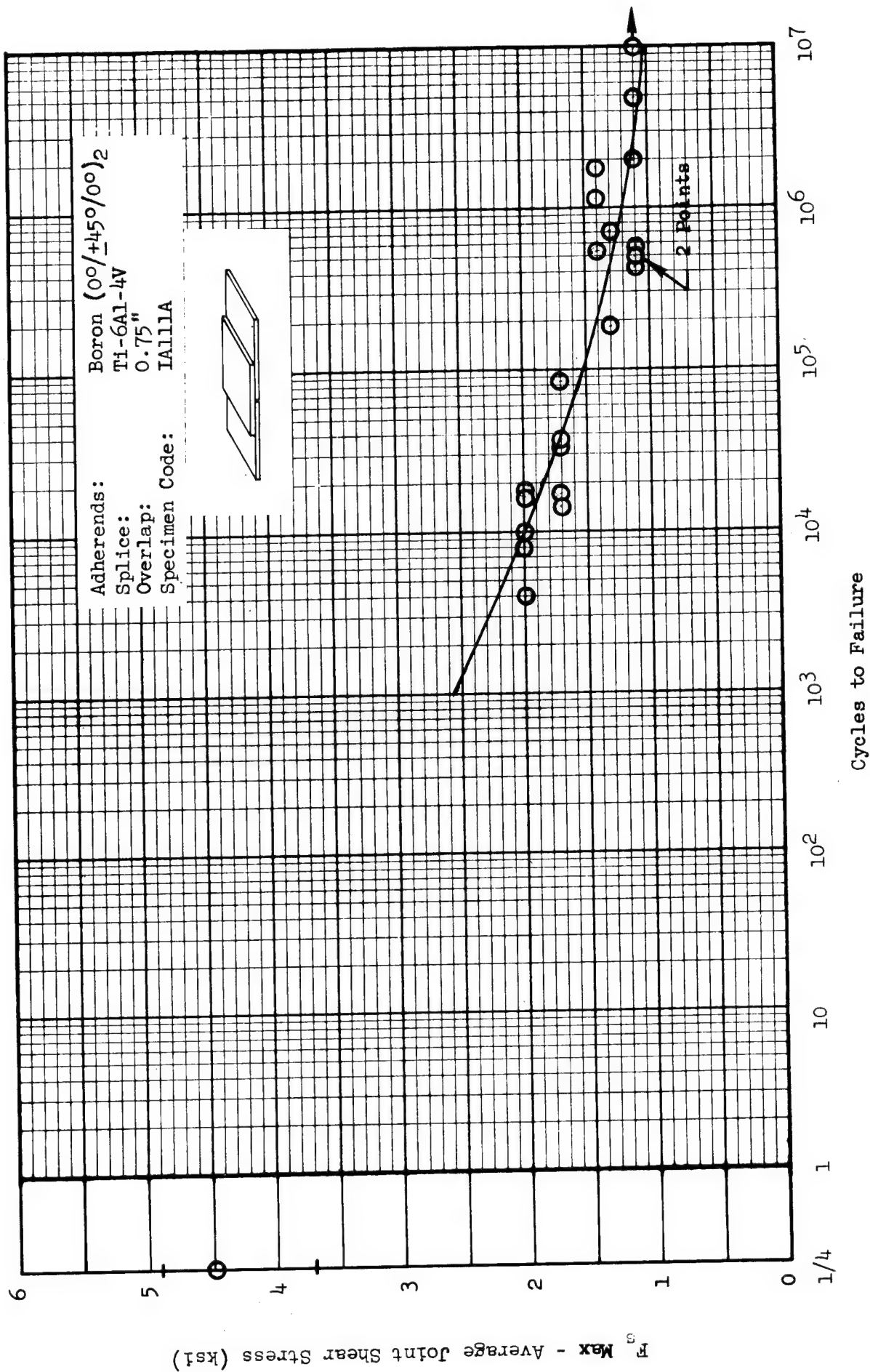


Figure 21 Fatigue Strength of Bonded Joints Baseline Data, Configuration IA, R = +0.10

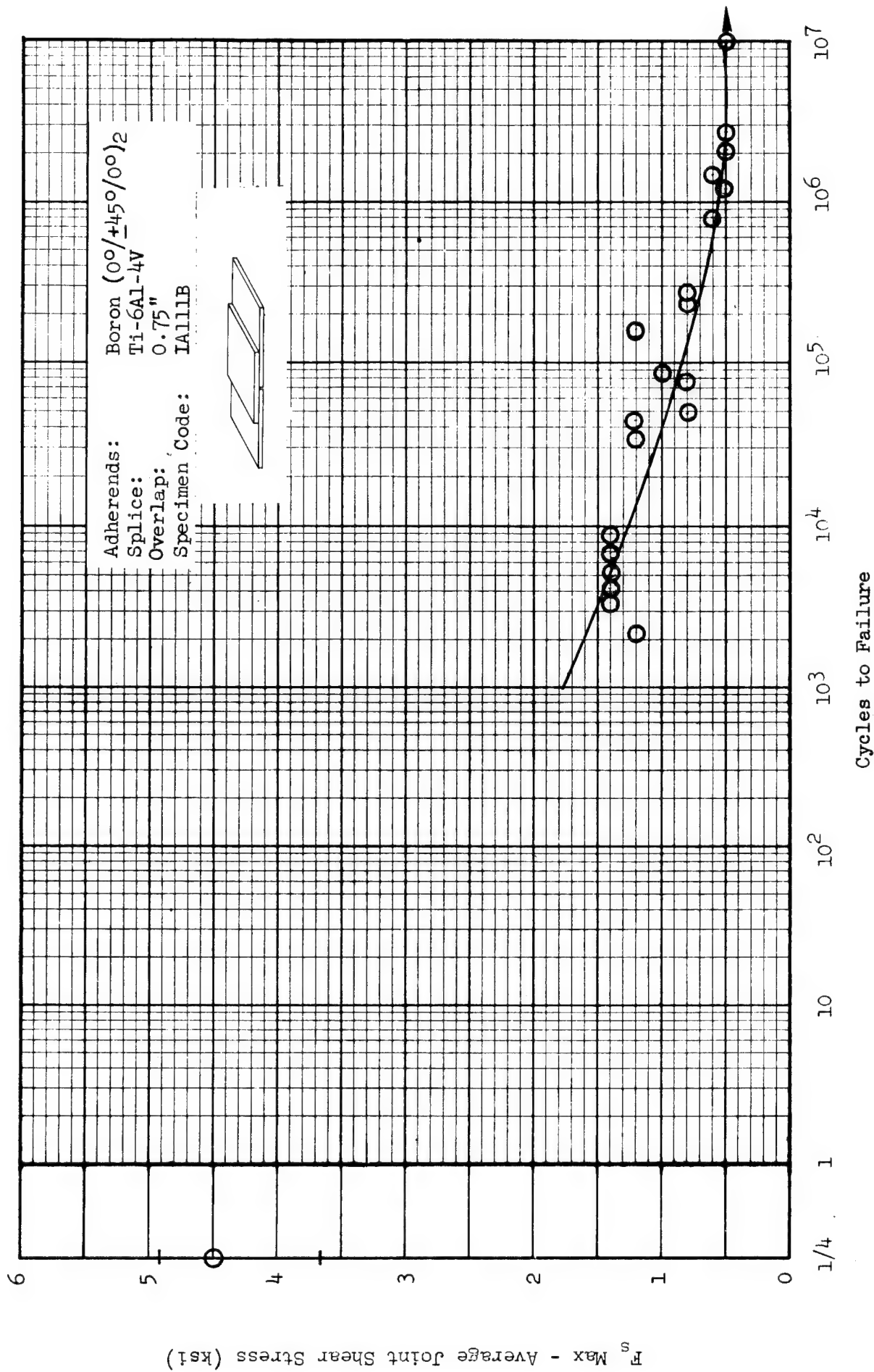


Figure 22 Fatigue Strength of Bonded Joints Baseline Data, Configuration IA, R = -1.0

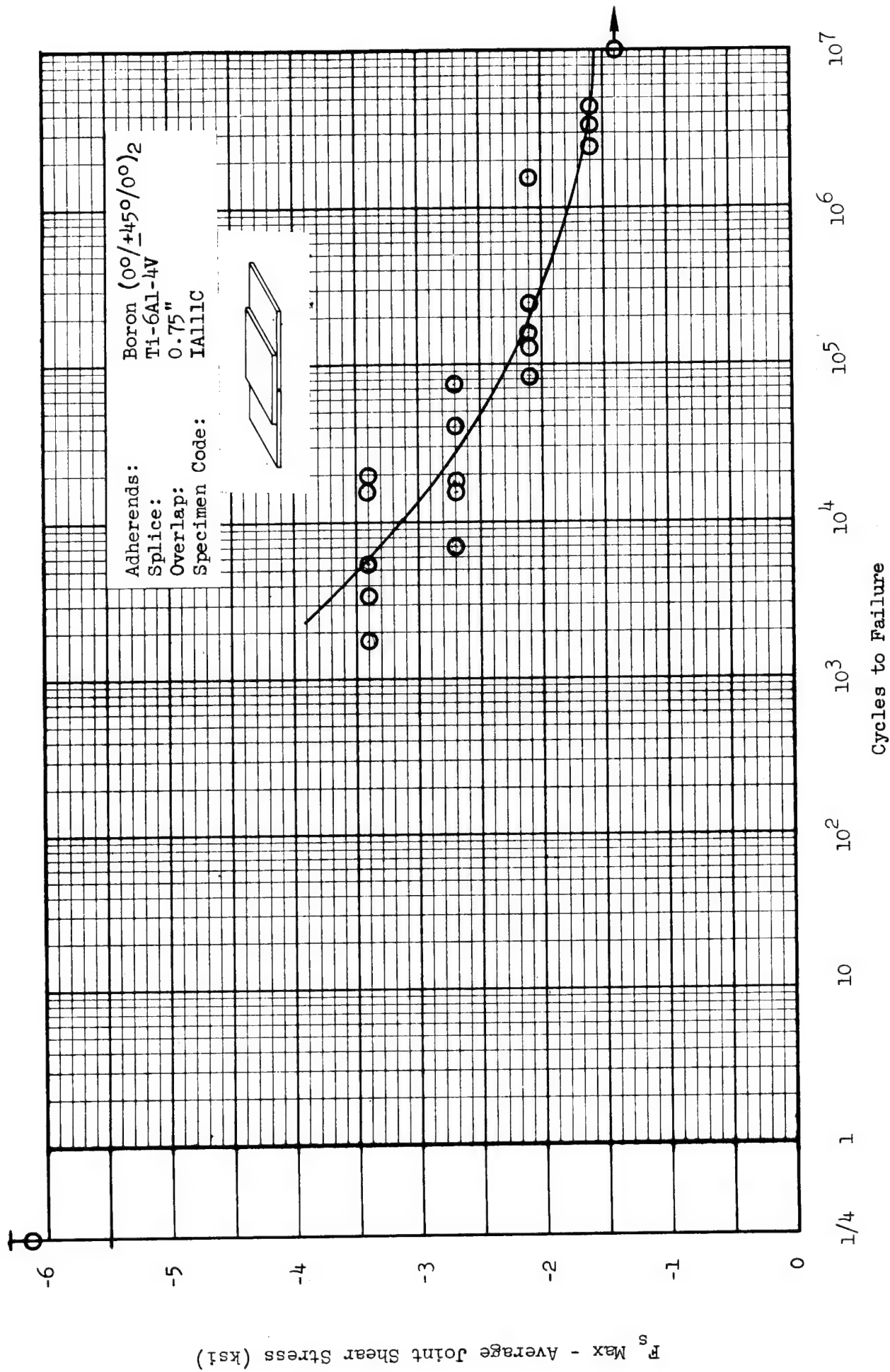


Figure 23 Fatigue Strength of Bonded Joints Baseline Data, Configuration IA, R = +10.0

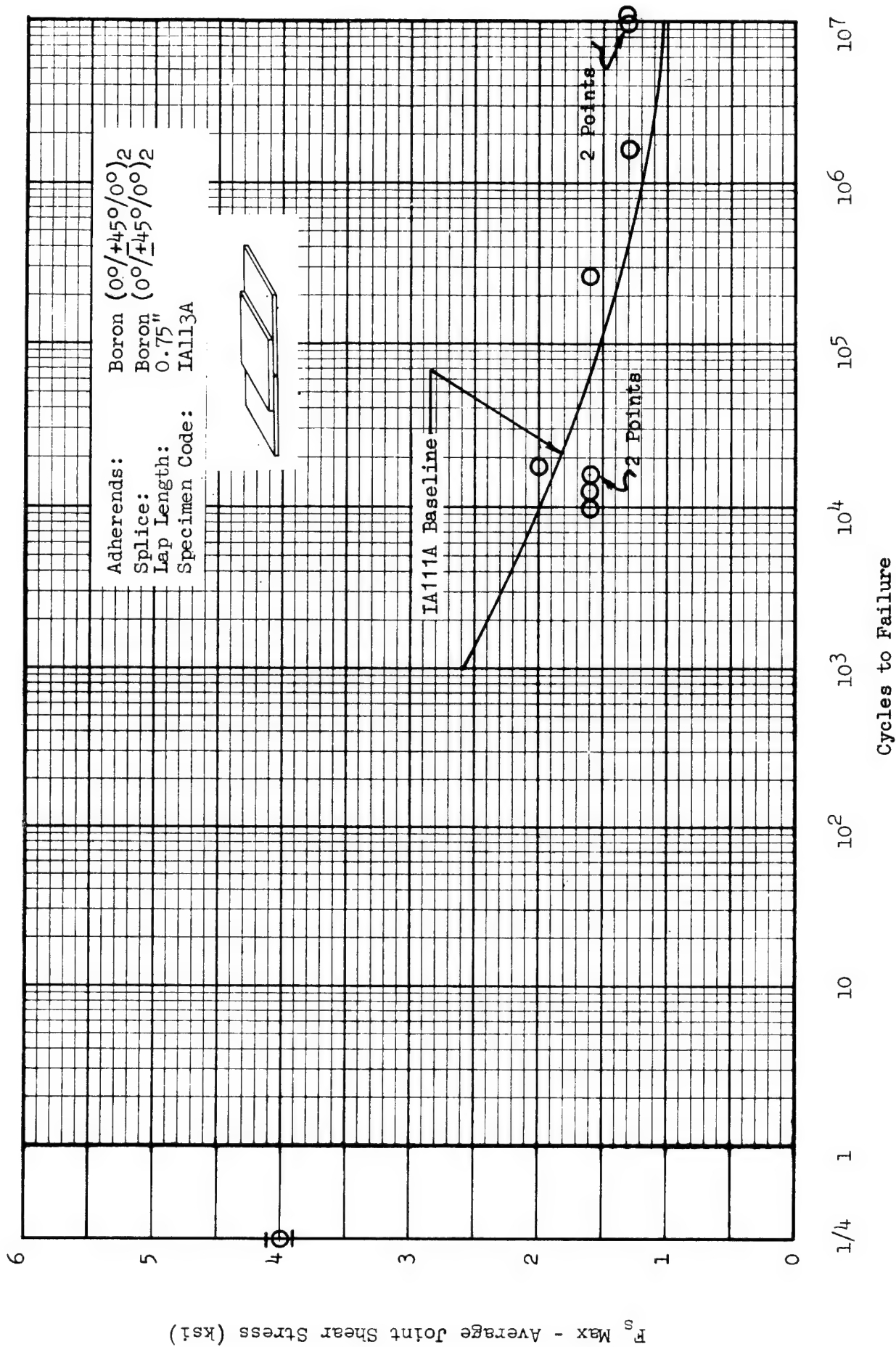


Figure 24 Fatigue Strength of Bonded Joints Baseline Data, Configuration IA, R = +0.10

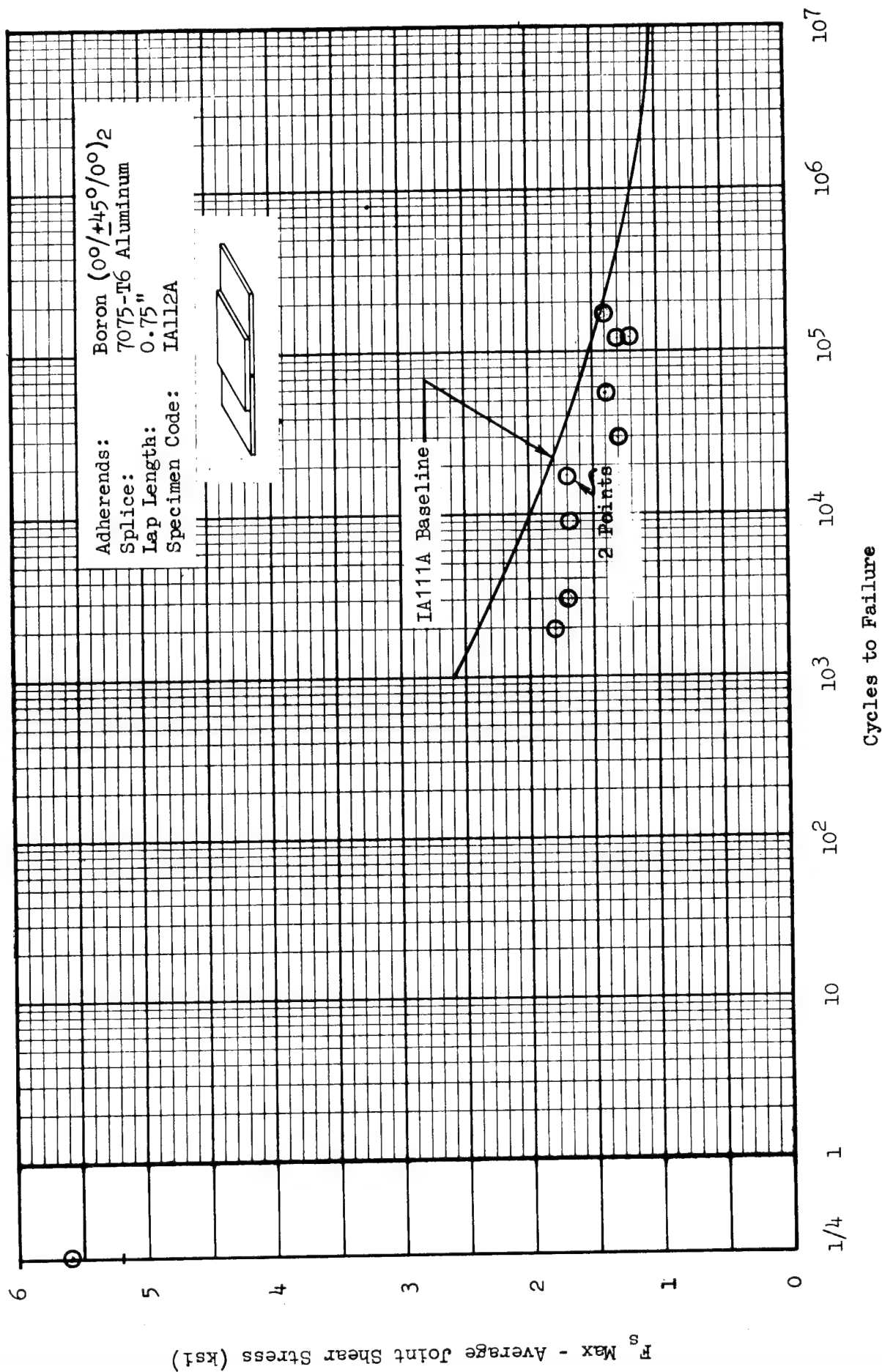


Figure 25 Fatigue Strength of Bonded Joints Baseline Data, Configuration IA, R = +0.10

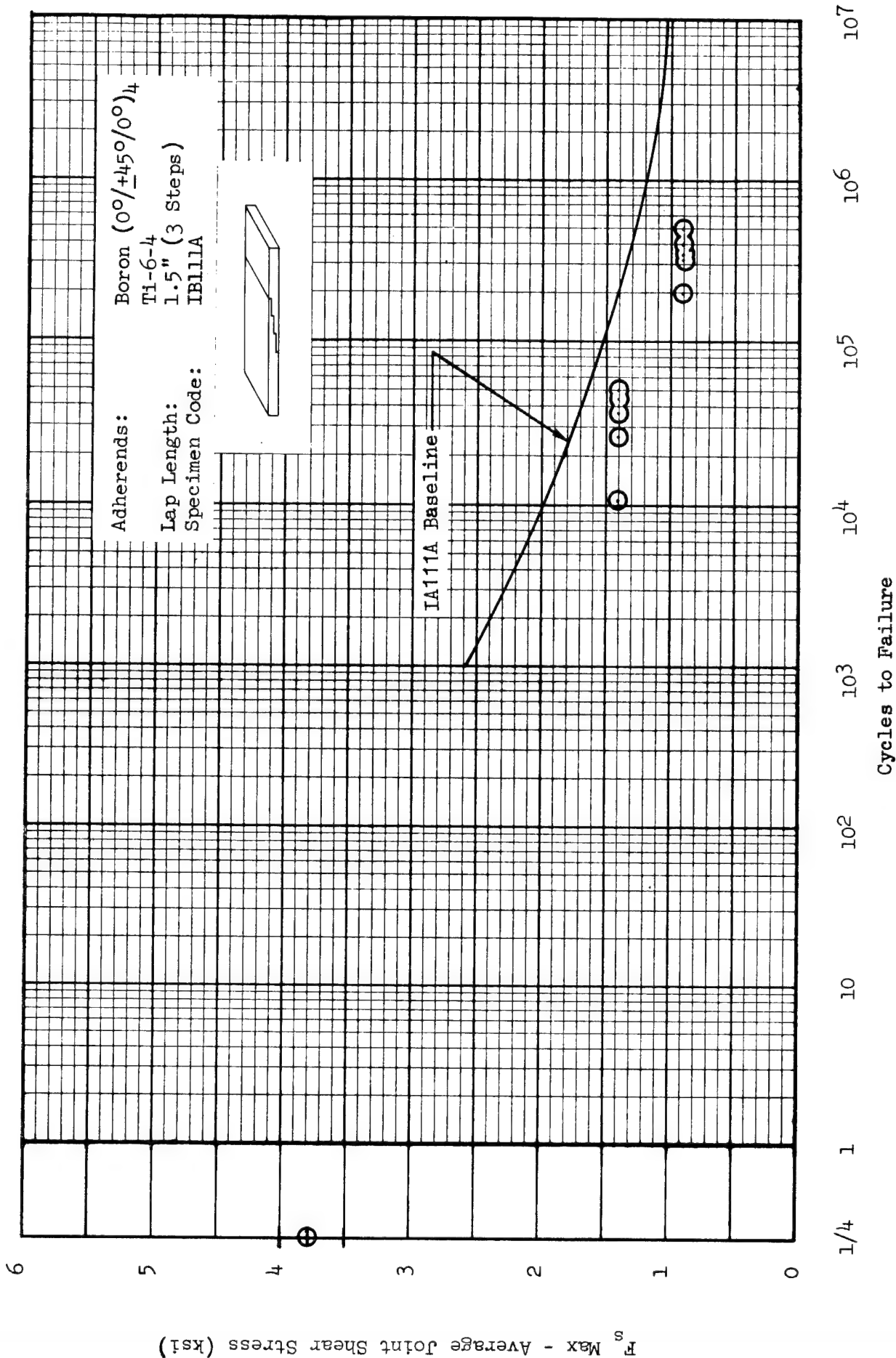


Figure 26 Fatigue Strength of Bonded Step Lap Scarf Joint
 Baseline Data, Configuration IB, $R = +0.10$

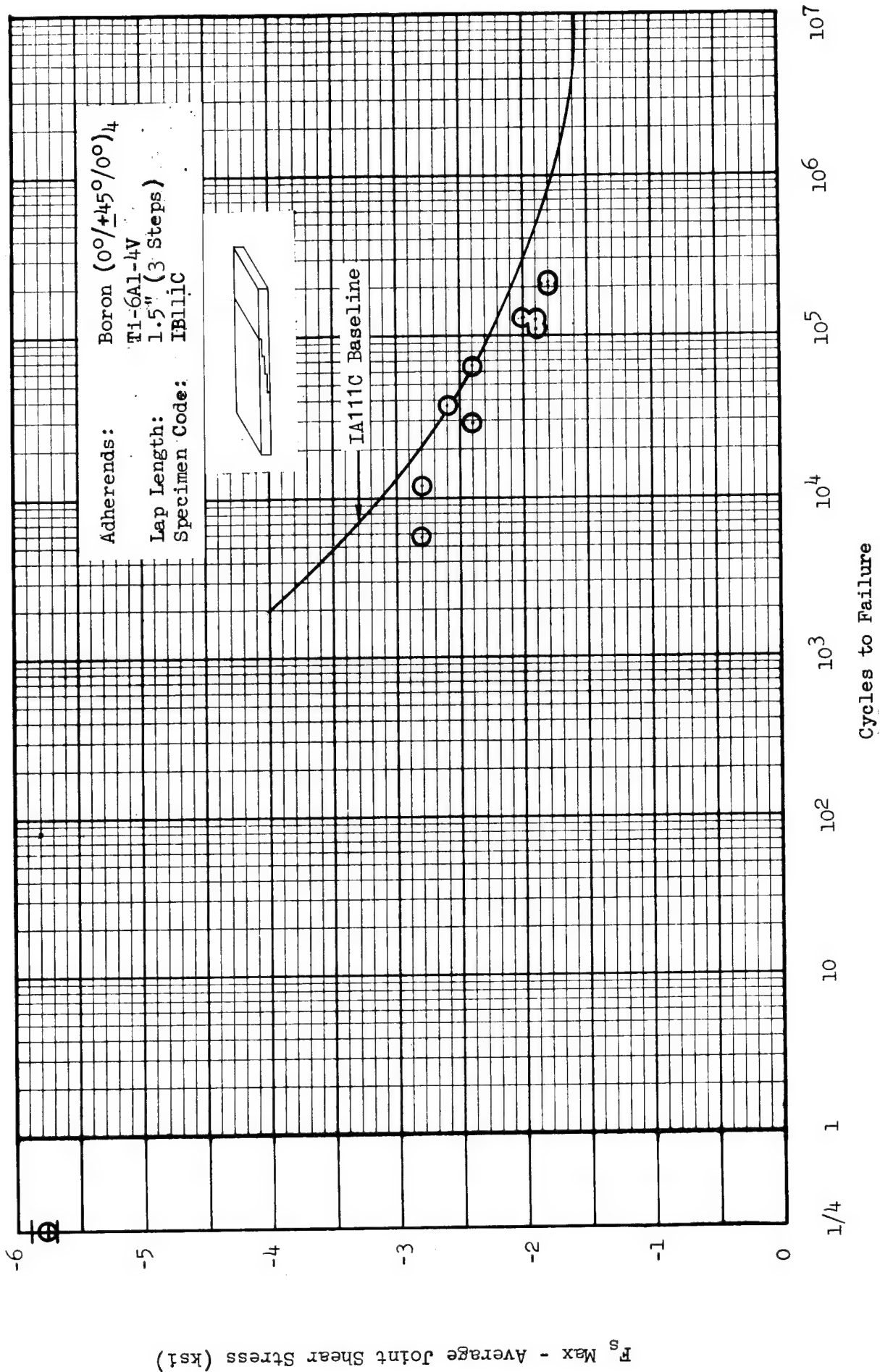


Figure 27 Fatigue Strength of Single-Scarf Butt Joints
 Baseline Data, Configuration IB, R = +10.0

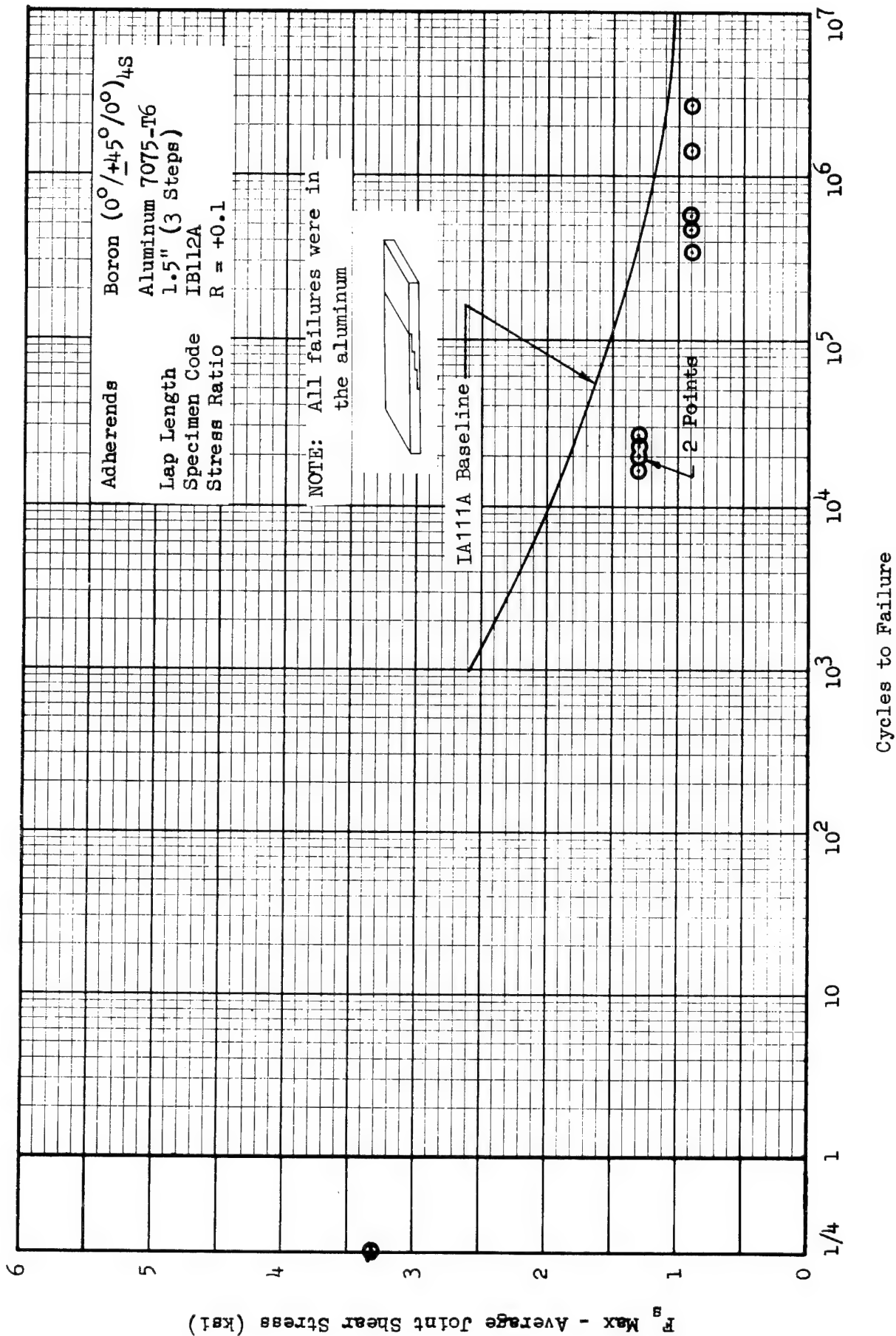


Figure 28 Fatigue Strength of Bonded Step Lap Scarf Joints:
 Configuration IB, Boron ($0^\circ/\pm 45^\circ$): Aluminum, Baseline Data

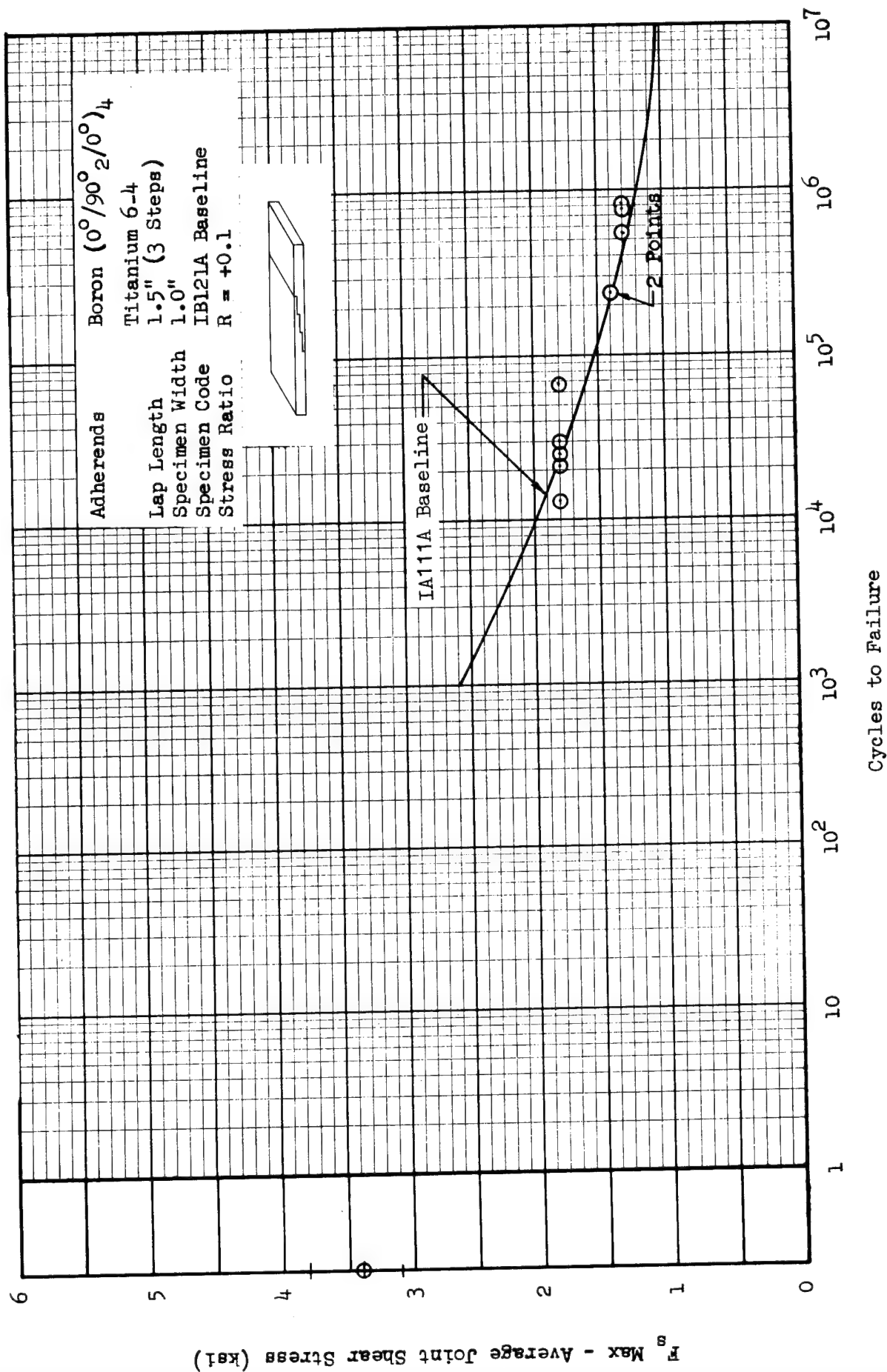


Figure 29 Fatigue Strength of Bonded Step Lap Scarf Joints:
 Configuration IB, Boron ($0^\circ/90^\circ$): Titanium, Baseline Data

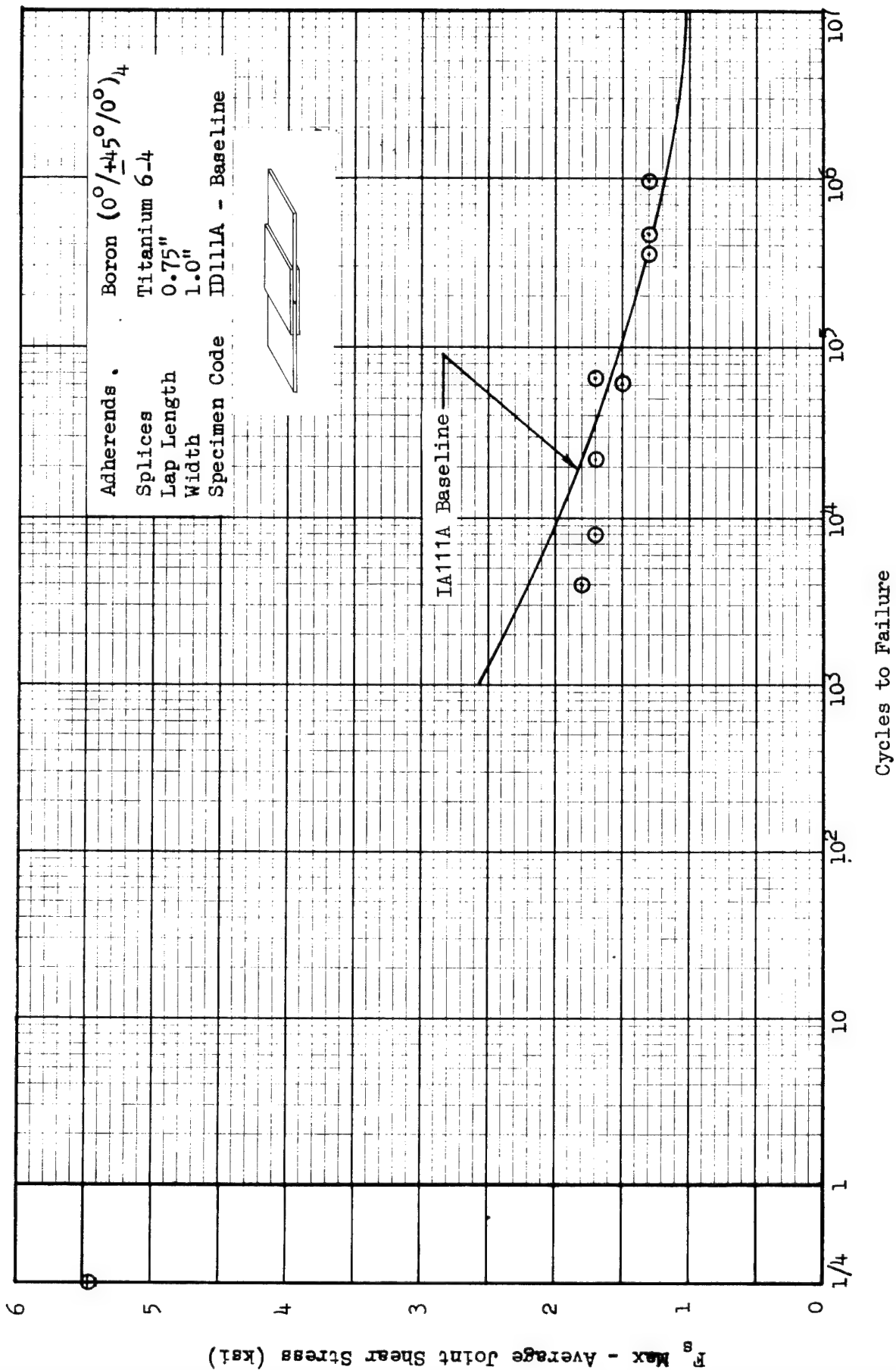


Figure 30 Fatigue Strength of Bonded Double Splice Butt Joint:
 Configuration ID, Boron:Titanium:Boron; R = +0.1

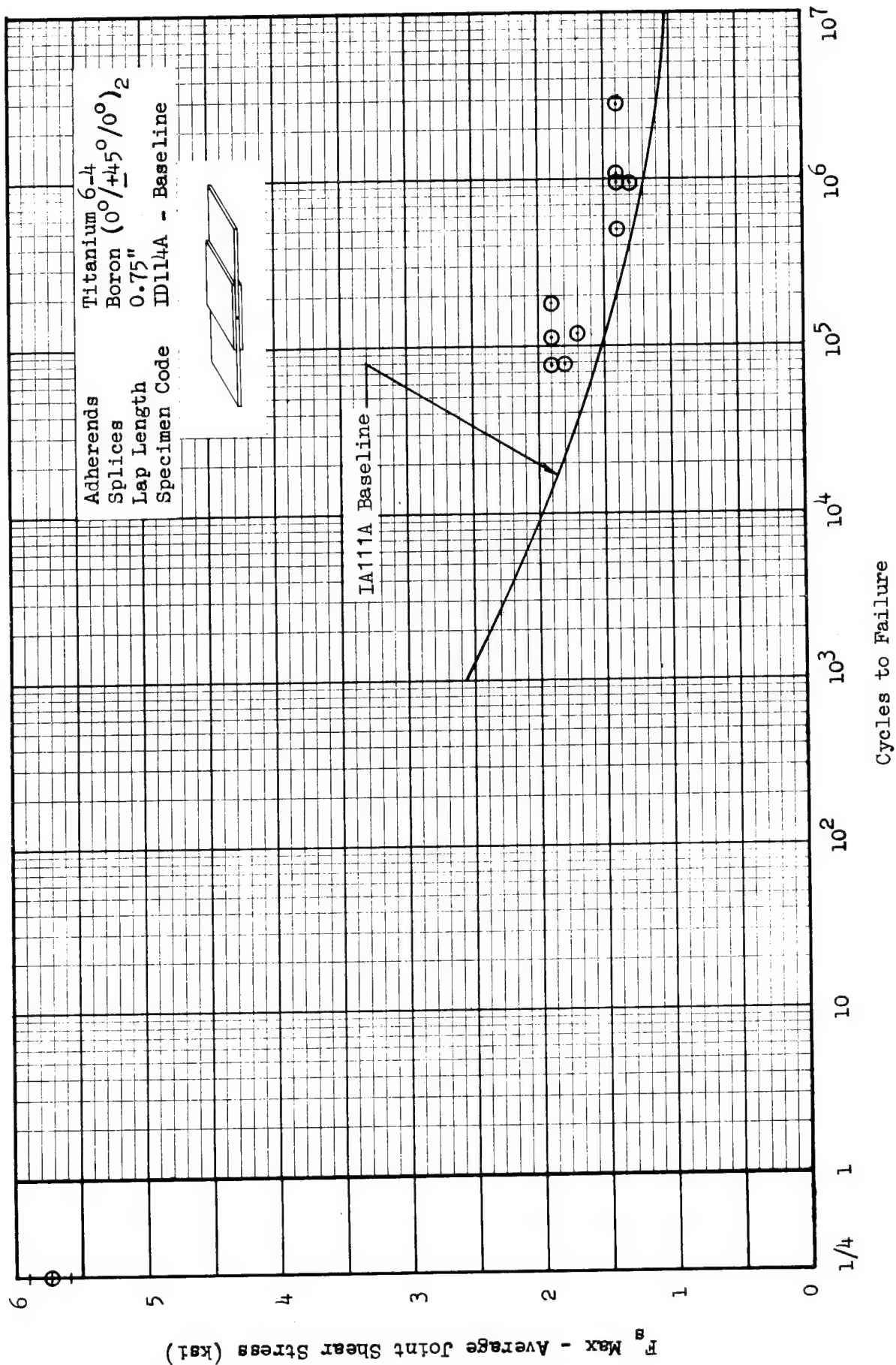


Figure 31 Fatigue Strength of Bonded Double Splice Butt Joints;
Configuration ID, Titanium: Boron: Titanium; R = +0.1

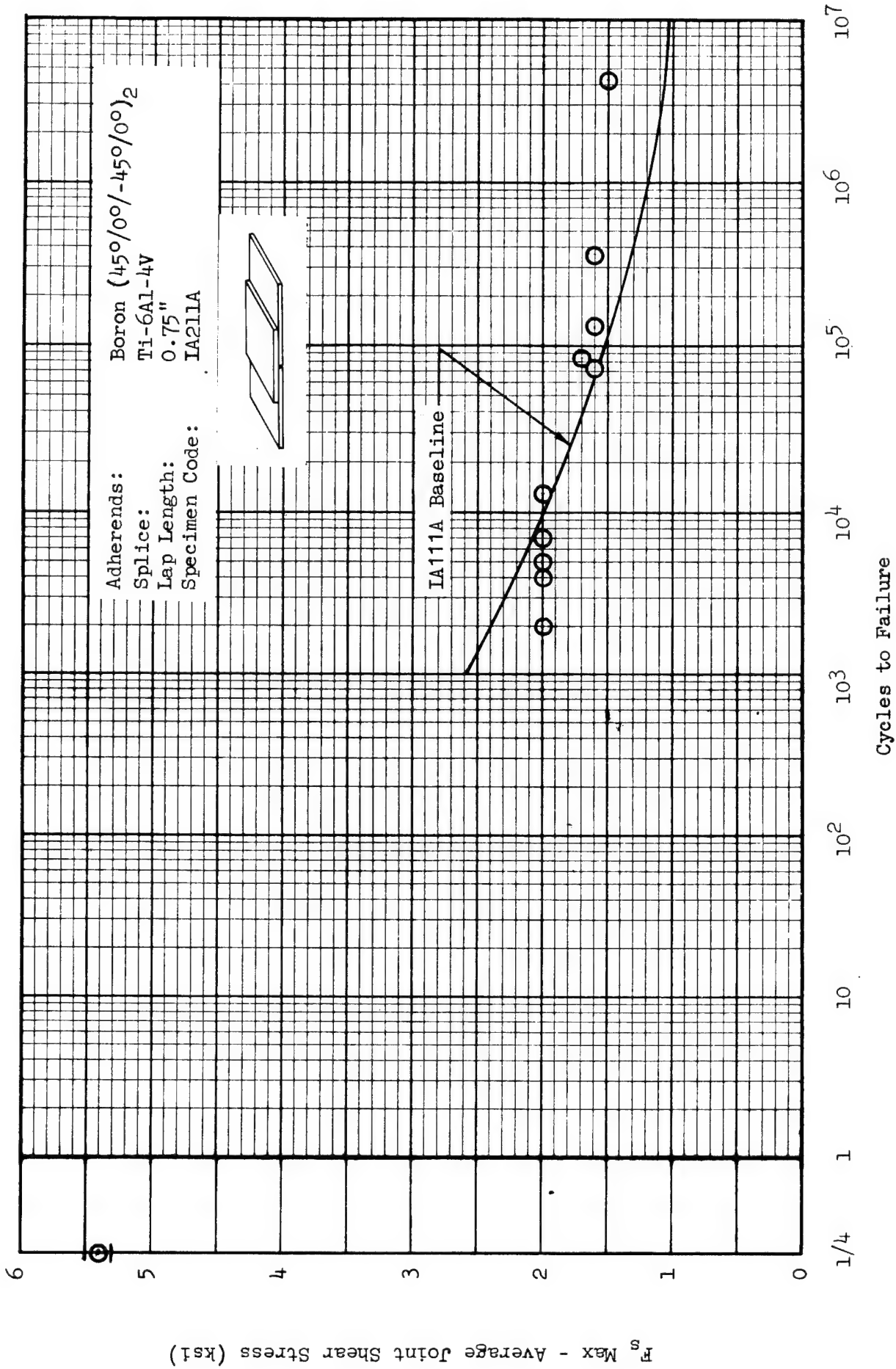


Figure 32 Fatigue Strength of Bonded Joints Ply-Stacking,
 Configuration IA, R = +0.10

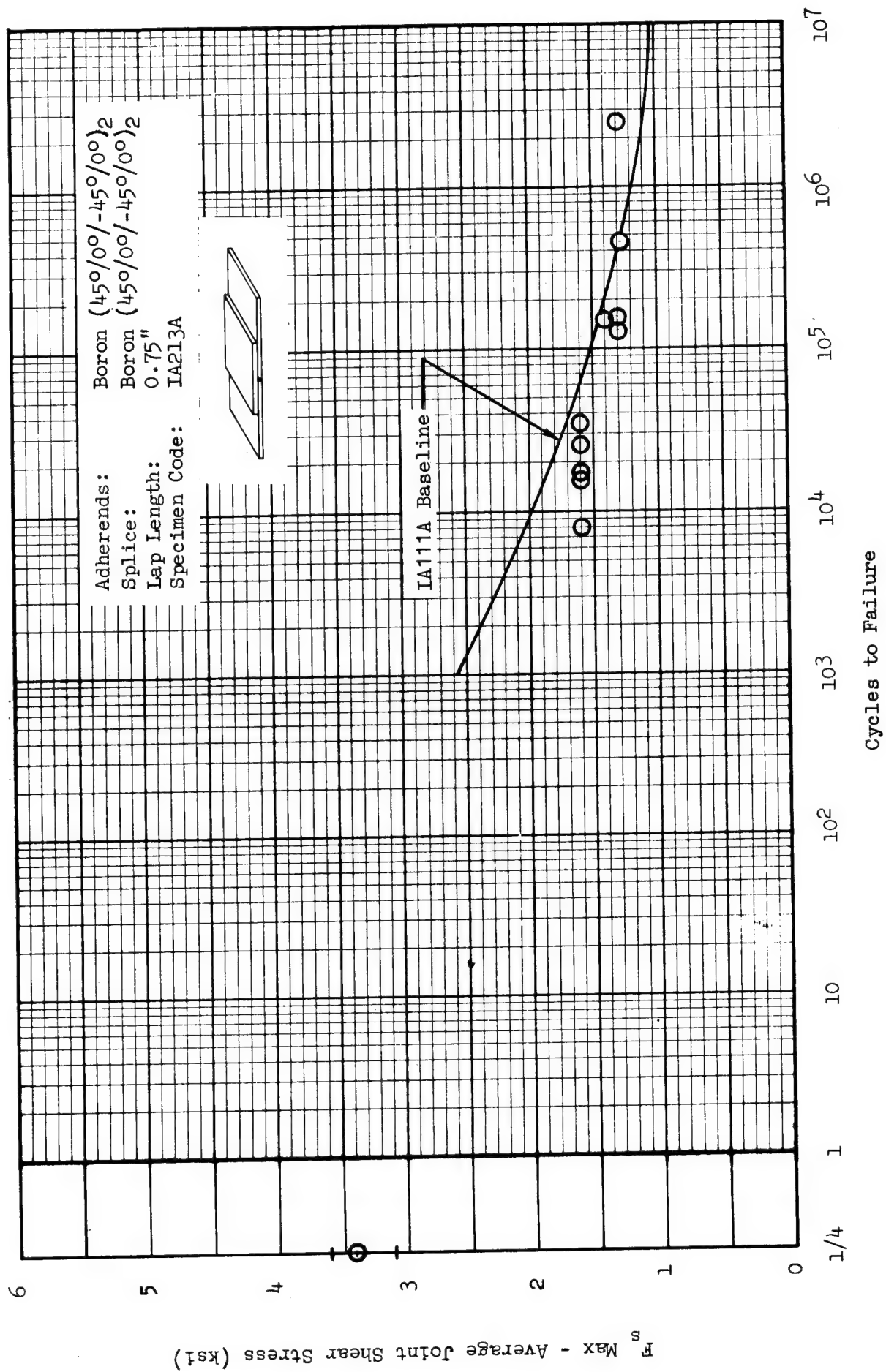


Figure 33 Fatigue Strength of Bonded Joints Ply-Stacking,
 Configuration IA, R = +0.10

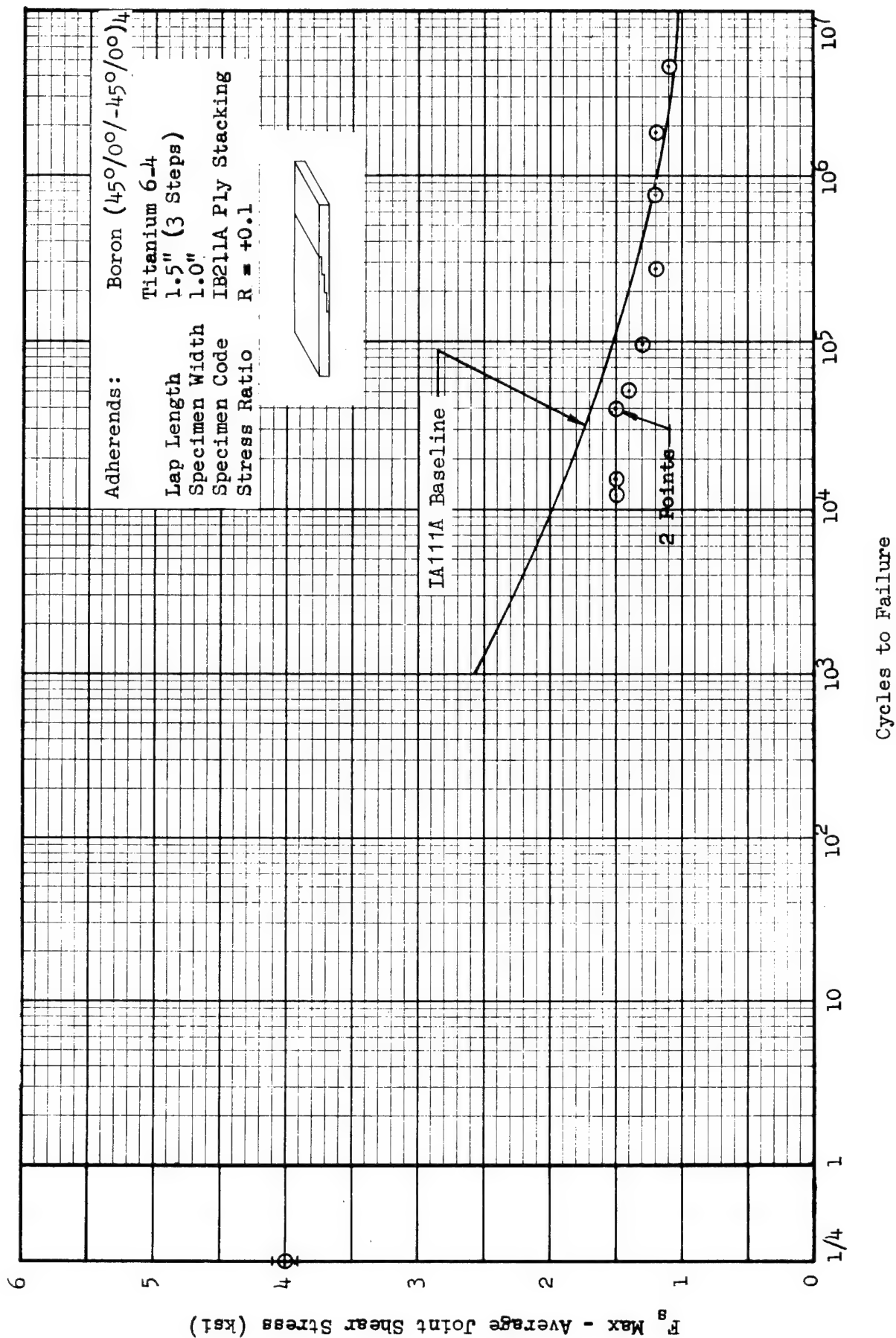


Figure 34 Fatigue Strength of Bonded Step Lap Scarf Joint; Configuration IB, Boron (0°/± 45°):Titanium, Ply-Stacking Effects

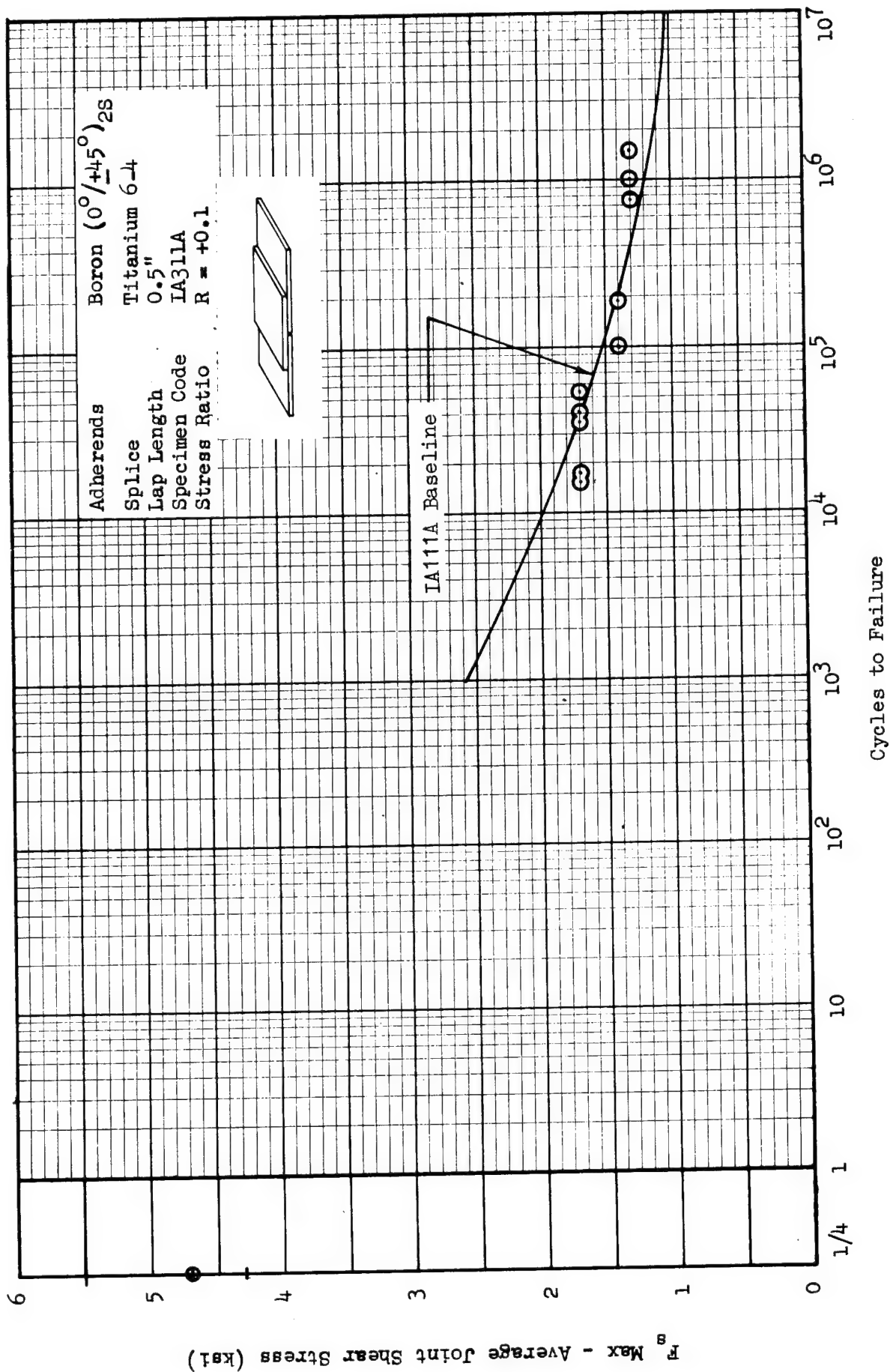


Figure 35 Fatigue Strength of Bonded Single Splice Butt Joint, Configuration IA, Boron: Titanium: Boron, Short Lap Effects

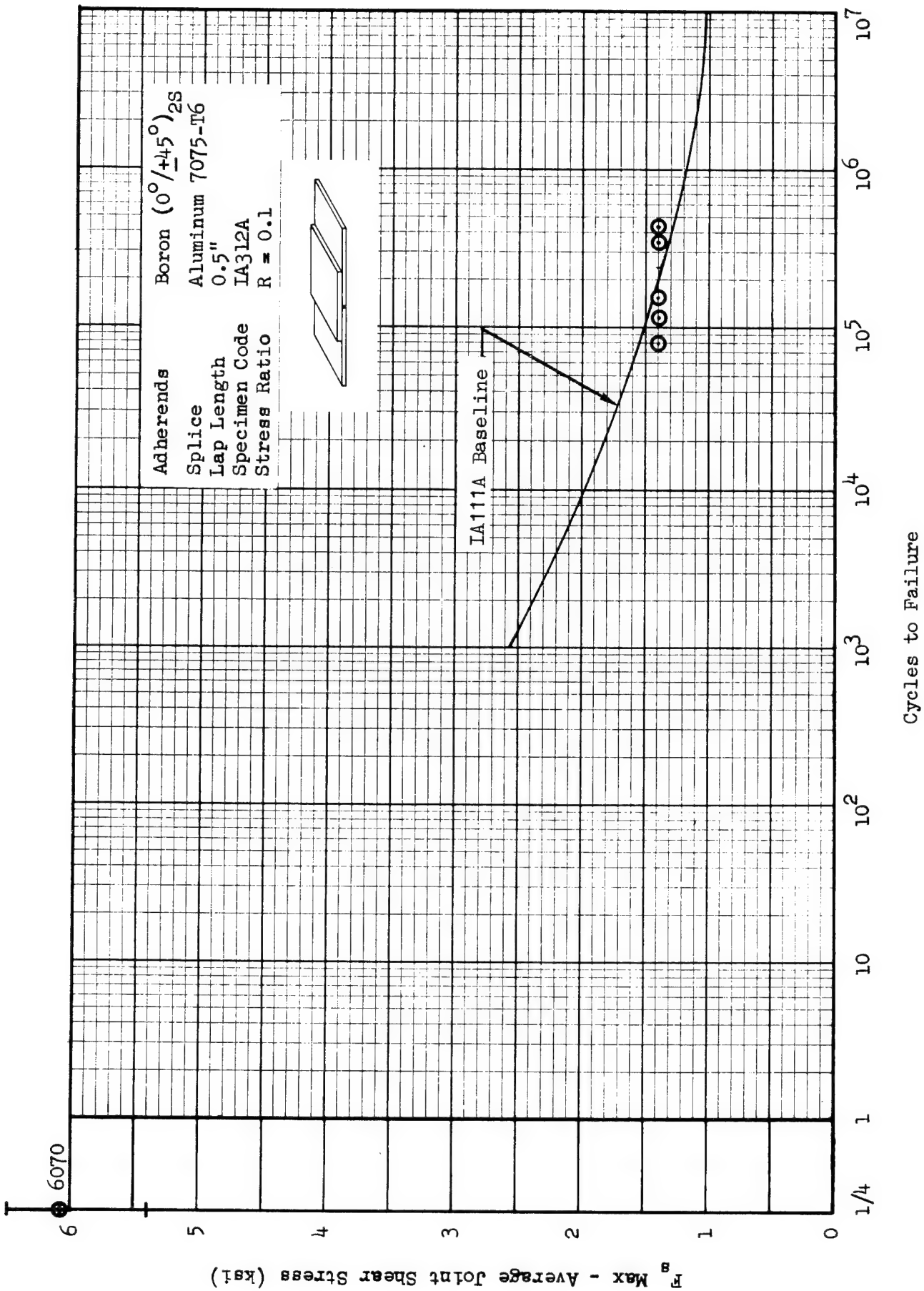


Figure 36 Fatigue Strength of Bonded Single Splice Butt Joints, Configuration IA, Boron:Aluminum:Boron, Short Lap Effects

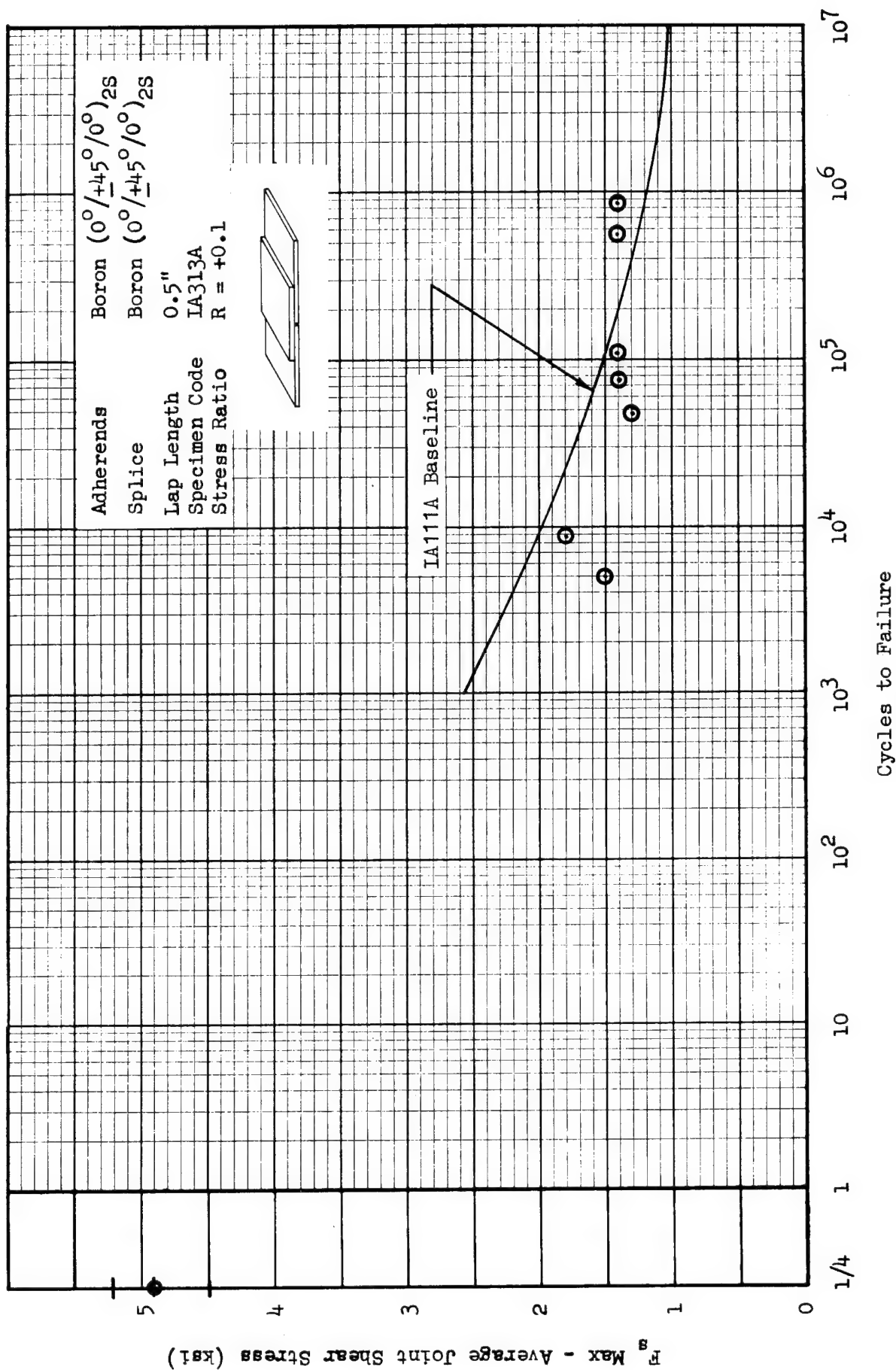


Figure 37 Fatigue Strength of Bonded Single Splice Butt Joints, Configuration IA, Boron:Boron, Short Lap Effects

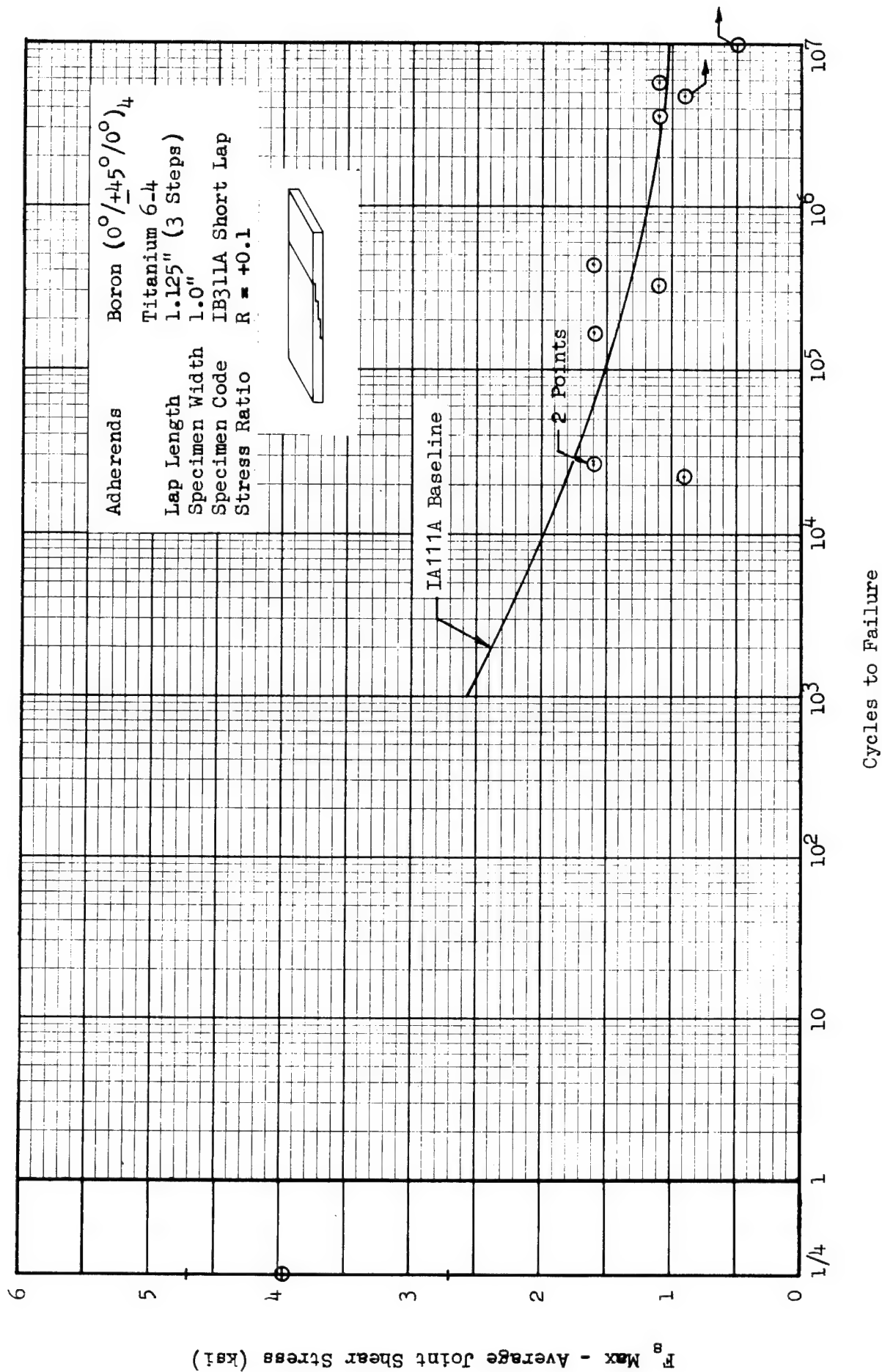


Figure 38 Fatigue Strength of Bonded Step Lap Scarf Joint; Configuration IB, Boron ($0^\circ/+45^\circ$):Titanium, Short Lap Effects

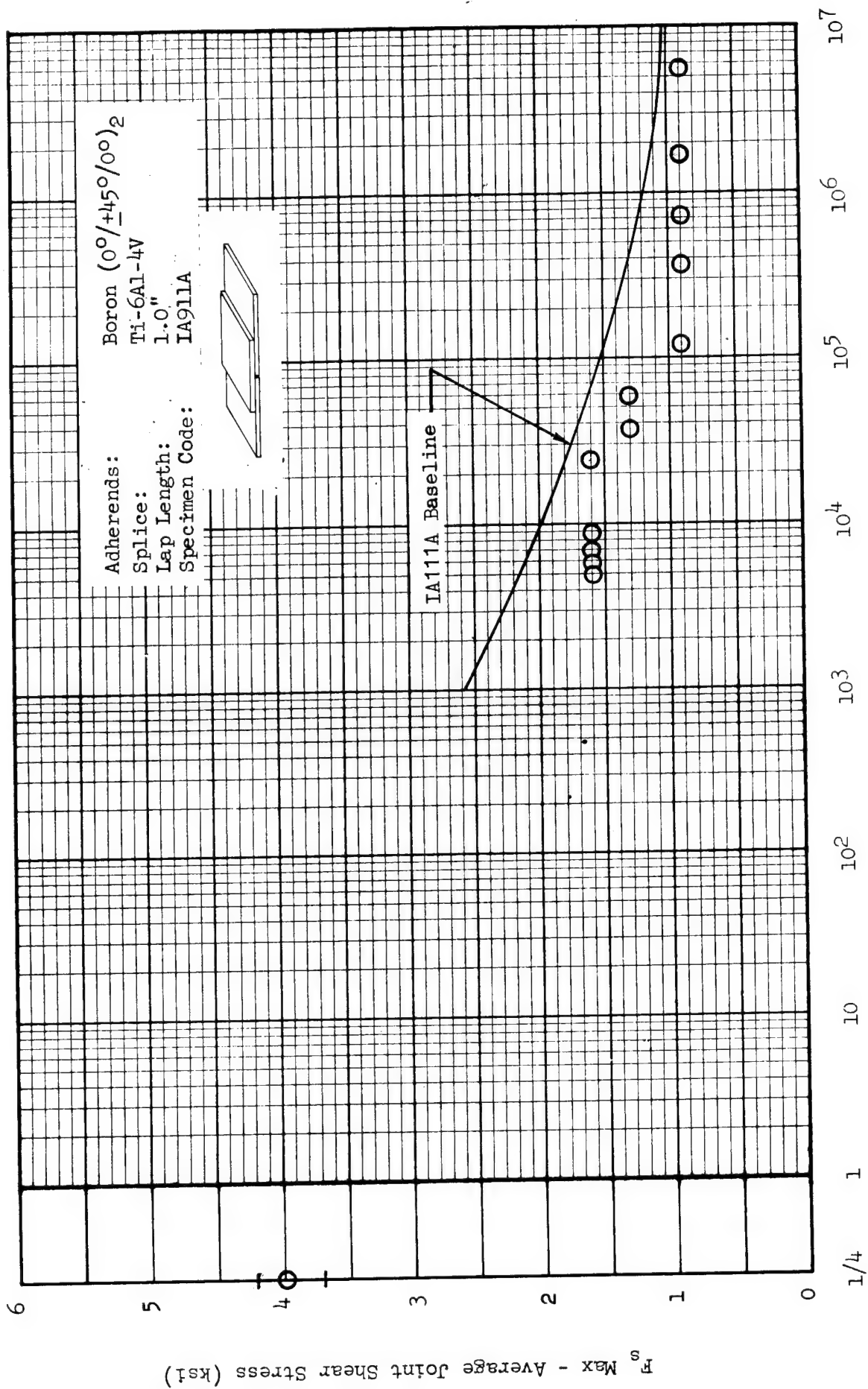
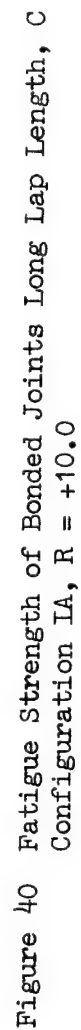


Figure 39 Fatigue Strength of Bonded Joints Long Lap Length,
 Configuration IA, R = +0.10



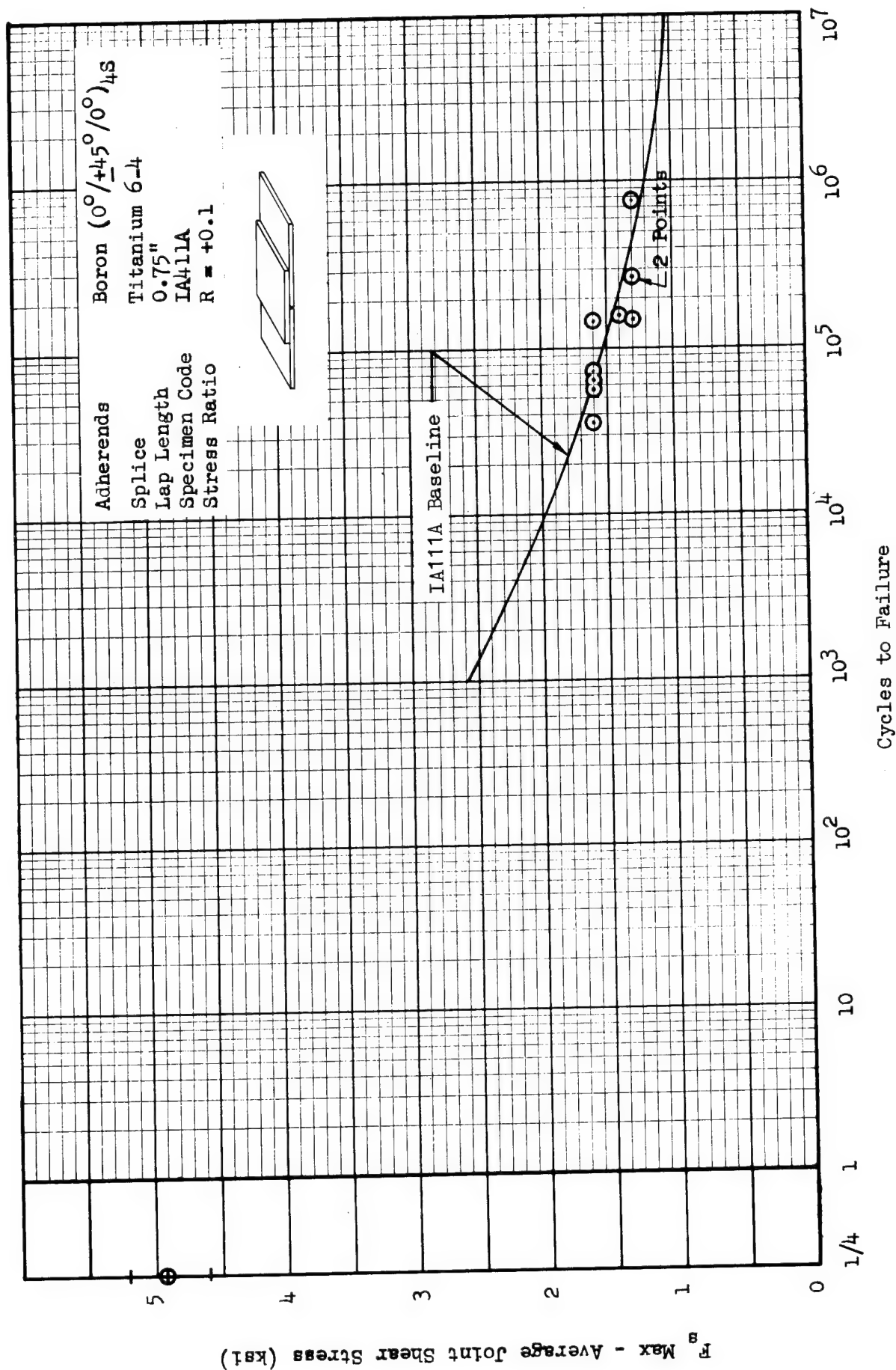


Figure 41 Fatigue Strength of Bonded Single Splice Butt Joints Configuration IA, Boron ($0^\circ/+45^\circ$):Titanium:6-4, Thickness Effects

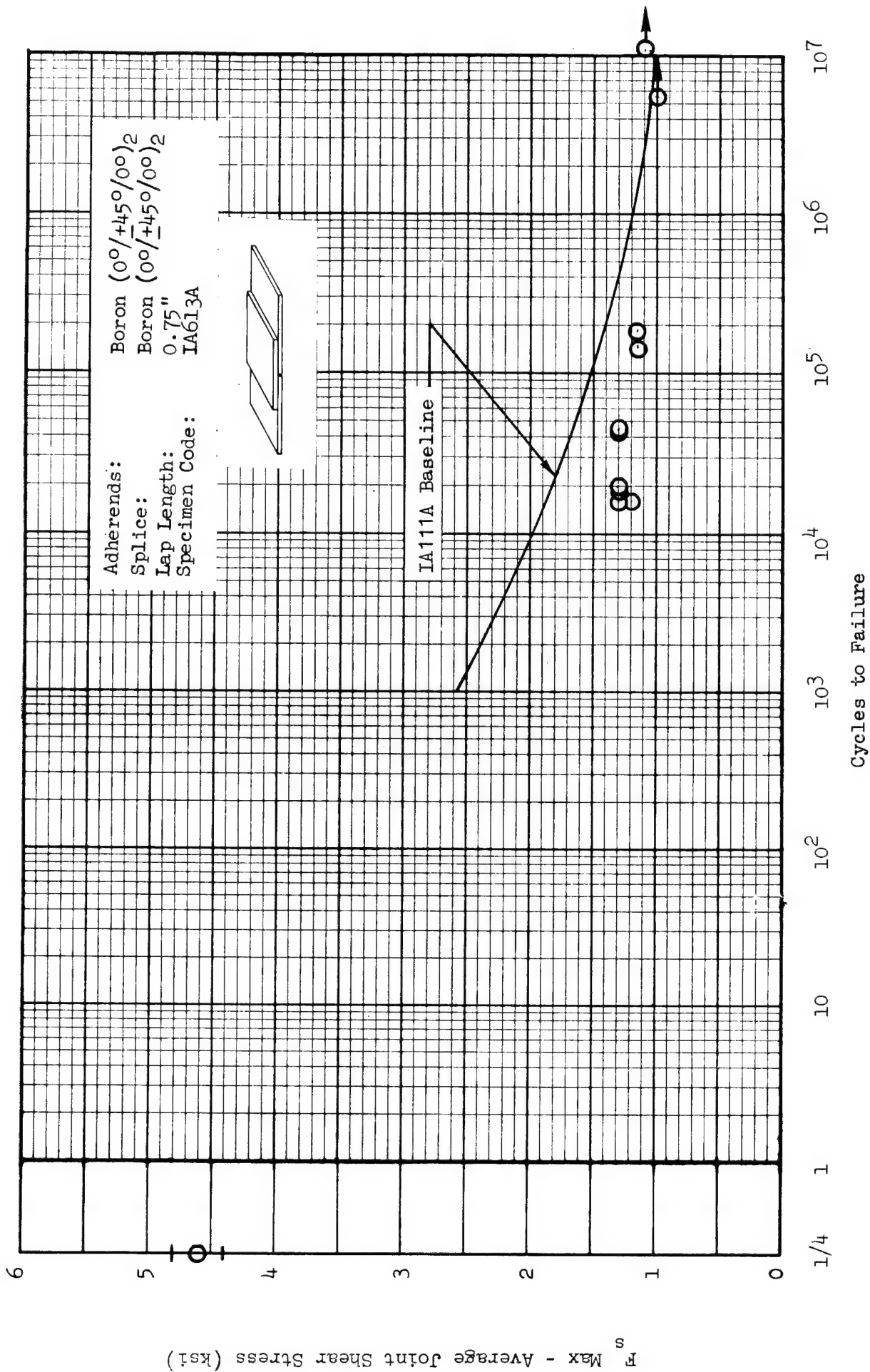


Figure 42 Fatigue Strength of Bonded Joints Second Adhesive, Configuration IA, R = +0.10

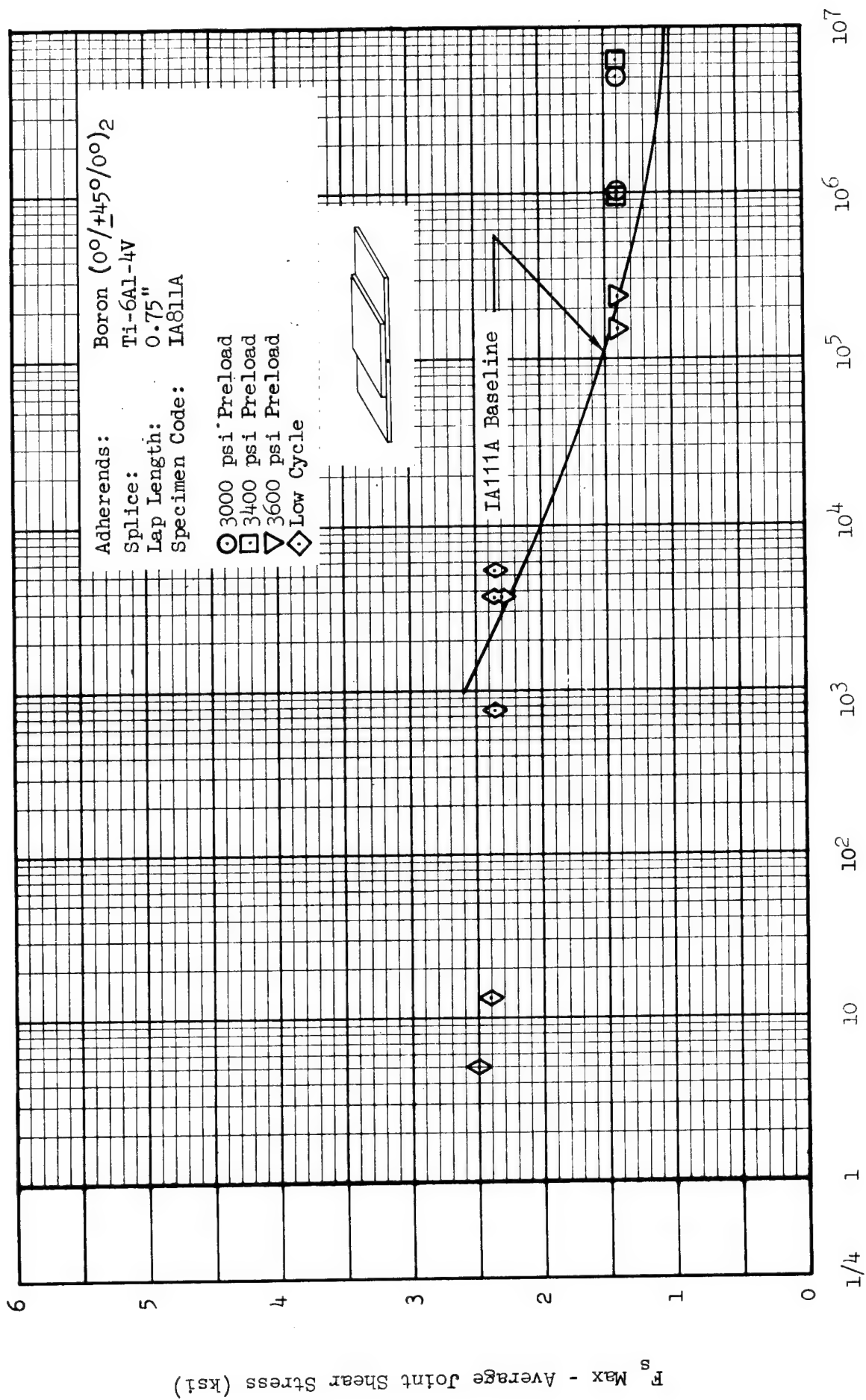


Figure 43 Fatigue Strength of Bonded Joints Low Cycle Data & Preload Data, Configuration IA, R = +0.10

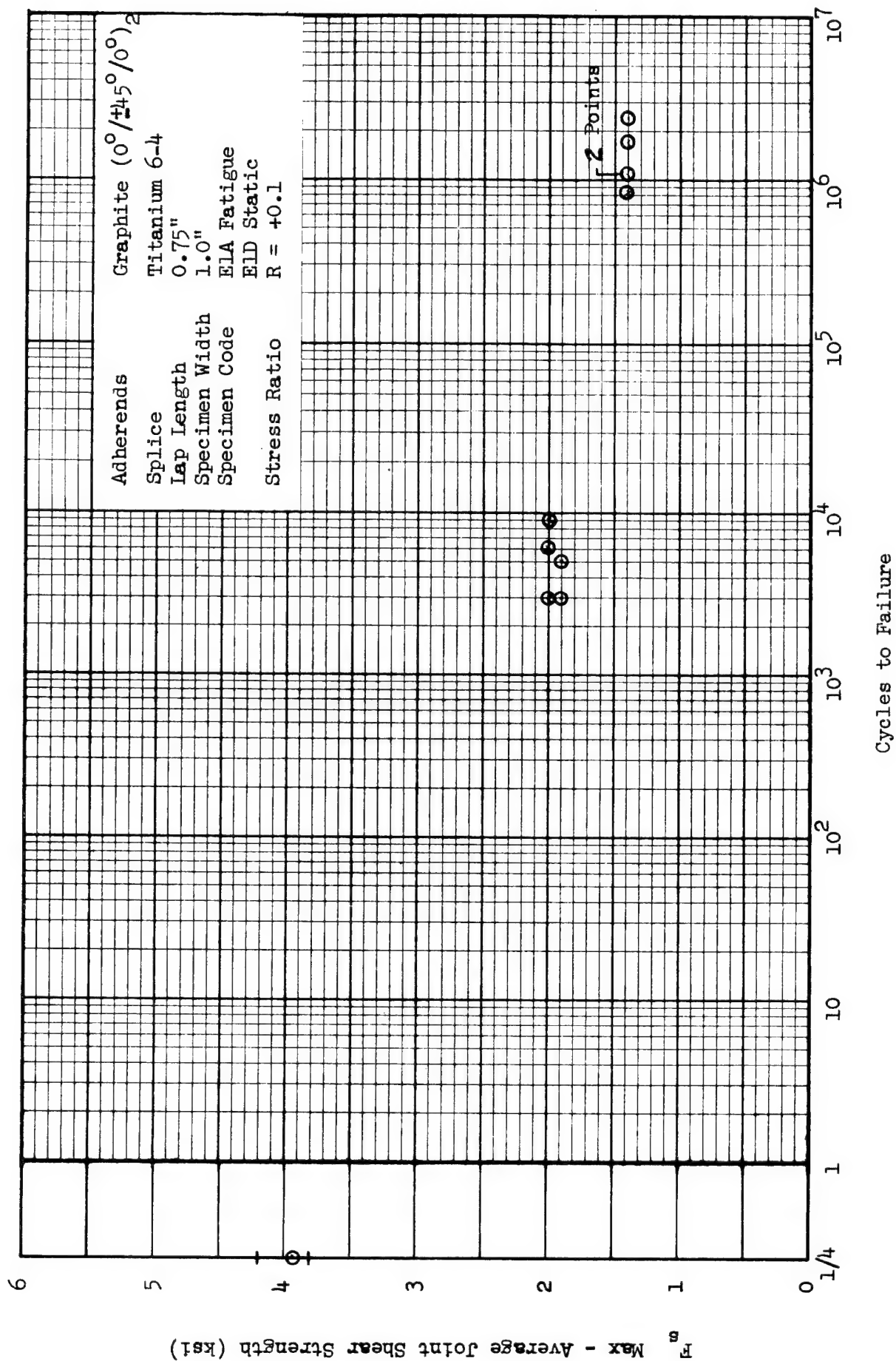


Figure 44 Fatigue Strength of Bonded Single Splice Butt Joints:
Configuration IA, Graphite: Titanium: Graphite

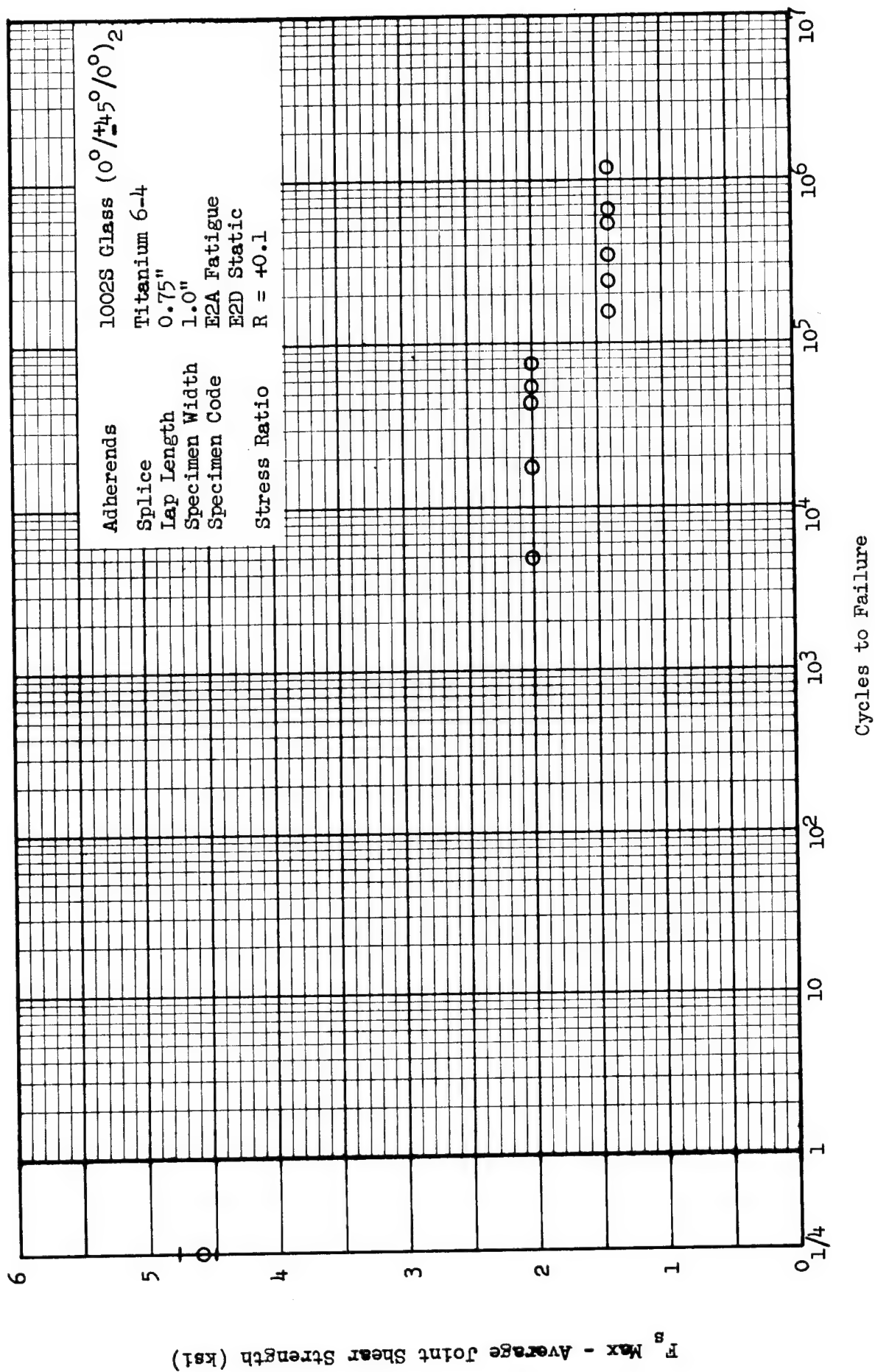


Figure 45 Fatigue Strength of Bonded Single Splice Butt Joints:
 Configuration IA, 1002S Glass: Titanium: 1002S Glass

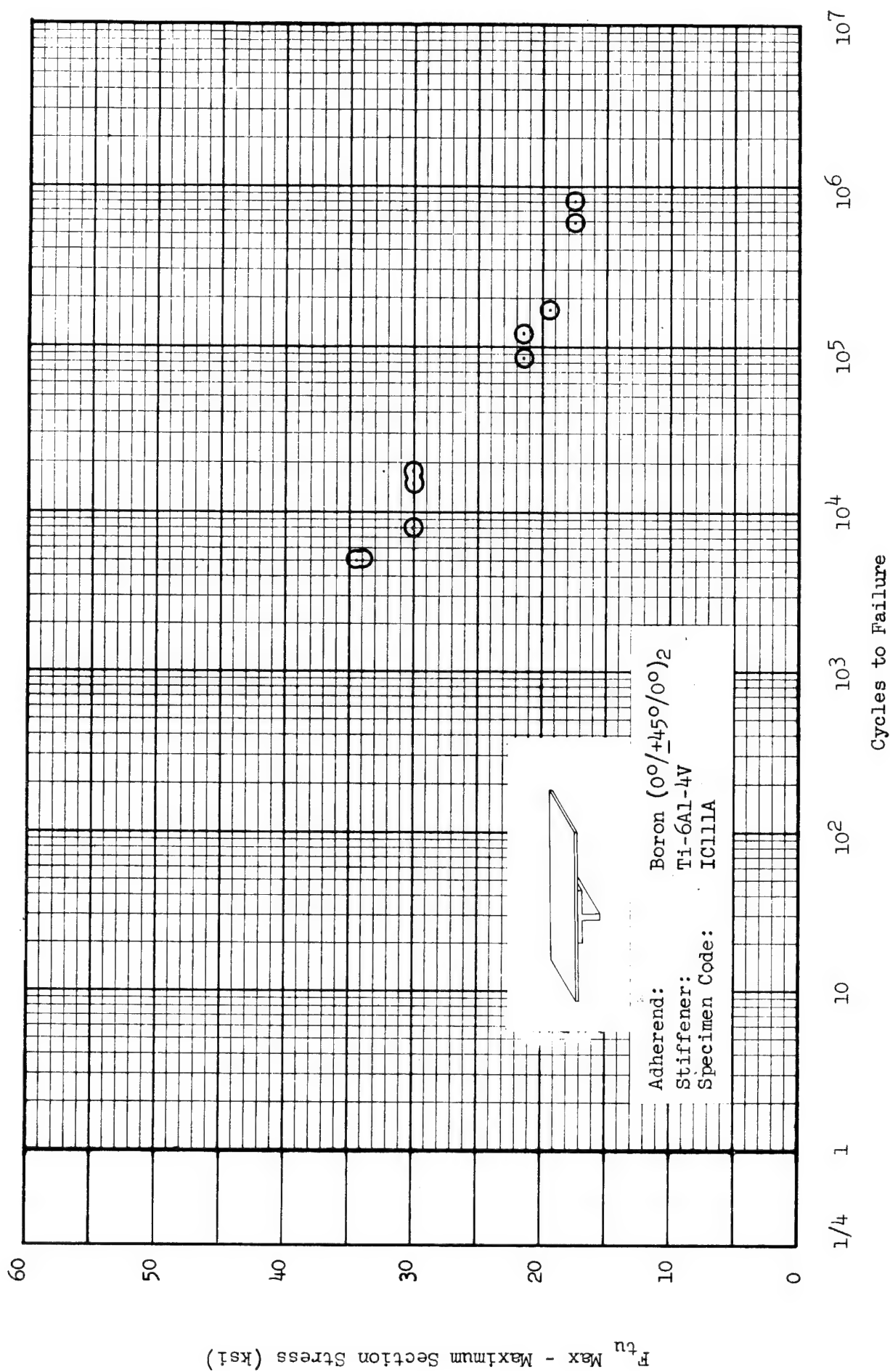


Figure 46 Fatigue Strength of Bonded Joints Baseline Data, Configuration IC, R = +0.10

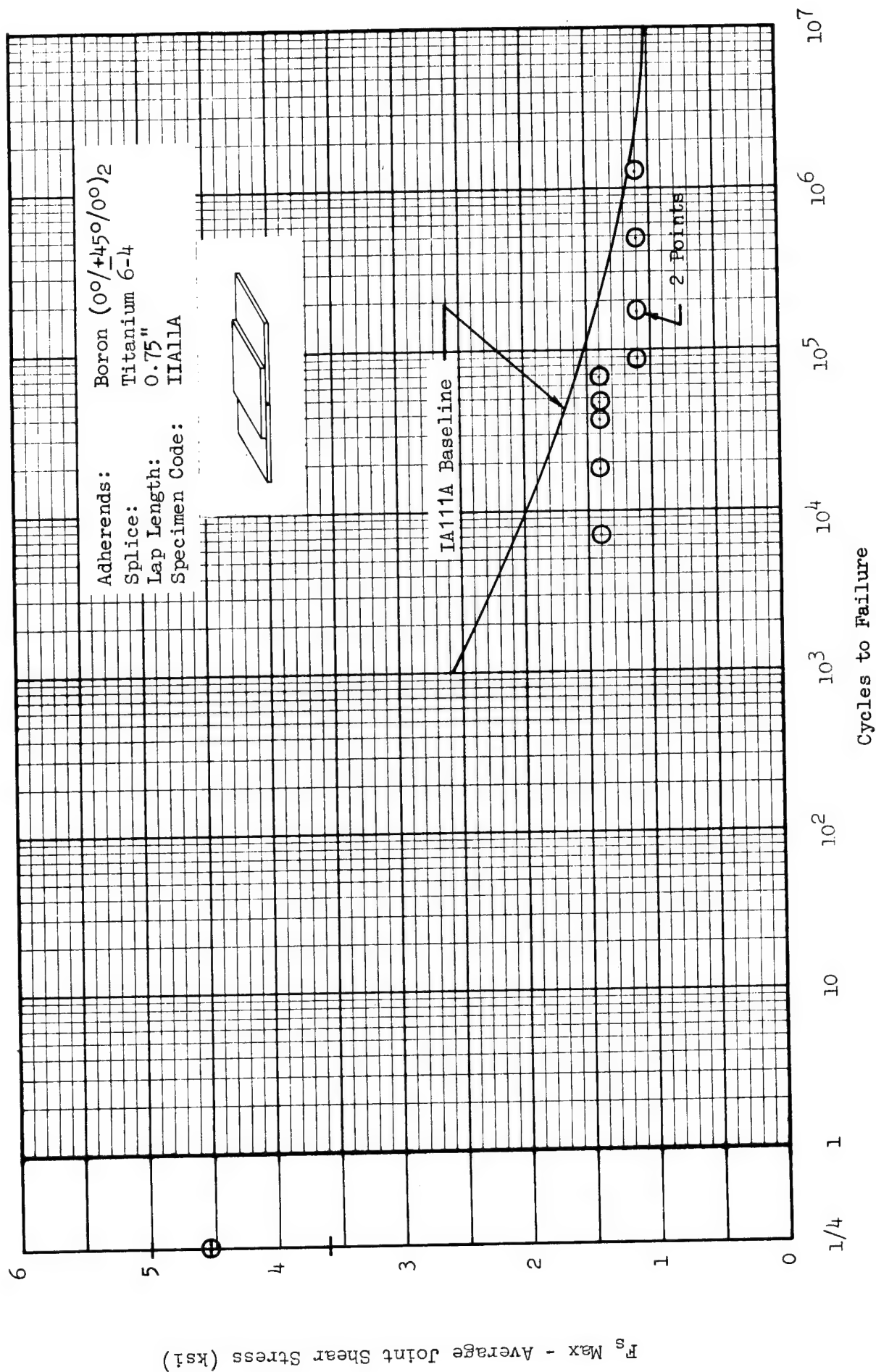


Figure 47 Fatigue Strength of Bonded Single Splice Butt Joints
 Baseline Data, Configuration IIA, $R = +0.10$

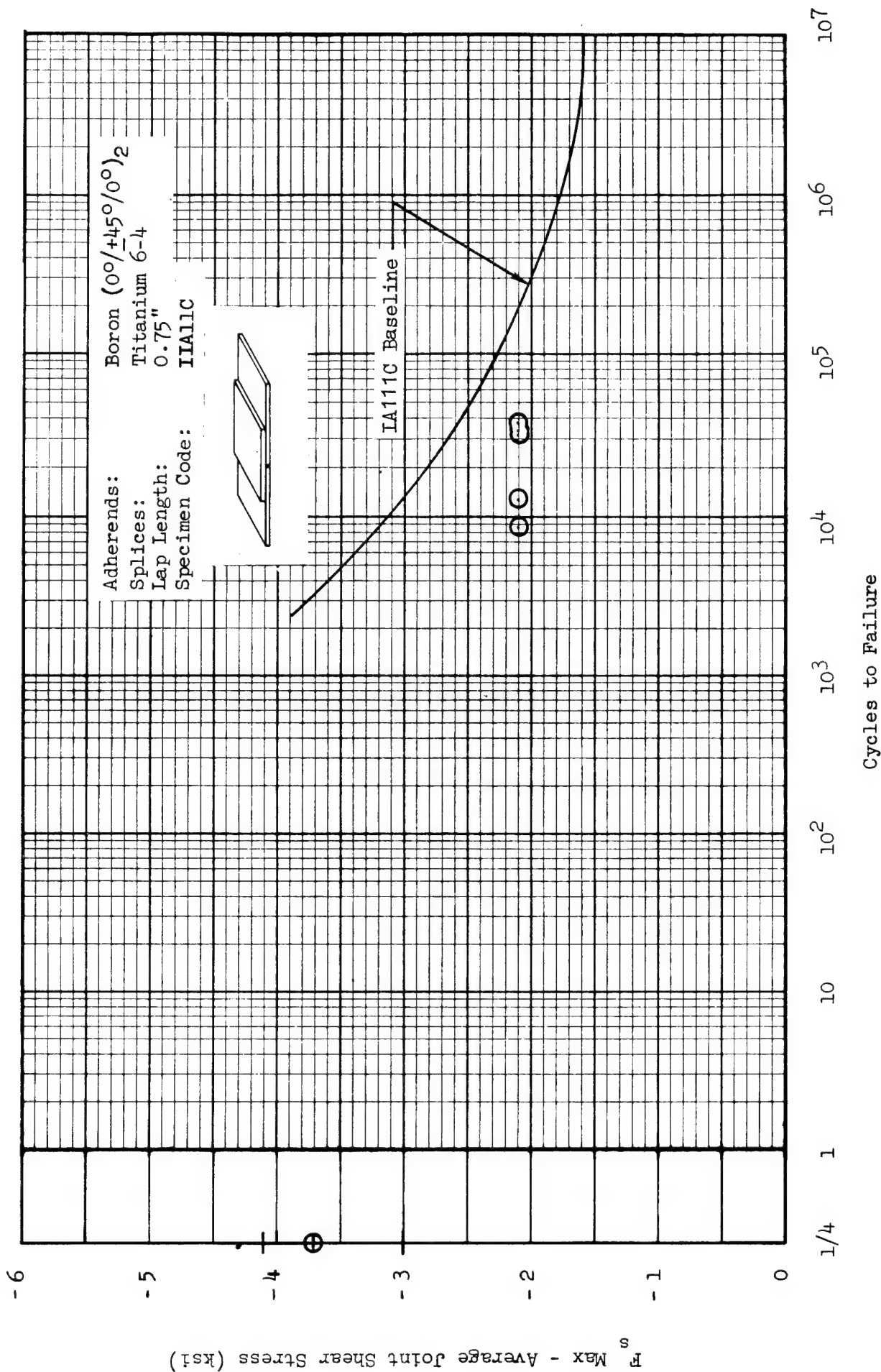


Figure 48 Fatigue Strength of Bonded Single Splice Butt Joints
 Baseline Data, Configuration IIA, R = +10.0

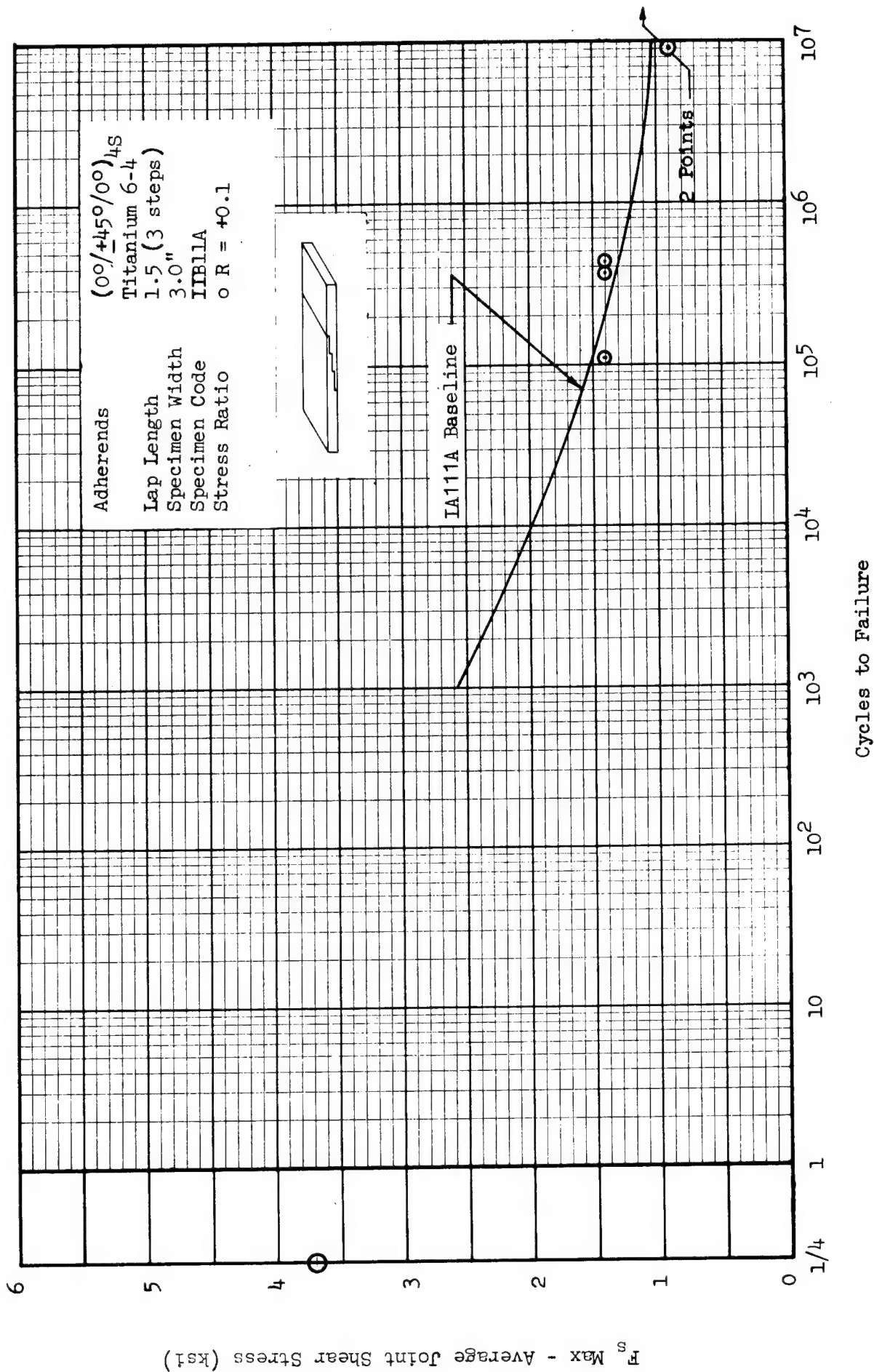


Figure 49 Fatigue Strength of Bonded Step Lap Joints;
 Configuration IIB, Boron: Titanium, Baseline Data

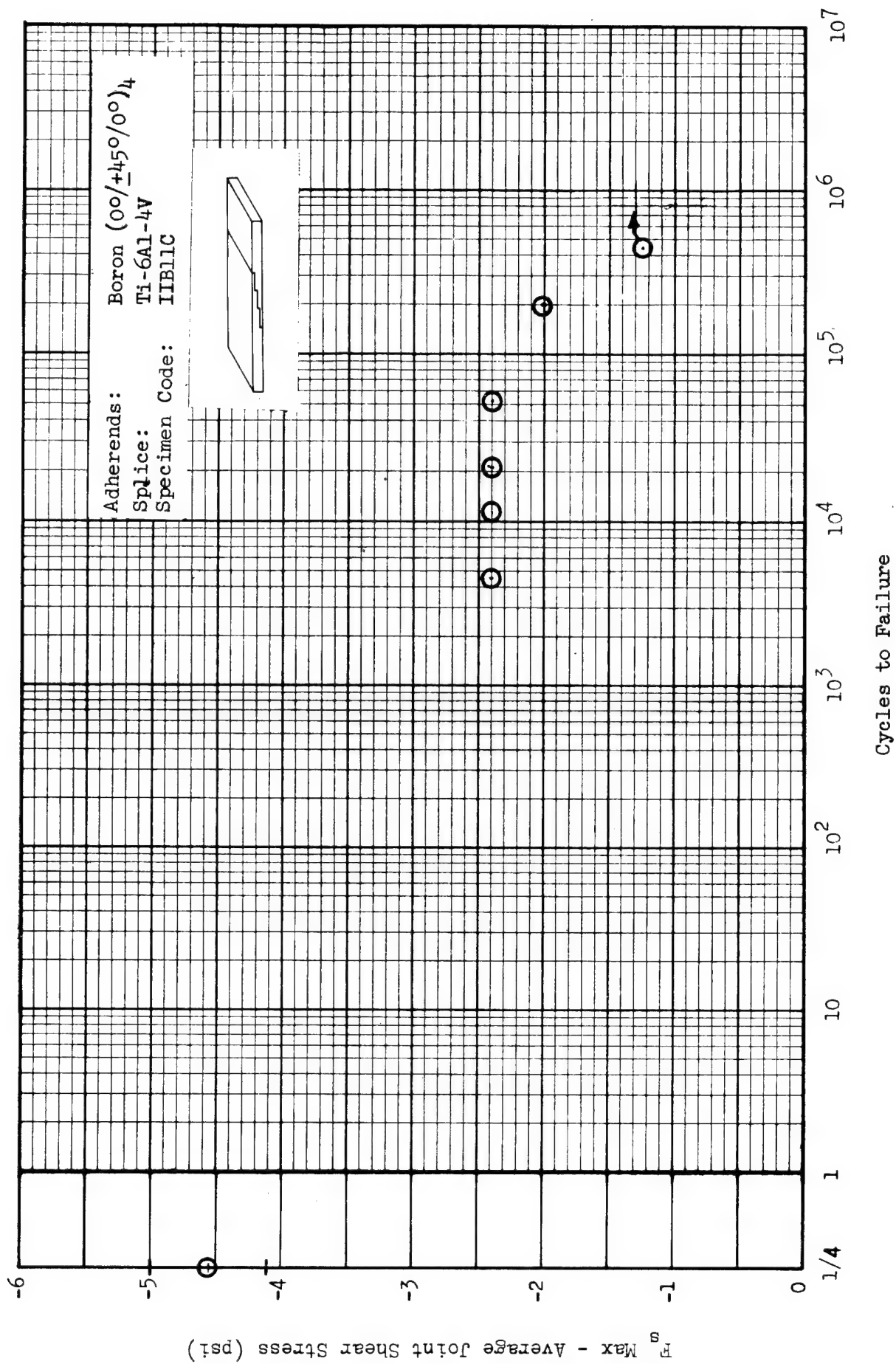


Figure 50 Fatigue Strength of Single-Scarf Butt Joints
 Baseline Data, Configuration IIB, R = +10.0

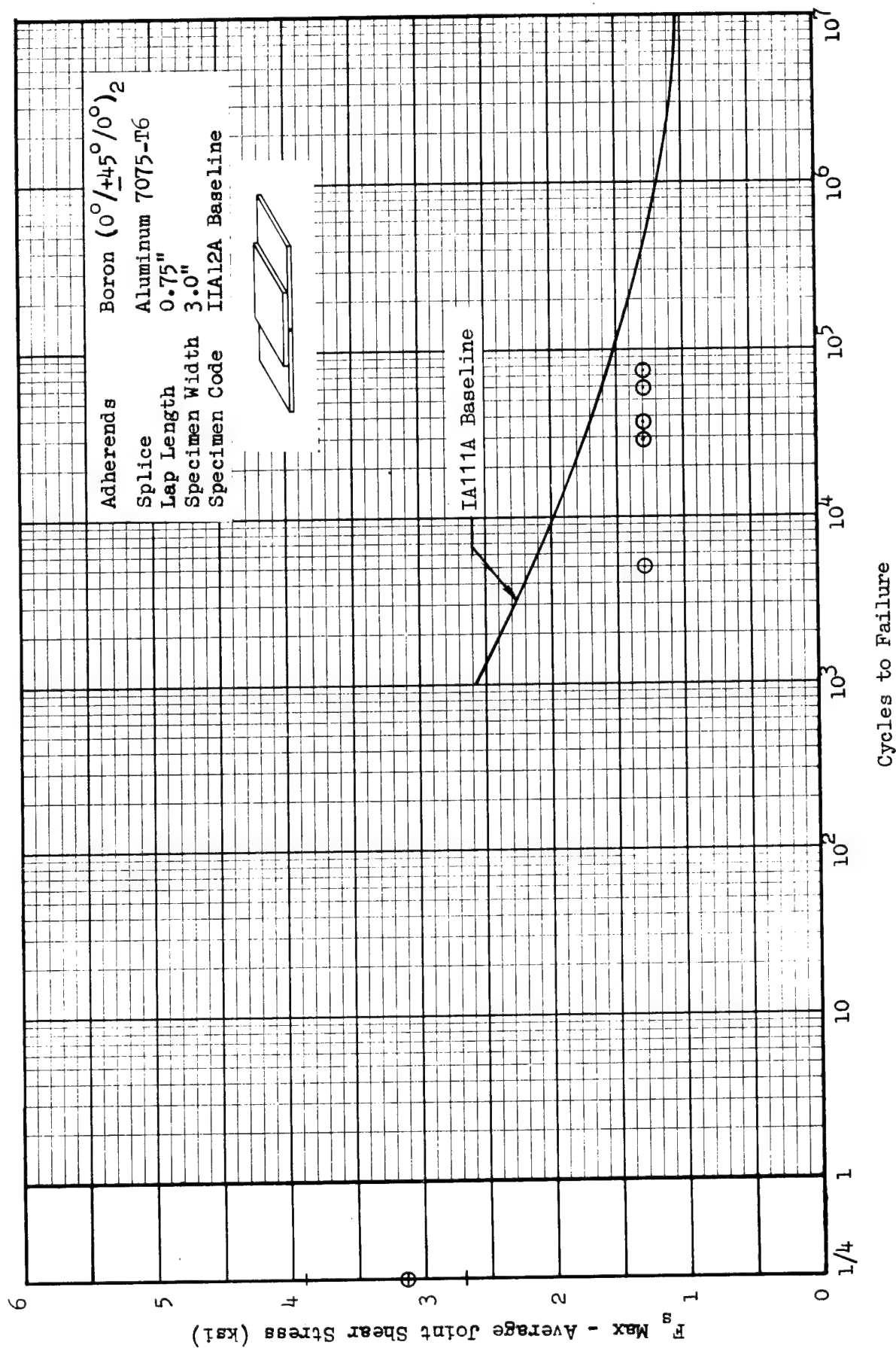


Figure 51 Fatigue Strength of Bonded Single Splice Butt Joints
 Configuration IIA, Boron:Aluminum:Boron; R = +0.1

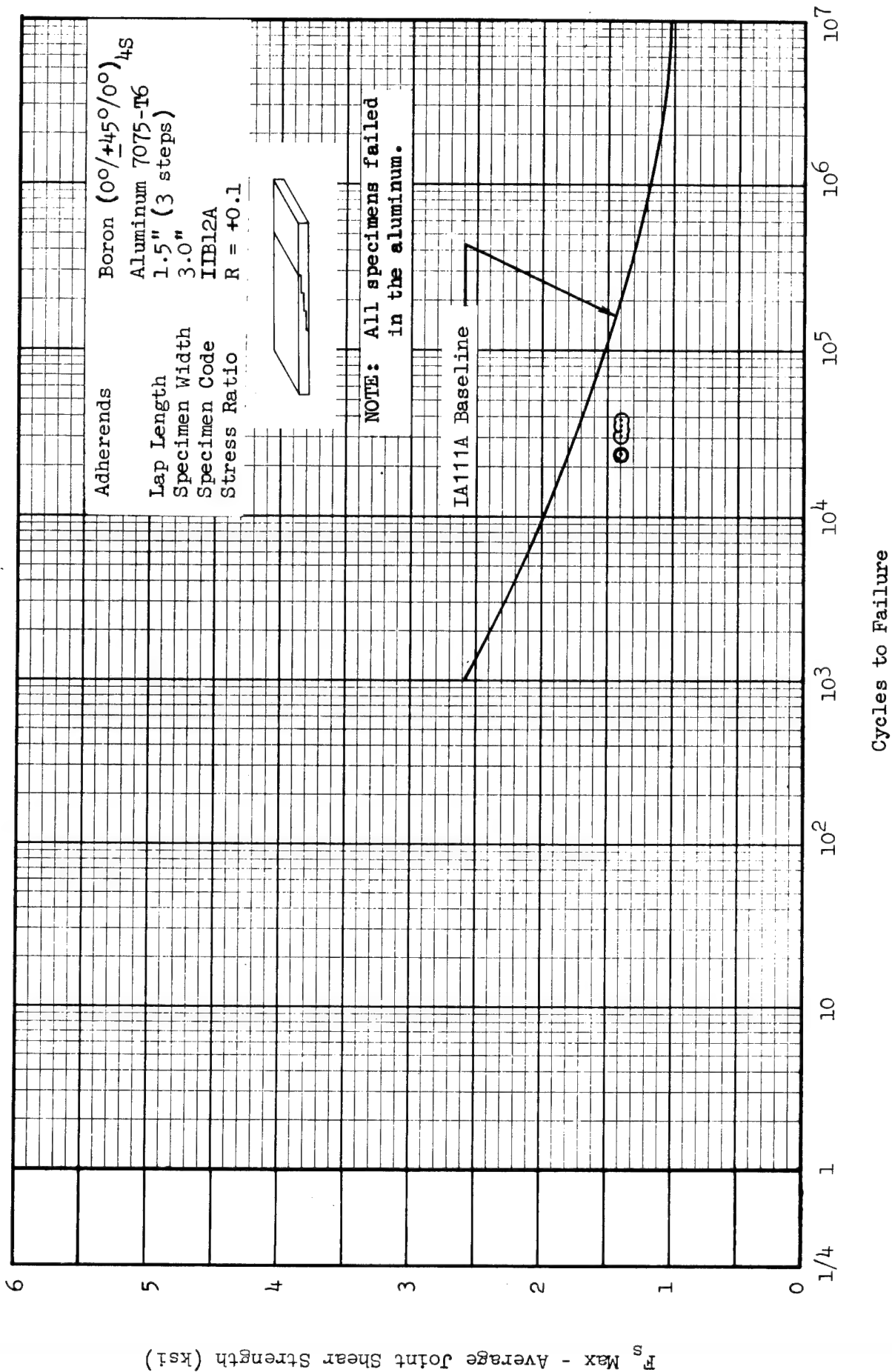


Figure 52 Fatigue Strength of Bonded Step Lap Joints,
Configuration IIB, Boron:Aluminum, Baseline Data

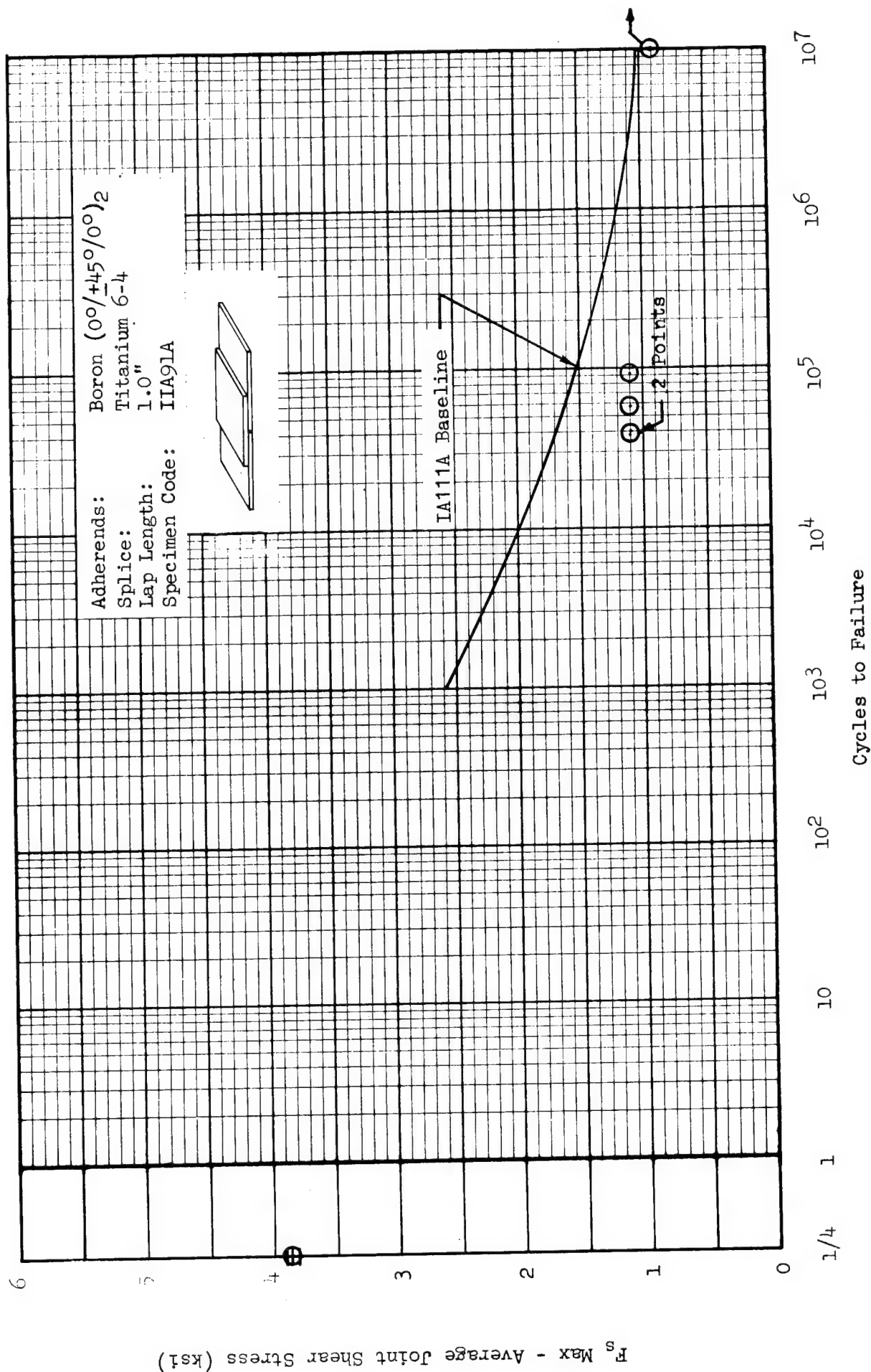


Figure 53 Fatigue Strength of Bonded Single Splice Butt Joints
 Long Lap Effects, Configuration IIA, R = +0.10

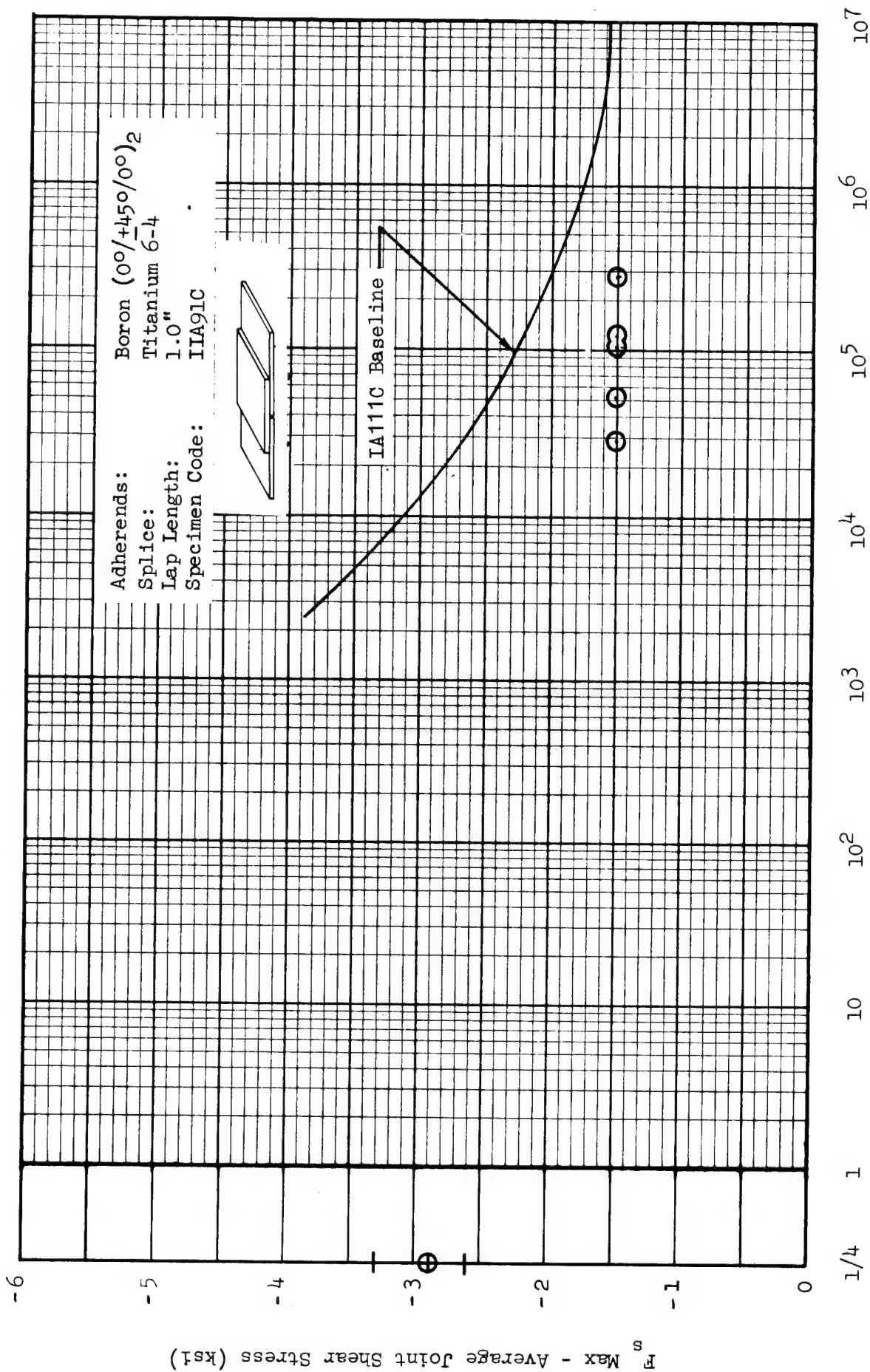


Figure 54 Fatigue Strength of Bonded Single Splice Butt Joints
 Long Lap Effects, Configuration IIA, R = +10.0

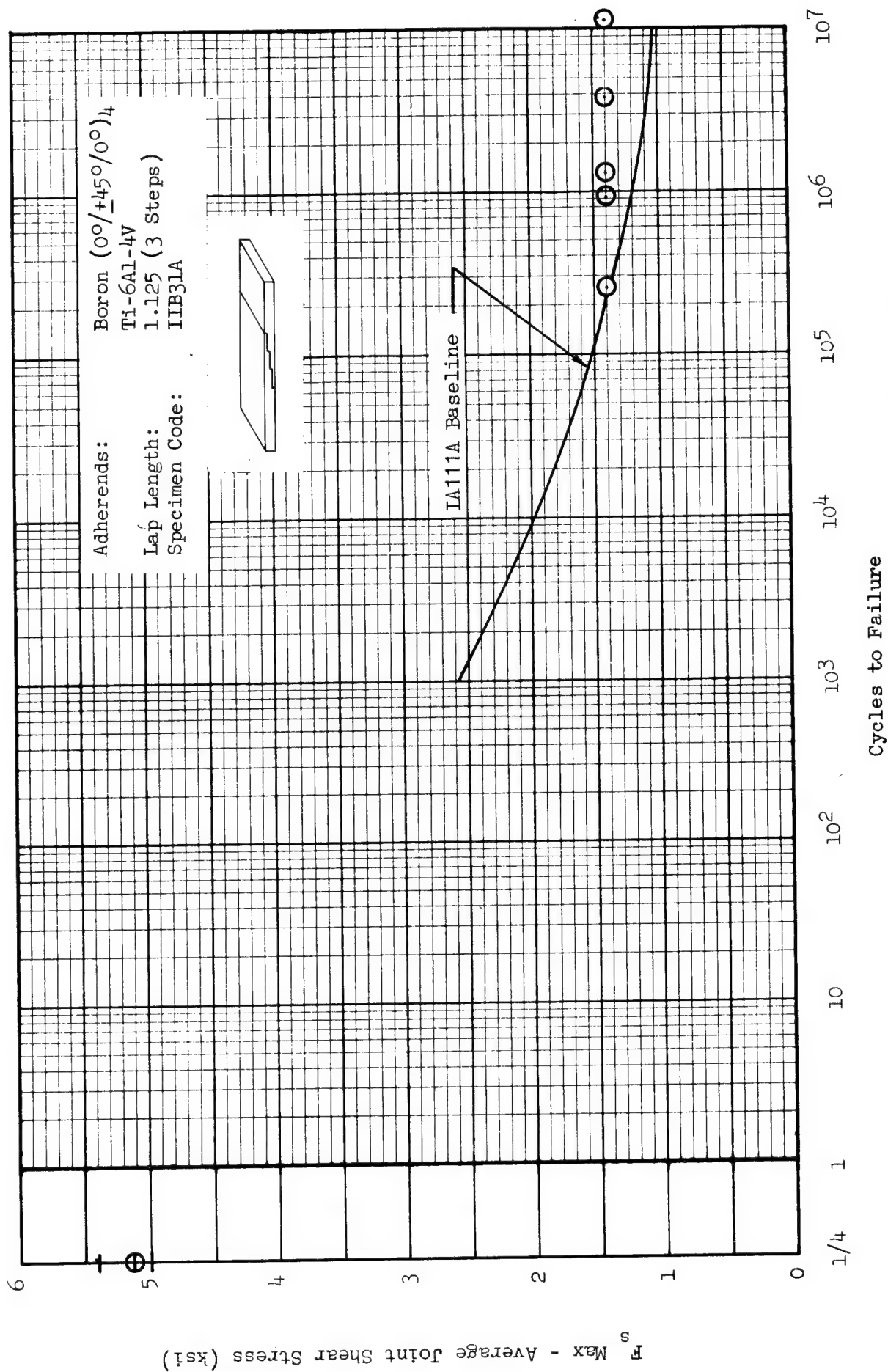


Figure 55 Fatigue Strength of Bonded Single Splice Butt Joints
 Short Lap Effects, Configuration IIB, R = +0.10

2.4.2.4 Phase I Mechanically Fastened Joint Analysis

Two of the four basic joint configurations have been evaluated, in this phase of the program, with mechanical fasteners used in lieu of adhesive in the joint assembly. These two joint concepts are the single splice butt joint and the simulated surface-to-under structure attachment. The joints are identified as Configuration E and F respectively and test specimen details are depicted in Figures 16 and 17.

In order to evaluate the Configuration E joints extensively, two variations were considered, one containing metallic reinforcing shims to improve fastener bearing strength and the second having additional plies of $\pm 45^\circ$ boron to accomplish the same task. Both one-inch and three-inch wide specimens are included in this evaluation with the one-inch specimen having received the most attention. Other parameters evaluated are similar to the bonded joint studies and include: adherend combinations, splice materials, fiber orientation, thickness, fastener edge distance, etc. Complete details of the mechanical joint evaluation program are included in Table XV. Specific program tasks are discussed in detail in the following sections.

2.4.2.4.1 Baseline Data - One specimen configuration was selected as the baseline or standard for comparison of all parametric study results, in the same manner as the bonded joint studies. For the mechanical joints, this baseline was the one-inch, single splice butt joint, Configuration IE111, and sufficient data has been obtained at $R=+0.10$ and -1.0 , with limited data at $R=+10.0$, to construct the constant life diagram shown in Figure 19. This baseline specimen has boron at $0^\circ/\pm 45^\circ$ orientation, titanium shims, and includes a titanium splice plate. Test data are presented in Figures 56 and 57 for $R=+0.10$ and -1.0 .

There is considerable scatter in both sets of data for the baseline specimen, considerably more than for the bonded joints test data. In each case the log-mean of the data has been determined at various stress levels and the smooth curves faired as close as possible to those mean data points. As noted in the low cycle region of each curve, there is no deviation from the joint ultimate strength from $1/4$ cycle to approximately 10^2 cycles. Data is not available in this area but the curve has been positioned based on the following rationale.

The average static strength of this joint was determined to be 42.0 ksi which is based on the failing load divided by the shimmed net section area. All static failures were in the boron adherend, however, at the ends of the reinforcing shims. This could lead to the use of the gross section stress (70.0 ksi in this case) at the 1/4 cycle except that almost all fatigue failures occur in the net section area. Also, the low cycle data (IE511A) tends to force the faired mean curve toward the 42.0 ksi net section stress, rather than the 70.0 ksi gross section stress. Further, an interesting phenomena associated with the fatigue of composites with a through hole was found in the C-5A Boron Slat Program, and reported in Reference 8. In this program, 8-ply, $0^\circ/\pm 60^\circ$ boron laminates with a $K_t = 2.8$ (a 1/16" diameter drilled hole) were tested at $R = +0.10$ and -0.30 . Plots of net section stress versus endurance show little difference between the allowable stress at 1/4 cycle and 10^7 cycles; i.e., the curves have practically zero slope. All failures were in the net section, however.

Combining these data, then, the low cycle portion of the baseline curves has zero slope from the 1/4 cycle average net section stress to approximately 10^2 cycles and then the curve is faired through the mean of the low cycle data and the IE111 baseline data points. The specimens here introduce bearing stresses in the adherend not present in the Reference 8 specimens, resulting in a deviation from the zero slope curves established for open holes.

Initial fatigue tests of the Configuration E specimens, composite-to-metal mechanical joint, resulted in failure of the metal portion of the joint. A number of attempts were made to correct this deficiency. The first attempt replaced the 7075-T6 aluminum portion of the joints with 8Al-1Mo-1V titanium of equal thickness but these specimens failed in the countersunk portion of the titanium. This led to the replacement of the HL19PB6 flush head fasteners by HL18PB6 button head fasteners for the metal-to-metal portion of the joint but this only moved the failure to the titanium splice plate. This second failure mode led to the final design which consisted of the boron portion joined to 8Al-1Mo-1V titanium which was 50 percent thicker than the composite. These specimens were assembled with flush head fasteners, HL19PB6 series, used on the boron-to-titanium half and button head fasteners, HL18PB6 series, used on the

titanium-to-titanium half. Fatigue tests on two specimens of this configuration resulted in fatigue failures of the boron portion of the joint. Based on these results, all of the Configuration E specimens were disassembled and new metal splice plates and metal joint halves were machined from 8Al-1Mo-1V titanium; 0.125" material was used with the 8-ply boron specimen halves and 0.250" material was used with the 16-ply boron specimen halves.

No further problems were encountered in testing the $R = +0.10$ specimens, but repeated attempts to obtain fatigue failures in the joints of the $R = +10$ baseline specimens were unsuccessful. The first specimen was tested at a maximum stress of -30.0 ksi with no failure after 7.5×10^5 cycles. Two additional specimens were tested at $F_{\max} = -40.0$ ksi with a compressive failure in the laminate and at the end tabs after 2.65×10^5 and 1.88×10^5 , respectively. Therefore, all $R = +10.0$ fatigue tests were discontinued and the remaining test specimens were used in other program tasks. For the specimens tested at a stress ratio of $R = -1.0$ the majority of failures occurred in the fasteners. Initially these failures were attributed to excessive bending action at the joint during the reversed cycling. It was believed that the 0.003-inch clearance between the joint and the support plates was allowing excessive bending of the splice plate which resulted in repeated tension loading of the fastener through the steel collar. However, subsequent testing with no clearance around the joint still resulted in fastener fatigue failures.

Two additional series of tests were run with the baseline configuration, one involved a boron splice plate with titanium shims rather than the titanium baseline and the other with 0° fiber orientation in the adherend and splice plate. These data are presented in Figures 58 and 59. The data in Figure 58 with the boron splice plate have approximately the same static strength as the baseline and the fatigue data is within the scatter of the baseline results. The same is true for the 0° fiber orientation and boron splice plate, Configuration IE122A.

2.4.2.4.2 Ply Stacking Order - For this parametric study, the 0.012" titanium reinforcing shims in the baseline specimen are replaced with two plies of boron at $\pm 45^\circ$ orientation. Tests have been conducted at $R = +0.10$ and $R = -1.0$ and data are

presented in Figures 60 and 61. In both instances only five specimens have been tested and the scatter is large; however, the fatigue endurance compares well with the baseline tests. The static ultimate stresses are lower than the baseline results, with failures in the net section, but the fatigue endurance is equivalent to the higher strength baseline. Comparison between the two sets of data on the basis of percent F_{tu} shows the boron reinforcing shims to have approximately a 15% improvement in fatigue strength.

2.4.2.4.3 Edge Distance Effects - To evaluate the effect of fastener edge distance on fatigue endurance, specimens with 1.5 edge distance (e/D) (compared to 2.0 on the baseline) have been tested. These specimens are identified as IE311A and IE321A and test results are presented in Figures 62 and 63. The IE311A configuration is identical to the baseline specimens except for fastener edge distance. Static test results are approximately the same, but based on these limited fatigue tests, the shorter edge distance results in a 20% decrease in fatigue strength.

The IE321A specimens have the boron adherend, shims, and splice plate and even though the average ultimate strength is low, the fatigue data does not show a significant reduction, compared to the baseline, with the short edge distance. Again this is based on limited data but the trend appears to be that when fatigue is the design criteria, the all boron, mechanically fastened joint is more optimum than the Boron/Ti combination. This is discussed further in 2.5, Fatigue Analysis.

2.4.2.4.4 Thickness Effects - To evaluate the effect of thickness on fatigue endurance, specimens IE411A and IE421A have been fabricated and tested. These specimens have a 16-ply, $0^\circ/\pm 45^\circ$ boron adherend as compared to the 8-ply baseline specimen. Five specimens of each configuration were tested and the data is presented in Figure 64. The data from the IE411A specimens with titanium reinforcing shims, exhibits reasonable scatter but shows a slight reduction in fatigue strength compared with the baseline data. The IE421A data (specimens with $\pm 45^\circ$ boron reinforcement) are widely scattered (two decades) but also show the same trend toward reduced allowables. This reduction in fatigue strength is associated with fastener clamp-up as discussed in 2.5.

2.4.2.4.5 Preload/Low Cycle Data - Ten IE411A specimens have been tested to evaluate the effect of preload on the specimen fatigue endurance and to obtain limited low cycle fatigue data. For the preload evaluation, the test specimens were statically loaded in tension then removed from the static test machines, reinstalled in the fatigue test apparatus, and cycled to failure. Two specimens were preloaded to 2800 lbs. tension and the remaining three were loaded to 2500 lb. Test results are presented in Figure 65 and show good agreement with the baseline data. Based on this, the preload for the mechanically fastened joints has little effect on fatigue endurance which is also true for the bonded joints as discussed previously.

The low cycle data is also presented in Figure 65. These tests were run at higher stress levels in order to induce failures in the lower cyclic range to aid in locating the mean fatigue curve. Also, the rate of cyclic loading was 10 cps compared with the higher loading rate (approximately 60 cps) for the other program tests. These data have been used along with the IE111 baseline data to establish the basic joint, mean fatigue curve. These results also indicate that the range of cyclic loading rates evaluated have no apparent effect on fatigue endurance.

2.4.2.4.6 Pinned Joints Evaluation - Pin bearing tests of the $0^\circ/\pm 45^\circ$ boron-epoxy laminate reinforced with titanium shims and $\pm 45^\circ$ plies of boron have been conducted. These test specimens as shown in detail in Figure 16 and are identified as the 7226-1302IE-15A, -17A, and -19A assemblies. Bearing loads were introduced through a 3/16" diameter steel pin loaded in double shear. Pin edge distances (e/D) evaluated were 1.5 and 2.0. Static test data developed from these tests is comparable to the data published in Reference 8 for e/D = 1.5 and 2.0. Fatigue tests of five specimens of each configuration were conducted at varying stress levels to establish trend curves as shown in Figure 66. The IE711 specimens with titanium shims and e/D = 2.0 shows the highest fatigue endurance of the three configurations tested. The decrease in edge distance to 1.5 has an accompanying reduction in fatigue endurance as expected. These results are comparable to the fastener edge distance evaluation discussed in 2.4.2.4.3. The specimens with the $\pm 45^\circ$ boron reinforcement and e/D = 2.0 show the same reduction in fatigue endurance as those with titanium shims and e/D = 1.5. This is most likely

associated with improved fatigue performance due to fastener clamp-up in the data in 2.4.2.4.3 which is not evident in these tests.

2.4.2.4.7 Configuration IF Data - As a part of the mechanically fastened joint constant amplitude testing, Configuration F joints representing a surface panel to support structure have been evaluated. Typical specimen details are included in Figure 17. These specimens were tested under combined axial loading and bending. The bending was introduced through side loads applied to the free leg of the support Tee.

All the tests were conducted in Lockheed designed resonant frequency fatigue machines. The 8-ply laminate specimens were tested at a maximum axial stress of 40,000 psi at the net section of the shimmed boron and at a stress ratio of $R = +0.1$. A side load of 100 pounds was used on five specimens and a side load of 250 pounds was used on the other five. The increased thickness effect specimens were tested in a similar manner but the maximum axial stress level was 35,000 psi and the side load was 500 pounds. Fatigue failures occurred at either the net section or at the edge of the shimmed boron section. As anticipated, the test data indicated that the fatigue strength of the joint decreased with increased side load. Test data are included in Figures 67 and 68.

2.4.2.5 Phase II Mechanically Fastened Joint Analysis

Phase II of the mechanically fastened joint program is included to extend the Phase I data from a one-dimensional to a two-dimensional evaluation of the basic single splice butt joint configuration. Specimen width has been increased from 1.0 to 2.0 inches with the investigation aimed at evaluating the effects of induced stresses such as those resulting from Poisson's Ratio and combined modes of stress. These test specimens are identified as IIE111 and are identical to the IE baseline specimens (same fiber orientation, shim material, splice plate, etc.) except for width. Test data are presented in Figure 69.

The fatigue data is comparable to the one-inch wide baseline data except that the scatter inherent in these mechanically fastened joints data is greatly reduced. The

trend of reduced fatigue strength with increased specimen width from the bonded single splice butt joint tests is not evident here. Since these specimens are joined with fasteners instead of the adhesive in the wider, bonded joint study, it was expected that the reduction in fatigue endurance associated with the Poisson Ratio in the bonded joints would not be reflected in these tests. Apparently this is the case and adds credence to the theory of brittle, plane strain failure associated with the wide bonded joints.

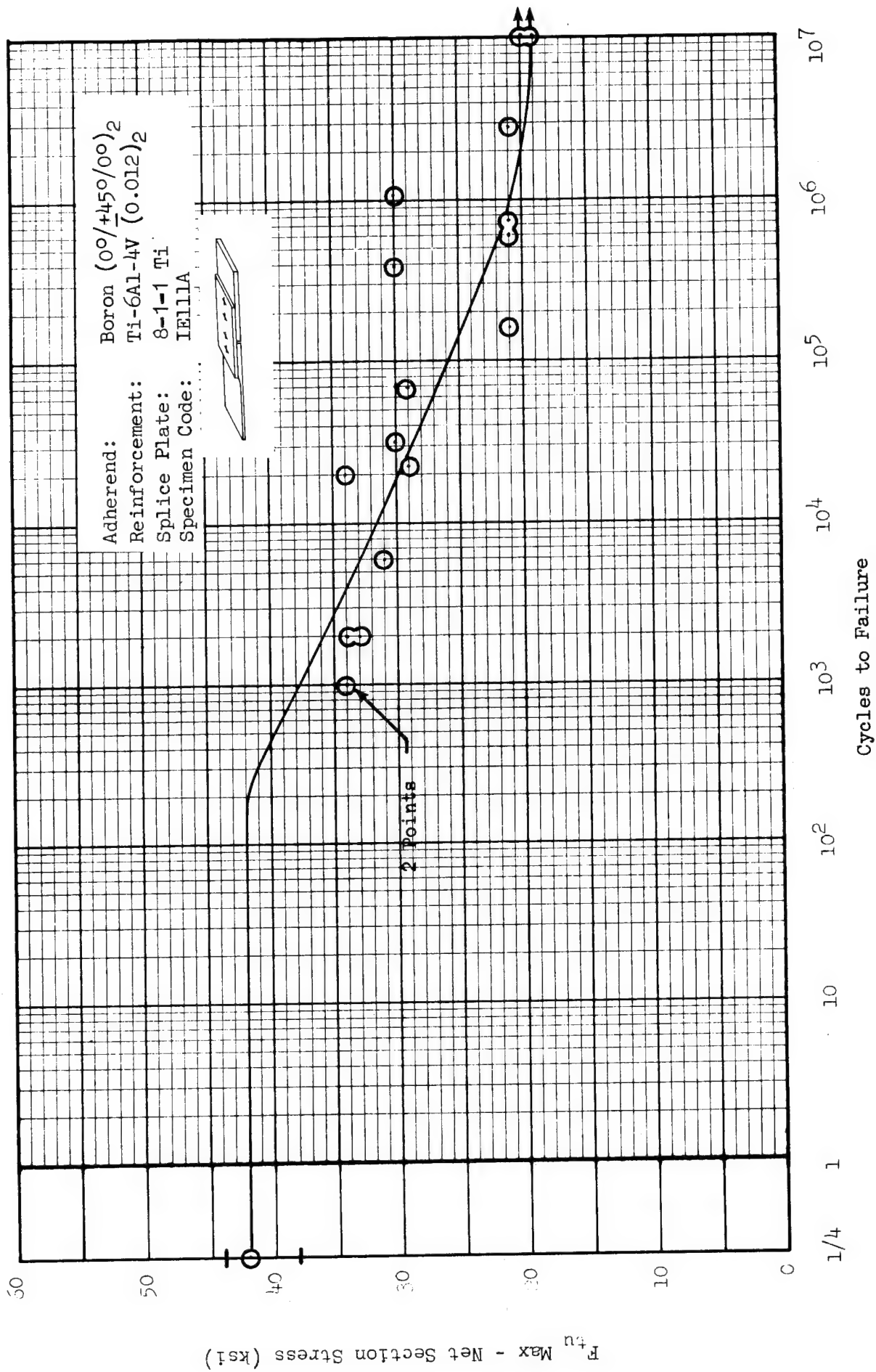


Figure 56 Fatigue Strength of Mechanical Joints Baseline Data, Configuration IE, $R = +0.10$

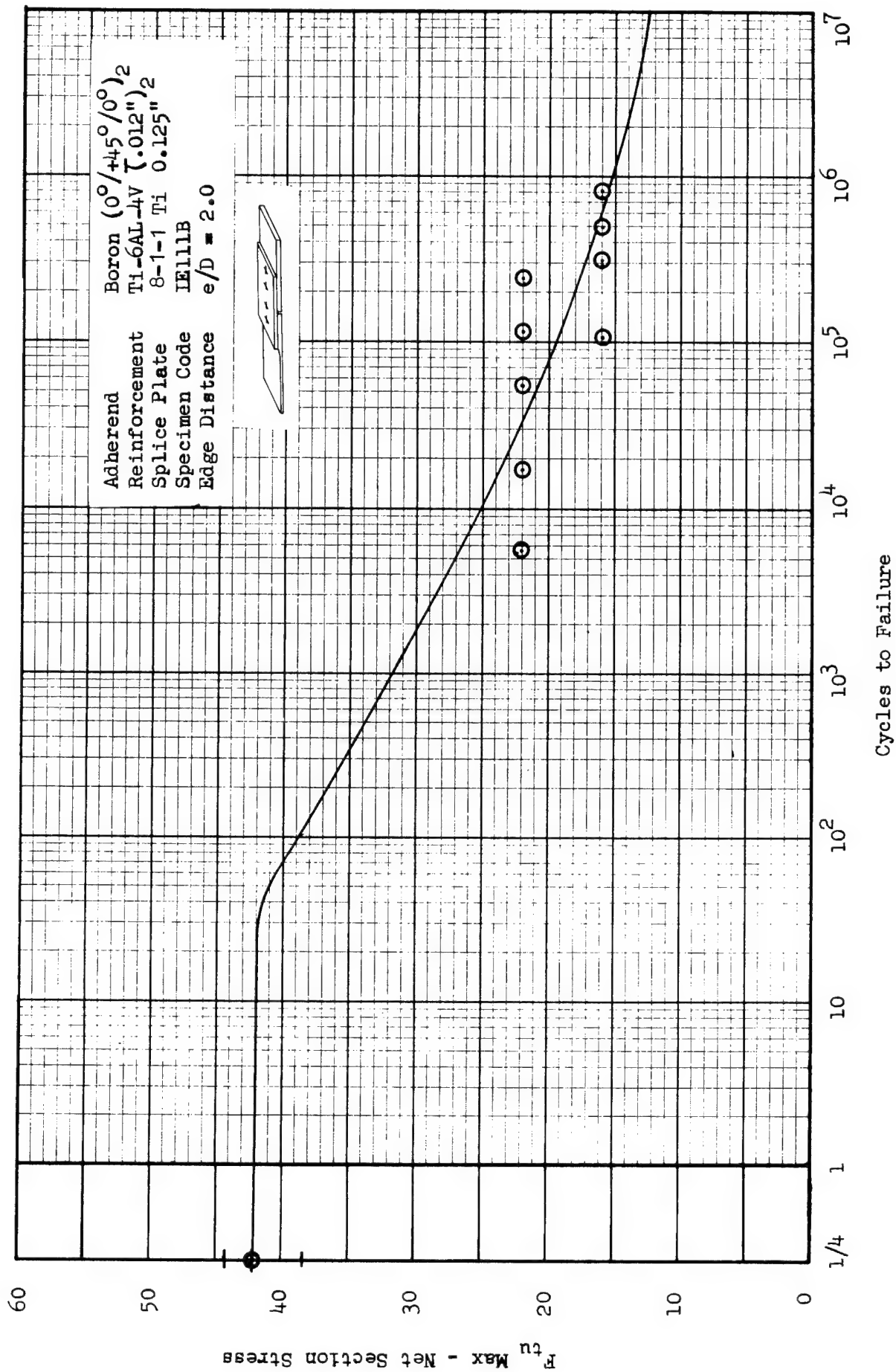


Figure 57 Fatigue Strength of Mechanical Joints, Baseline Configuration IE, Boron: Titanium R = -1.0

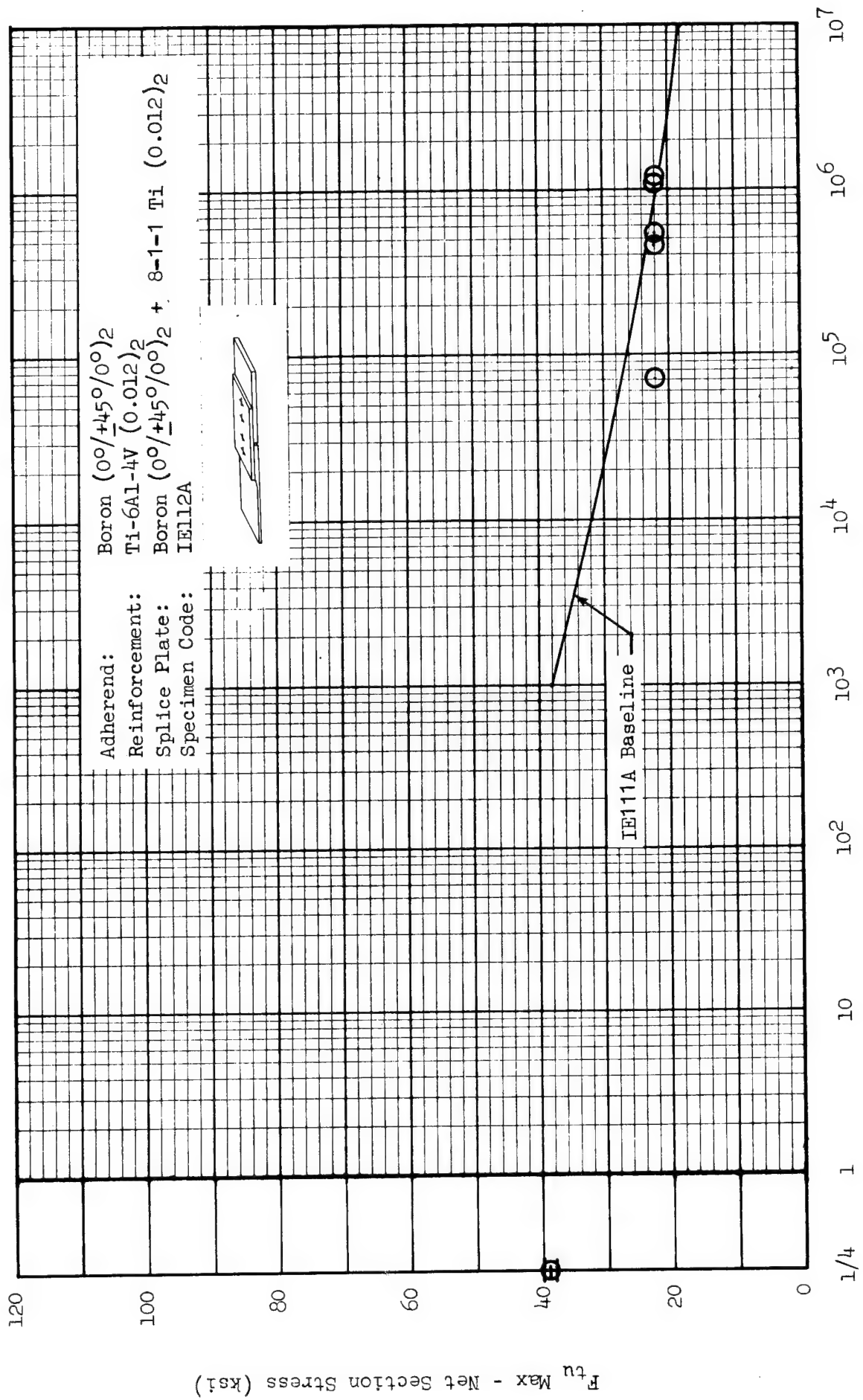


Figure 58 Fatigue Strength of Mechanical Joints Baseline Data, Configuration IE, R = +0.10

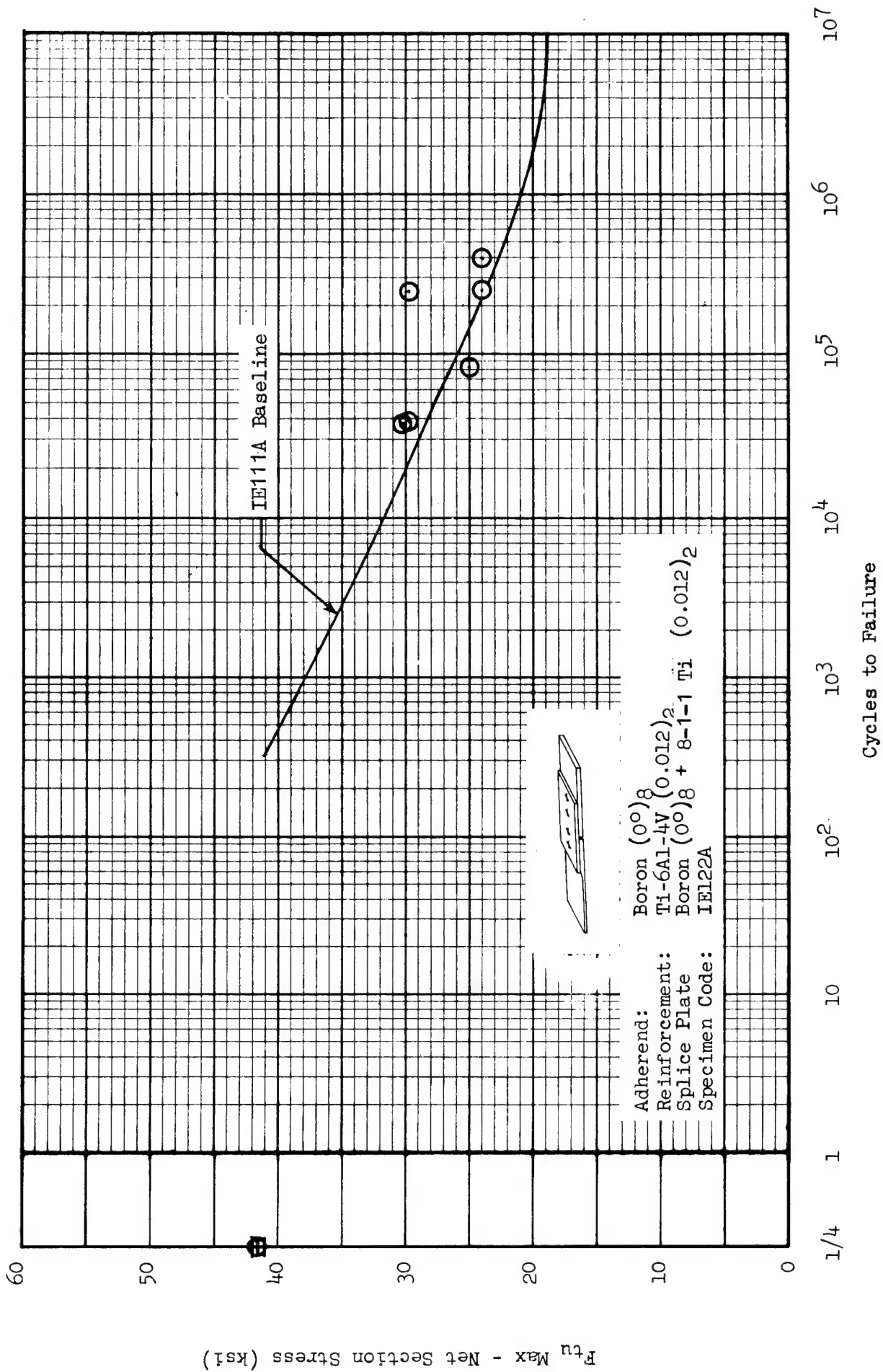


Figure 59 Fatigue Strength of Mechanical Joints Baseline Data, Configuration IE, R = 0.10

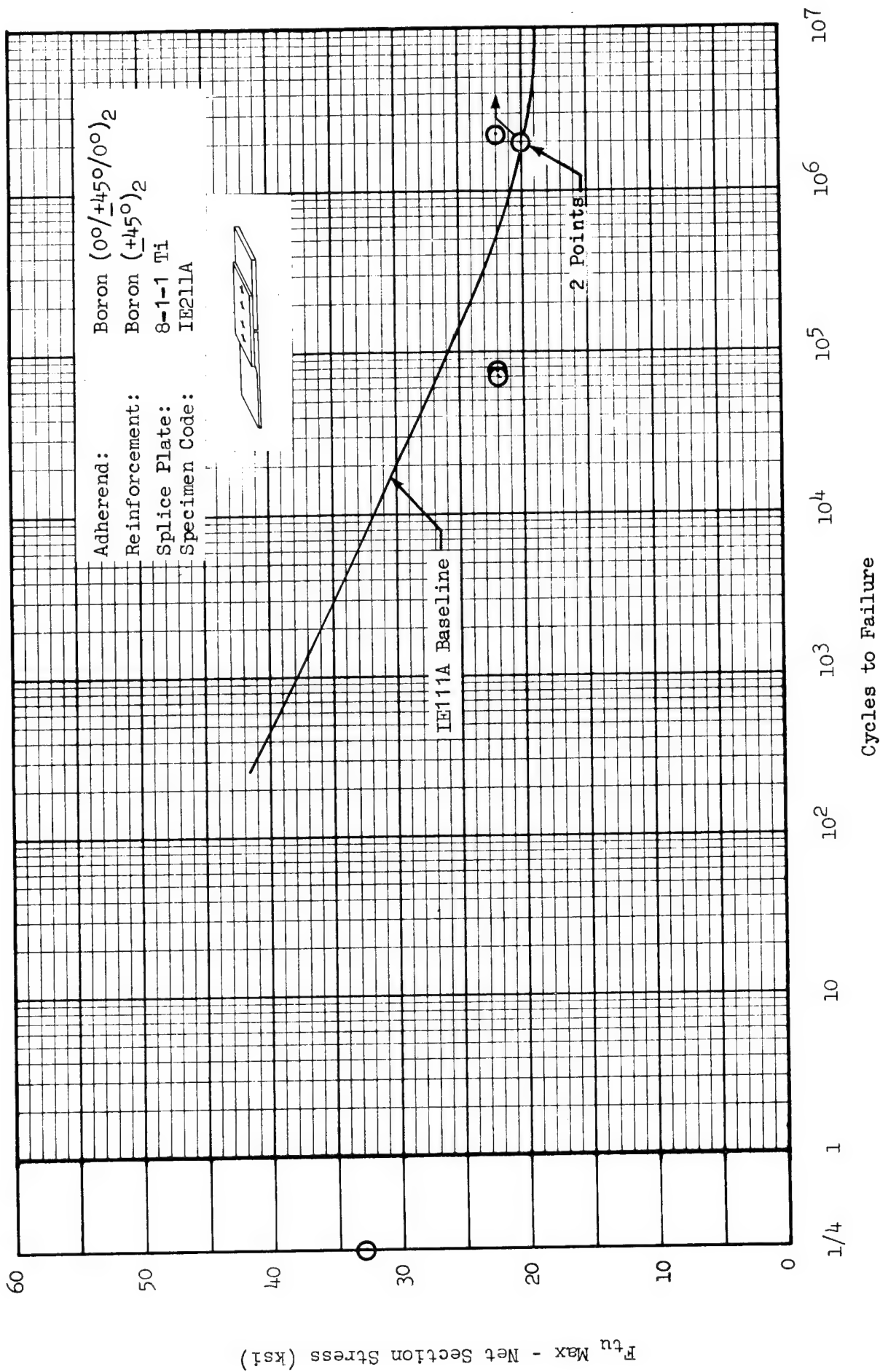
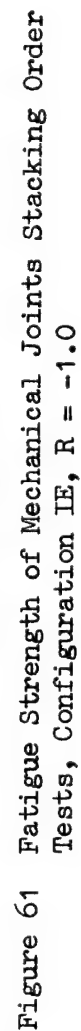


Figure 60 Fatigue Strength of Mechanical Joints Stacking Order Tests, Configuration IE, R = +0.10



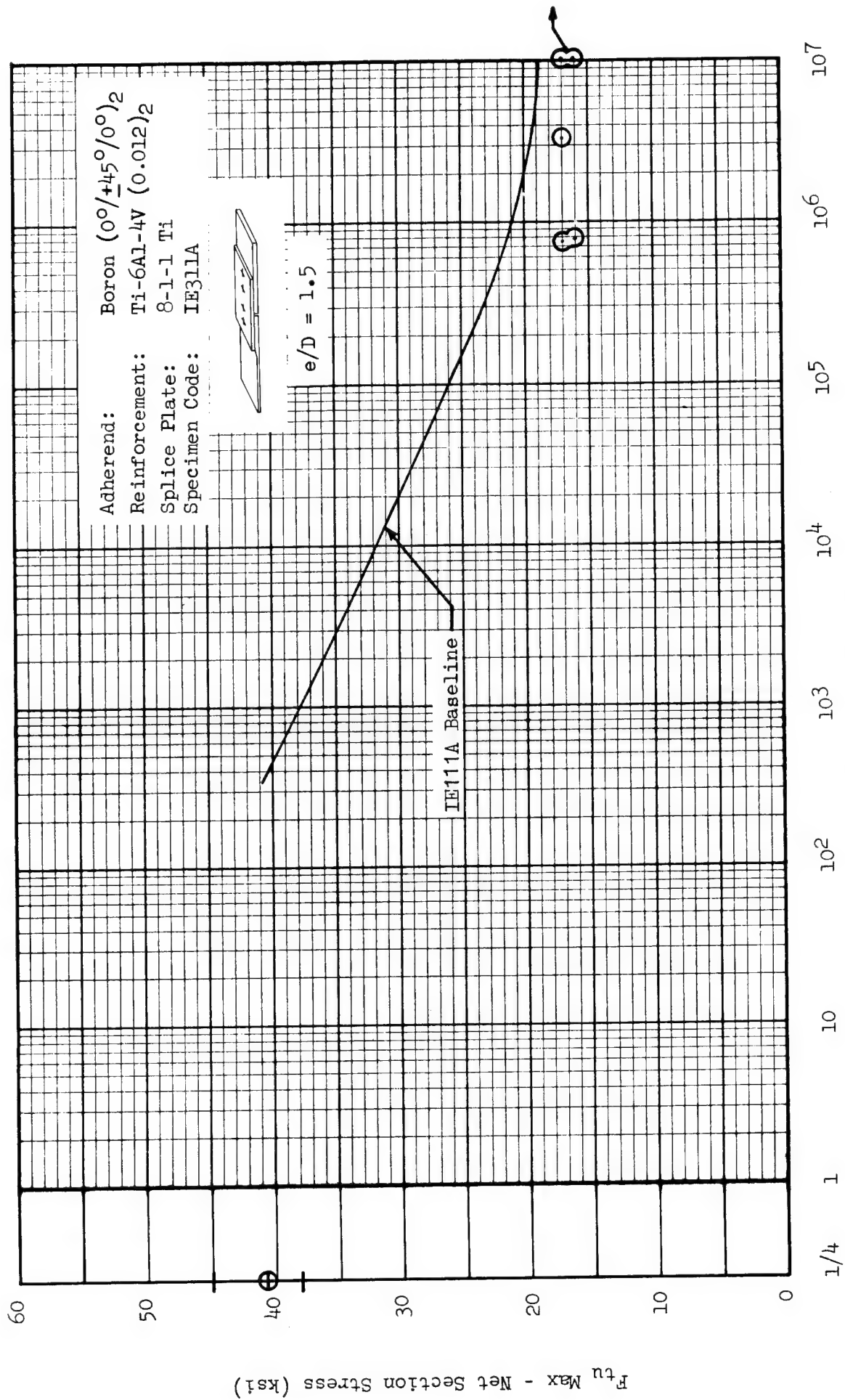


Figure 62 Fatigue Strength of Mechanical Joints Edge Distance Evaluation, Configuration IE, R = +0.10

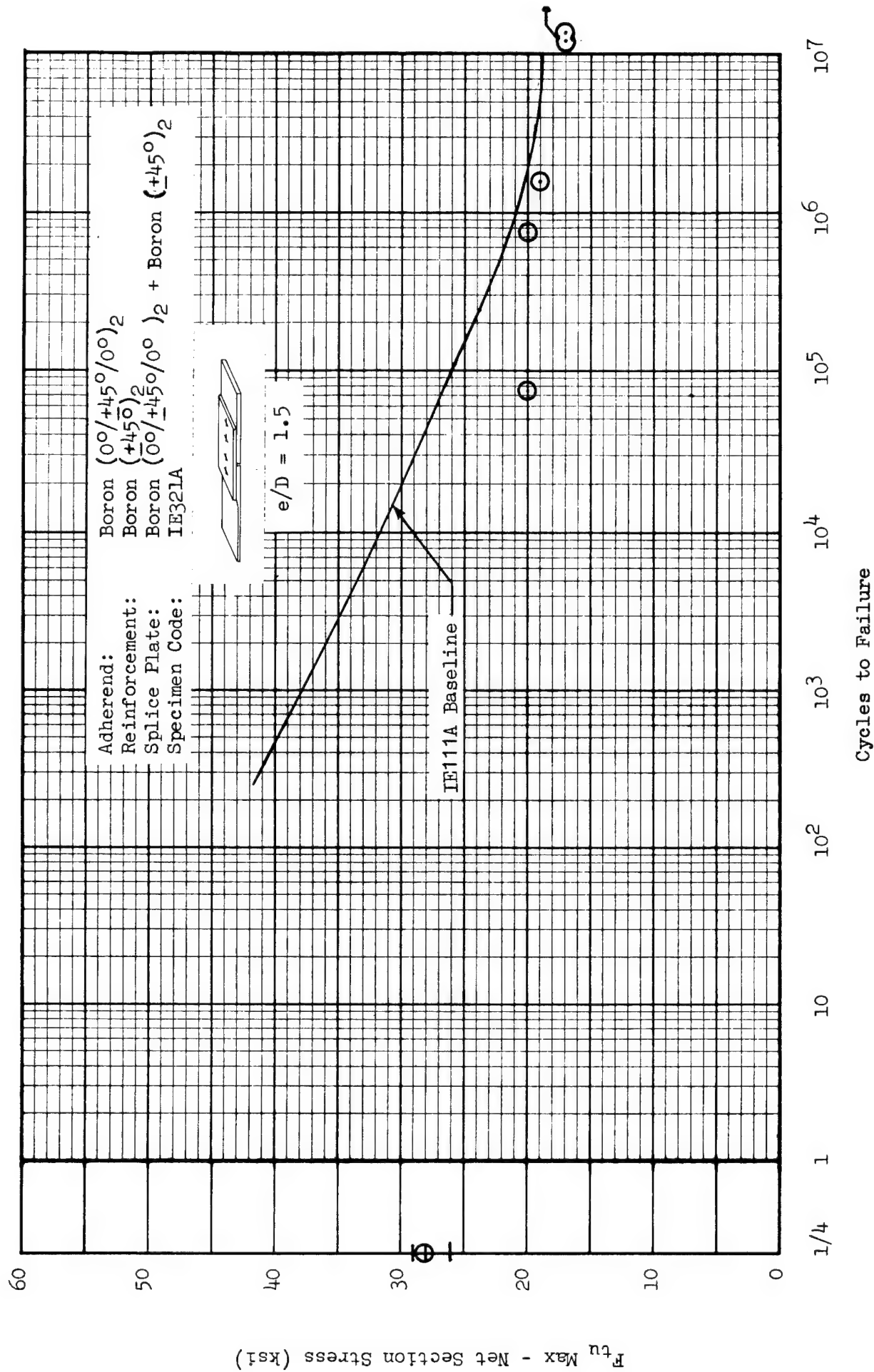


Figure 63 Fatigue Strength of Mechanical Joints Edge Distance Evaluation, Configuration IE, R = + 0.10

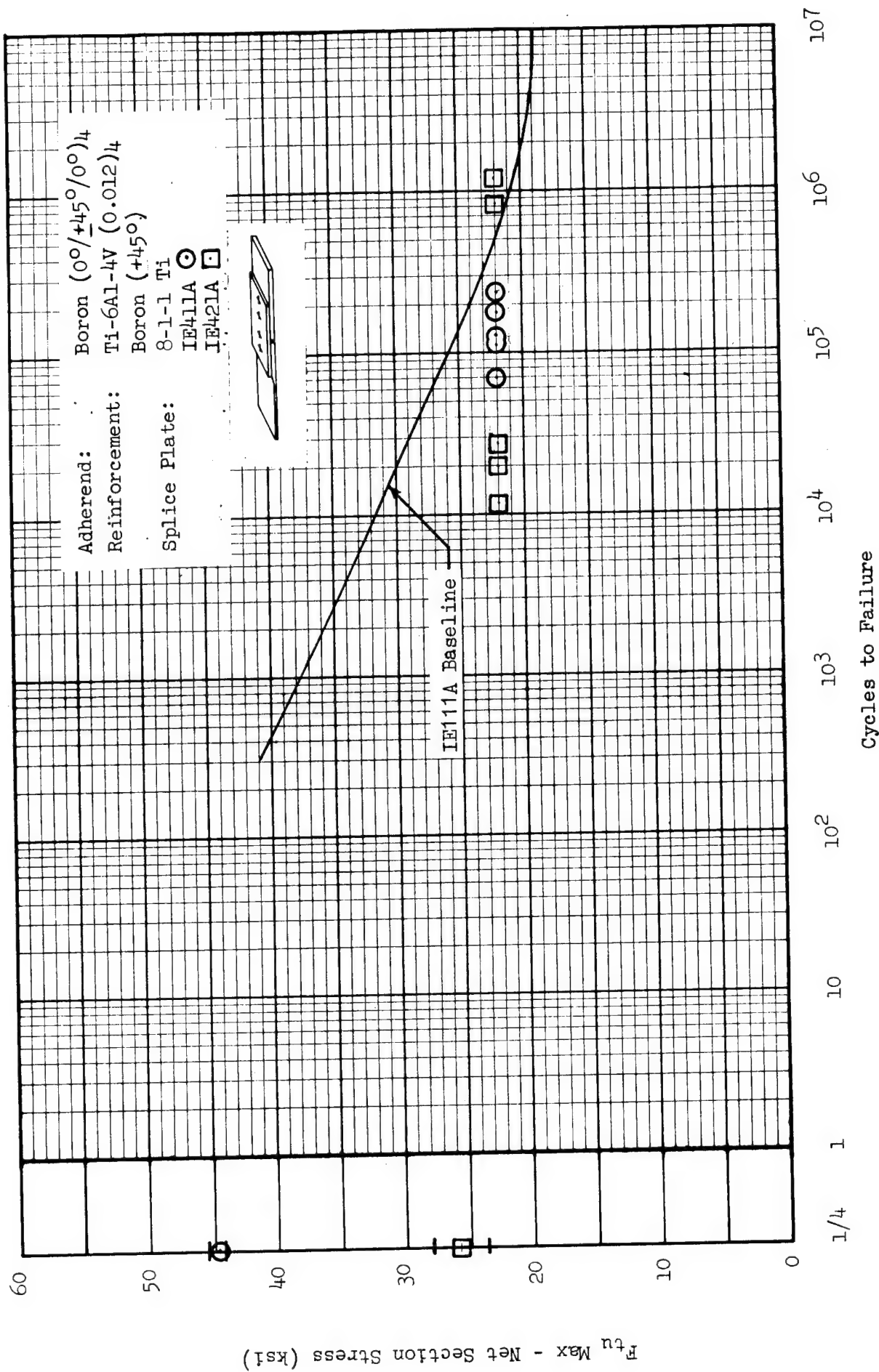


Figure 64 Fatigue Strength of Mechanical Joints: Thickness Effects Tests, Configuration IE, R = +0.10

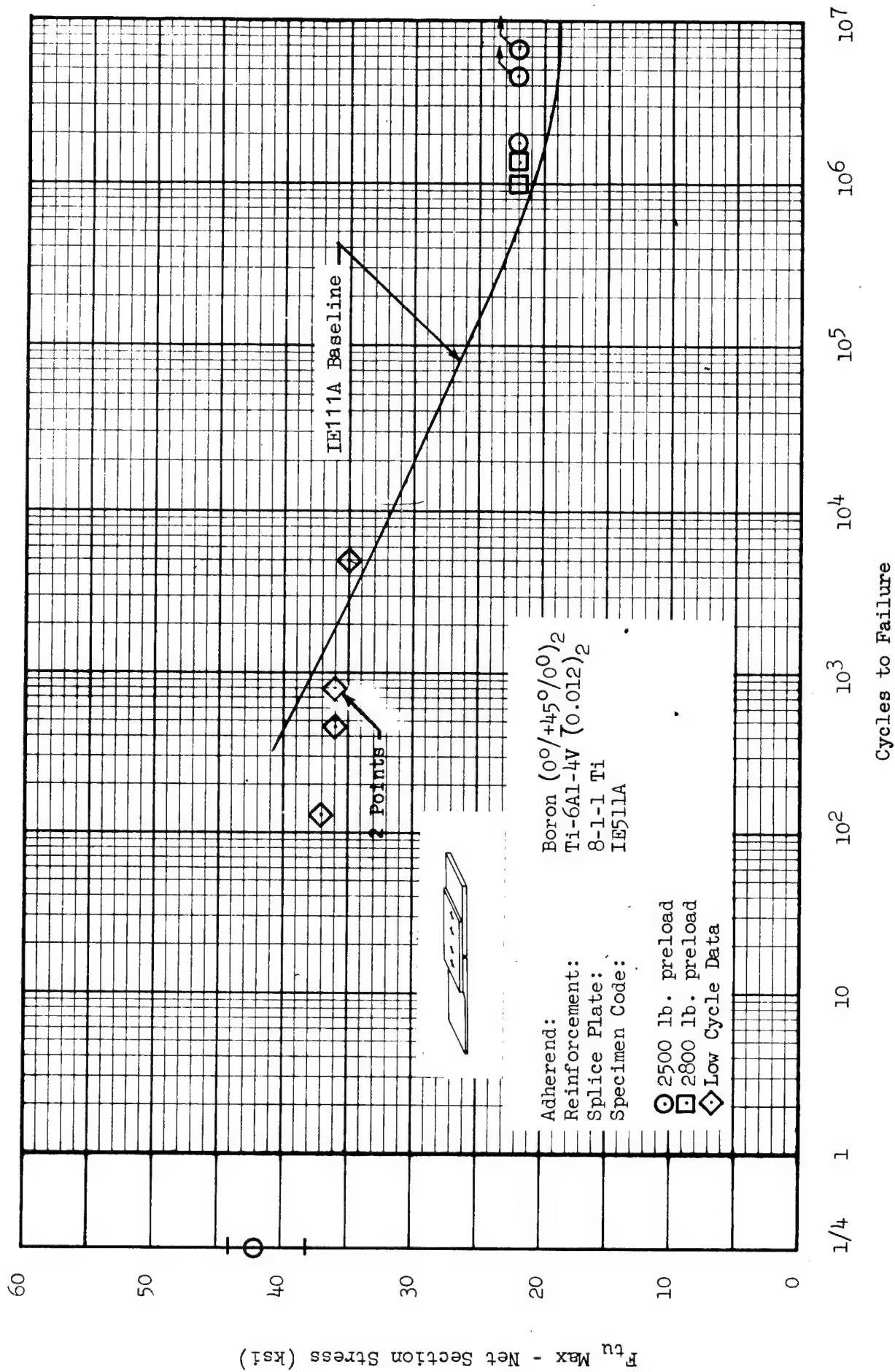


Figure 65 Fatigue Strength of Mechanical Joints, Preload and Low Cycle Data, Configuration IE, R = +0.1

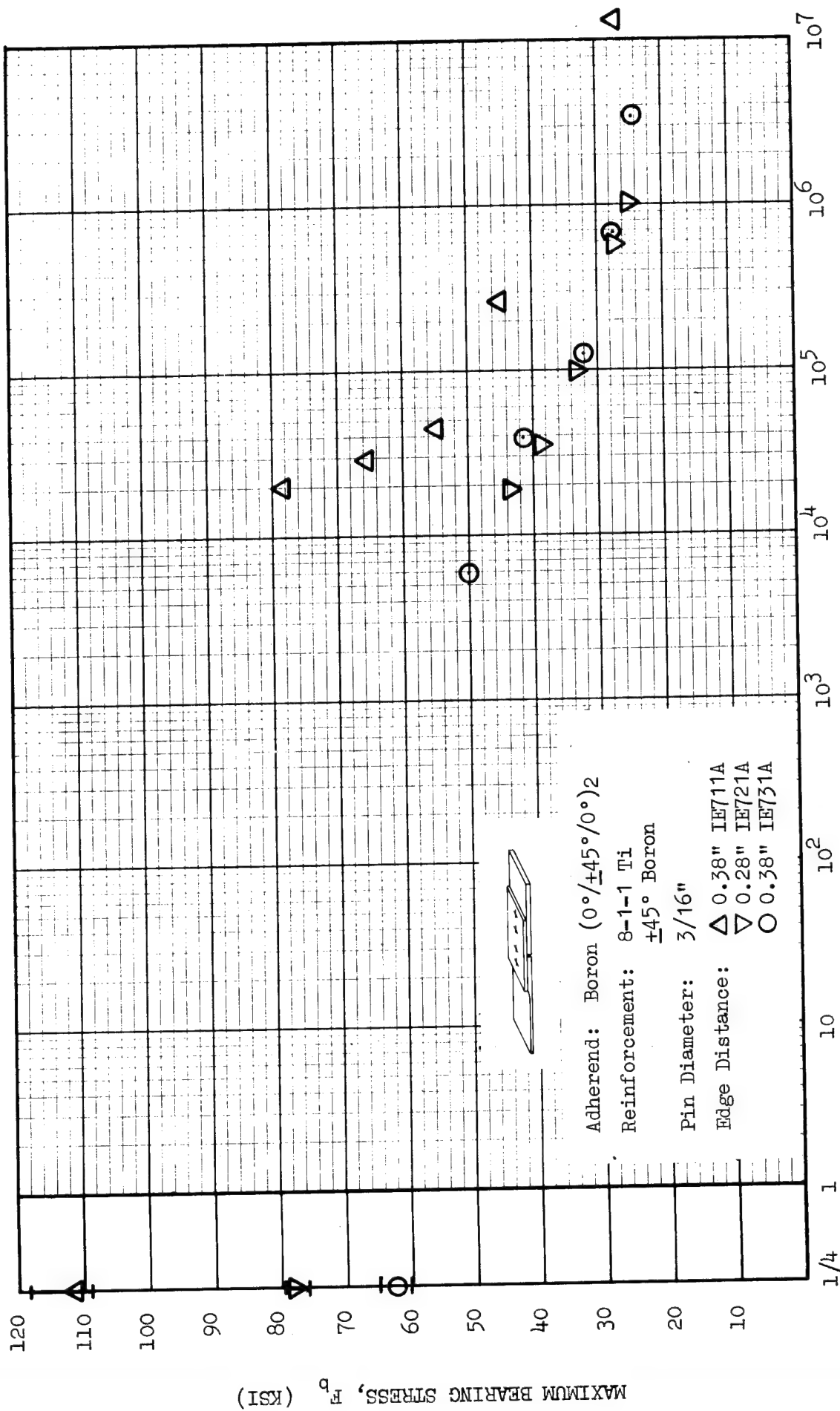


Figure 66 Fatigue Strength of Mechanical Joints
 Pinned Joints/Edge Distance Evaluation

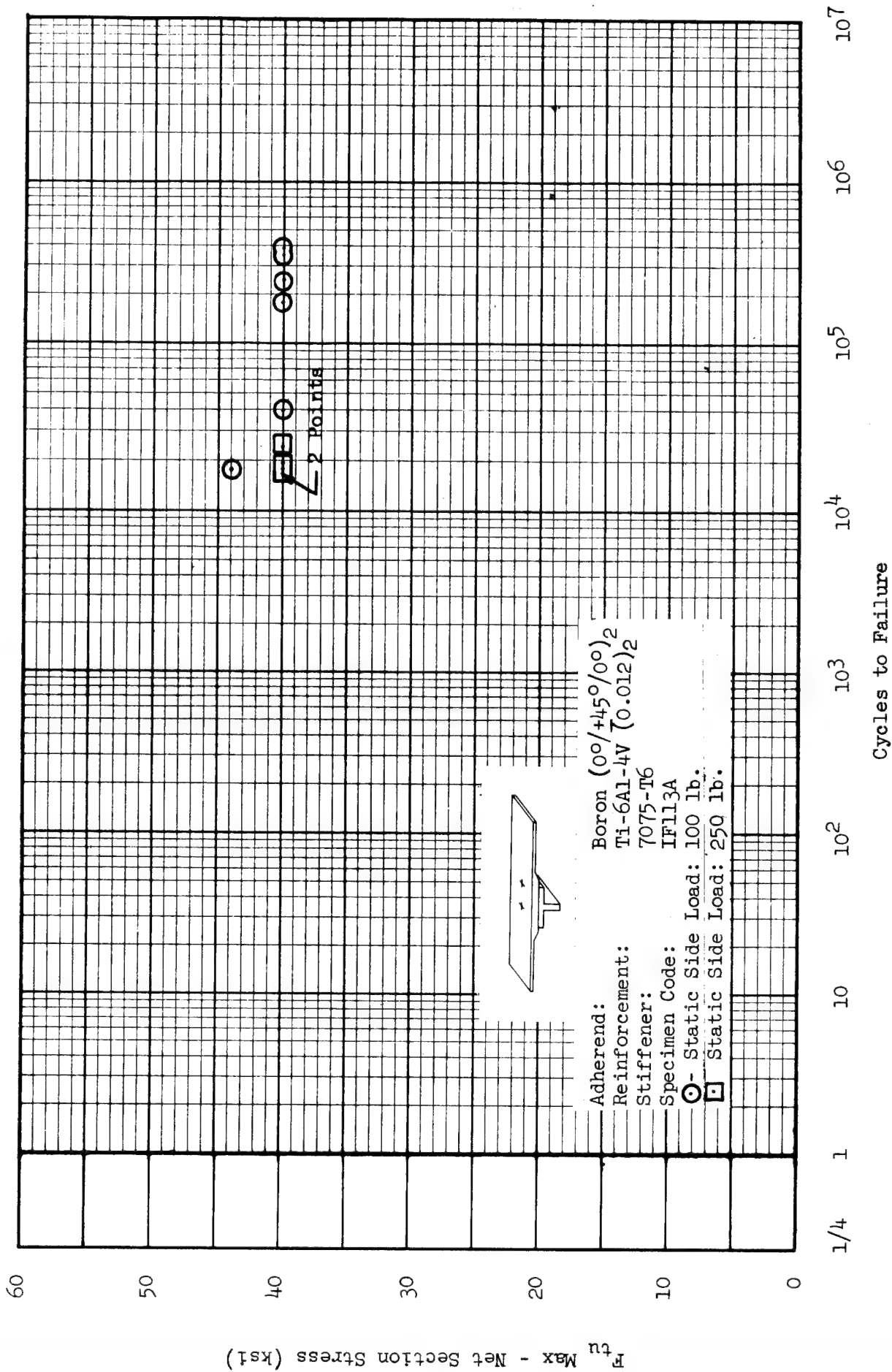


Figure 67 Fatigue Evaluation of Mechanical Joints Baseline Data Configuration IF, R = +0.10

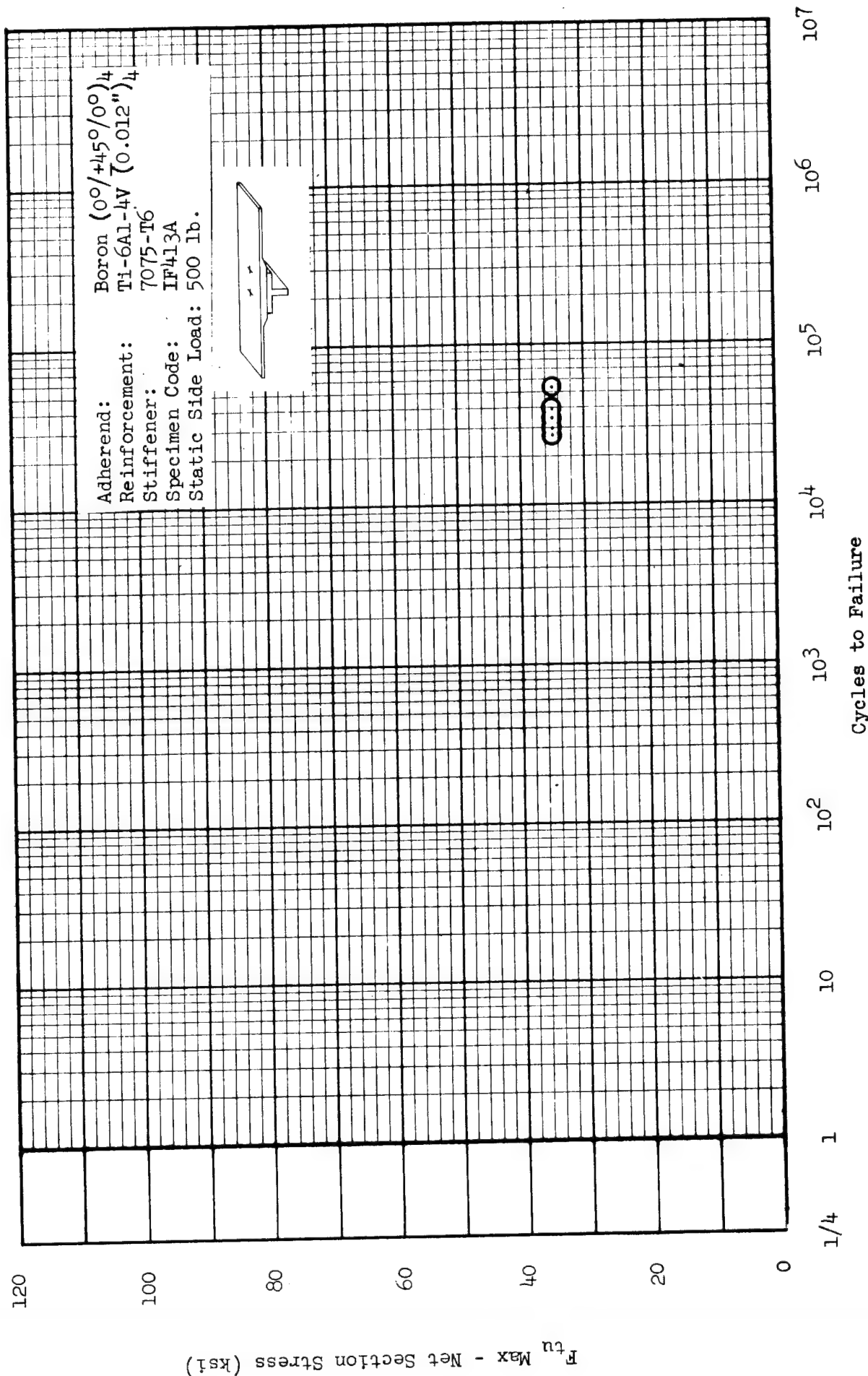


Figure 68 Fatigue Strength of Mechanical Joints Thickness Effects Data. Configuration IF, R = +0.10

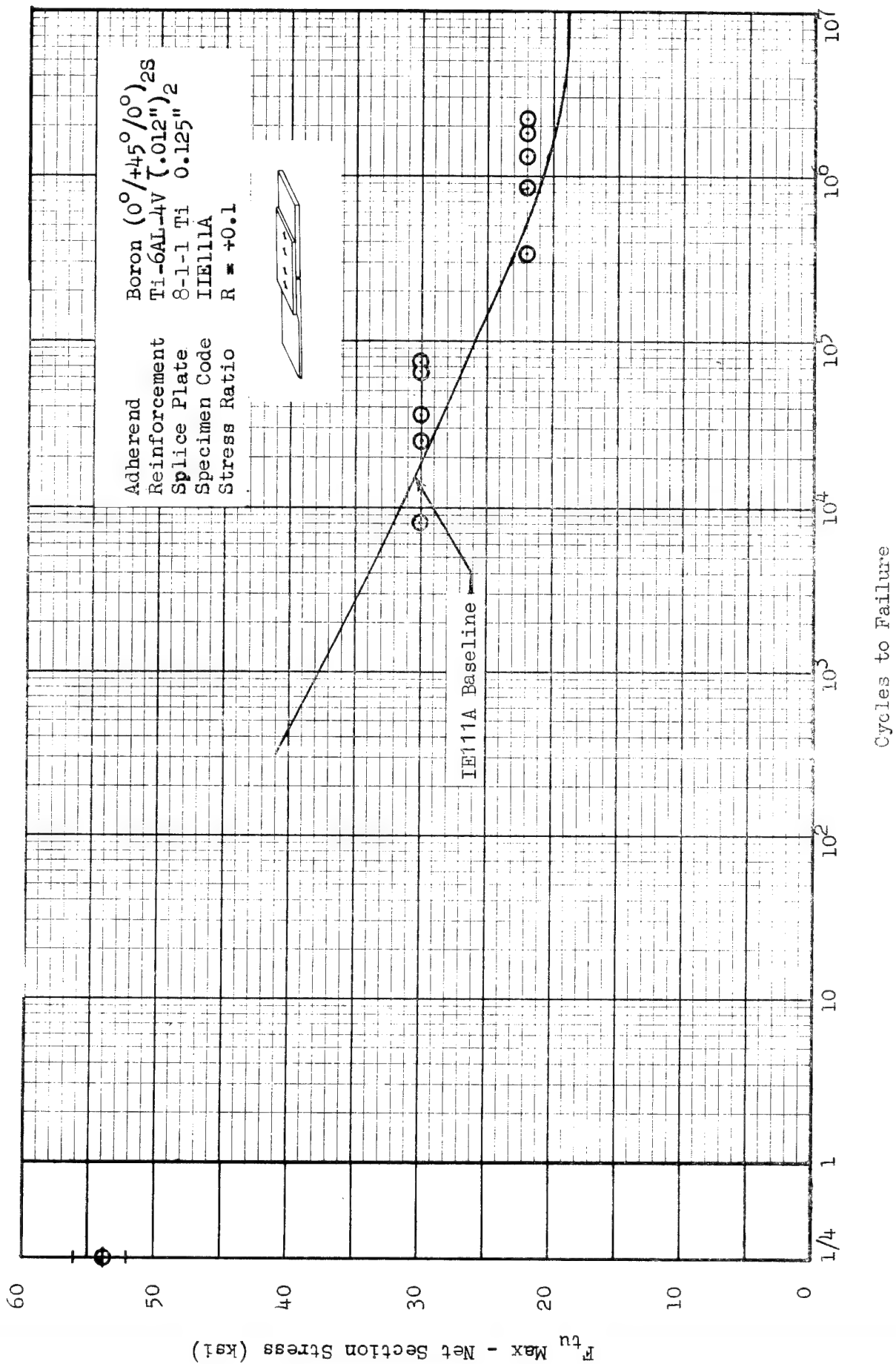


Figure 69 Fatigue Strength of Mechanical Joints, Baseline Configuration IIE, Boron: Titanium

2.4.3 Cumulative Damage Analysis

In the systems development program for a typical air vehicle, the overall fatigue evaluation is a systematic progression of analyses and substantiating test programs. The analysis is, of course, dependent upon accurate S-N data developed from simple specimen fatigue tests of the materials under consideration. This is then substantiated and/or refined with component tests of structural assemblies identified as critical from a fatigue standpoint and ultimately by full scale testing of a complete vehicle. The materials S-N data are generally developed from constant amplitude fatigue tests whereas the component and full scale tests are program fatigue tests and may involve block loading, flight-by-flight loading, or spectrum loading. The constant amplitude data are used for analytical life predictions, component and full scale test program development, and data analysis and correlation with predictions. The problem of predicting the fatigue life of these structures subjected to program fatigue tests (varying loads and stress spectra) is of course dependent upon cumulative damage theories.

Since this program has been directed toward the development of a better understanding of the fatigue phenomena of advanced composites joints, it is prudent that the constant amplitude fatigue tests be extended to include variable loads spectra testing and data analysis based on the theory of cumulative damage. This has been accomplished with a two-part program:

- o Realistic Loading Spectrum
- o Block Loading Spectrum

The realistic loading test spectrum has been developed to represent a typical fighter aircraft wing maneuver loading spectrum and includes both frequency and amplitude variation. A detailed description of the realistic spectrum development is presented in 2.3. This spectrum is comprised of four basic missions or simulated flight loads repeated in random order, 4000 times. A typical loads trace showing all the load levels in each of the four different missions is shown in Figure 70.

As can be seen, these loads spectra include both frequency and amplitude variation and, for the purpose of discussion, these are considered to be narrow-band random spectra.

An equivalent block loading spectrum has been developed from the realistic spectrum discussed above and is also discussed in 2.3. For the block loading spectrum, the fighter maneuver occurrence loadings for 4000 flights plus 4000 occurrences of "-1.0g" have been combined into 10 approximately equal blocks.

The basic constant amplitude S-N data for the bonded and mechanically fastened joints, as presented in the constant life diagrams in Figures 18 and 19, have been used to predict the specimen endurance under the block loading tasks. The predicted fatigue endurance and test data analysis for all the variable loads spectra testing has been accomplished by using the well-known Palmgren-Miner Theory for cumulative damage. Shockey, Reference 9, has evaluated some of the more well-known cumulative damage theories to determine applicability to advanced composite materials and has concluded that Miner's Theory appears most applicable for design purposes.

The realistic and block spectrum test program included both bonded and mechanically fastened joint specimens representing the baseline configurations evaluated in the constant amplitude testing phase. A listing of the specimens involved is included in Table XXIII. The specific details of each configuration are as defined in Figures 12 through 17.

TABLE XXIII CUMULATIVE DAMAGE TEST SPECIMENS

Block Spectrum		Realistic Spectrum	
Specimen	Number	Specimen	Number
IA711F	11	IA711G	10
IIIA21F	1	IIA41G	5
IIIB21F	1	IE611G	5
IE611F	2	IIE611G	<u>5</u>
IIE611F	<u>5</u>		25
	20		

The following paragraphs present a detailed discussion of these variable amplitude loading tests and evaluation of the test data.

2.4.3.1 Block Loading Spectrum

Twenty specimens representative of typical bonded and mechanically fastened joints have been subjected to the block loading spectra presented in Tables VIII and IX. All testing was axial loading, with each block representing 400 flight hours or 10 percent of the required fighter life of 4000 hours. For each test, the first block loads are applied in a low-to-high order and the second in a high-to-low order. This procedure is followed through the application of ten blocks, representing one lifetime.

The baseline constant life diagram developed for the single splice butt joint was used to predict the damage and fatigue endurance for the IA bonded joints. This analysis shows that the average strength specimen (4500 psi ultimate shear) should have a damage of approximately 0.25 per block or a fatigue endurance of 4.0 blocks of load application. Miner's Theory was used for this prediction. There is not sufficient S-N data available to analytically predict the damage/block for the IIIA and IIIB ten-inch wide specimens; however, the IIIB specimen should accumulate somewhat less damage and longer endurance than the IA specimen while the IIIA specimen should have a shorter fatigue endurance. These assumptions are based on the trends established for these two joint concepts from

the constant amplitude tests of the ten-inch wide specimens. The fatigue predictions for the IE and IIE average specimens are a damage/block of 0.140 and a fatigue endurance of 7 blocks.

Cumulative damage has been calculated for all specimens tested using Miner's Theory and the actual cycles at failure. Table XXIV is a summary of this cumulative damage analysis. Miner's Theory predicts failure at a damage of 1.0. For an average bonded or mechanically fastened specimen, failure was predicted after 4.0 and 7.0 blocks of applied load, respectively. As can be seen in Table XXIV, the majority of the one-inch wide specimens (both configurations) fail in significantly less time than predicted and in all but one case the calculated damage at failure is less than 1.0. The average damage for ten IA specimens is 0.293 and the average for the IE specimens is 0.204, or approximately 25% of the predicted damage at failure. The data grouping or scatter in the sample is considered good and the trend established is considered realistic.

The applied loads and resulting stresses in the 10-inch wide IIIA and IIIB specimens were low compared to the IA specimens and, as a result, the predicted damage per block and fatigue endurance are not in keeping with the other specimens tested. The predicted endurance for these specimens is 500 blocks, for $\sum \frac{n}{N} = 1.0$. As noted in Table XXIV, however, the actual damage at failure and fatigue endurance are significantly less than the predictions. Even at these lower applied load levels, failures were encountered long before the damage theory predicted, which follows the trends of the one-inch baseline specimens.

The two-inch wide mechanically fastened joints (IIE) specimens generally exhibited longer fatigue endurances than predicted. These specimens were tested at stress levels comparable to the one-inch wide, IE specimens; however, the trends for those specimens is reversed with the increased width. The constant amplitude data for the two widths compare well as discussed in 2.5.1.6 and offer no explanation for these block spectrum test results.

Another significant point from these data is that in all the mechanically fastened joint specimens the failing load was the highest load level in the spectrum (8.0g in this case). The majority of the bonded joints also failed at load levels greater than 8.0g. The trend for these composite joints appears to be similar to that shown in constant amplitude fatigue tests of basic composite laminates; that is, if the composite will sustain the first application of a high load, the fatigue life could vary several decades. In other words, the slope of the composite laminate curve is very small and the laminate may have a fatigue endurance approaching its static strength.

These test results and trends are discussed further in 2.5.2.

2.4.3.2 Realistic Loading Spectrum

Twenty-five specimens including both bonded and mechanically fastened joints have been subjected to a realistic spectrum loading. The test spectrum development is discussed in 2.3 and consists of four basic missions and a 4000-flight lifetime. This required life was divided into 400-flight spectrum blocks with each block repeated 10 times to obtain the desired life. Single flight loading charts for each of the four missions are presented in Tables I through IV with additional "odd-ball" loadings shown in Table V. These 400 flights were then randomized with a random numbers table to establish the testing sequence as shown in Table VII. Details of this realistic spectrum testing are discussed in Volume II of this report. Figure 70 depicts the first occurrence realistic spectrum for each of the four missions included in the program. As noted in 2.3.1 and Tables I through V, some loadings are non-regular; that is, they occur one time in a given number of flights. All loads are applied during the first occurrence of each mission (Figure 70) but subsequent mission occurrences contain fewer load levels and cycles. Figure 71 depicts an average spectrum for Missions 1 and 4 where these non-regular loadings do not appear. The first occurrence and "average" occurrence nomenclature is pertinent to the data analysis of these realistic spectrum test results.

Since these realistic spectrum tests are considered to have narrow band random test spectra, the question of data analysis is quite important. There are various methods of analysis to consider; however, the approach taken here is analogous to that used in sonic fatigue analyses where random loading and structural response are the framework of the fatigue analysis.

To calculate the actual cumulative damage for each specimen tested with these narrow band random spectra applied, rms stress (σ) and rms fatigue curves (σ -N) have been utilized rather than peak or sinusoidal stresses and S-N curves. The root-mean-square (rms) of a narrow band or broad band random load or stress time history is the best analytical tool for describing and/or utilizing these random data. The damage calculations again employ Miner's Theory and utilize rms stress (σ) and σ -N fatigue curves.

There are no σ -N curves available for composite structures, specifically the joints evaluated here, so the constant amplitude fatigue curves developed for this program were "randomized" via the procedures of Reference 10. These σ -N curves for both bonded and mechanically fastened joints are shown in Figures 72 and 73 and have been used in the cumulative damage analyses here.

Since there was a difference in the first occurrence (in any 400-flight block) of a given mission and subsequent occurrences of the same mission, the rms stress and number of cycles for each mission are determined for the first occurrence and then an "average" occurrence. There are then 8 rms stresses and 8 values of applied cycles per flight for the four basic missions, for the damage calculations. The rms stress is simply the square root of the average of the squared values of the time histories. Applied cycles were counted as number of stress reversals within a given flight, first and average occurrence of each mission. Table XXV lists the rms and mean voltage recorded from the test equipment load cell and the number of applied cycles per mission. Also, the load/volt conversion factor for each specimen type is included.

With the σ -N curves, the mean and rms variable loads, stress to load ratio, and the applied cycles (number of cycles per mission type times the number of occurrences of that mission), damage calculations for the realistic spectrum were run. Table XXVI is a summary of this data. In 2.3.2 it is noted that two blocks of applied loads for the block spectrum tests are approximately the same as the application of two 400-flight realistic spectrum blocks. This then says for an average IA or IIA specimen, the damage per 400-flight block should be 0.25 (0.14 for the IE and IIE specimens) and an endurance of four 400-flight blocks or 1600 flights. The IE and IIE specimens should have an endurance of seven, 400-flight blocks or 2800 flights.

Based on this analysis, the cumulative damage theory grossly over-estimates the fatigue endurance of composite joints. The realistic spectrum should be more damaging than a block spectrum as is apparently the case here, due to shorter relative life and high damage summations. Again the trends noted in the block spectrum results are apparent here as regards failing load and the ability to sustain higher loads. These results are discussed further in 2.5.2.

TABLE XXIV BLOCK LOADING CUMULATIVE DAMAGE SUMMARY

Specimen Number	Cycles to Failure Block/Cycles/Load ⁽¹⁾	Total Cycles	Damage At Failure - $\sum \frac{n}{N}$	Predictions	
				Damage $\sum \frac{n}{N}$ /Block	Endurance Total Blocks
IA711F01	1/1.25/19	17,595.25	0.126	0.25	4.0
F02	1/0.25/20	17,601.25	0.183		
F03	1/0.25/20	17,601.25	0.239		
F04	1/156/17	17,469.0	0.092		
F05	1/1743/15	16,446.0	0.017		
F06	1/0.25/19	17,594.25	0.201		
F07	4/71/17	52,935	0.851		
F08	3/42/18	52,800	0.776		
F09	1/0.25/20	17,601.25	0.291		
F10	1/0.25/18	17,550.25	0.151		
F11	5/0.25/19	88,010.25	3.720	0.25	4.0
IIIA21F1	25/1.0/19	438,000	0.052	0.002	500
IIIB21F1	61/200/17	1,074,000	0.135	0.002	500
IE611F06	1/7/10	6,479	0.092	0.140	7.0
IE611F07	3/45/10	19,567	0.316	0.140	7.0
IIE611F01	3/44/10	19,566	1.672	0.140	7.0
F02	12/25/10	78,172	3.931		
F03	9/1/10	60,673	1.244		
F04	9/25/10	60,697	1.341		
F05	13/1/10	84,673	3.443	0.140	7.0

(1) See Tables VIII and IX for block spectrum loadings and cycles.

TABLE XXV RMS LOADS DATA

<u>Mission Number</u>	<u>RMS Voltage (Variable Load)</u>	<u>Mean Voltage (Mean Load)</u>	<u>Stress Reversals/ Mission</u>
1st Occ. No. 1	2.18V	1.76V	106
No. 2	2.03	1.71	104
No. 3	1.94	1.64	112
No. 4	2.24	1.79	120
Ave. No. 1	2.08	1.75	60
No. 2	1.74	1.49	80
No. 3	1.74	1.51	70
No. 4	1.97	1.63	70

<u>Specimen Number</u>	<u>Load/Volt (lbs)</u>
IA	360
IIA (G01-03)	930
IIA (G04 & 05)	835
IE	500
IIIE	1000

TABLE XXVI DAMAGE SUMMARY - REALISTIC SPECTRUM TESTS

Specimen Number	Mission Occurrence No.	Failure Data		Total Number Of Applied Cycles	Damage at Failure $\Sigma \frac{n}{N}$
		End Point Number	Failure Load (lbs)		
IA711G01	134	19	1910	9.22×10^3	80.0
G02	401	20	2010	2.73×10^4	252.0
G03	5	21	2160	450	8.0
G04	127	18	1700	8.76×10^3	94.0
G05	36	19	1720	2.60×10^3	33.0
G06	142	20	2120	9.76×10^3	92.0
G07	178	18	1700	1.22×10^4	113.0
G08	124	19	1810	8.45×10^3	81.0
G09	142	20	2180	9.76×10^3	92.0
G10	69	19	1900	4.83×10^3	48.0
IIA41G01	196	18	4450	2.0×10^4	54.0
G02	5	21	5850	450	2.0
G03	184	19	5175	1.26×10^4	35.0
G04	142	20	4950	9.76×10^3	11.0
G05	142	20	4950	9.76×10^3	11.0
IE611G01	1157	19	2650	7.88×10^4	250.0
G02	1815	19	2870	1.23×10^5	380.0
G03	5	20	2670	450	4.0
G04	710	19	2880	4.84×10^4	155.0
G05	1660	19	2750	1.13×10^5	359.0
IIE611G01	1854	16	3600	1.23×10^5	219.0
G02	810	19	5800	5.52×10^4	267.0
G03	1703	19	5820	1.16×10^5	509.0
G04	810	19	5800	5.52×10^4	442.0
G05	1830	19	5620	1.24×10^5	730.0

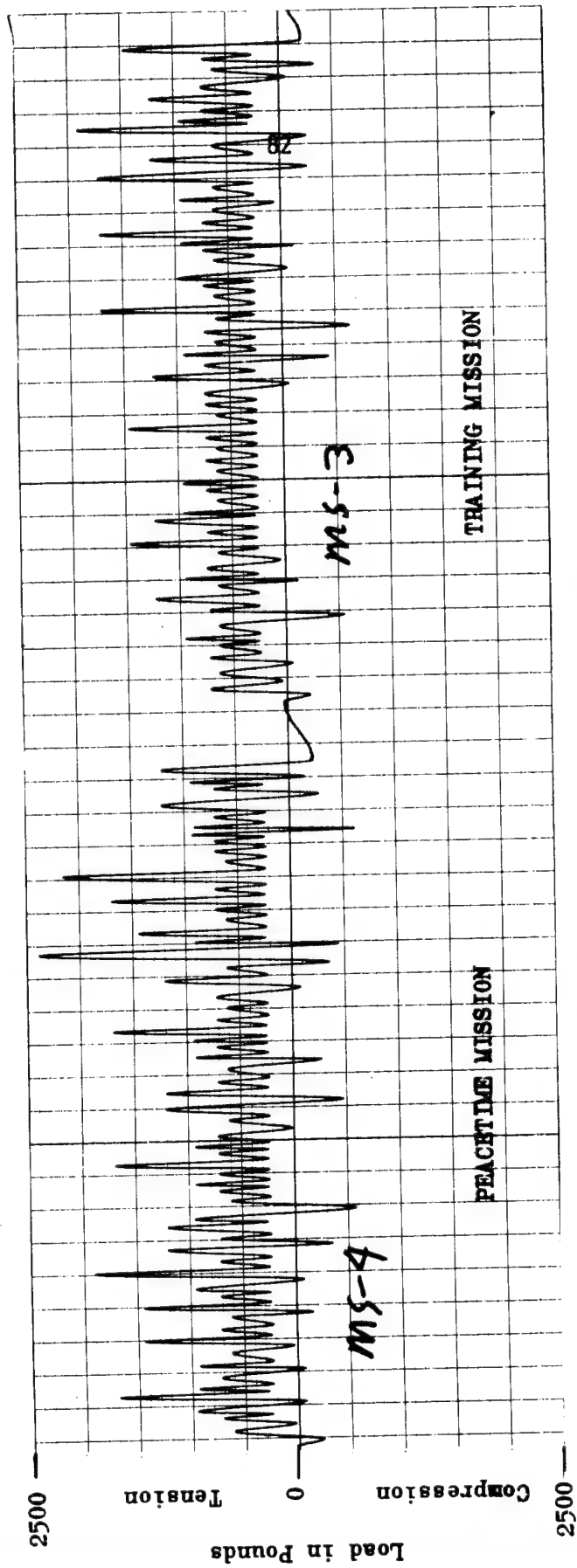
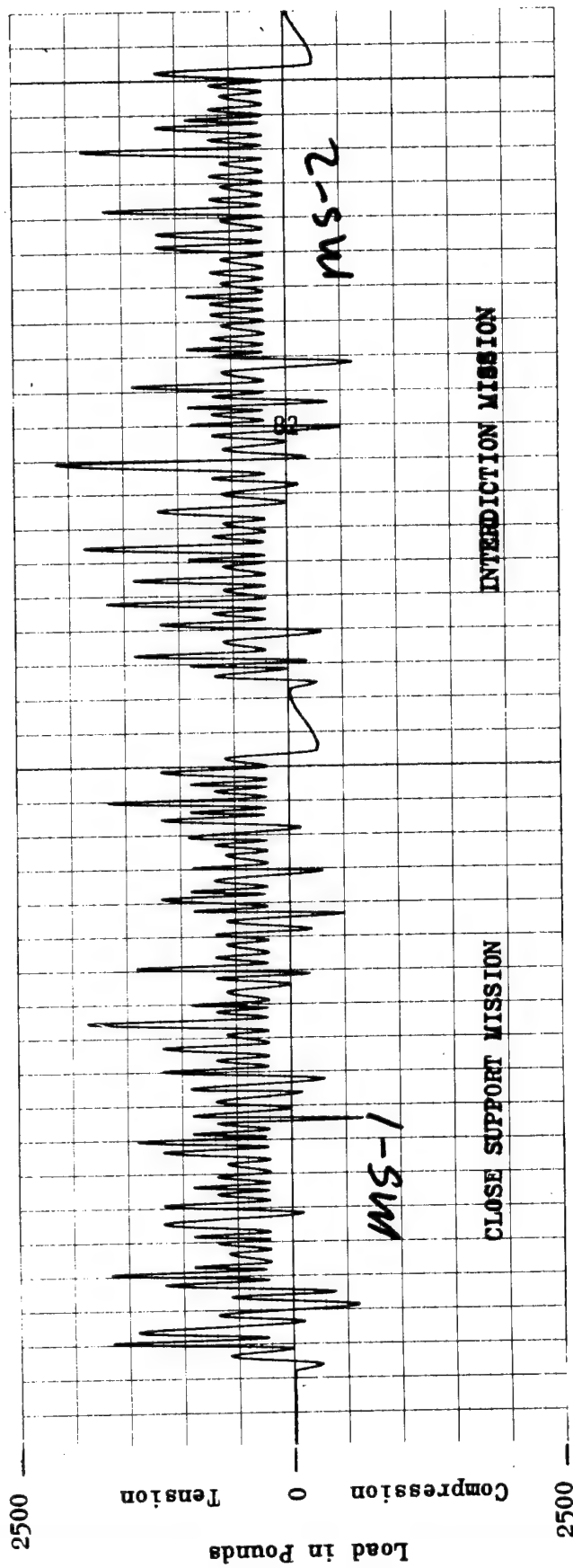


FIGURE 70 Typical Strip-Chart Recording of Individual Load Levels in Each Mission, Realistic Load Spectrum

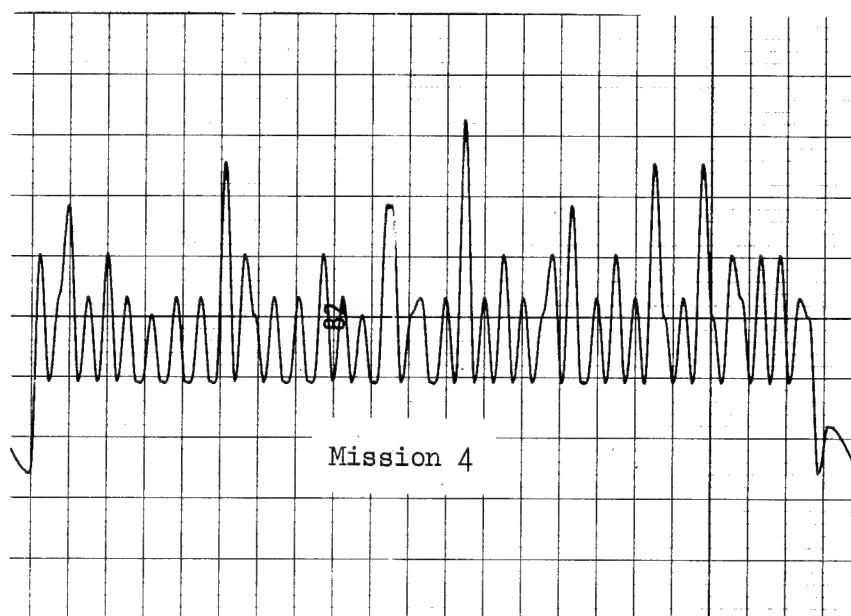
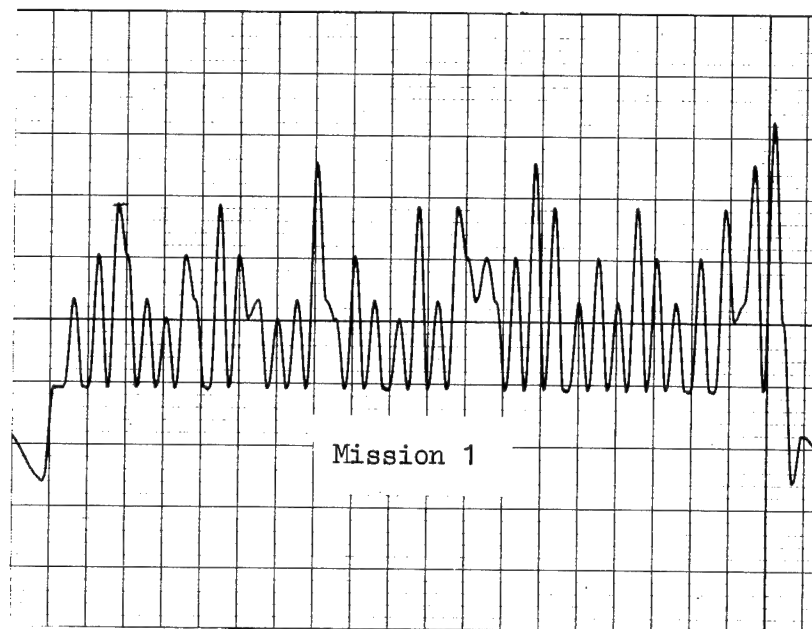


FIGURE 71 Average Realistic Spectrum
Missions 1 and 4

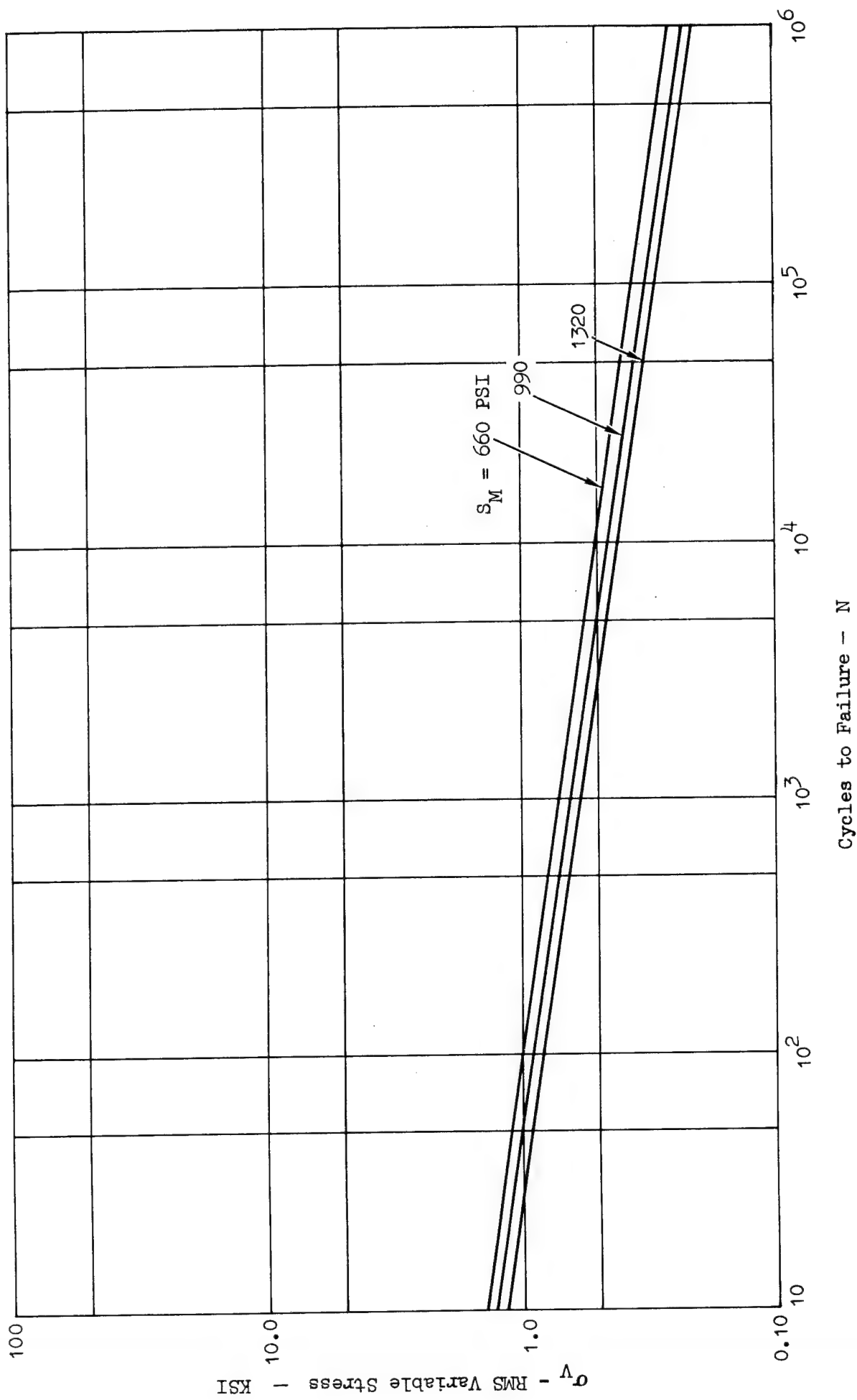


Figure 72 RMS Fatigue Curve Bonded Joints

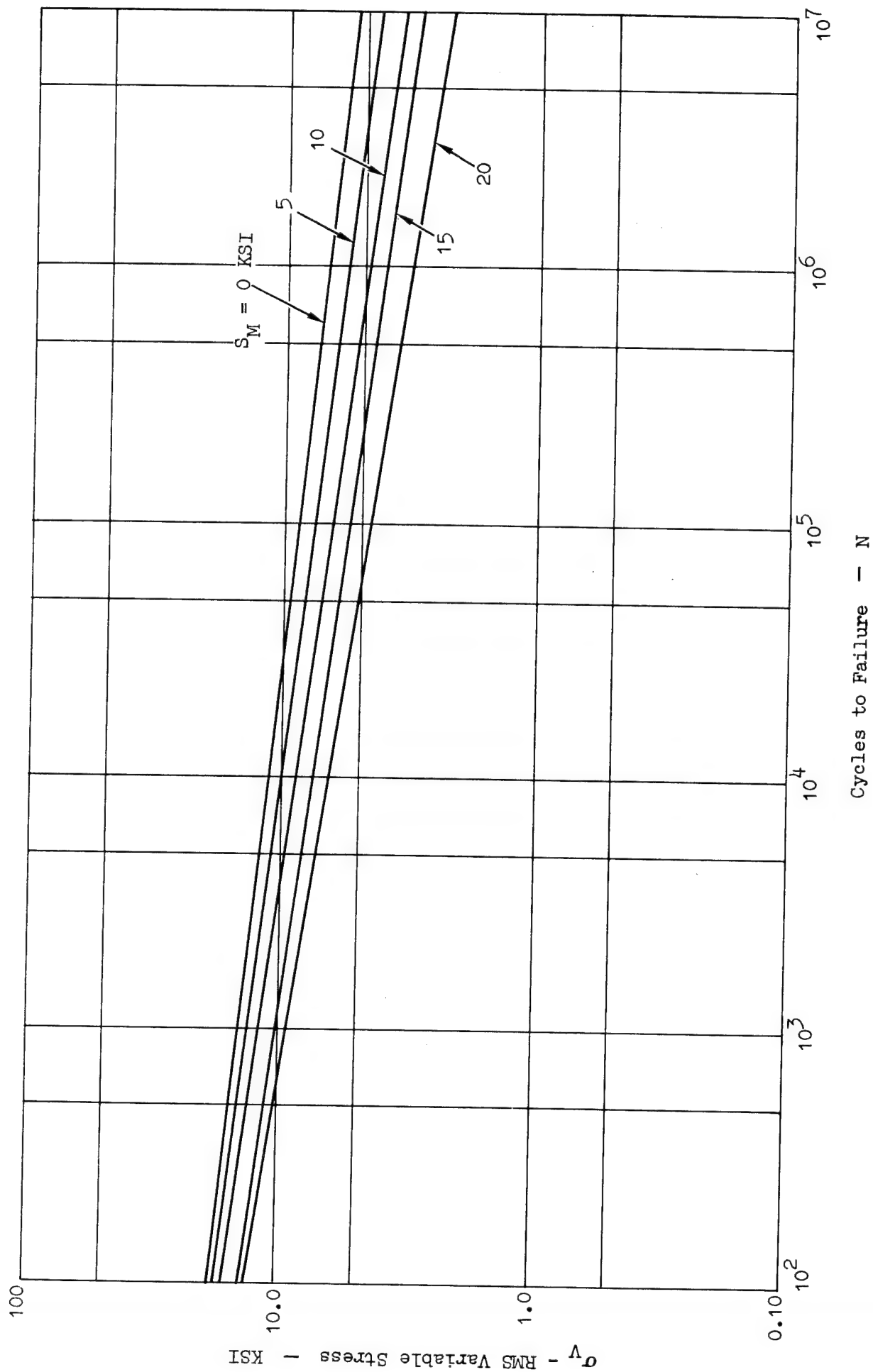


Figure 73 RMS Fatigue Curve Mechanical Joints

2.5 FATIGUE ANALYSIS

In this section of the report, the results of the constant amplitude and program fatigue tests for the bonded and mechanically fastened advanced composites joints are evaluated for applicability to design. These data analyses and general conclusions are based on the trends observed from the data presented in 2.4 and are intended to provide a better understanding of the fatigue phenomena of advanced composites joints. This discussion is addressed to the specific parametric program tasks initiated to develop realistic composites joints design criteria. The following sections present recommendations for joint design based on the constant amplitude testing and a discussion of cumulative damage applicability from the program fatigue tests.

2.5.1 Constant Amplitude Design Data

The constant amplitude test data is considered applicable for developing the basic understanding of the phenomena of fatigue of advanced composites joints. The basic recommended design criteria from this program is discussed in 2.5.1.1 and specific variations of joint geometry and loading conditions are discussed in subsequent paragraphs.

2.5.1.1 Basic Design Criteria

Several significant conclusions with respect to the overall evaluation of the fatigue behavior of composite joints have been formed from analysis of the constant amplitude test data. These relate specifically to the following:

- o Joint static properties versus fatigue endurance
- o Adherend/splice combinations
- o Optimum bonded joint concept
- o Joint reinforcement for mechanical fasteners
- o Scatter in fatigue data
- o Residual strength

In 2.4 the basic data developed from the fatigue tests are presented as S-N curves and general comparisons between the baseline data and joint variables are discussed. Here, attempts are made to expand on these comparative data and present criteria guidelines for composite joints design.

In previous fatigue tests of basic composite laminates, Reference 8, the resultant S-N curves have very little slope and for notched specimens, fatigue strengths at 10^7 cycles have been found to be higher than the static strength of the laminate. Based on these results alone, this could lead to a detailed composites structures design where the fatigue life is based solely on the allowable strength of the alternates under consideration. The designer may elect to utilize the structural concept which has the highest static strength assuming this will also be the optimum configuration for fatigue. Detailed analysis of the various joint concepts evaluated in this program indicate that fatigue endurance should not be based on static allowables only. There is a definite trade between strength, fatigue, weight, cost, and joint complexity.

The trend discussed above is further substantiated by comparison of the test data from the various joint concepts evaluated. In Table XXVII, for example, the average static strength, allowable fatigue stresses at 10^6 cycles, and fatigue strength as a percentage of ultimate strength are listed for four typical joint configurations. As can be seen, joint fatigue endurance and subsequent detail design based strictly on static strength may result in a non-optimum structure. Configuration D, with the double splice butt joint will develop the highest static strength but the single splice butt joint (Configuration A) has comparable fatigue strength. If fatigue is the design criteria, the single splice butt joint will result in weight and possibly cost savings for the same fatigue endurance. The all boron bonded joint (single splice Configuration A) appears to offer the optimum strength-to-weight concept where fatigue is the critical design criteria.

For the mechanically fastened joints, the same trend holds. The Boron-Boron, adherend/splice combination, with titanium reinforcing shims does not exhibit the highest strength but is the best strength-to-weight concept evaluated for fatigue. This is true if the joint envelope is restricted such that titanium reinforcing shims are required for load

carrying capability. The joint may be further optimized if the structural envelope is not a restriction, and the titanium shims are replaced by alternating $\pm 45^\circ$ plies of boron. Considering the net section area of each configuration on the basis of equivalent density, the all boron joint (boron reinforcing shims) will have a higher load carrying capability than the boron with titanium shims. This together with the higher fatigue strength as a percentage of joint static strength for the boron with boron reinforcing shims listed in Table XXVII ($64\% F_{ult}$) indicate that this configuration is optimum for the mechanical joints considered.

In the mechanically fastened joints, Configuration E, the basic composite laminate has been reinforced locally with either titanium or boron shims, for added bearing strength. Each configuration has been static tested as well as fatigue tested to develop data for this program. The static tests of the specimens with titanium shims result in gross section failures in the basic laminate at the ends of the titanium shims rather than in the net section. The boron reinforced specimens, on the other hand, all experienced static failures in the net section through fastener holes. When fatigue tested, both configurations generally failed in the net section.

With titanium shims, the boron adherend has two geometric stress concentration factors in the build-up area. One stress concentration factor is associated with the fastener hole and the other at the shim ends where there is an abrupt change in stiffness in the transition area between the build-up and basic laminate. This stress concentration at the shim ends apparently is the more significant at high loads (the static failures occur here) whereas with the lower load, fatigue cycling, the stress concentration at the hole is the governing parameter in specimen failure. These same two stress concentration factors occur in the adherends containing additional plies of boron as the reinforcement. The stress concentration at the ends of these reinforcing plies, however, is apparently small compared to the stress concentration occurring at the ends of the titanium shim reinforcement. This is due to less abrupt changes in fiber lay-up, laminate thickness, and a more uniform change in stiffness. This lends further credence to the conclusion earlier that the all boron mechanically fastened joint is more optimum than the boron laminate with titanium reinforcement.

Although not a specific design criteria, it should be noted that the scatter in fatigue data from these tests is much less than that generally found in the literature, Reference 8 for example, for notched and unnotched composites laminates. Definite trends have been established from these tests, with limited numbers of specimens, that possibly could not be attained with a basic laminate fatigue program. This information is significant in that it results in increased confidence in fatigue results and can result in maximum utilization of a limited number of fatigue test specimens.

The tests to evaluate the residual strength and stiffness of the bonded joints have provided additional data to aid in the understanding of the fatigue of composite joints. The basic S-N data for these composite joints differs significantly from those developed with the basic composite but the residual strength after cycling and at fatigue run-out is only slightly (approximately 15%) less than the average static strength of the particular joint. In Table XXVII the fatigue strength of typical bonded joints ranges from 24 to 30% F_{Ult} at 10^6 cycles, but from the degradation of joints testing after cycling at approximately the same stress for 2×10^6 cycles without failure, the average residual strength is approximately 85% F_{Ult} . There is no apparent stiffness loss for any of the bonded specimens evaluated. Again this data adds confidence to vehicle structural designs incorporating bonded composites joints.

2.5.1.2 Stacking Order and Thickness Effects

In general, the ply stacking and thickness variations evaluated here for the bonded joints have no effect on the fatigue endurance of the joint. This is of course specifically related to the Narmco 5505 boron-epoxy and the $0^\circ/\pm 45^\circ$ fiber orientation. Previous data indicated that higher strength was developed with outer plies at $\pm 45^\circ$ rather than 0° , but in this program no apparent differences were noted in the static or fatigue properties of $0^\circ/\pm 45^\circ$ versus $\pm 45^\circ/0^\circ$. Limited data for $0^\circ/90^\circ$ fiber orientation was obtained for the bonded stepped lap joint and fatigue strength is slightly higher than comparable data with $0^\circ/\pm 45^\circ$ fiber orientation at higher stress levels, but no definite trends have been established based on these tests.

The thickness increase from the standard 8-ply to a 16-ply laminate for the bonded joints does result in a decrease in joint L/t ratios. The increased thickness while maintaining a standard lap length results in fatigue data comparable to that discussed in 2.5.1.3 for the short lap specimens. Increased thickness (16-ply) with the Configuration E, mechanically fastened joints shows some reduction in fatigue strength compared to the 8-ply baseline data. This reduction in strength can be attributed to the ratio of fastener clamp-up to pin bearing strength for the two thicknesses, i.e., as specimen thickness is doubled the pin bearing load is doubled; however, the fastener clamp-up remains constant due to constant fastener torque. This leads to the conclusion that joint capability should be based on pin bearing strength plus an added constant value for joint clamp-up.

Variations in the stacking order for the mechanically fastened joints consisted of the boron reinforcing shims in lieu of the baseline titanium shims. The resulting effects on the joint fatigue endurance have been discussed in detail in 2.5.1.1.

2.5.1.3 Lap Length Effects

The effect of overlap length on the fatigue endurance of bonded Configuration A and B joints has been extensively evaluated in this test program. The range of lap lengths evaluated was 0.375" to 1.0" with L/t ratios of 9.375 to 25.0. There is no apparent degradation in fatigue endurance with lap lengths of 0.75" or less, in fact, the data are equivalent for the two joint concepts tested where lap length is varied from 0.375" to 0.75". There is a decrease in fatigue strength with the 1.0" lap length. When considering average joint shear stress versus specimen L/t , there is apparently a plateau in the range of $0.375 < L/t < 0.75$ and a reduction in fatigue strength at L/t greater than 0.75.

2.5.1.4 Preload/Sideload Effects

As a part of the constant amplitude fatigue test program, typical Configuration A and E specimens were preloaded in tension prior to fatigue testing to determine what effect, if any, this type of loading has on the fatigue life of composite joints. Test data are

presented in Figures 43 and 65. For the range of load levels considered, static preload has no effect on the fatigue endurance of bonded or mechanically fastened joints.

An additional parameter evaluated in this program was the application of side loads to specimens IC and IF during the axial load fatigue testing. Test data is presented in Figures 46, 67, and 68. Side loads varied for each specimen (from low to high) and the increase in side load is accompanied by a decrease in fatigue strength. The mechanically fastened joints (IF) exhibit higher allowable fatigue strength than the baseline IE specimens. This combined loading phenomena should be evaluated further to develop more complete fatigue design data for composite joints.

2.5.1.5 Cyclic Rate and Low Cycle Fatigue

As a part of this program, the rate of cyclic loading during fatigue testing has been evaluated for $R = +0.10$ and $R = -1.0$. Cyclic rates from 1 Hz to approximately 30 Hz have been evaluated. These test results show no effect of cyclic rate on the fatigue endurance of either the bonded or mechanically fastened joints. This conclusion is in keeping with results from fatigue tests of basic composite laminates as reported in Reference 8.

Limited low cycle data has been obtained as a part of this program and is included with the baseline data for the bonded and mechanically fastened joints to establish mean fatigue curves and constant life diagrams. There is, however, a need to develop additional low cycle fatigue data for both configurations to better define the fatigue phenomena of this type of structure. There are still questions relative to the low cycle portion of the S-N curve for mechanical joints that need answers such that the higher cycle data points and mode of failure is tied to the static strength and static failure mode. (See 2.4.2.4.1 for further discussion.)

2.5.1.6 Specimen Width

The major portion of the constant amplitude fatigue test program has been directed towards evaluating one-inch wide specimens; however, this has been extended to wider specimens to evaluate the effect of Poisson's Ratio and transverse residual thermal stresses. Two specimen widths were tested for the bonded joints and include 3-inch and 10-inch width. The bonded single splice butt joint and stepped scarf lap joint have been tested. For the Configuration E mechanically fastened joints, the increased width effect was evaluated with 2-inch wide specimens only.

There are specific trends in the wide bonded joint tests which are discussed in detail in 2.4.2.2.1 and 2.4.2.3. The single splice, bonded butt joint data shows a decrease in fatigue strength with increased width which has been associated with Poisson's Ratio and substantiated in part by the failure modes of the one-inch wide specimens. It was theorized that Poisson effects result in transverse strains which produce a plane strain state in the adhesive toward the specimen center resulting in crack initiation in this brittle adhesive area. Hence, the reduction in fatigue life.

The wide, bonded stepped lap joints show increasing fatigue endurance with increasing width for tension-tension fatigue loading ($R = +0.10$). This phenomena is contrary to the trend for the wide single splice butt joint and needs further evaluation to develop detailed design data. It is felt that the 3-step lap joint results in a softer interface between the adherends than with the other bonded joints evaluated and approaches a true scarf with an attendant increase in fatigue endurance.

The S-N data for the 2-inch wide mechanically fastened joints is comparable to the results of the one-inch specimen tests. This is as expected since the Poisson effect which apparently leads to a reduced fatigue endurance in the similar bonded single splice lap joint is not significant here.

2.5.1.7 Bearing Strength and Edge Distance

Pin bearing fatigue tests and fatigue tests with two different fastener edge distances have been conducted for the Configuration E, mechanically fastened single splice butt joint. In the fatigue evaluation of this type of joint, in advanced composites, it is prudent that bearing fatigue strength be determined with and without the effect of fastener clamp-up, since some primary modes of failures are associated with bearing tear-out. The pin bearing tests, then, are intended to give an indication of the bearing capabilities of the basic reinforced laminate without the benefit of joint clamp-up.

For this evaluation the $0^\circ/\pm 45^\circ$ boron laminate with titanium shims was tested with pin edge distances of 2.0D and 1.5D. The same configuration but with $\pm 45^\circ$ boron shims was also included and had an e/D of 1.5. Test data are presented in Figure 66 as bearing strength versus cycles to failure. The data trend is very good considering the limited number of specimens and shows decreasing fatigue endurance with decreasing e/D , as expected.

Fastener edge distance effects have been evaluated in a similar manner. Configuration E specimens with both titanium and boron reinforcing shims and fastener edge distances of 1.5 were tested for comparison with the baseline data with $e/D = 2.0$. Tests with the titanium shims and short edge distance show a reduction in fatigue endurance which is in keeping with the pin bearing results. The test results with boron shims, however, are within the scatter of the baseline data and is an improvement over the pin bearing results for the identical reinforced laminate. This is attributed to an improvement in the fatigue endurance of this concept with fastener clamp-up and further substantiates the conclusion that the all boron configuration is the more optimum of the mechanically fastened joints evaluated.

2.5.2 Cumulative Damage Design Data

The results of the block and realistic spectrum tests discussed in 2.4.3 and subsequent data analyses have provided useful information for better understanding the fatigue phenomena of bonded and bolted composite joints. Some of the more pertinent data as regards fatigue design criteria are discussed in the following paragraphs.

All cumulative damage analyses of the program fatigue tests conducted here were done using Miner's Cumulative Damage Theory. Shockey, Reference 9, evaluated several damage theories for application to composite structures and concluded that Miner's Theory is as applicable as any existing, more complex theory. The author agrees with this conclusion; however, cumulative damage theories as they presently exist may not be applicable to composite structures. This is based on the data presented in Tables XXIV and XXVI where, in general, the actual fatigue endurance (either in blocks or flights) is significantly less than the predicted endurance.

For the IA and IE baseline, 1.0-inch wide specimens tested under block loading, the actual endurance averages approximately one-fourth that predicted by theory. The same specimens tested with the realistic spectrum applied have actual fatigue endurance of one-tenth and one-half the predicted values, for the IA and IE specimens, respectively. The same trend is true for the wider bonded and bolted specimens with the exception of the IIE block loading results where the actual endurance exceeds the predictions. When evaluating cumulative damage of metallic structures using Miner's Theory, the results for any data sample (similar specimens, etc.) tend to scatter about 1.0, but for the composite joints tested here the data for a particular specimen type or group do not follow this trend and tend to be less than or greater than 1.0. In general, Miner's Theory greatly overestimates the fatigue endurance of the composite joints evaluated here. Table XXVIII is a comparison of the average test endurance versus predictions for the block and realistic test spectra.

It is felt that the lack of correlation between the actual endurance and predictions is attributed to the combination of shortcomings in an applicable damage theory and the phenomena related to the durability of the specimen as regards sustaining higher applied loads. In 2.5.1.1, it was noted that a basic composite laminate often has a fatigue endurance at 10^7 cycles approaching the static strength of the laminate. That is, the S-N curve has little slope from $1/4$ cycle to 10^7 cycles. It has been shown that a load approaching ultimate can fail a specimen early, say at 10 cycles, or after millions of applied cycles; i.e., large scatter. Almost all the failing loads in both test series were approaching the static strength envelope for that particular joint configuration. It

is apparent that, if the specimen would sustain the first application of these loads, the fatigue endurance varies and there is considerable scatter, which follows the same trends for the basic composite laminate. The constant amplitude tests did not show this trend, but it is apparent in these cumulative damage results.

TABLE XXVIII ACTUAL VERSUS PREDICTED FATIGUE ENDURANCE

Specimen	Block Spectrum		Realistic Spectrum	
	Actual	Predicted	Actual	Predicted
IA	2 ⁽¹⁾	4 ⁽¹⁾	150 ⁽²⁾	1600 ⁽²⁾
IIA	-	-	166	1600
IIIA & B	44	500	-	-
IE	2.5	7	1585	2800
IIE	9	7	1400	2800

Note: (1) Number of blocks - see Tables VIII and IX
 (2) Number of flights - see Table VII

With the present state-of-the-art, care must be taken in fatigue analysis of composite joints where variable amplitude environmental loads exist to preclude premature fatigue damage. This of course assumes utilization of an existing cumulative damage theory. On approach which apparently has been used successfully in composite structures is to establish fatigue cutoff stresses such that the most damaging, higher loads are minimized. The maximum stresses for this program as percent of average F_{tu} for each specimen tested are listed below:

<u>Specimen</u>	<u>% Ave. F_{tu}</u>
IA	73%
IIA	73%
IIIA	41%
IIIB	54%
IE	90%
IIE	90%

For all specimens except the block loading IIE data, the existing methodology overestimates the fatigue endurance. The IIIA and IIIB specimens follow this trend but at the lower maximum stresses, 40 to 60% F_{tU} , these specimens did have an endurance greater than two lifetimes.

These test results show a definite need for significant improvement in cumulative damage analysis methodology as pertains to composite structures, and emphasis should be directed to additional development in this area to achieve the true potential of advanced composites in a broader spectrum of hardware applications.

TABLE XXVII
JOINT STATIC STRENGTH VERSUS FATIGUE ENDURANCE

<u>Joint Concept</u>	<u>Adherend/Splice Combination</u>	<u>Static Strength Fult.</u>	<u>Fatigue Strength F_{MAX} @10⁶ Cycles</u>	<u>Fatigue Strength F_{MAX}/Fult.</u>
		<u>PSI</u>	<u>PSI</u>	<u>Percent</u>
<u>Bonded Joints</u>				
Configuration A	Boron/Ti	4500	1200	27
	Boron/Boron	4000	1200	30
Configuration B	Boron/Ti	3800	900	24
Configuration D	Boron/Ti	5450	1200	22
<u>Mechanical Joints</u>				
Configuration E	Boron/Ti (Ti Shims)	42000	21000	50
	Boron/Boron (Ti Shims)	39500	21000	53
	Boron/Ti (Boron Shims)	33000	21000	64

NOTE: 1. All tests at R = +0.10
2. All specimens 1.0" wide

2.6 CONCLUSIONS

The general conclusions stated here are based on the trends observed from the data presented in 2.4 and 2.5.

- o Test data scatter for both the bonded and mechanically fastened joints is small compared to that observed from basic laminate fatigue tests.
- o In structural designs involving composite joints, there are definite trade studies to be made in considering strength, fatigue, weight, and joint complexity.
- o An all boron joint appears to be the most optimum of the configurations evaluated. For the bonded joints this includes adherend and splice plate; and for mechanically fastened joints, the boron reinforcing shims appear optimum.
- o Low cycle fatigue for the mechanically fastened joints should be evaluated further to better define the trends established here.
- o There are both positive and negative effects on fatigue endurance with increased bonded specimen width as evidenced here from the IIA and IIB test data.
- o The optimum L/t ratio for bonded joints appears to range from 9.0 to 25.0.
- o These composite joints compare favorably with basic laminates as regards residual strength and stiffness after fatigue cycling.
- o Mechanically fastened joint capability should be based on pin bearing strength plus an added constant for joint clamp-up.
- o Miner's Theory grossly overestimates the fatigue endurance of composites joints and a relevant and usable cumulative damage theory needs to be developed.

- o These joints behave similar to a basic composite laminate as regards ability to sustain higher loads. There is considerable scatter in the results due to this phenomena.
- o The realistic spectra applied here are apparently four times more damaging than the block spectra.
- o Utilization of rms stress and σ -N curves is a reasonable method for approaching the evaluation of realistic spectrum test data.

III. FAILURE MODE STUDIES

3.1 GENERAL

In conjunction with other analyses and evaluations, failed bonded joints were studied to ascertain the mode of failure. The effects of variations in stress ratios, loading conditions, joint overlap and bond width were considered. Shear and peel failure modes were established for boron-epoxy composites. Specimens of various joint configurations having boron epoxy as one of the adherends were evaluated.

The initial step in the investigation of these specimens was to obtain 5.6X magnification photographs of the failure surfaces. By close examination of these photographs and by macroscopic examination of the specimens, areas of general modes of failure were outlined for more extensive investigation by scanning electron microscope (SEM) photomicrographs. SEM photomicrographs with a magnification of approximately 20X were the first shots taken. These photographs provided a map of a selected sample (from the specimen) and covered an area which may be as large as 3/16 inch in width. The 20X SEM photographs were then enlarged (approximately 200 percent) by conventional methods and were used for selecting smaller areas for more detailed study at 100X or 200X magnification. These final SEM photomicrographs were used in conjunction with the lower magnification shots to define the various failure modes present. The failure surface on the splice plate is identified as Surface A and the failure surface on the loaded adherend is identified as Surface B.

3.2 DETERMINATION OF SHEAR AND PEEL FAILURE MODES

The shear and peel failure modes were defined utilizing a failed 15-ply flexure specimen. The specimen was subjected to a beam bending load and initial failure was a shear failure along the midplane of the laminate. This initial failure plane is evident in Figure 74. The specimen was then physically pulled apart by hand, resulting in a true peel or cleavage mode of failure over the remainder of the specimen. In Figure 75 the facing fractured surfaces are shown and the two failure mode zones are defined. Electron scan photomicrographs of these two surfaces in the transition zone, Figure 76, illustrate the difference between the shear and peel modes of failure. The difference is still more pronounced in the 560X magnification of the shear surfaces, Figure 77, and in the 570X magnification of the peel surfaces, Figure 78. The shear failure of the resin between the fibers has the appearance of being stressed in biaxial compression and tension (shear) with failure occurring normal to the tensile load.

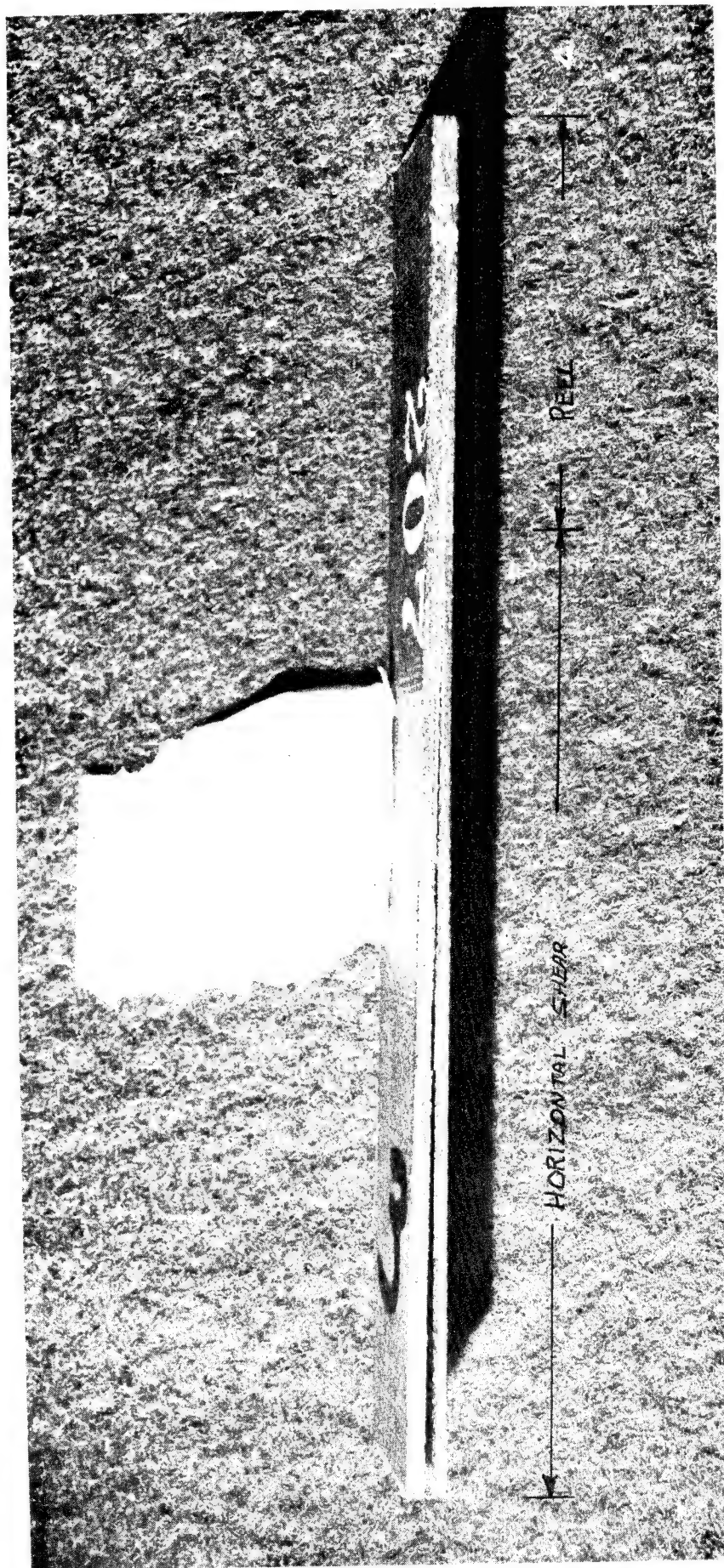


Figure 74 Boron Flexure Specimen - Horizontal Shear Failure

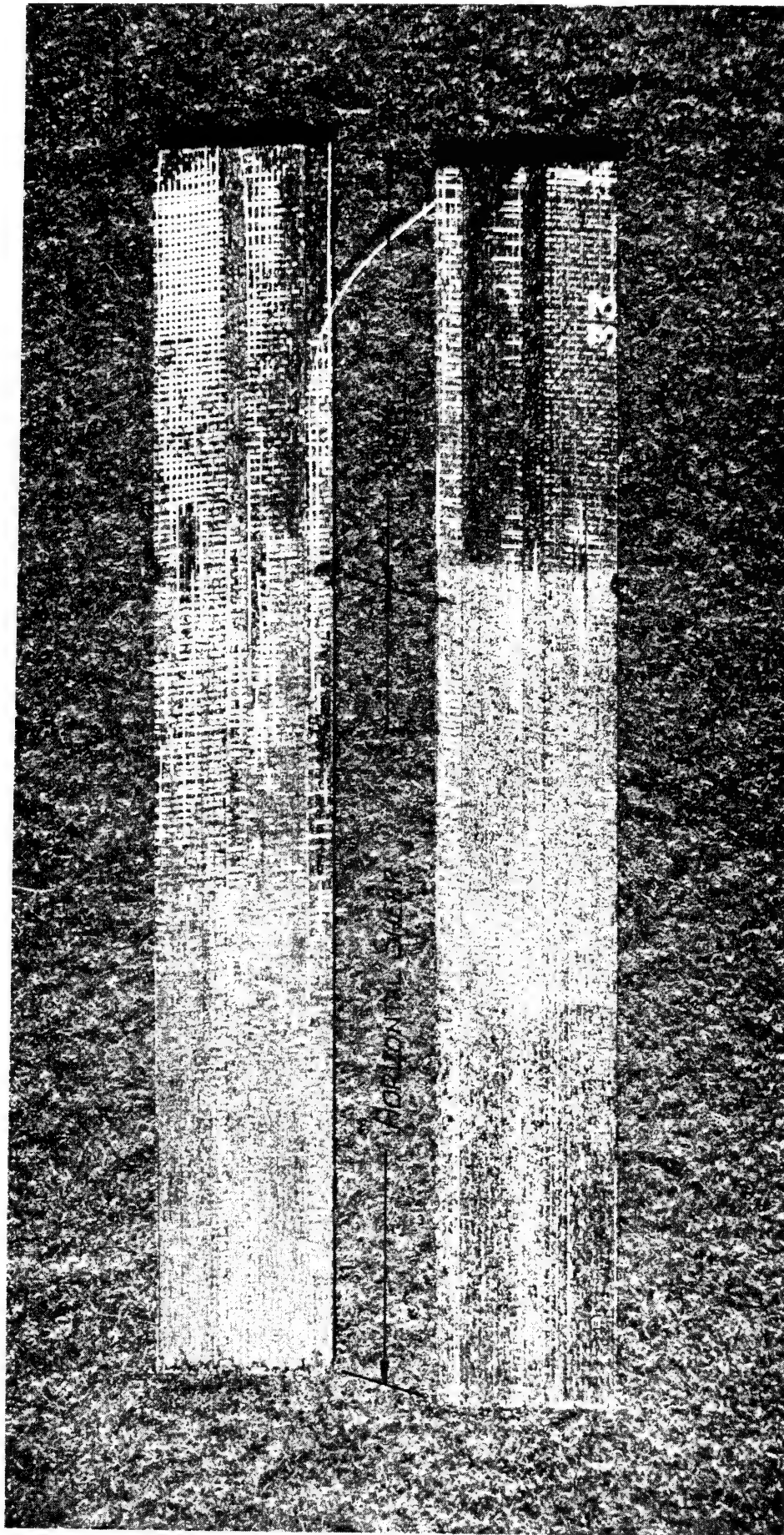
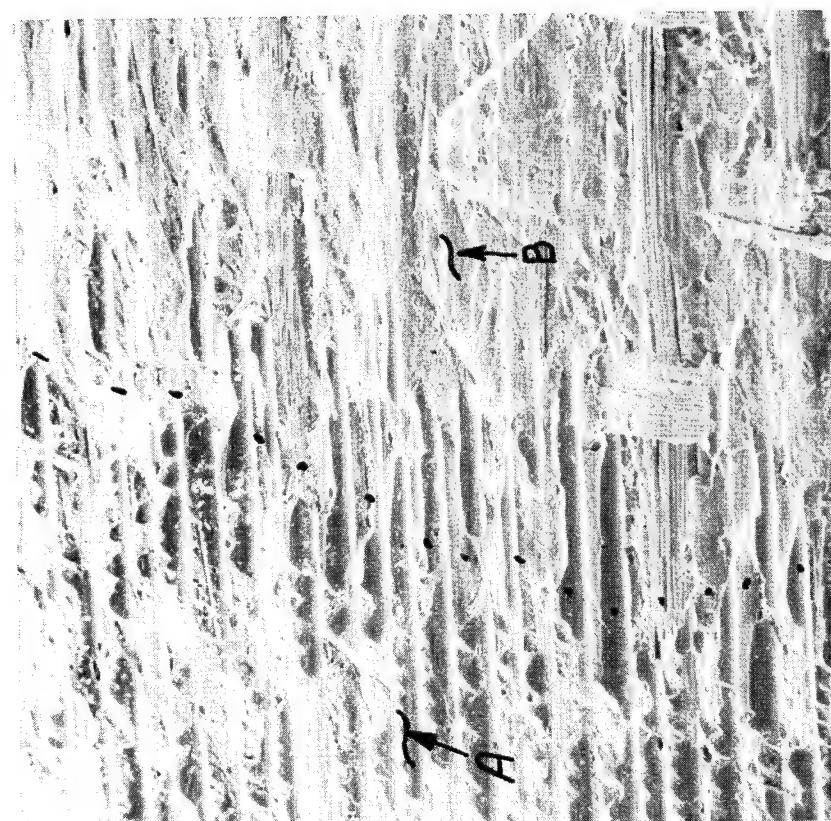
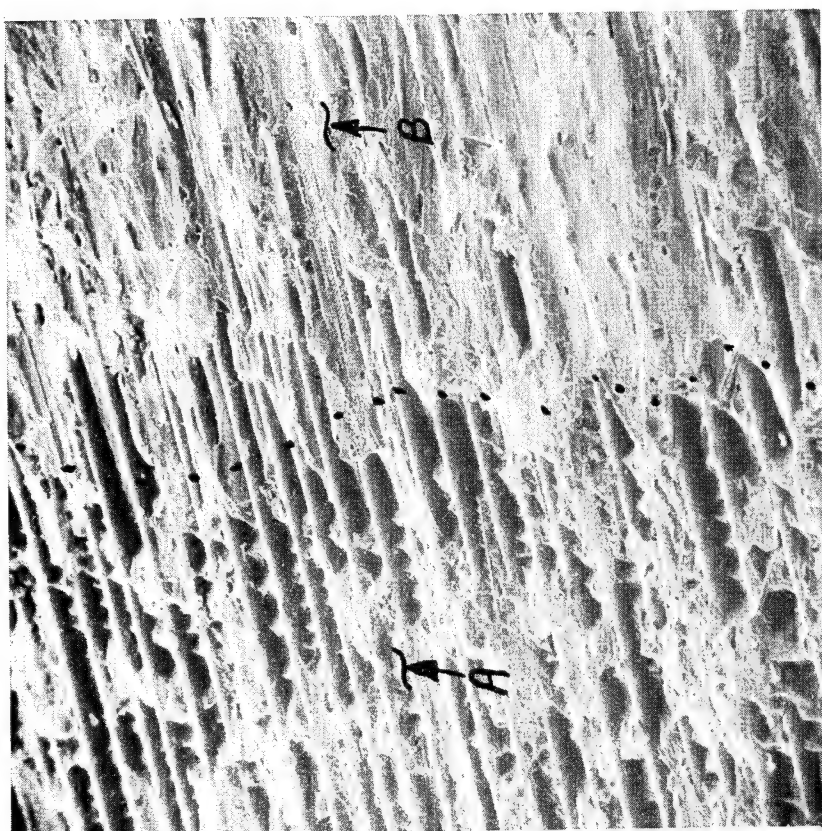


Figure 75 Boron Flexure Specimen Peel Apart - Shear and Peel Zones Defined



Surface A



Surface B

NOTES: (1) Surface A does not mate identically to Surface B.

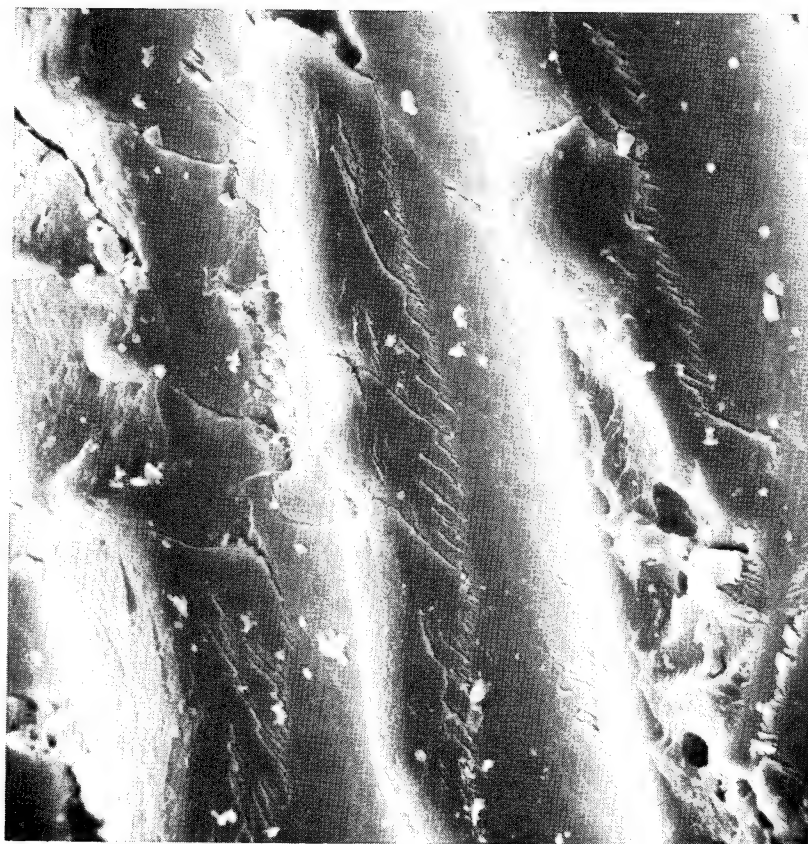
(2) Dotted line indicates area where failure mode shifted from horizontal shear to peel.

(3) Arrow A indicates shear zone.

(4) Arrow B indicates peel zone.

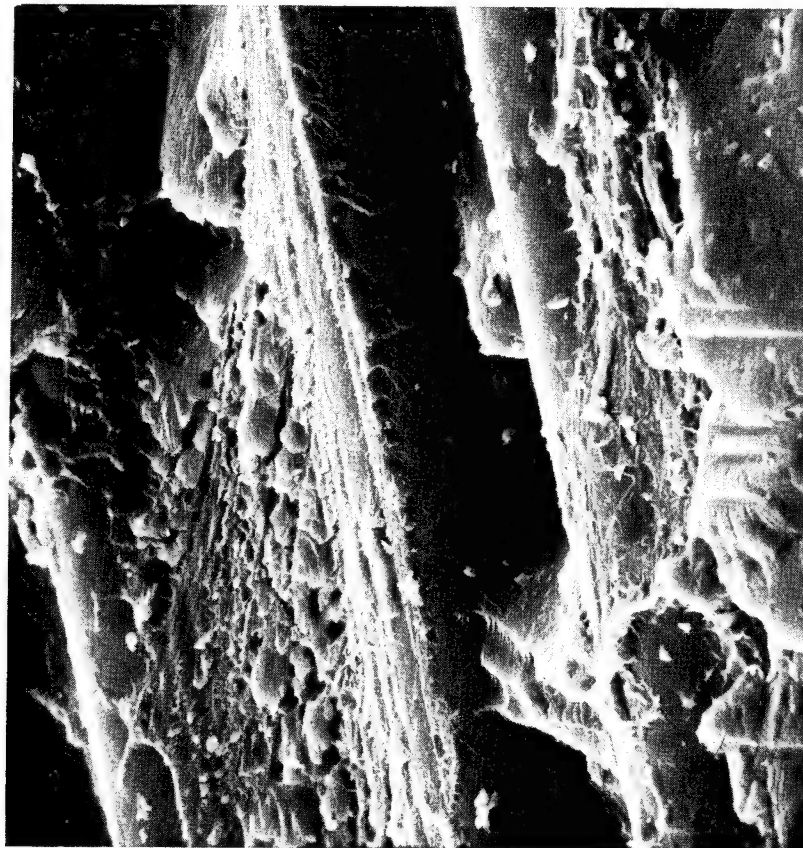
(5) Intralaminar separation of the specimen as a result of horizontal shear occurred during flexural testing and extended from one end toward the other for approximately three-fourths of the specimen length. The peel zone was produced by extending the intralaminar separation for the remainder of the specimen length by pulling apart the delaminated ends by hand.

Figure 76 Facing Fracture Surfaces Along the Fracture Plane of a Boron-Epoxy Longitudinal Flexure Specimen



Surface A

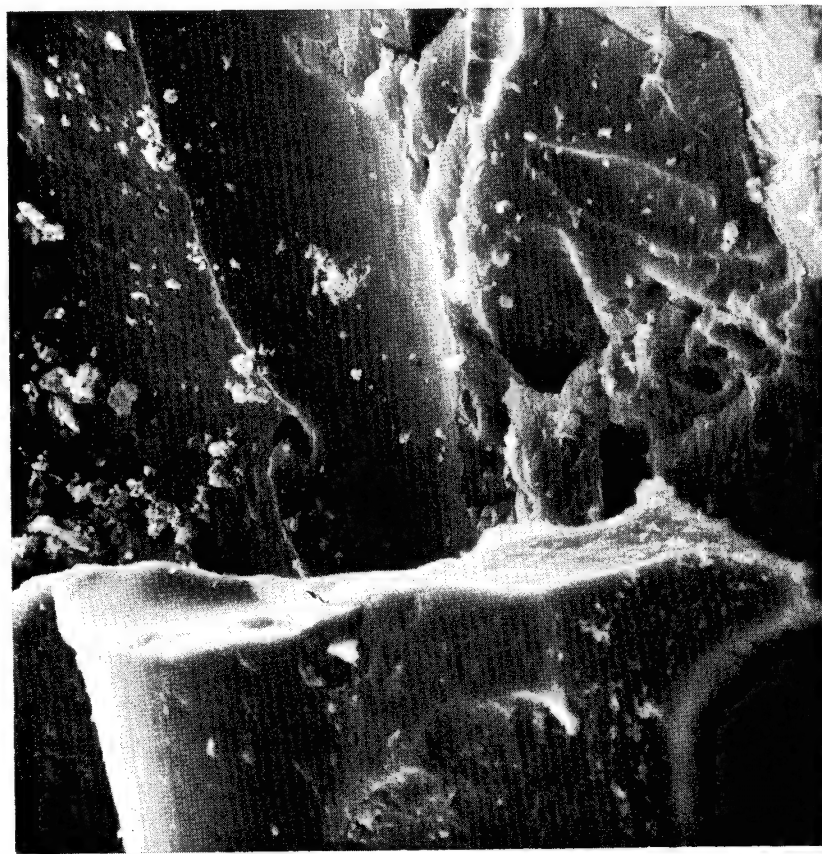
Magnification 565X



Surface B

Magnification 556X

Figure 77 Facing Surfaces in the Horizontal Shear Fracture Zone of a Boron-Epoxy Longitudinal Flexure Specimen



Surface A

Magnification 580X



Surface B

Magnification 570X

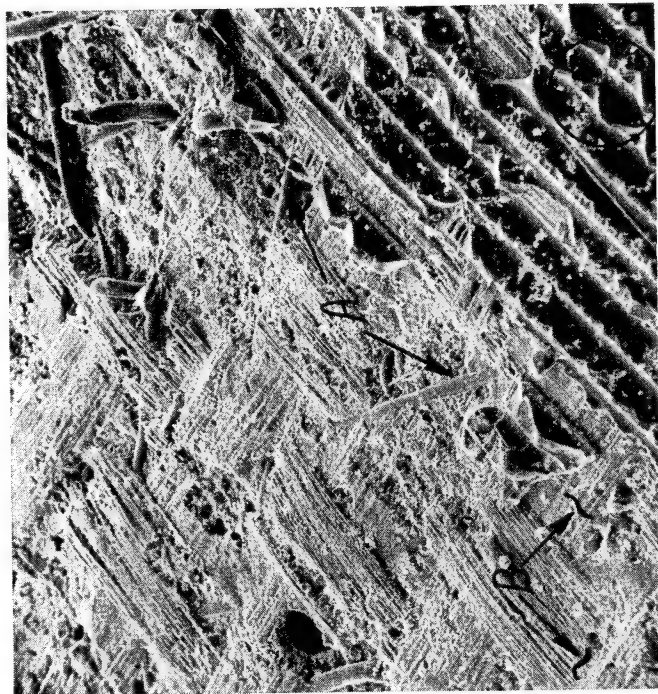
Figure 78 Facing Surfaces in the Peel Fracture Zone of a Boron-Epoxy Longitudinal Flexure Specimen

3.3 INITIAL JOINT FAILURE STUDIES

The first joint specimens to be subjected to failure mode studies were two specimens used in establishing test set-up procedures, cyclic rate limits, specimen support methods, and specimen heating due to fatigue loading. These specimens were IA111E02 and IA111E06.

One specimen, -E06, was fatigue cycled at a stress ratio $R = -1.0$, while the other specimen, -E02, was fatigued cycled at a stress ratio $R = +10.0$. Since these specimens were used to evaluate cyclic rates for various maximum loads, the only comparison that can be made is the effects of stress ratios, $R = -1.0$ vs. $R = +10.0$.

The 52X magnification, Figure 79, of specimen -E06 shows the general appearance of the failed surface whereas the 575X magnification of the same failure surface shows finer details of the fracture mode. The saw tooth effect so prominent in these photos indicates that the reversal in specimen loading resulted also in the reversal of principal tension stress within the resin causing the tensile failures. This fracture mode differs from the basic shear mode as evidenced on the flexure specimen. On the flexure specimen the tensile fractures were in one direction and were not as sharply defined whereas on this $R = -1.0$ fatigue failure the fractures are sharp, well defined, and the tensile fractures are nearly normal to each other. The 50X magnification, Figure 80, of specimen -E02 shows the general appearance of the failed surface whereas the 500X magnification of the same failure surface shows details of the fracture mode. The tensile fracture that was defined in the flexure specimen as a shear mode is also illustrated in this photograph. However, the fracture for this specimen has a rounded appearance along the length of the tension fracture indicating the direction of the principal tensile stress is varying through the thickness of the resin.



Surface "A"

Magn. 52X

- NOTES: 1) Arrows A indicate filament of woven adhesive carrier (scrim).
 2) Arrows B indicate glass scrim cloth used with the boron-epoxy tape.
 3) Area shown at 575X is similar to that enclosed by circle (c).
 Notice topographical features (cracks) of resin matrix that was adjacent to boron filaments.



Magn. 575X

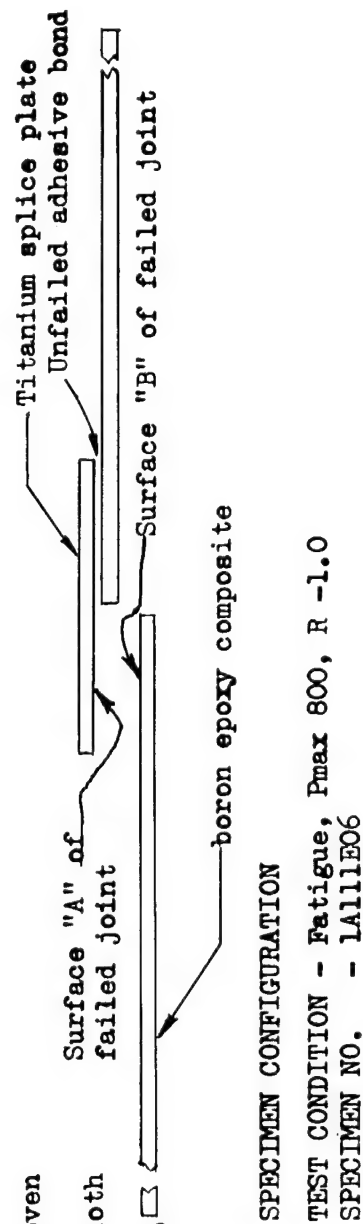
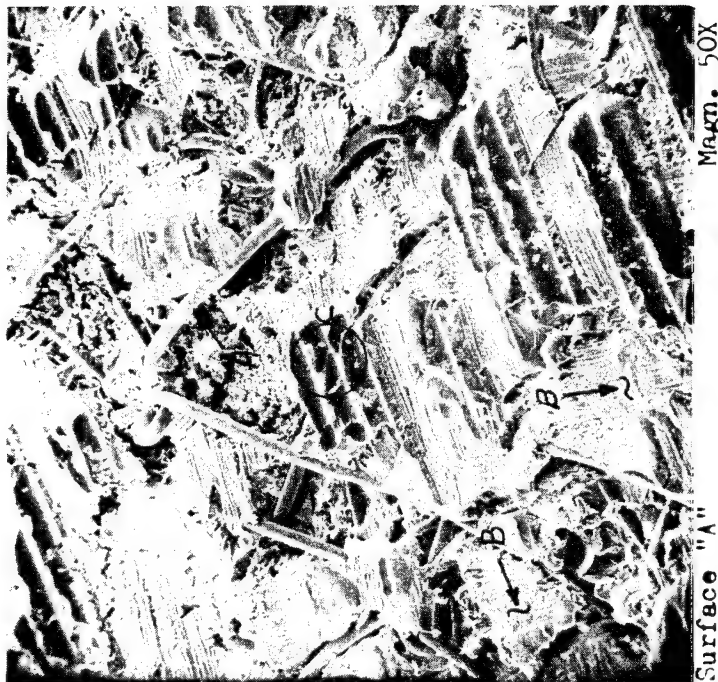
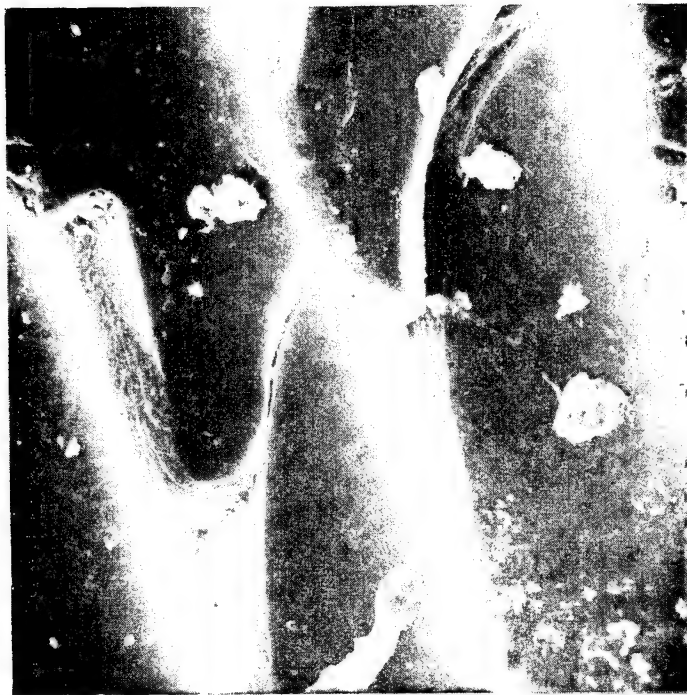


Figure 79 Typical View of Fracture Surface "A" in Adhesive Bonded Joint Specimen



Surface "A"

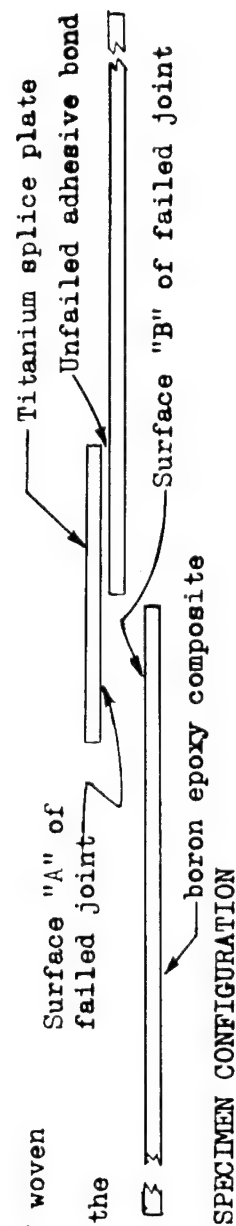
Magn. 500X



Area C Surface "A"

Magn. 500X

- NOTES:
- 1) Arrows A indicate filament of woven adhesive carrier (scrim).
 - 2) Arrows B indicate imprint of the glass scrim cloth used with the boron-epoxy tape.
 - 3) Area enclosed by circle (c) is shown at 500X. Notice topographical features (cracks) of resin matrix that was adjacent to boron filaments.



SPECIMEN CONFIGURATION

TEST CONDITION - Fatigue Pmax 2100-115,000 cycles, 3000-5650 cycles, R +10
SPECIMEN NO. - 1A11E02

Figure 80 Typical View of Fracture Surface "A" in Adhesive Bonded Joint Specimen

3.4 CONFIGURATION A STUDIES

Configuration A specimens are single splice butt joints of boron-epoxy adherends bonded to titanium, aluminum or boron-epoxy splices. The specimens on which failure mode studies were conducted are defined below:

<u>Specimen Number</u>	<u>Adherend Combination</u>	<u>Loading History</u>
IA111A03	Boron/Titanium 0.75" Overlap	Fatigue, $R = +0.1$ $F_{s \max} = 2000 \text{ psi}$ Fatigue Life = 8000 Cycles
IA111D01	Boron/Titanium	Static Tension $F_{tu} = 4600 \text{ psi}$
IA111D09	Boron/Titanium	Static Compression $F_{su} = -6300 \text{ psi}$
IA113A01	Boron/Boron	Fatigue, $R = +0.1$ $F_{\max} = 1300 \text{ psi}$ Fatigue Life = 10,660,000 Cycles
IA113D03	Boron/Boron 0.75" Overlap	Static Tension $F_{su} = 3900 \text{ psi}$
IIA11C03	Boron/Titanium 0.75" Overlap	Compression Fatigue, $R = +10.0$ $F_{s \max} = 2100 \text{ psi}$ Fatigue Life = 12,500 Cycles
IIIA12A01	Boron/Titanium 0.75" Overlap	Fatigue, $R = +0.1$ $F_{s \max} = 1300 \text{ psi}$ Fatigue Life = 9210 Cycles

3.4.1 Specimen IA111A03

This is a Configuration A specimen having boron adherends and a titanium splice plate. The failure bond joint area is 1" wide with a 0.75" overlap. Failure Surface A (titanium splice plate) is shown in Figure 81 and failure Surface B (boron adherend) is shown in Figure 82.

In Figure 81, Section #1 is cohesive shear failure of the adhesive immediately adjacent to the titanium splice plate. The fracture surface visible in Section #2 is the resin matrix sheared from the outer surface of the boron and the whitish look of this section is due to a secondary failure at the adhesive-titanium interface. The remainder of the fracture was predominately shear between the resin matrix and the boron filaments with some tensile failure of the boron filaments. The two white streaks were areas of shear between the resin matrix and the 104 glass scrim cloth. A 200X magnification of a portion of this area is shown in Figure 83. This photograph shows where the fibers had been imbedded in the resin but were sheared out under fatigue loading. The resin ridges show the angled tension failures in the resin with some areas being rounded similar to those exhibited in the $R = +10.0$ fatigue specimen (Figure 80). However, the rounding is not as pronounced and the fracture along the top of these ridges has sharper peaks similar to those exhibited by the shear mode in the flexure specimen.

In Figure 82, Section #1 is a cohesive failure of the adhesive adjacent to the titanium splice plate and coincides with Section #1 in Figure 81. The remainder of the fracture was shear between the resin matrix and boron fiber leaving the upper surface of the boron fibers exposed. A 100X magnification of a portion of this area is shown in Figure 84. This photograph is of the facing surface to that shown in Figure 83, and the fractures in the resin between the fiber are mating fractures to those along the ridges in Figure 83.

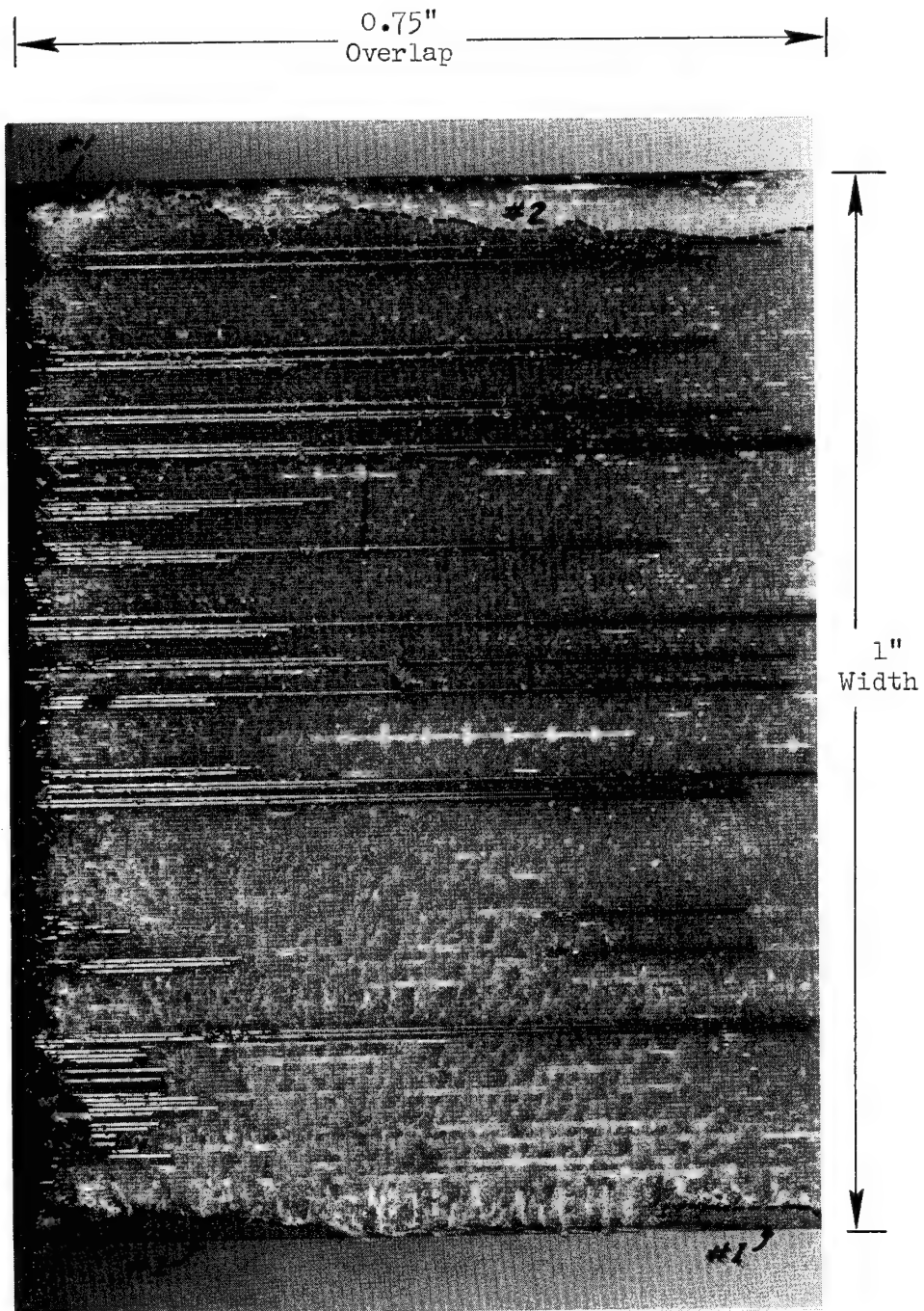


Figure 81 IA111A03 - Failure Surface "A"
Titanium Splice Plate

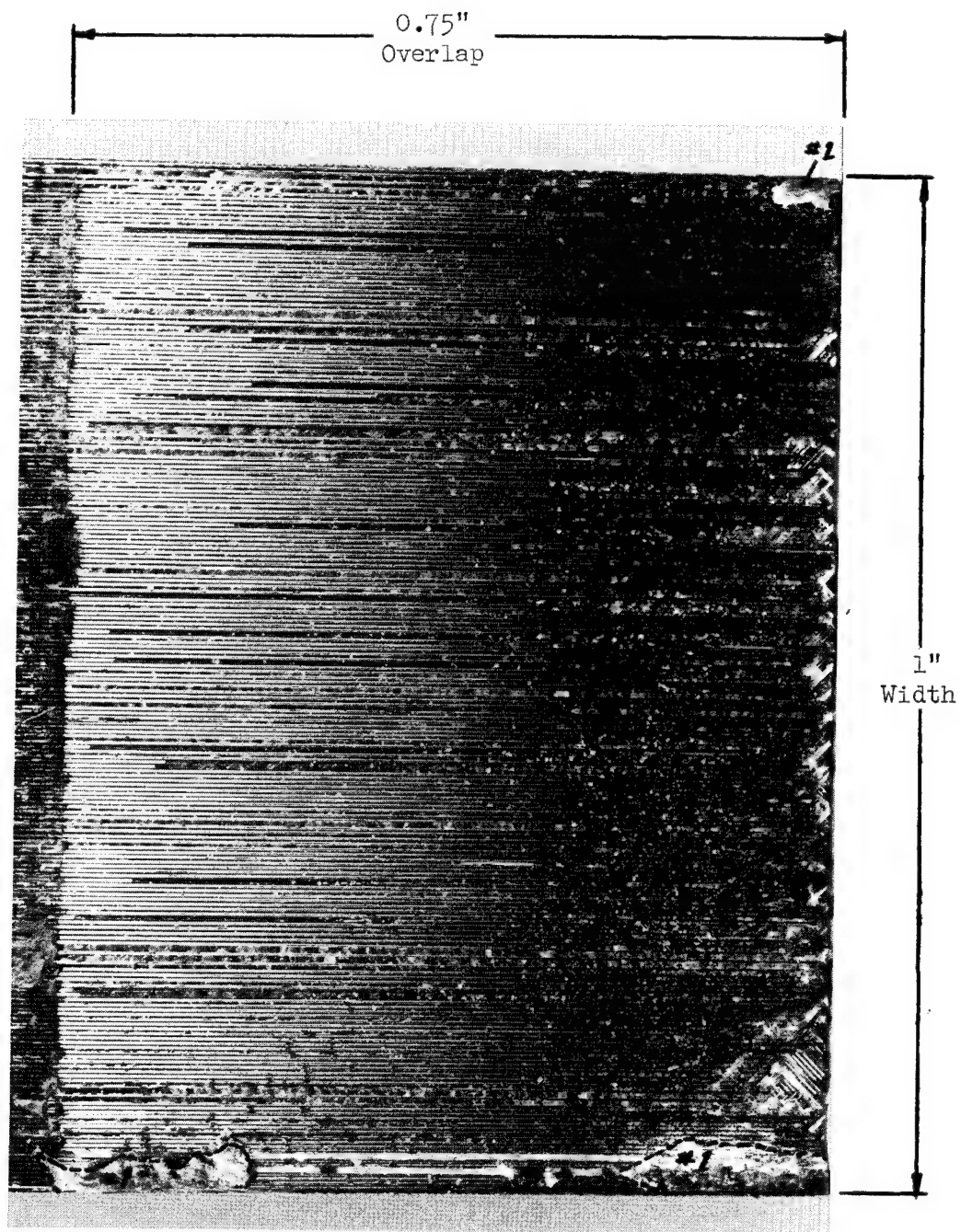


Figure 82 IA111A03 - Failure Surface "B"
Boron Adherend

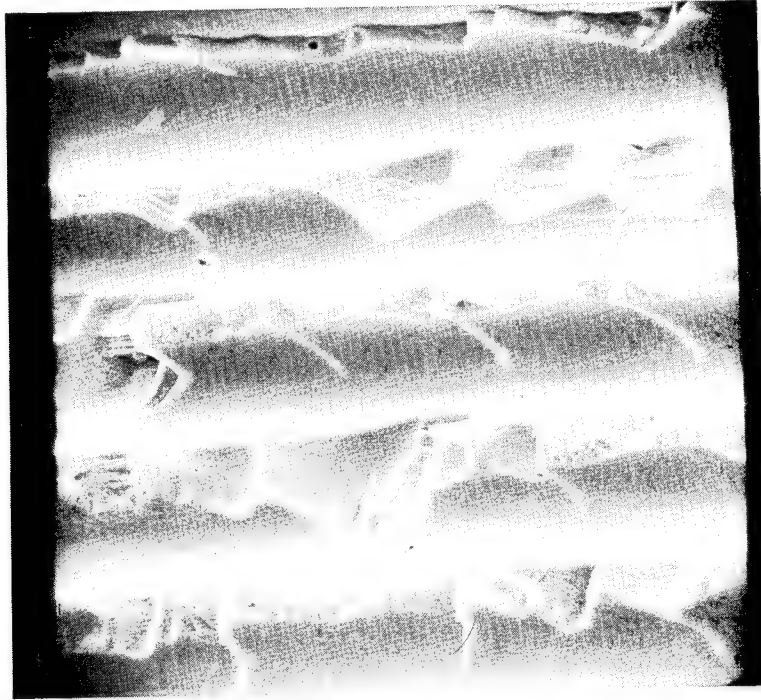


Figure 83 IA111A03 - Failure Surface "A"
200X Magnification

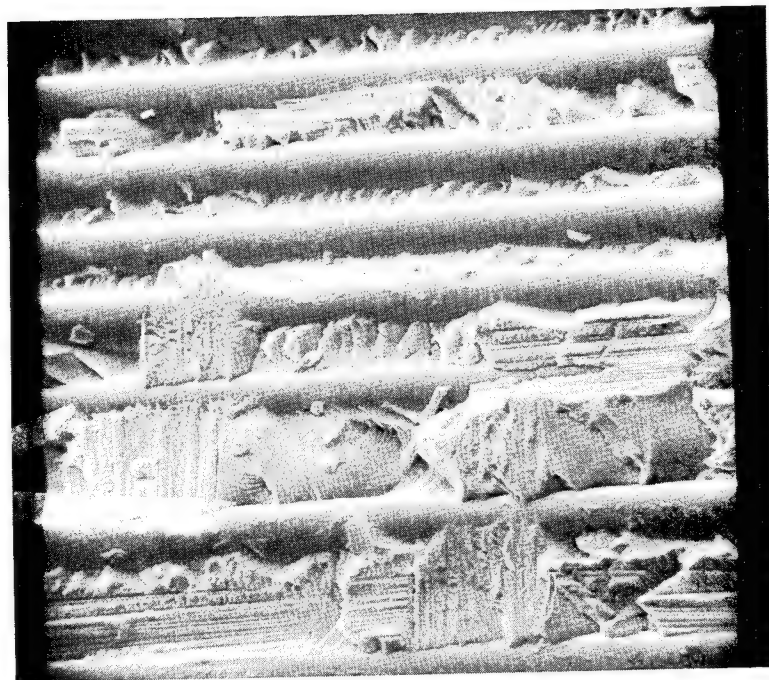


Figure 84 IA111A03 - Failure Surface "B"
100X Magnification

3.4.2 Specimen IA111D01

This is a Configuration A specimen having boron adherends and a titanium splice plate. The specimen was subjected to static loading in tension and failed at 4600 psi. Figures 85 and 86 show failure Surfaces A and B respectively. The major modes of failure for this specimen were shear between the resin matrix and the boron fiber and tensile failure of a large number of boron fibers. A small area across the end of the titanium splice plate had an adhesive failure between the EA9601 adhesive and the titanium splice plate. Only one high magnification, 100X, photograph was taken of this specimen, Figure 87. This photograph shows the exposed fiber of Surface B and the broken resin between the fibers. The appearance of this fracture mode is similar in nature to that shown in Figure 84 for specimen No. IA111A03 (fatigue test, $R = +0.1$). Again by this similarity it may be indicated that the direction of load is the major controlling factor in the type of failure mode.

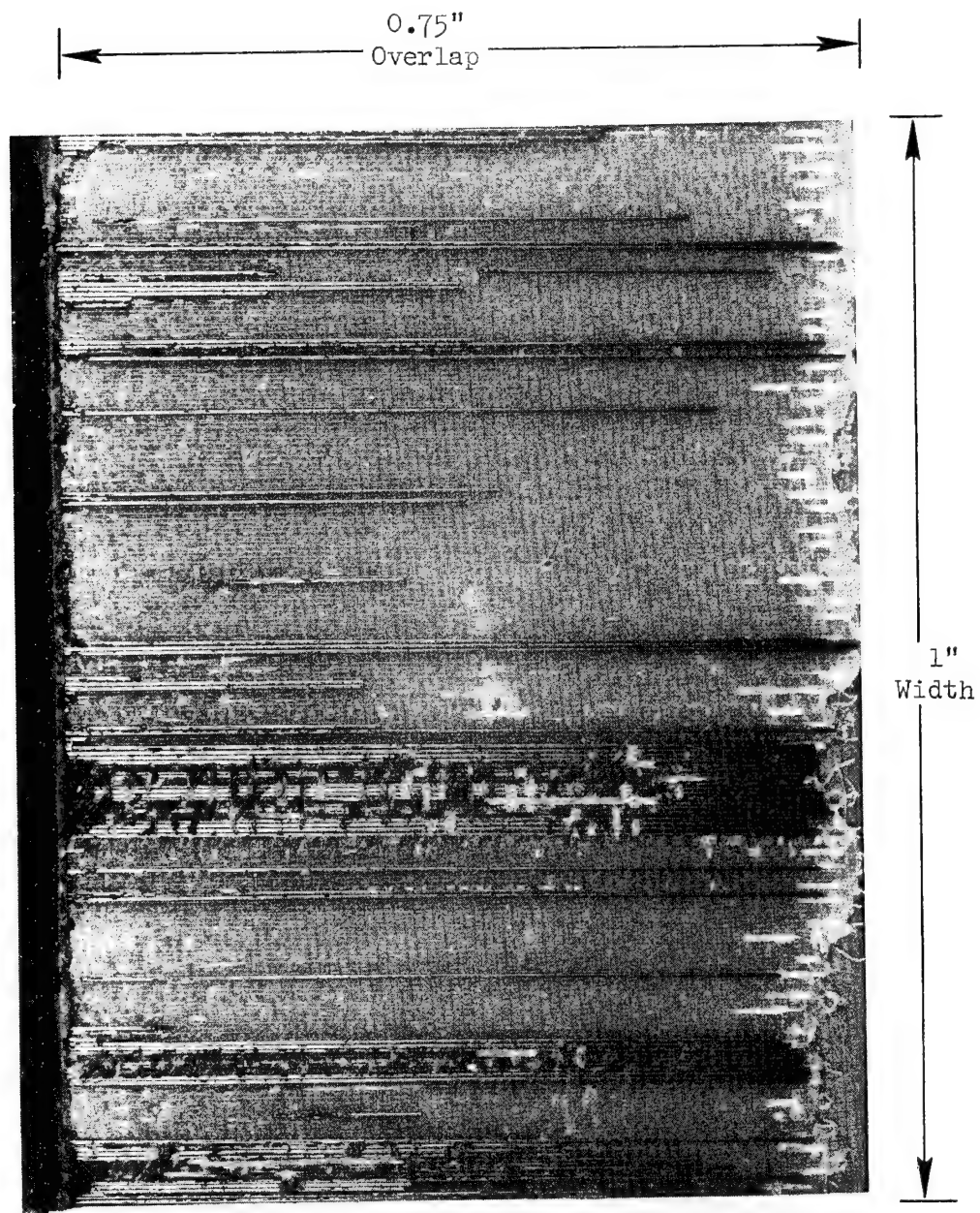


Figure 85 IA111D01 - Failure Surface "A"
Titanium Splice Plate

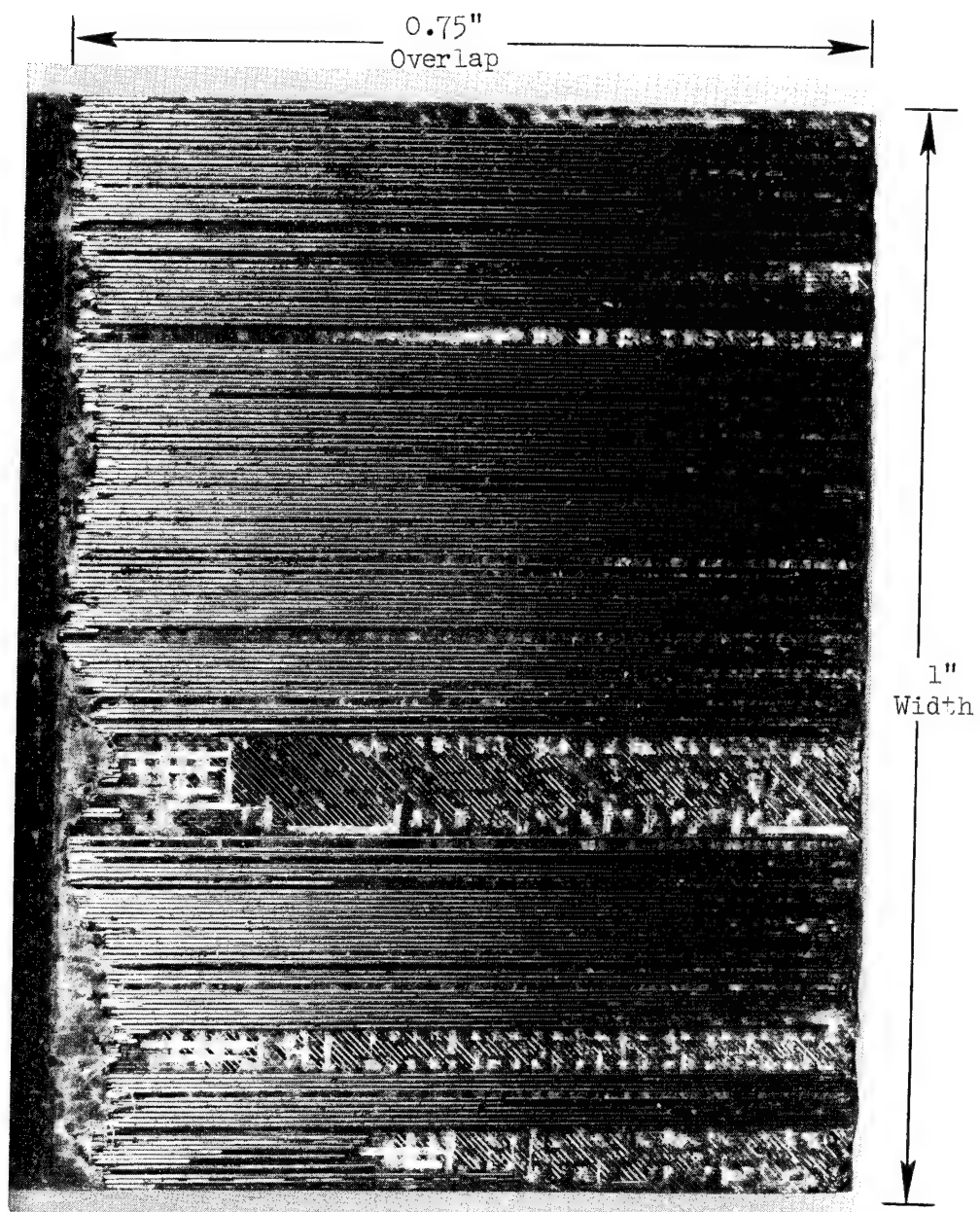


Figure 86 IA111D01 - Failure Surface "B"
Boron Adherend

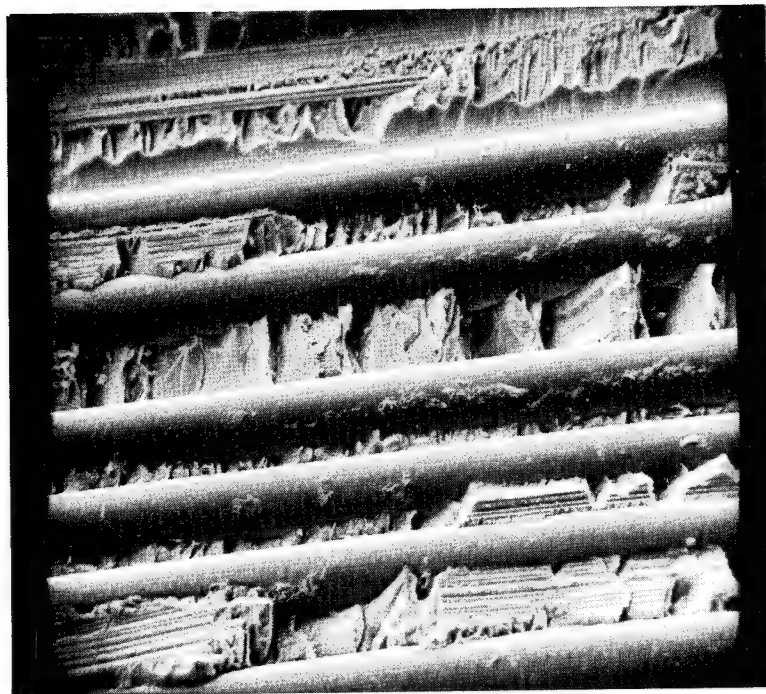


Figure 87 IA111D01 - Failure Surface "B"
100X Magnification

3.4.3 Specimen IA111D09

This is a Configuration A specimen having boron adherends and a titanium splice plate. The specimen was subjected to a static compression load. Average ultimate shear stress was 6300 psi and is representative of a high quality bond. Failure Surface A (titanium splice plate) is shown in Figure 88 and Failure Surface B (boron adherend) is shown in Figure 89.

In Figure 88, Section #1, the major mode of failure was shear between the resin matrix (adjacent to the splice plate adhesive) and the first or outer ply of boron filaments of the specimen half. The longitudinal area outlined by dots is the location of an 0.05 inch wide gap between boron filaments in the first or outer ply.

The major mode of failure in Section #2 was cohesive shear of the adhesive along the plane of the adhesive scrim cloth. This is a failure mode not often detected in composite joints since the adhesive is usually much stronger than the resin. The failure mode in Section #3 was an adhesive failure of the adhesive to the titanium surface.

The fracture surface of Figure 89 is a mirror image of the splice plate surface shown in Figure 88. The small square area outlined in this figure is the area selected for investigation by SEM photomicrographs. Figure 90 is the larger area outlined in Figure 89 and was used as a map for more extensive investigation. Three different failure modes were studied with this specimen. One failure mode, Figure 91, was associated with shear at the adhesive surface; the second, Figure 92, was associated with shear within the adhesive along the adhesive scrim carrier (cohesive mode); and the third, Figure 93, illustrated once again the resin/fiber interface shear mode associated with compression loading.

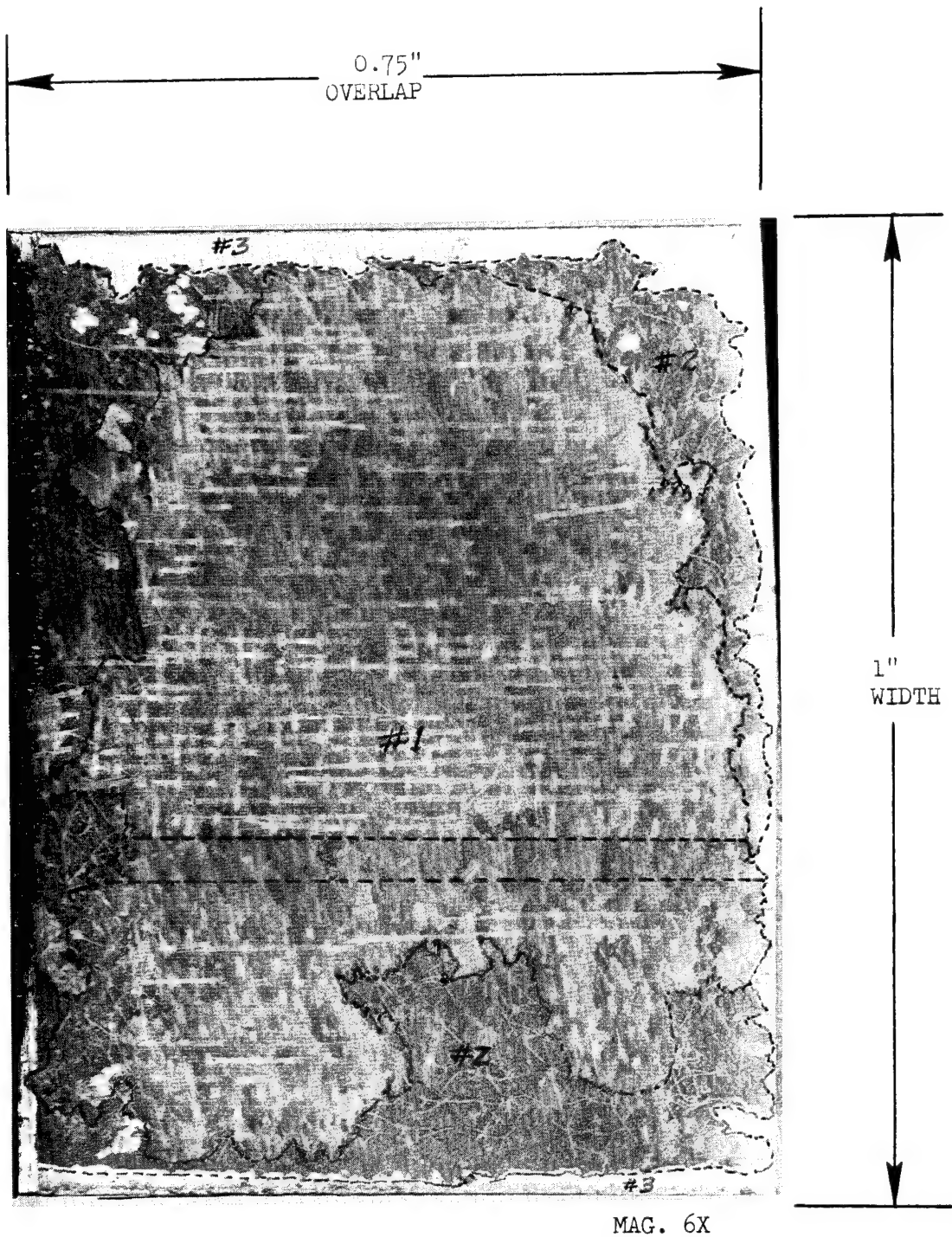


Figure 88 IA111D09 Failure Surface "A" -
Titanium Splice Plate

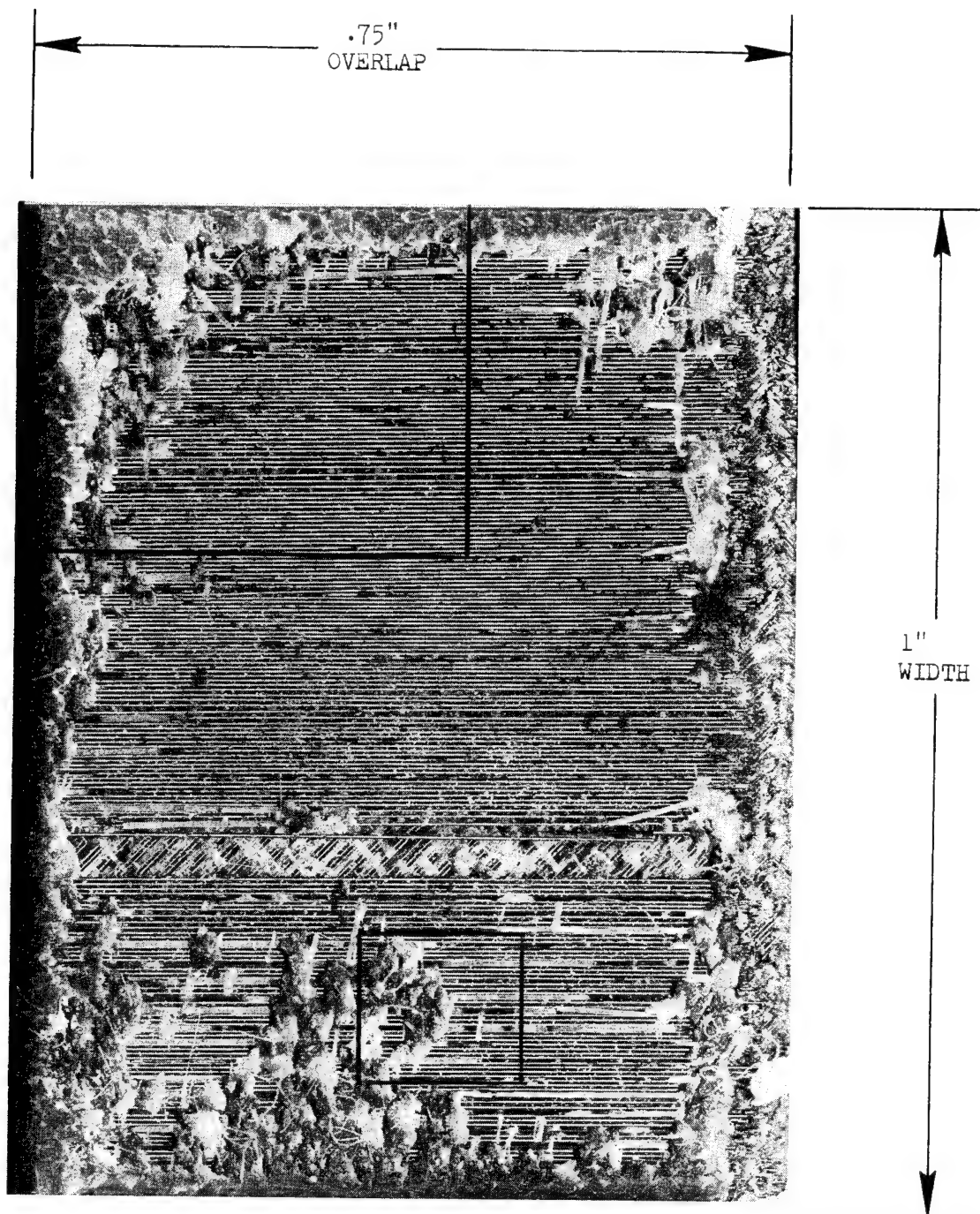
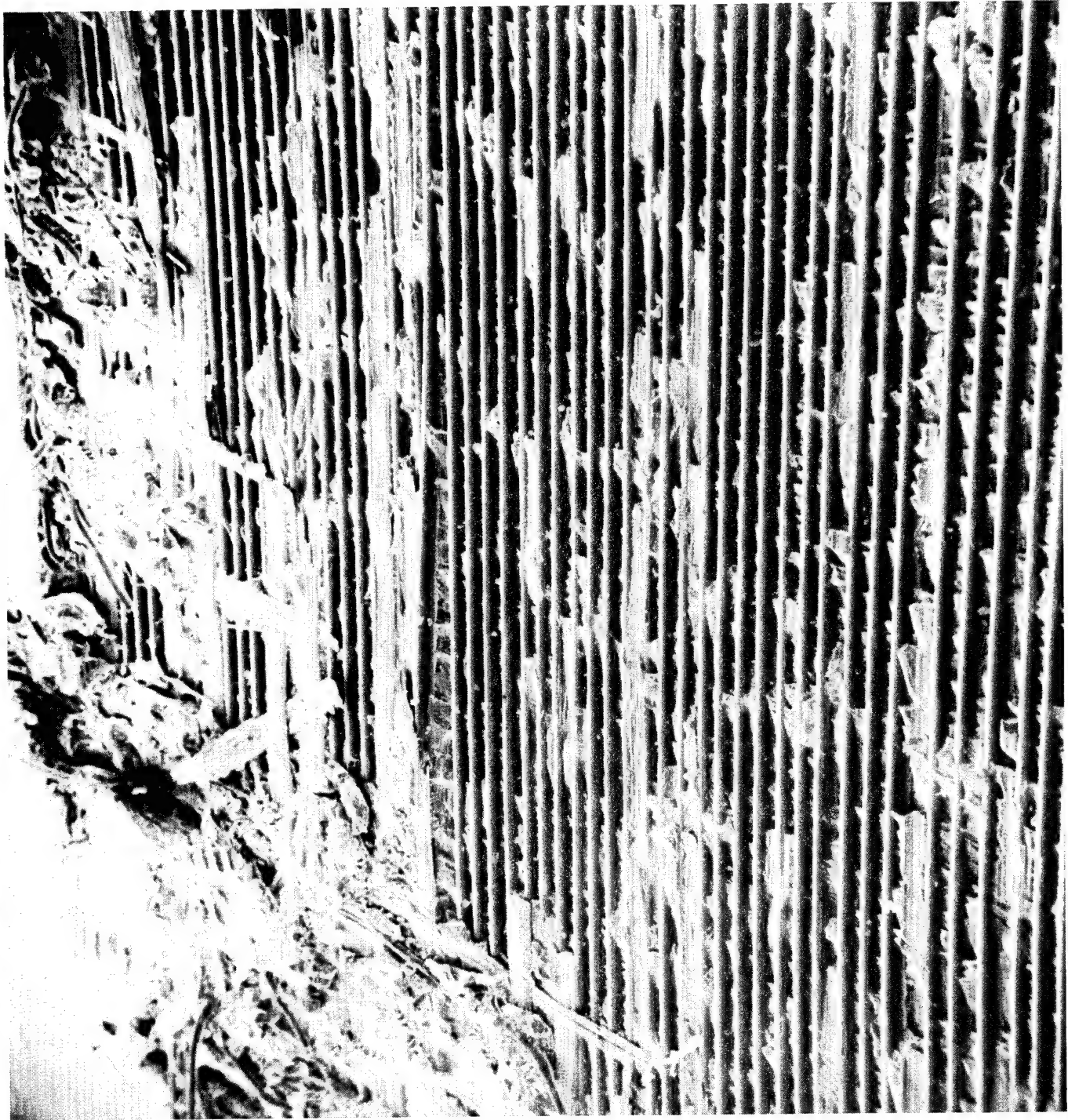


Figure 89 IA111D09 Failure Surface "B" -
Boron Adherend - Mag. 6X



UP

Figure 90 IA111D09 Failure Surface "B" Map - 40X Magnification, 45° Tilt
(Reference Figure 89)

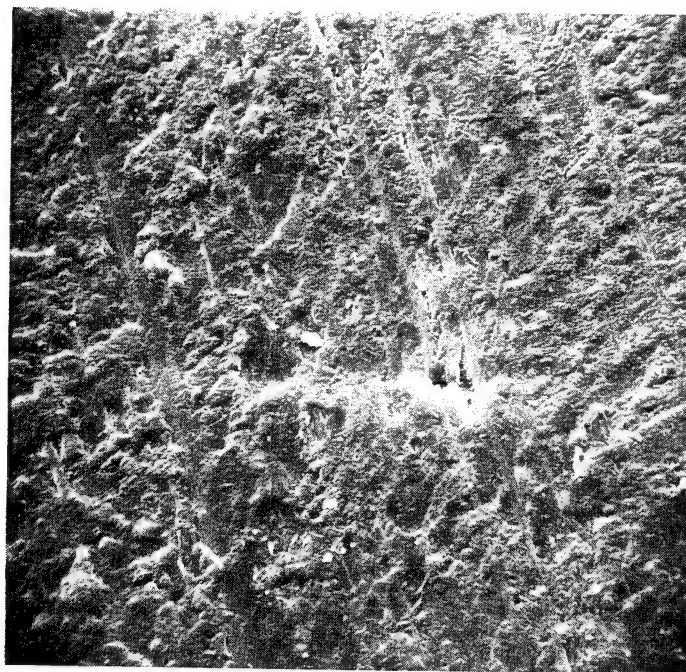


Figure 91 IA111D09 Surface "B", 48X Magnification,
Adhesive Surface (Reference Figure 90)



Figure 92 IA111D09 Surface "B", 51X Magnification
(Reference Figure 90, Adhesive Surface
Upper Left)

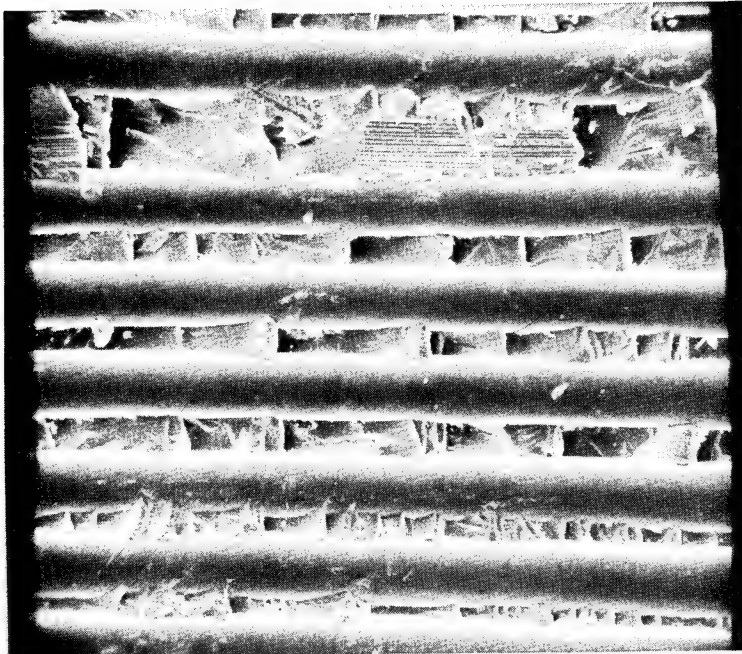


Figure 93 IA111D09 - Surface "B"
100X Magnification, 0° Tilt
(Reference Figure 90)

3.4.4 Specimen IA113A01

This is a Configuration A specimen having boron adherends and a boron splice plate. The specimen was subjected to fatigue cycling at a stress ratio $R = +0.1$ and a maximum stress of 1300 psi. Its fatigue life was 10,660,000 cycles. Failure Surface A (boron splice plate) is shown in Figure 94, and Failure Surface B (loaded boron adherend) is shown in Figure 95.

In Figure 94, Section #1, the mode of failure was shear between the resin matrix and the first or outer layer of boron filaments of the loaded boron specimen half (Surface B). The failure mode of Section #2 is just the reverse of Section #1, i.e., shear between the resin matrix and outer or surface layer of boron filaments of the boron splice plate.

Section #3 exhibits a failure mode different from failure modes previously investigated. The failure in this area occurred between the first set of $\pm 45^\circ$ plies. The failure mode was shear of the resin matrix adjacent to the 2nd 45° ply of boron. The light area indicated by the arrow is powdered resin matrix.

In Figure 95, the failure modes of Sections #1 and #2 are mirror images of those shown in Figure 94. The major portion of Section #2 shows the outer portion of the resin matrix that was adjacent to the outer ply of boron filaments in the splice plate.

The major portion of Section #3 shows the resin matrix that was adjacent to the boron filaments in the 2nd 45° ply of the boron splice plate. The dashed roughly circular area denotes considerable fretting or rubbing.

The square areas outlined in Figures 94 and 95 are the areas investigated by SEM photomicrographs. Figure 96 is the area outlined in Figure 94 and was used as a map for further investigation. Two different failure modes were evaluated at higher magnifications. Figure 97 illustrates two different failure modes. One failure mode is a shear failure between the resin and the first layer of boron parallel to the load direction. This failure mode is the same as that previously defined for tension-tension fatigue loading. However,

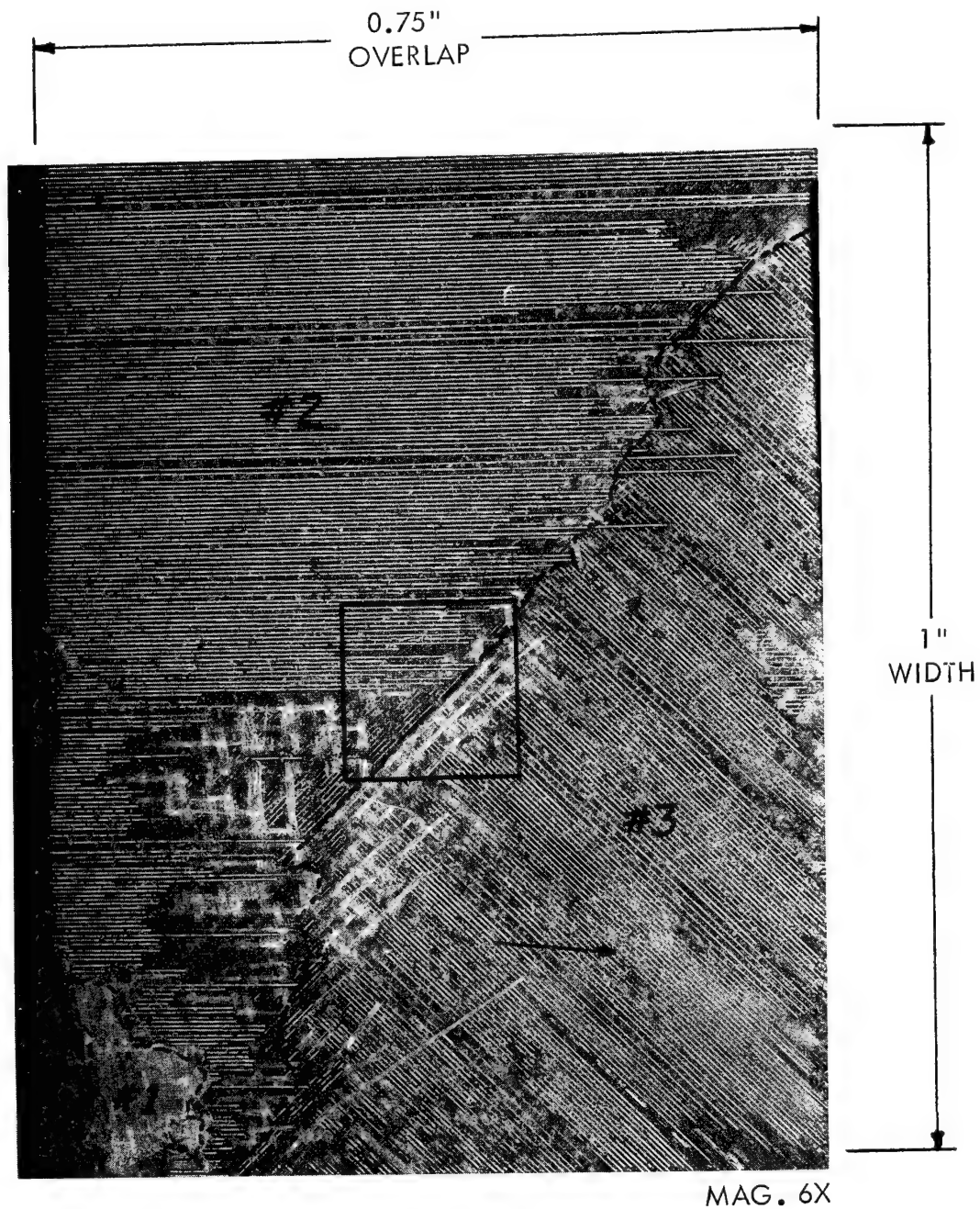


Figure 94 IA113A01 Failure Surface "A"
Boron Splice Plate

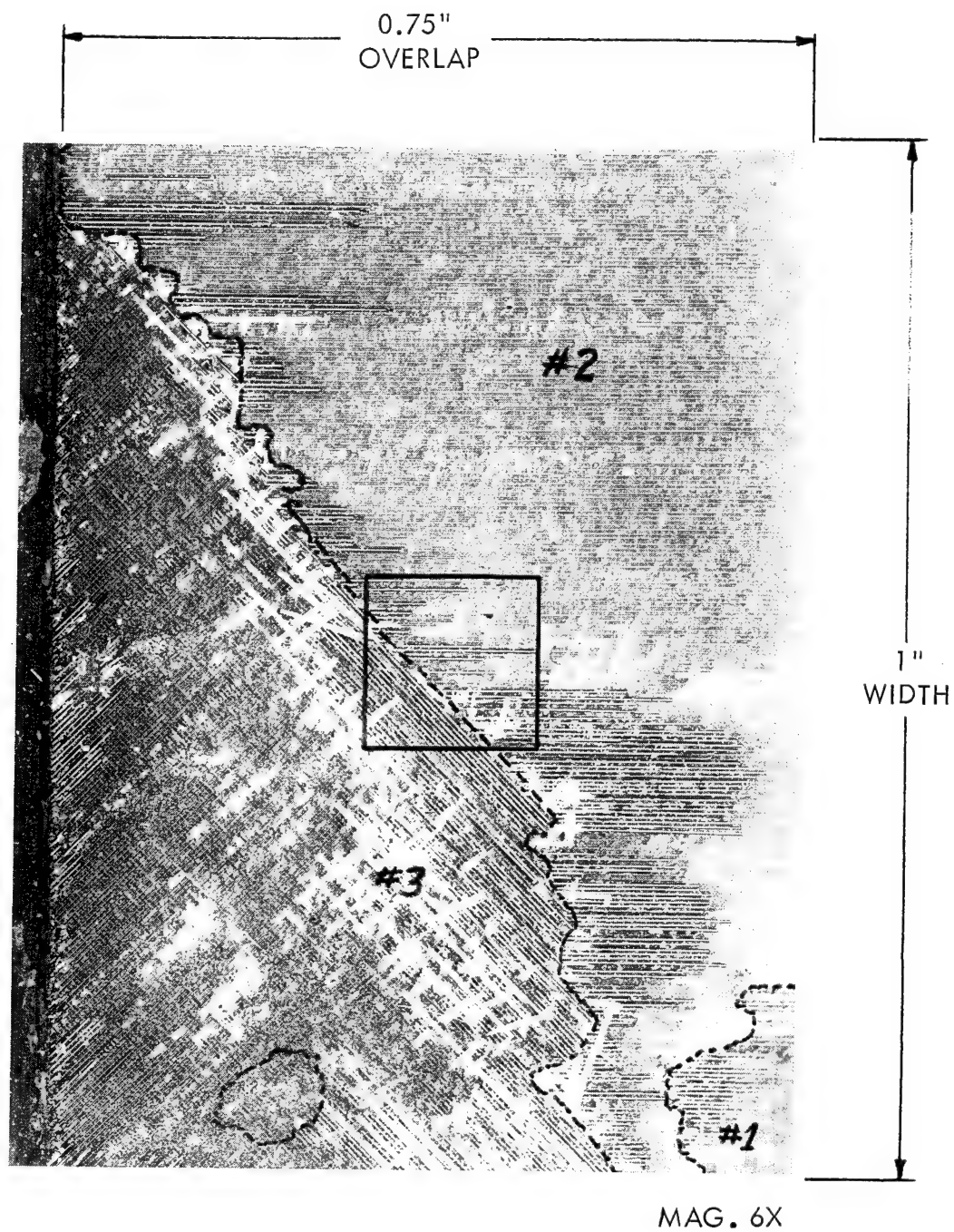


Figure 95 IA113A01 Failure Surface "B"
Loaded Boron Adherend

UP
←

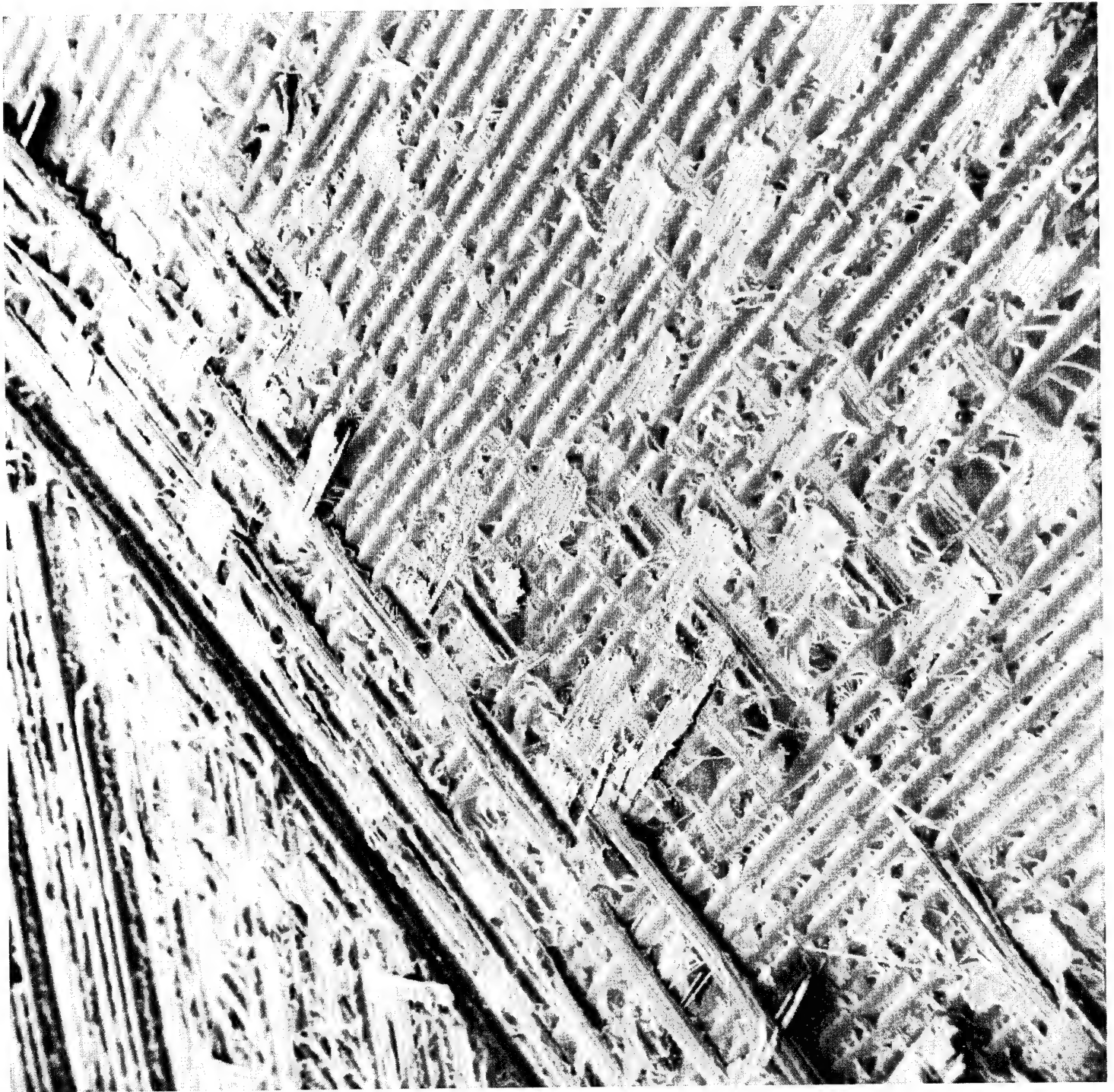


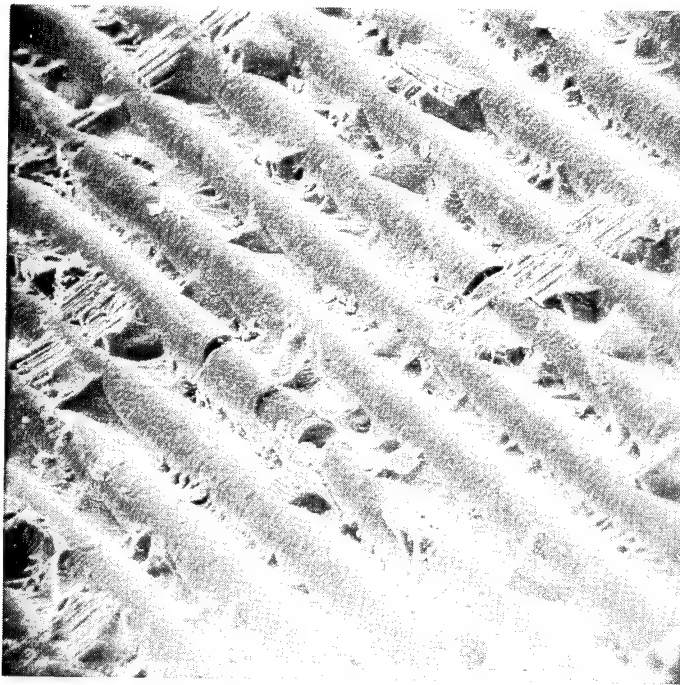
Figure 96 IA113A01 Failure Surface "A" Map
40X Magnification
(Reference Figure 94)



Figure 97 IA113A01 Failure Surface "A"
53X Magnification
(Reference Figure 96 Upper Left)

the fracture surface in the resin adjacent to the 45° ply exhibits a different type of failure mode. This difference is attributed to the difference in support provided to the resin by the off angle ply. This failure mode is further investigated in the photomicrographs shown in Figure 98. The surface exposed in these SEM photomicrographs is the same as designated as Section #3 in Figure 94. The failure mode in these photomicrographs is shear in the resin adjacent to the 45° ply resulting from a tension-tension fatigue load applied at 0° . The 117X and the 235X magnifications reveal a failure associated with the boron fiber which has not been detected in previous failure mode studies. The failure illustrated in this figure has the appearance of fiber surface spalling.

The square area outlined in Figure 95 is shown in Figure 99. The two different failure modes illustrated in Figures 96 through 98 are also visible in Figure 99. Figure 100 illustrates the same failure mode as Figure 97 and Figure 101 illustrates the same failure mode as Figure 98 since these represent the mirror images of those figures.



117X Magnification



235X Magnification

Figure 98 IA113A01 Failure Surface "A"
(Reference Figure 96 Right of Center)

↑ UP

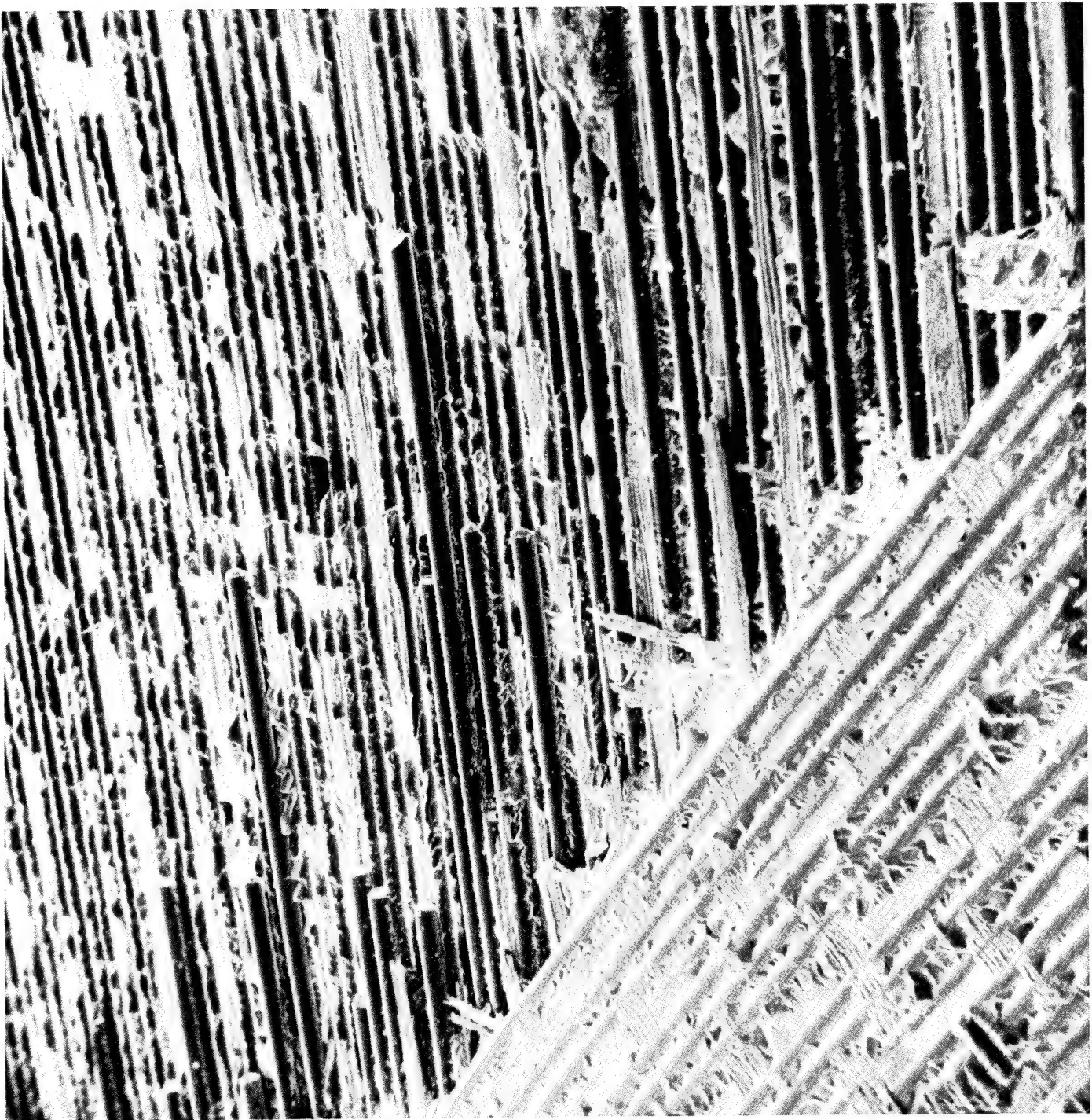


Figure 99 IA113A01 Failure Surface "B" Map
40X Magnification
(Reference Figure 95)

3.4.5 Specimen IA113D03

This is a Configuration A specimen having boron adherends and a boron splice plate with a standard 0.75" overlap. The specimen was subjected to a static tension load, and failed at an ultimate average shear stress of 3900 psi. The failure bond area is 0.75" x 1.0". Failure Surface A is shown in Figure 102 and has the standard resin-to-fiber shear mode. Failure Surface B is shown in Figure 103, and although it is a mirror image of Figure 102, close examination reveals this failure mode to be different than previously investigated fracture surfaces. For this reason, two samples were removed for SEM inspection and these are shown in Figures 104 and 105.

Figure 104 was taken from near the center of the specimen and Figure 105 was taken near the end of the specimen. Extensive shear fracture can be detected over the entire photograph with the exception of a few areas that appear as a peel fracture mode. This peel mode can be seen more clearly in Figure 106. This fracture compares closely with the peel mode reported in the first fracture studies conducted under this program. Figure 107 illustrates that the shear fracture is not confined to one interface at a given location. This figure shows failure occurring between the resin and the 0° ply and the 45° ply in the same location. These same failures are shown in Figures 108 and 109. Presence of some peel mode failure and multi-layer shear failure are believed to be the reasons why this boron-to-boron specimen exhibited a lower strength, generally, than the boron to metal specimens.

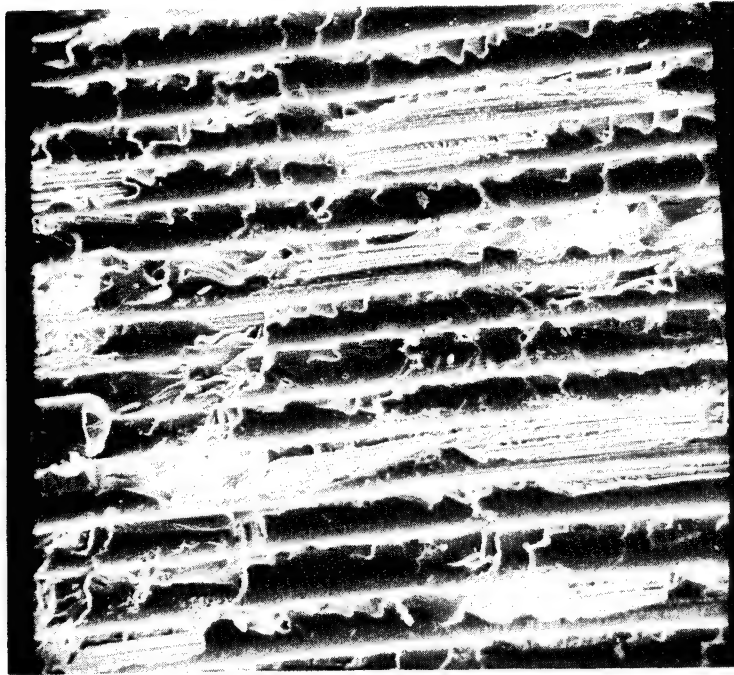


Figure 100 IA113A01 Failure Surface "B"
98X Magnification
(Reference Figure 99 Upper Center)

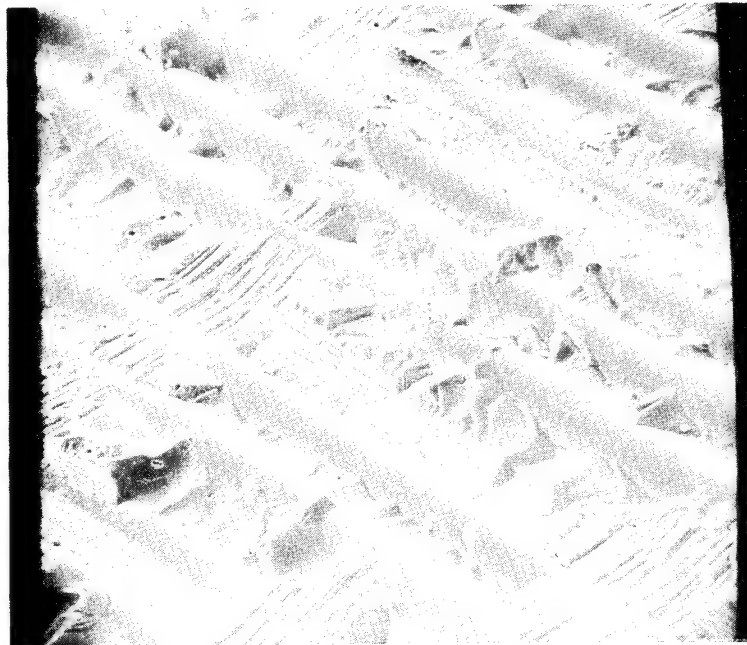


Figure 101 IA113A01 Failure Surface "B"
110X Magnification
(Reference Figure 99 Lower Left)

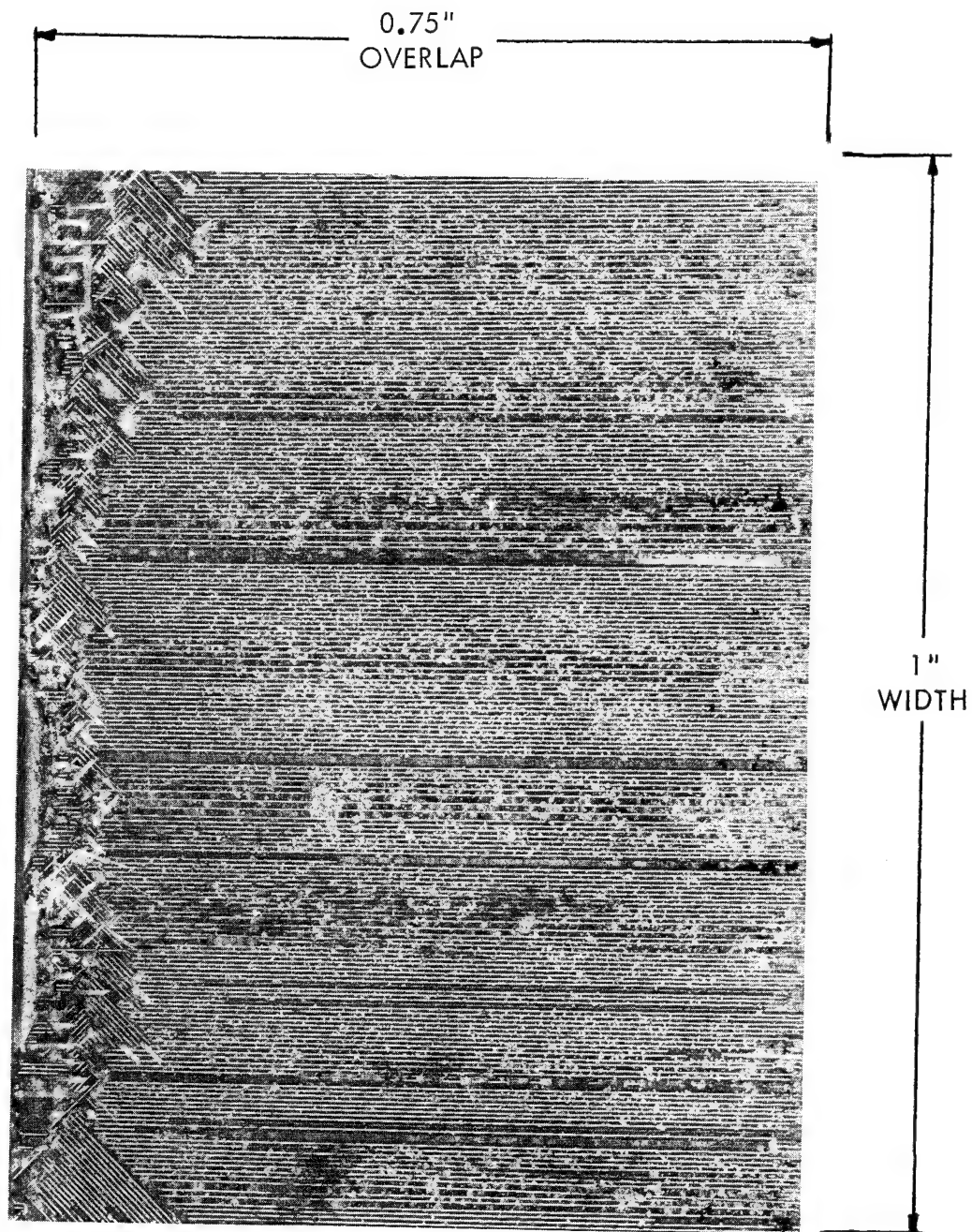


Figure 102 IA113D03 Failure Surface "A"
Boron Splice Plate
6X Magnification

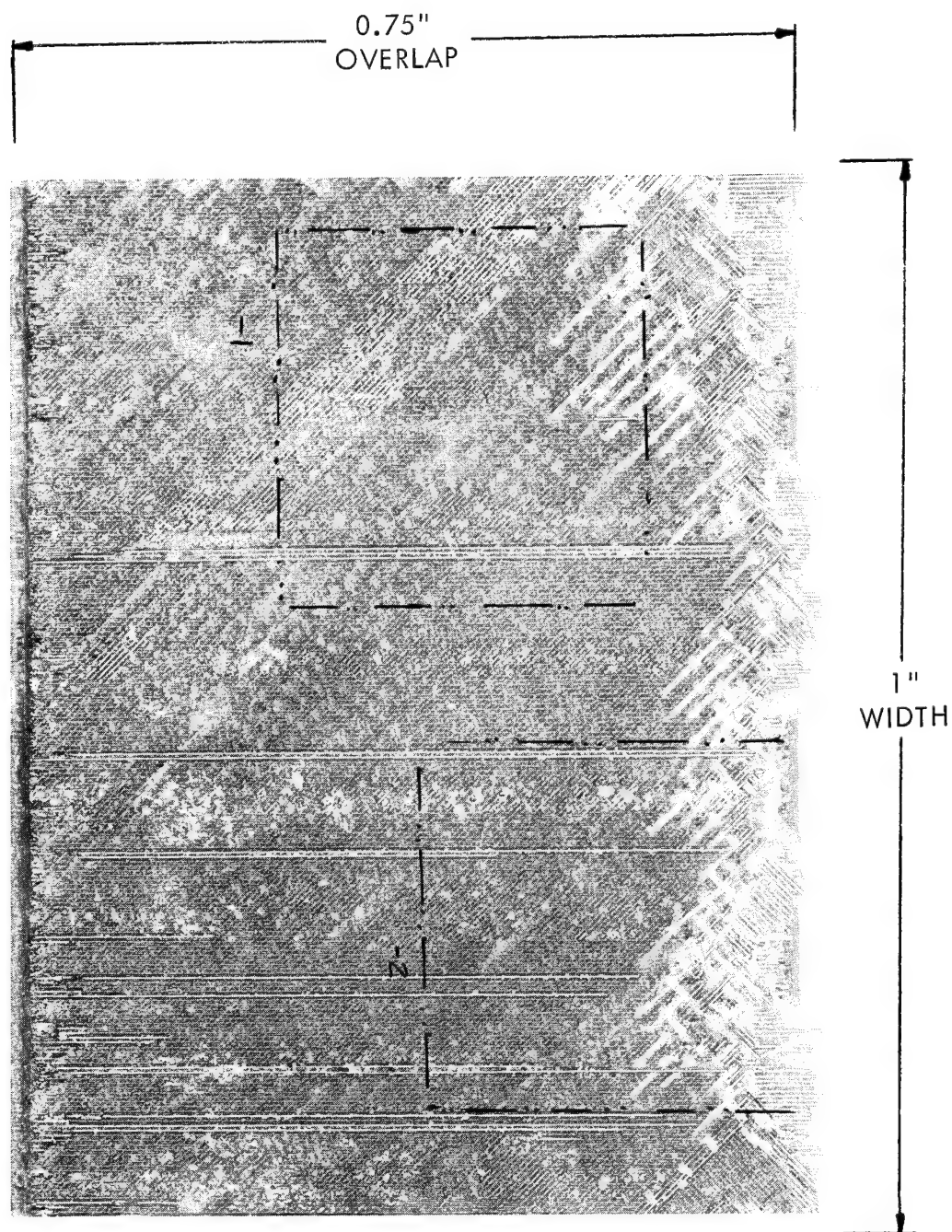


Figure 103 IA113D03 Failure Surface "B"
Boron Adherend
6X Magnification

UP ↑

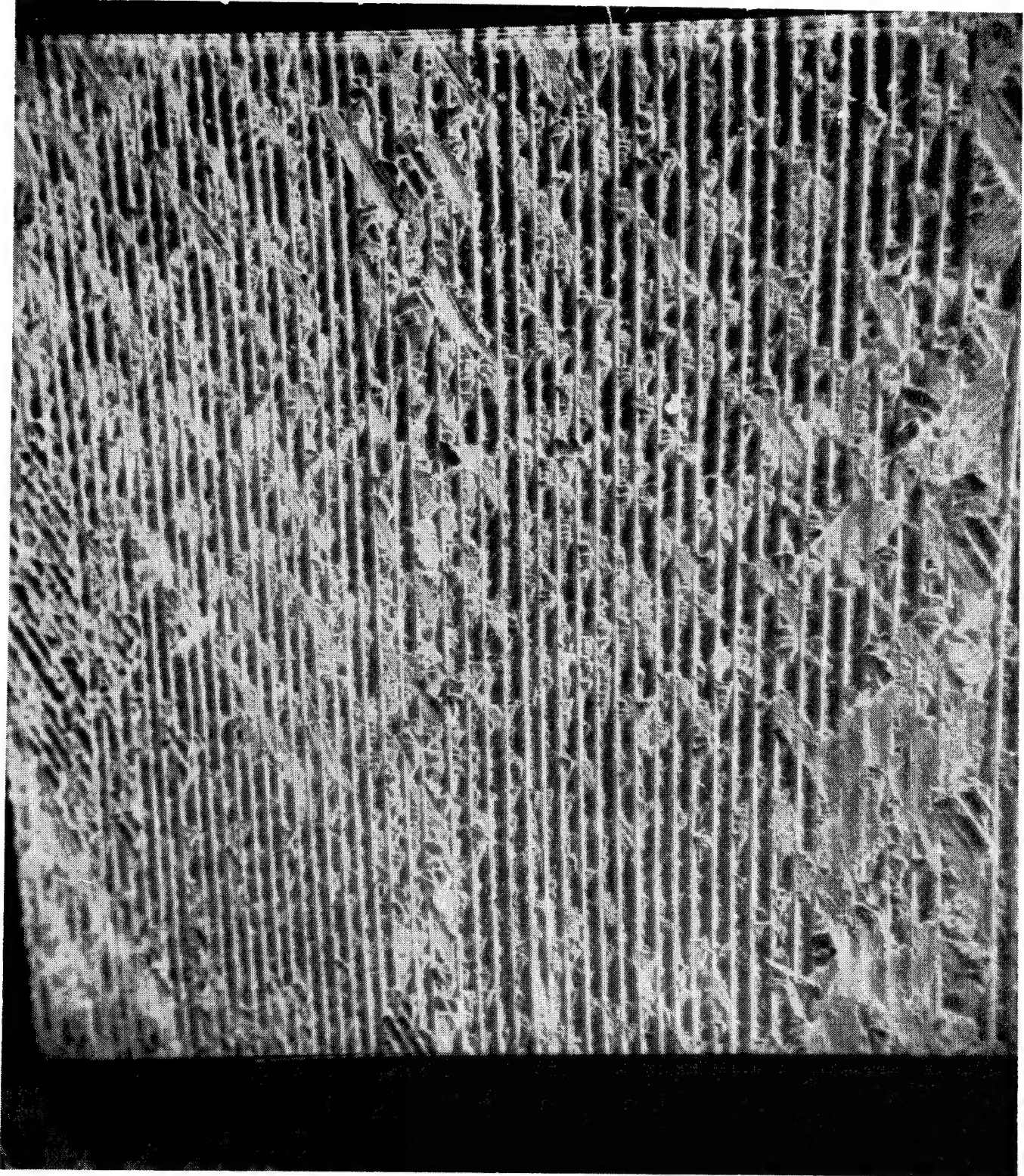


Figure 104 IA113D03 Failure Surface "A", 40X Magnification

UP ←

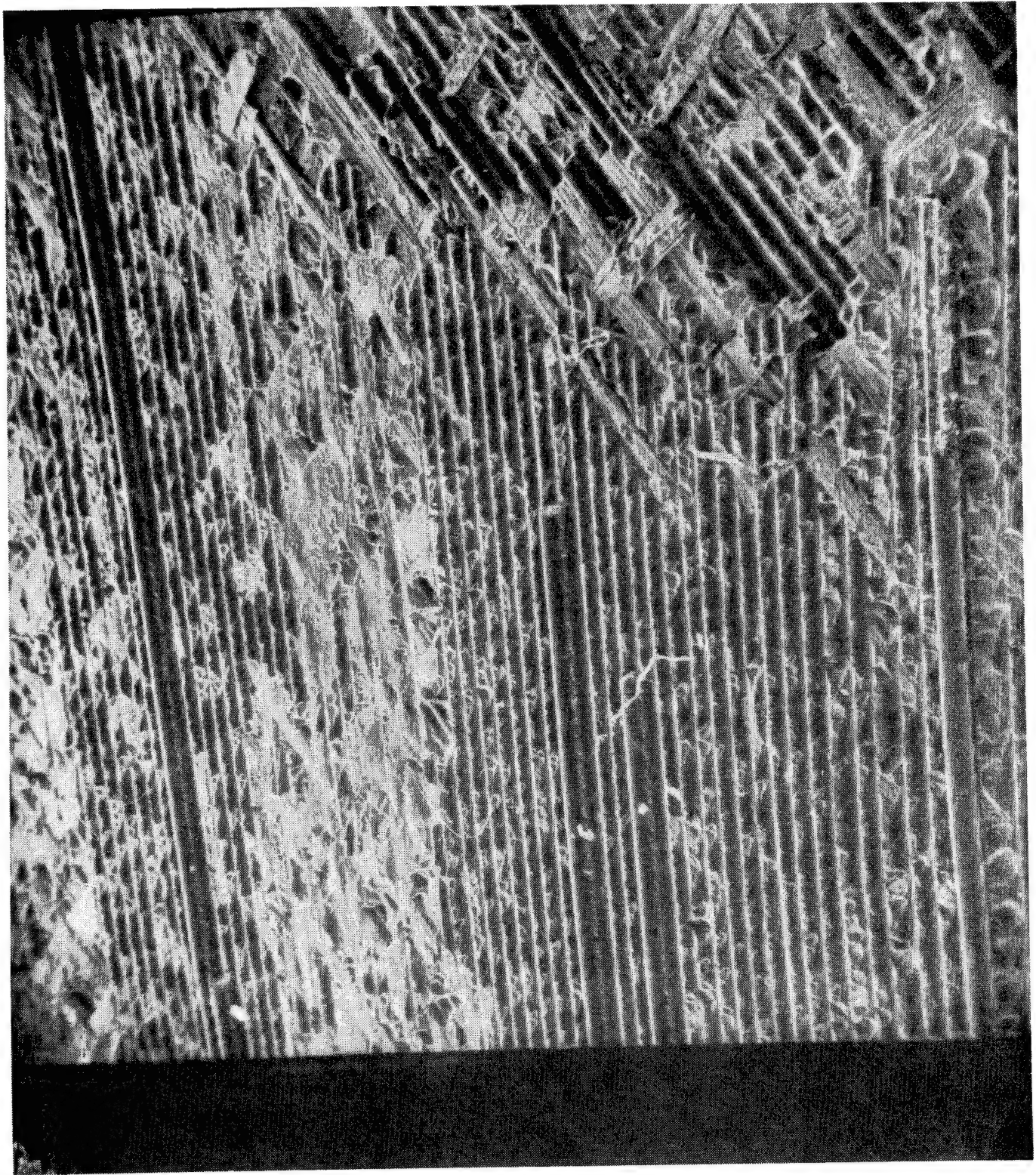


Figure 105 IA113D03 Failure Surface "B", 40X Magnification
(Reference Figure 103 Near Edge)

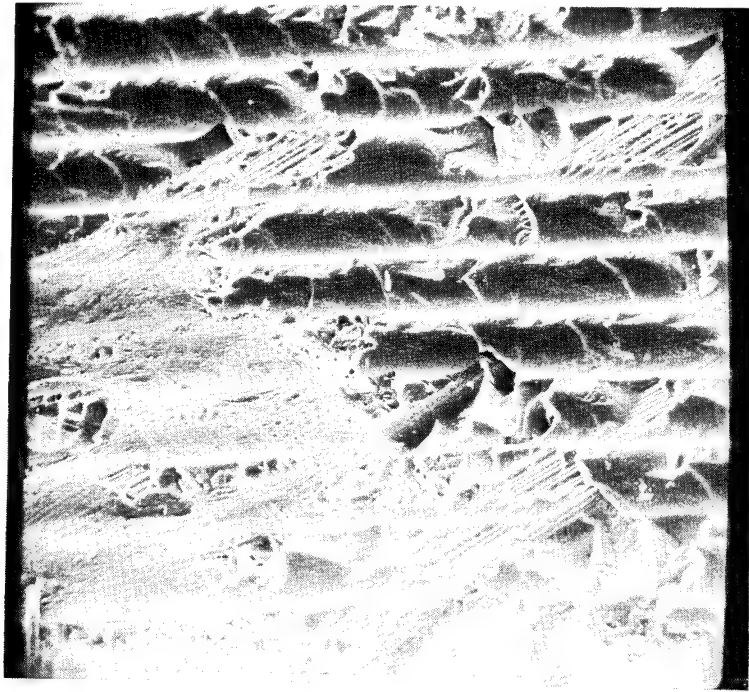


Figure 106 Enlargement of Figure 104
Lower Left Hand Corner 122X Magnification

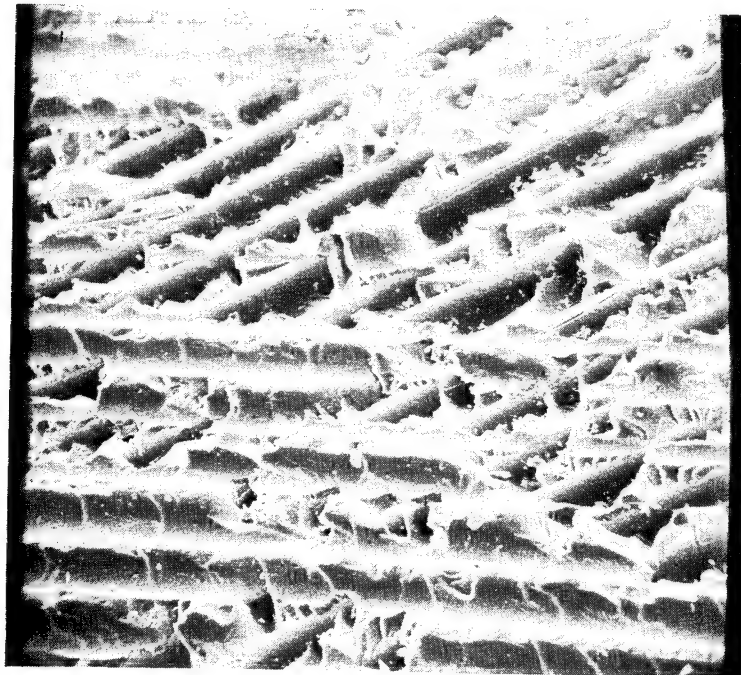


Figure 107 Enlargement of Figure 104
Upper Center, 100X Magnification

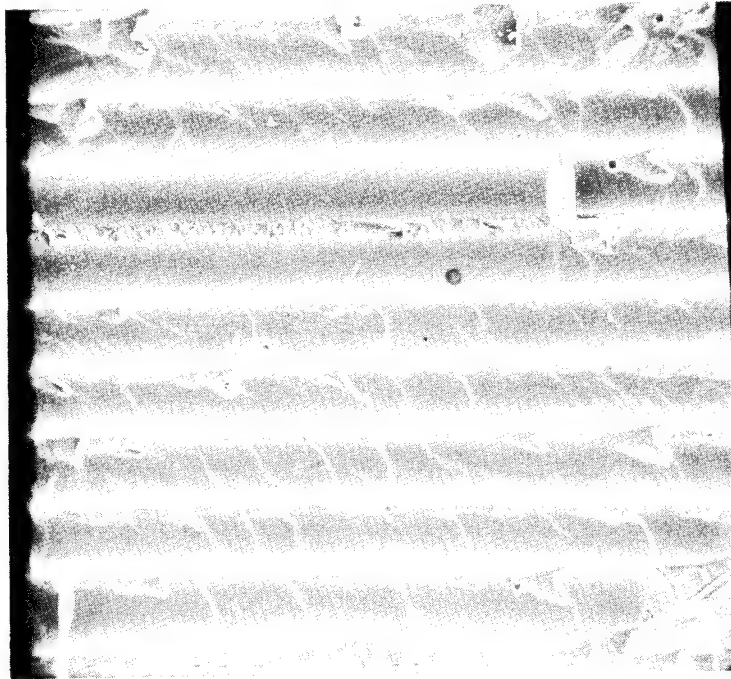


Figure 108 Enlargement of Figure 105
Just Below Center, 117X Magnification

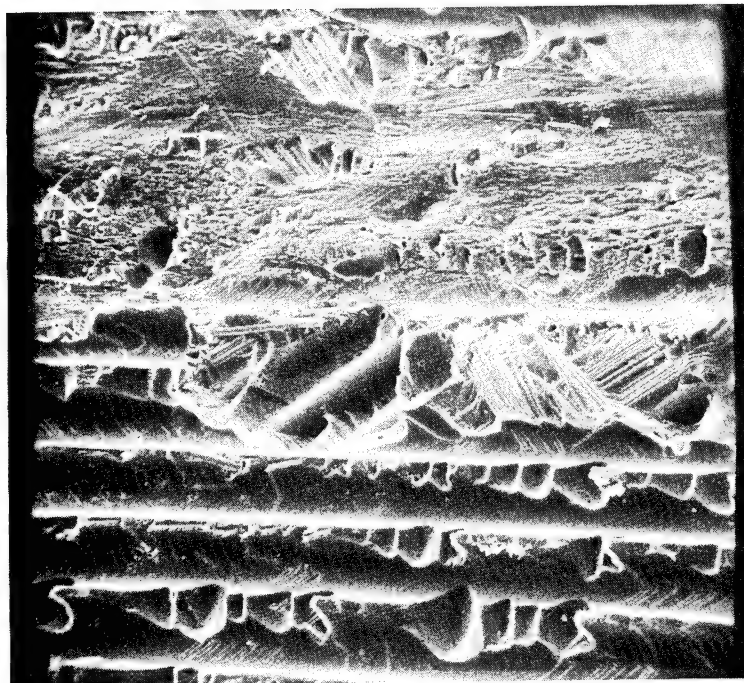


Figure 109 Enlargement of Figure 105
Near Center, 110X Magnification

3.4.6 Specimen IIA11C03

This is a 3-inch wide Configuration A single splice lap joint compressive fatigue loaded to a stress ratio of $R = +10.0$. Figure 110 is a 2X magnification overall view of the fractured surface. No new failure modes are apparent in any of the 3-inch wide specimens investigated. However, the increase in joint area allows for more fracture modes within one specimen as illustrated in Figure 110. One factor noted in the wider joints was the increased amount of crazed or granular resin over the entire fracture surface.

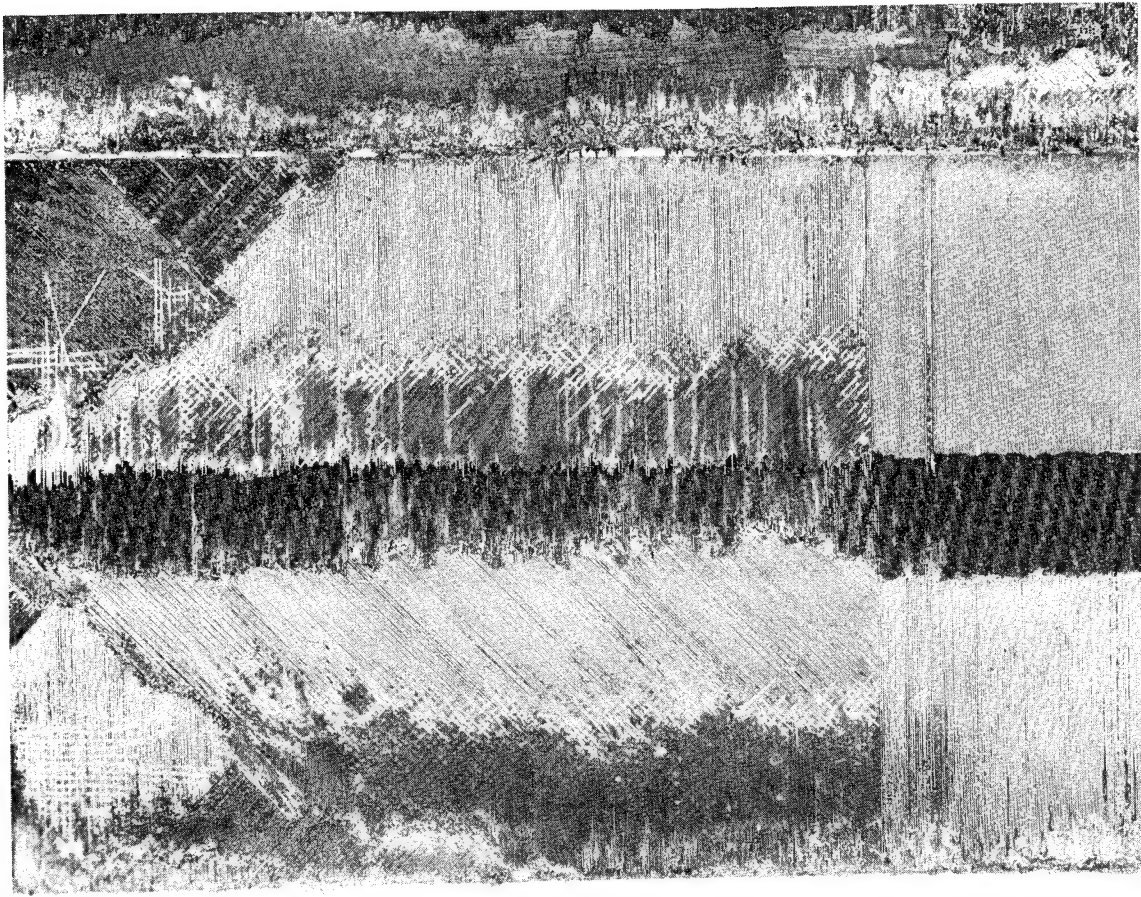


Figure 110 Specimen IIA11C03 - Overall View, 2X Magnification

3.4.7 Specimen IIIA12A01

This is a 10-inch wide Configuration A single splice lap joint loaded in tension-tension fatigue to a stress ratio of $R = +0.1$. As may be seen in Figure 111, three separate and different fracture areas are apparent. It is assumed that the fracture initiated in one area, propagated to the next, where the net section was reduced to a minimum, leading to a catastrophic static failure on the next cycle of loading.

Examination of Failure Surface A indicated shear failure initiating in the adhesive at the outer edges of the joint. Although difficult to demonstrate photographically, a definite pattern appeared in the adhesive, under microscopic examination, indicative of combined applied loads and transverse thermal stresses at the edge of the panel and resultant loads peaking at the ends of the overlap.

In Figure 111, Surface B, Section #1, the failure mode was shear within the adhesive along the plane in the scrim cloth. In Section #3 the failure mode was primarily shear between the boron filaments and resin matrix with some shear between the resin matrix and 104 carrier scrim.

In Section #2 the failure mode was shear between the boron filaments and resin matrix and tensile failure of the boron filaments.

The square areas outlined in Figure 111, Surface B, were investigated by SEM photomicrographs. Figure 112 represents the -1 area and illustrates the failure modes discussed under Section #1 above. Figure 113 represents the -2 area and illustrates the failure modes discussed under Section #2 above.

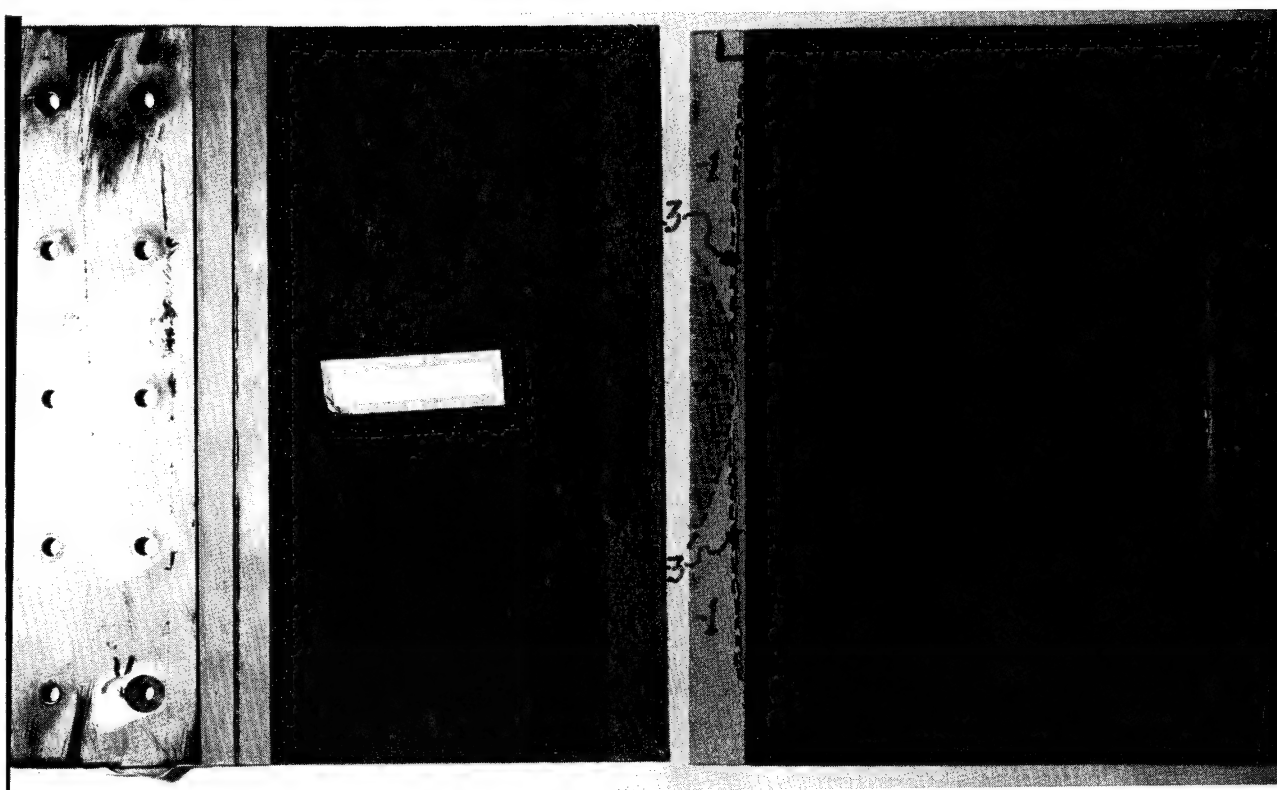


Figure 111 Specimen IIIA12A01 - Overall View, 1/3X Magnification

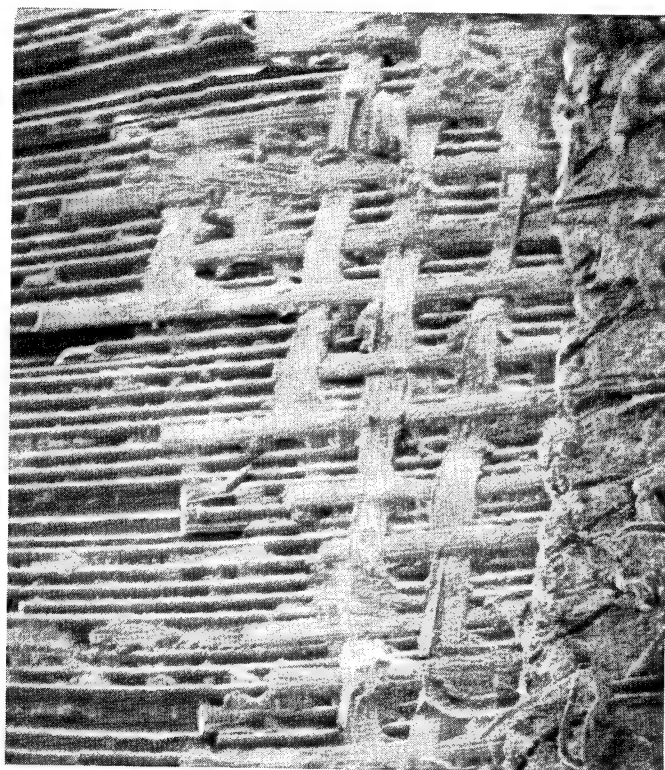


Figure 112 SEM Photomicrograph of -1 Square in Figure 111
Surface B

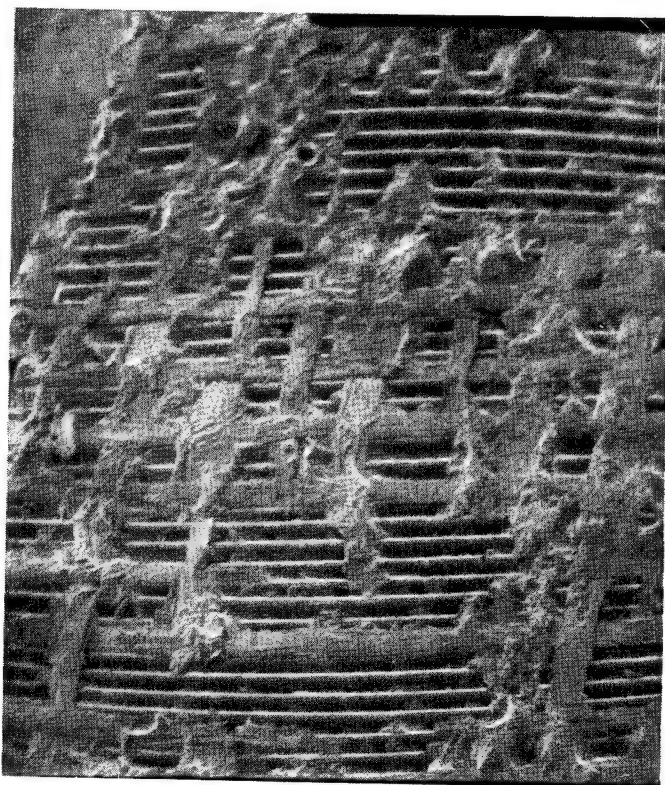


Figure 113 SEM Photomicrograph of -2 Square in Figure 111
Surface B

3.5 CONFIGURATION B

Configuration B specimens are single scarf step joints having boron-epoxy adherends bonded to titanium or aluminum. These are 3-step joints with each joint consisting of 1/2 or 3/8-inch steps. The specimens on which failure mode studies were conducted are defined below:

<u>Specimen Number</u>	<u>Adherend Combinations</u>	<u>Loading History</u>
IB111C01	Boron/Titanium 1.50 Overlap	Compression Fatigue, $R = +10.0$ $F_{s \max} = 2500$ psi Fatigue Life = 315, 130 Cycles
IIB31A05	Boron/Titanium 1.125 Overlap	Fatigue, $R = +0.1$ $F_{s \max} = 1400$ psi Fatigue Life = 939, 000 Cycles

3.5.1 Specimen IB111C01

This is a one-inch wide Configuration B step-lap joint specimen, loaded in compression to a stress ratio of $R = +10.0$. A 4X view of the failure surface is shown in Figure 114. For step-lap joints, the failure modes are generally mixed; i.e., some bond failure, some delamination, and some net section for the thinnest step in the boron. However, when loaded in compression fatigue, the bondline is usually the weakest link, as evidenced in the micrograph.

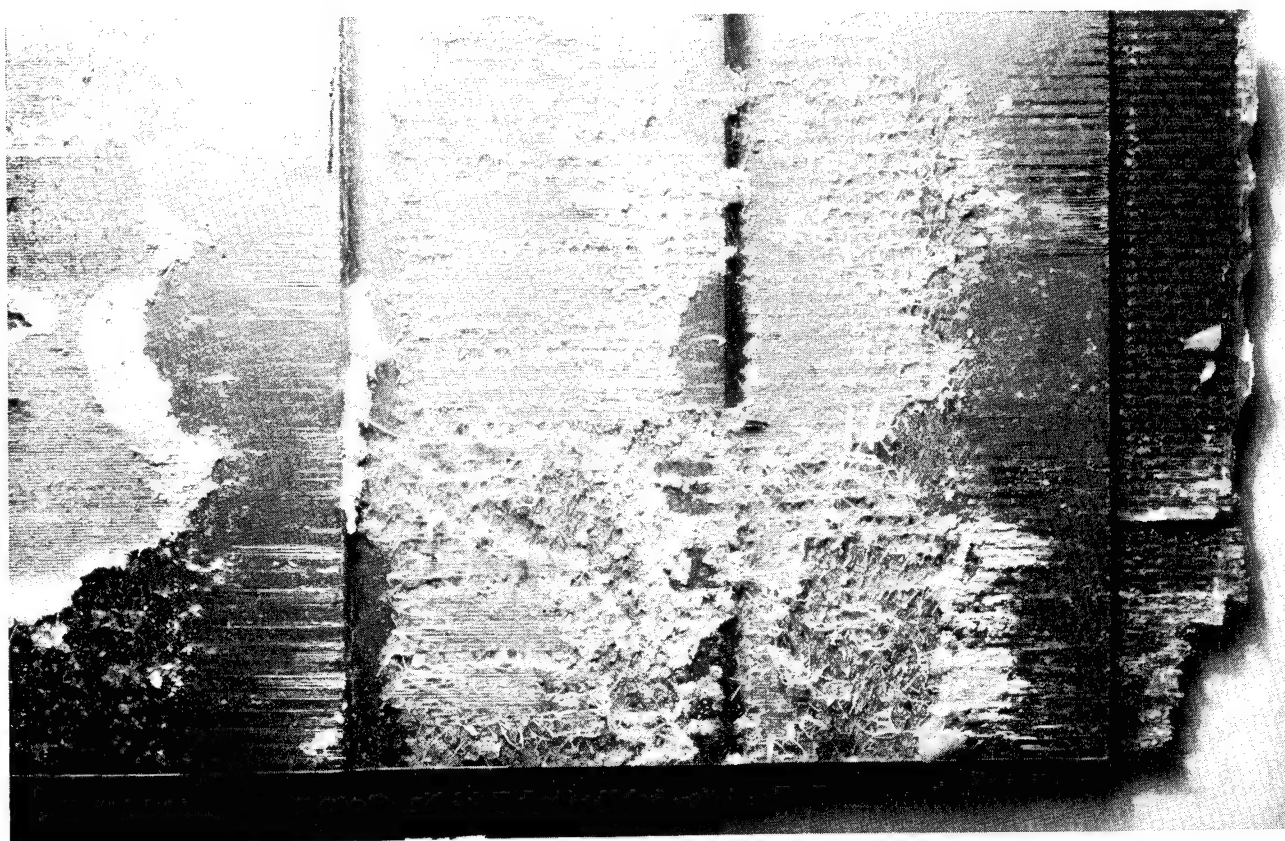


Figure 114 Specimen IB111C01 - Surface A - 4X Magnification

3.5.2 Specimen IIB31A05

This is a three-inch wide Configuration B step-lap joint specimen, loaded in tension-tension fatigue at a stress ratio of $R = +0.1$. An overall view of the joint is shown in Figure 115. It will be seen in magnified view (6X) Figure 116, that the joint failed in the bond line on two steps and in net section tension in the third step.

As seen in Figure 115, when failure takes place in the bond line, much damage occurs to the adhesive layer. Sections #1 and #2 noted on Figure 116 were examined further on the SEM. As evidenced in Figure 117, the failure mode at the first step consists of shear failure within the adhesive (along the plane of the scrim cloth) changing abruptly to shear failure between the resin matrix and the outer ply of boron filaments. Figure 118, representing Section #2 of Figure 116, shows the shift in failure mode from shear between the resin matrix and outer ply of boron filaments (in the first step) to shear within the adhesive along the plane of the adhesive scrim cloth.

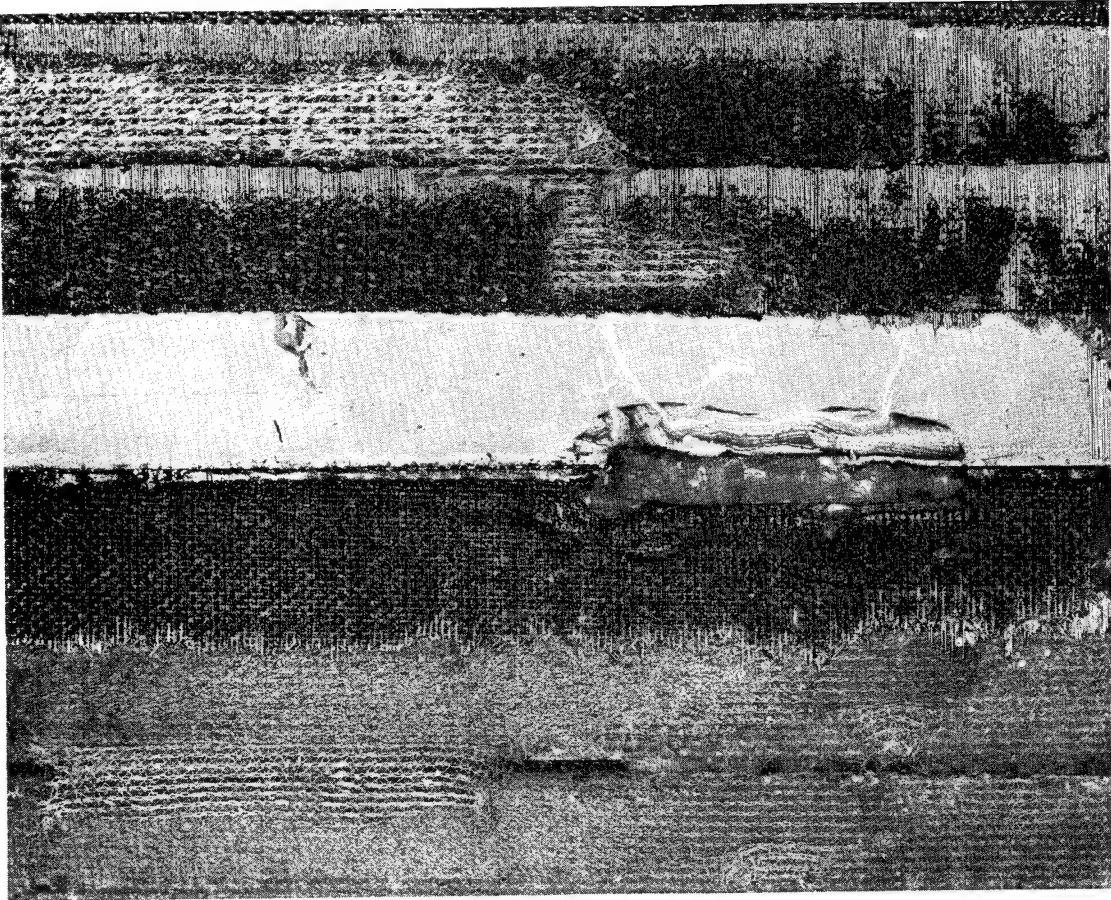


Figure 115 Specimen IIB31A05 - Overall View - 2X Magnification

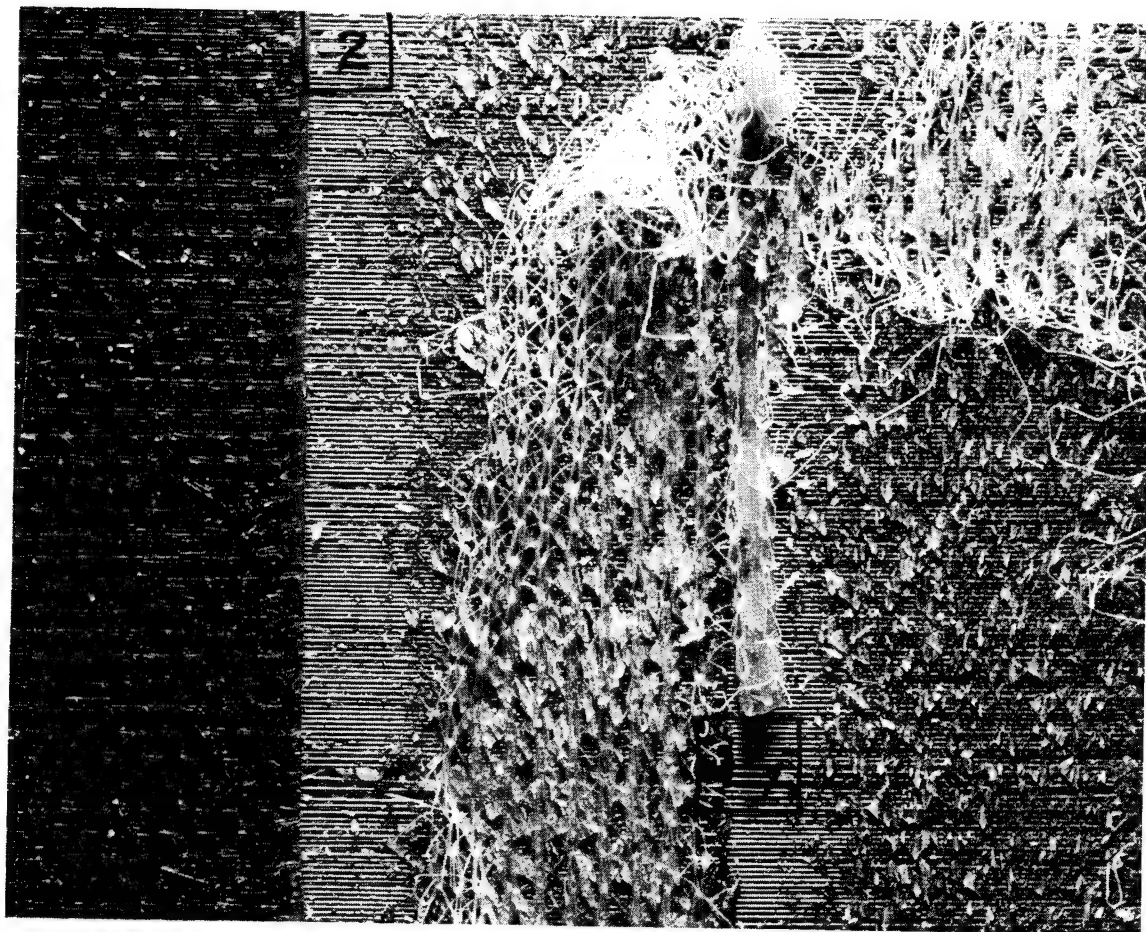


Figure 116 Specimen IIB31A05 - Surface B - 6X Magnification



Figure 117 SEM Photomicrograph of -1 Square in Figure 116
20X Magnification

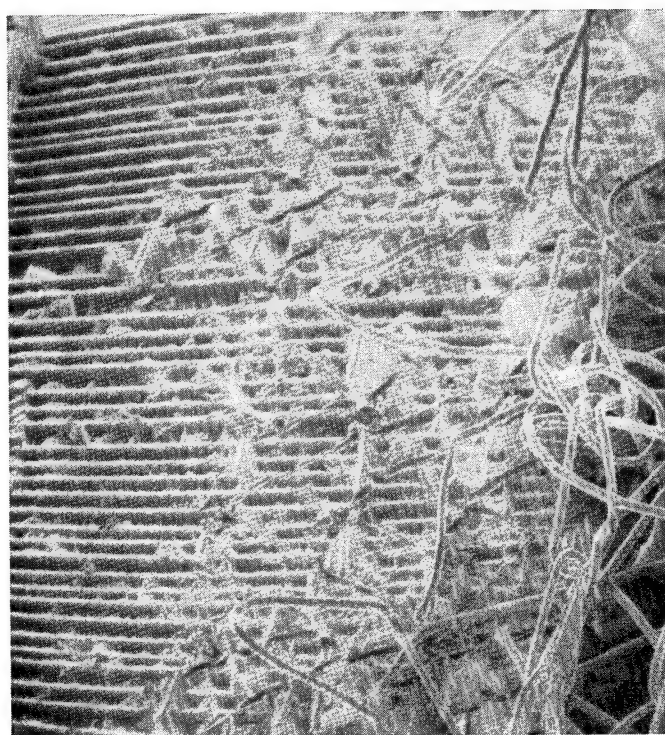


Figure 118 SEM Photomicrograph of -2 Square in Figure 116
20X Magnification

3.6 CONFIGURATION C STUDIES

Configuration C specimens are T-joint specimens consisting of a titanium "T" section bonded to a boron-epoxy adherend. The T-section is bonded perpendicular to the length of the specimen in such a fashion that when the specimen is loaded axially, a transverse load can be introduced to the bond area through tension applied to the upstanding leg of the tee. The specimens on which failure mode studies were conducted are defined below:

<u>Specimen Number</u>	<u>Adherend Combinations</u>	<u>Loading History</u>
IC111A01	Boron/Titanium 1.0 x 1.25 Overlap	Fatigue, R = +0.1 $F_{t \max} = 21,500 \text{ psi}$ Side Load = 50 lbs Fatigue Life = 86,000 Cycles
IC111A02	Boron/Titanium 1.0 x 1.25 Overlap	Fatigue, R = +0.1 $F_{t \max} = 30,000 \text{ psi}$ Side Load = 60 lbs Fatigue Life = 18,000 Cycles
IC111D03	Boron/Titanium	Static Tension, Axial Load = 47,500 psi Side Load = 105 lbs at Failure Deflection = 0.190 in. at Failure

3.6.1 Specimen IC111A01

This is a Configuration C or T-joint specimen having a titanium tee bonded to a boron adherend over a 1.0 x 1.25 inch area. The specimen was subjected to an axial tension-tension fatigue loading at a stress ratio of $R = +0.1$ and maximum tensile stress of 21,500 psi. In conjunction with this, a sustained side load of 50 lbs was introduced through the bonded tee.

Figure 119 shows the general failure modes of this specimen which consist of a laminate-to-tee disbond, and fracture of the laminate. Failure Surface B, Figure 120, magnification 4X, indicates that the bond failed primarily in shear at the glass carrier scrim/resin interface in the surface ply of boron culminating in a static peel mode. It is apparent that the effects of side loading and laminate bending have caused plies near the surface to fail, thus propagating into total laminate failure.

A SEM specimen was removed from the area indicated on the specimen fracture surface in Figure 120. Figure 121, a 20X SEM photomicrograph of a section of this area, shows the change in surface topography where the fracture mode shifted from shear to peel. A higher magnification (100X) SEM photomicrograph of the fracture transition zone is shown in Figure 122.

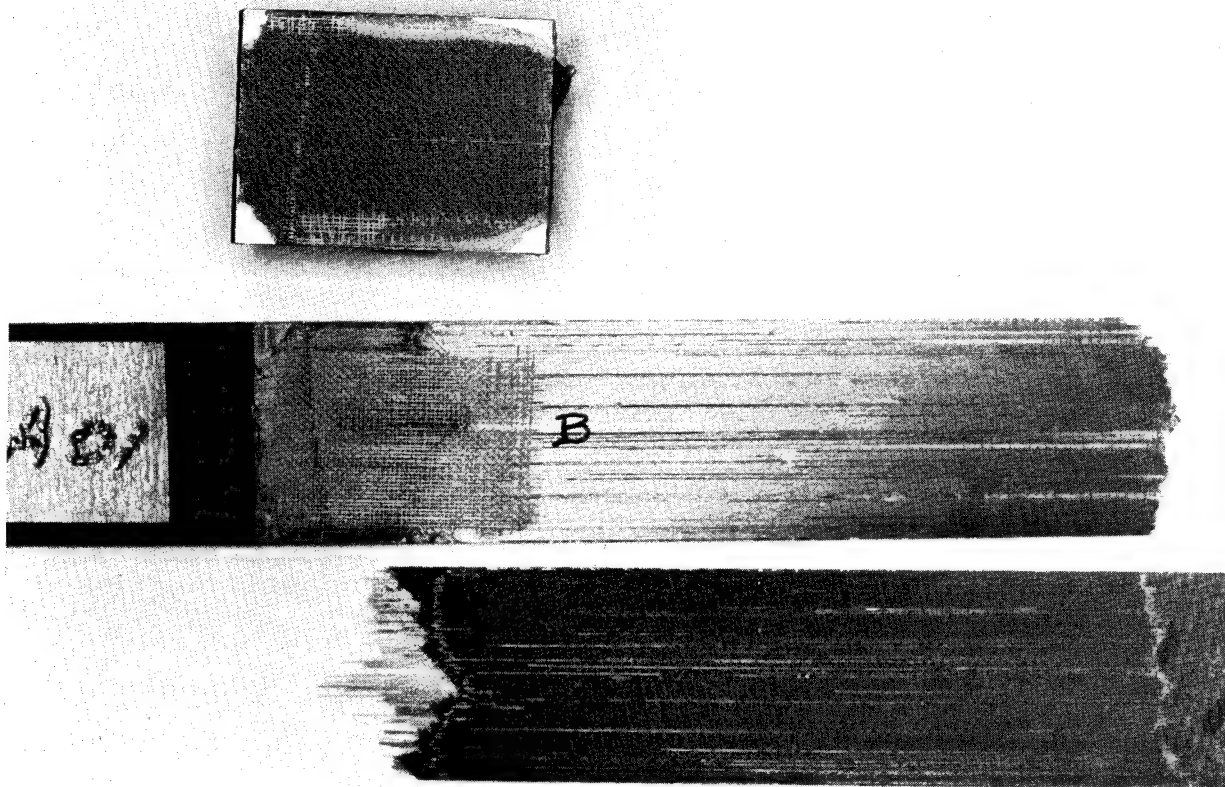


Figure 119 Specimen IC111A01 - Overall View

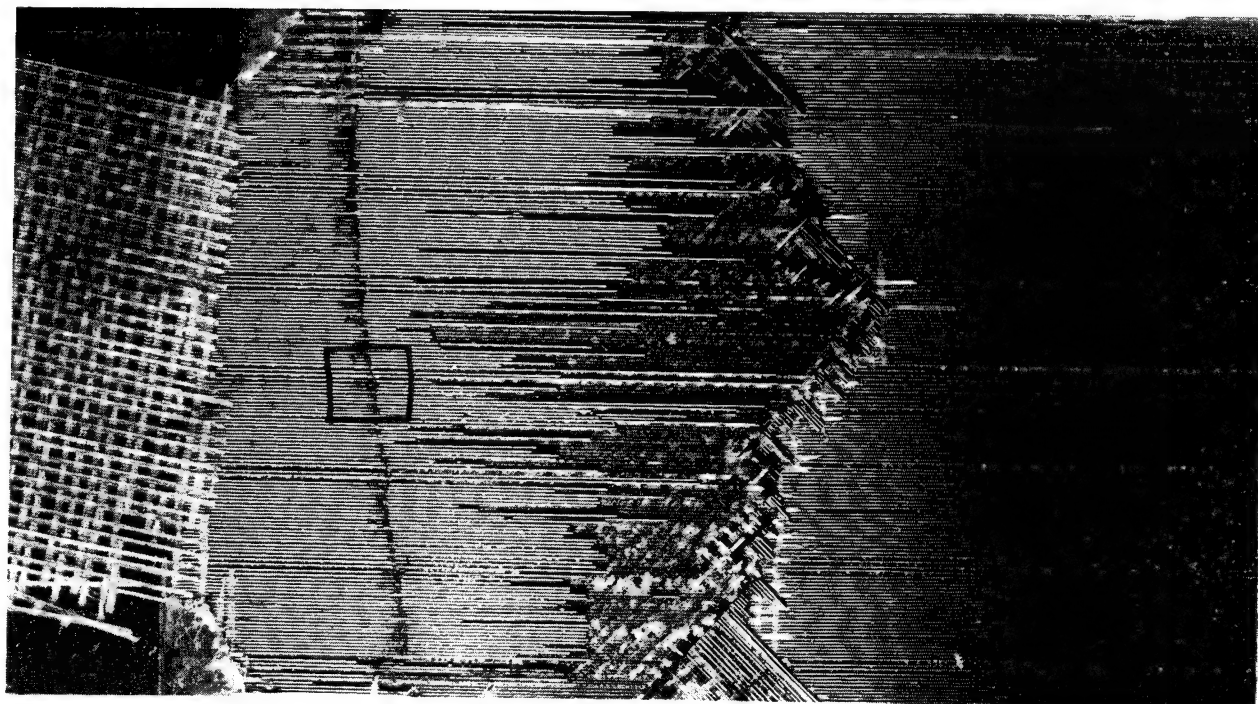
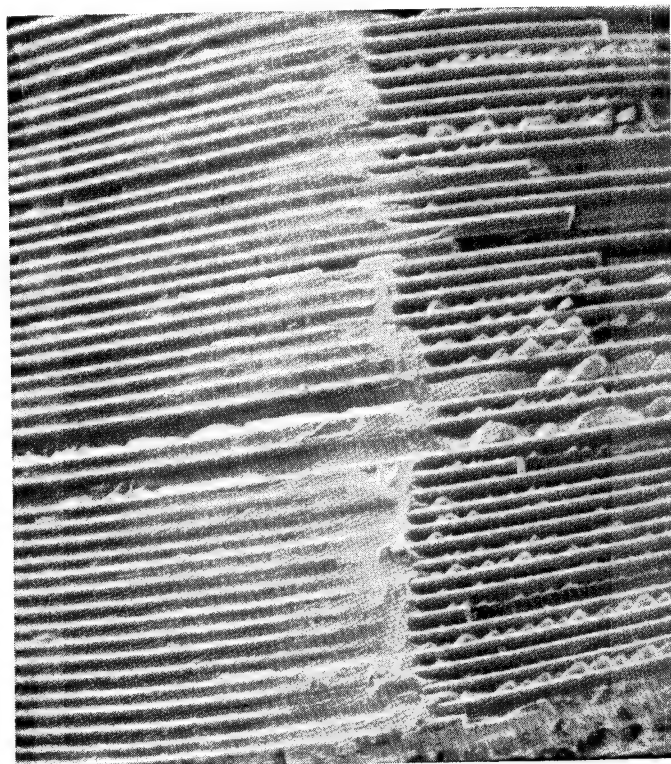
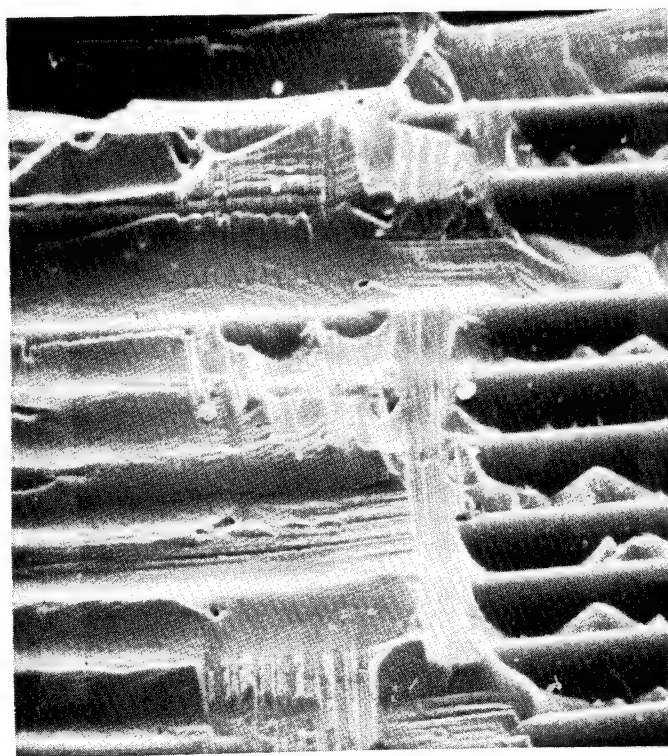


Figure 120 Specimen IC111A01 - Magnification 4X - Surface "B"



MAG. 20X

Figure 121 SEM Photomicrograph of Area Outlined in Figure 120



MAG. 20X

Figure 122 SEM Photomicrograph of Area Outlined in Figure 121

3.6.2 Specimen IC111A02

This specimen was loaded similar to IC111A01 except that the maximum tensile stress was 30,000 psi with a side load of 60 lbs. An overall view of the joint, Figure 123, shows that failure again initiated at the ends and propagated toward the center.

Microscopic inspection, Figure 124, revealed a tension shear fracture mode at the ends but changing to a peel mode at final failure. A 20X SEM photomicrograph of a section of this specimen is shown in Figure 125. A pronounced narrow band of peel, or flat-wise tension fracture mode, is evident (arrow) with striations also being visible. The striations initiated in the area where the failure mode changes from shear to peel. Although apparent on only one side of the final fracture site, the striations were observed microscopically on both sides of the final failure zone.

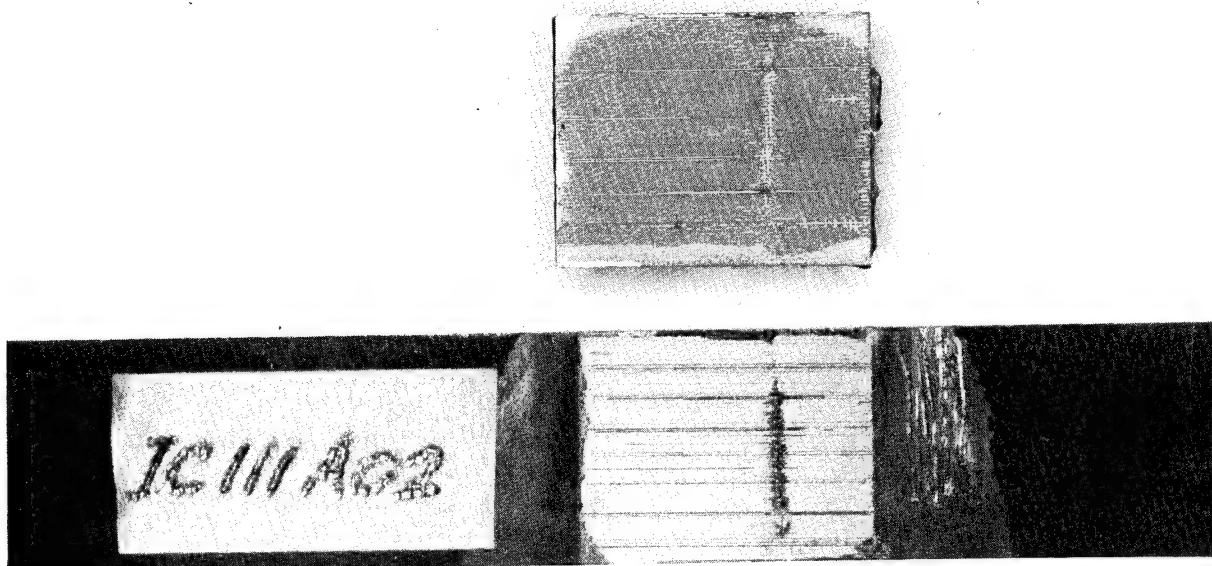


Figure 123 Specimen IC111A02 - Overall View

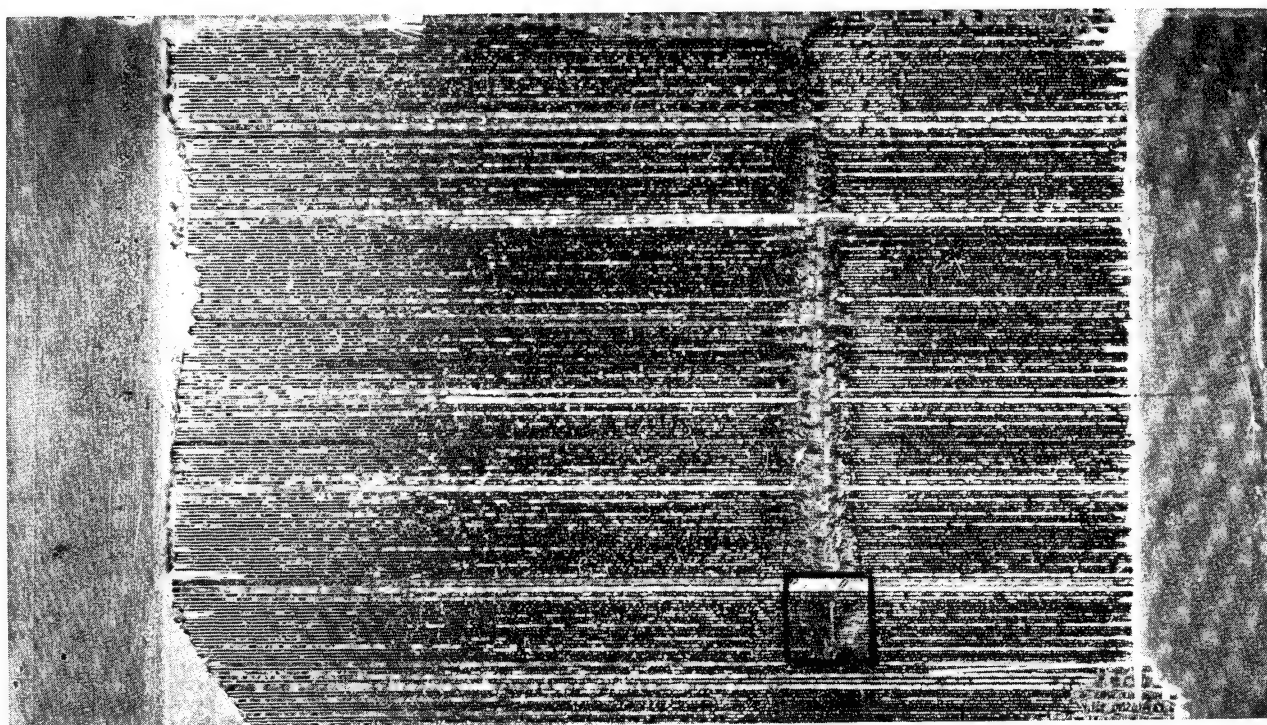
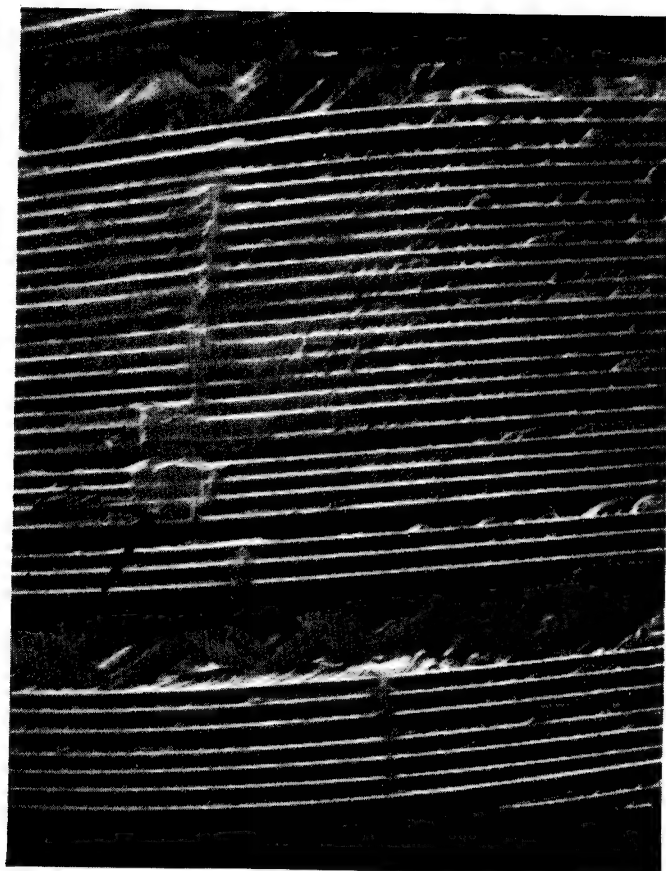


Figure 124 Specimen IC111A02 - Magnification 4X - Surface "B"



MAG. 20X

Figure 125 SEM Photomicrograph of Section from Area
Designated by Square in 124

3.6.3 Specimen IC111D03

This is a Configuration C specimen which was subjected to an axial load of 47,500 psi and an increasing side load which reached 105 pounds, and incurred a deflection of 0.190 inches at failure. An overall view of the fracture surfaces is shown in Figure 126. Microscopic examination (Figure 127) indicates failure due to overload normal to the bond line. Without the presence of cyclic axial loads, the initial failure at the ends of the tee joint appear to be a tension or a tension/peel combination. This fracture then rapidly changed into a shear plus tension mode.

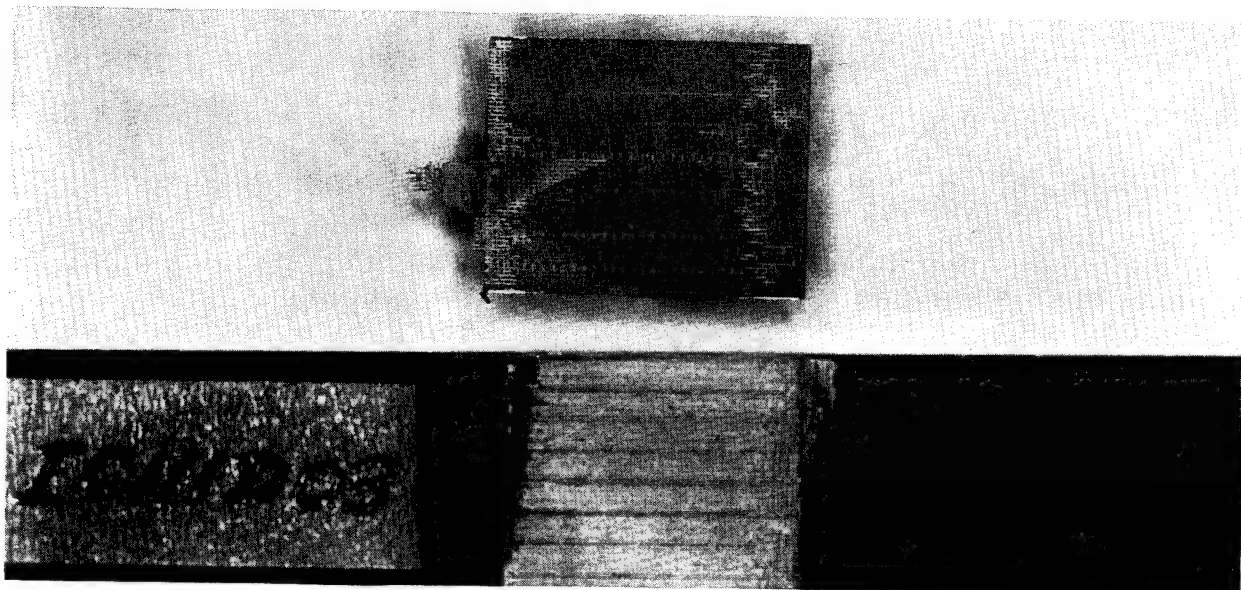


Figure 126 Specimen IC111D03 - Overall View

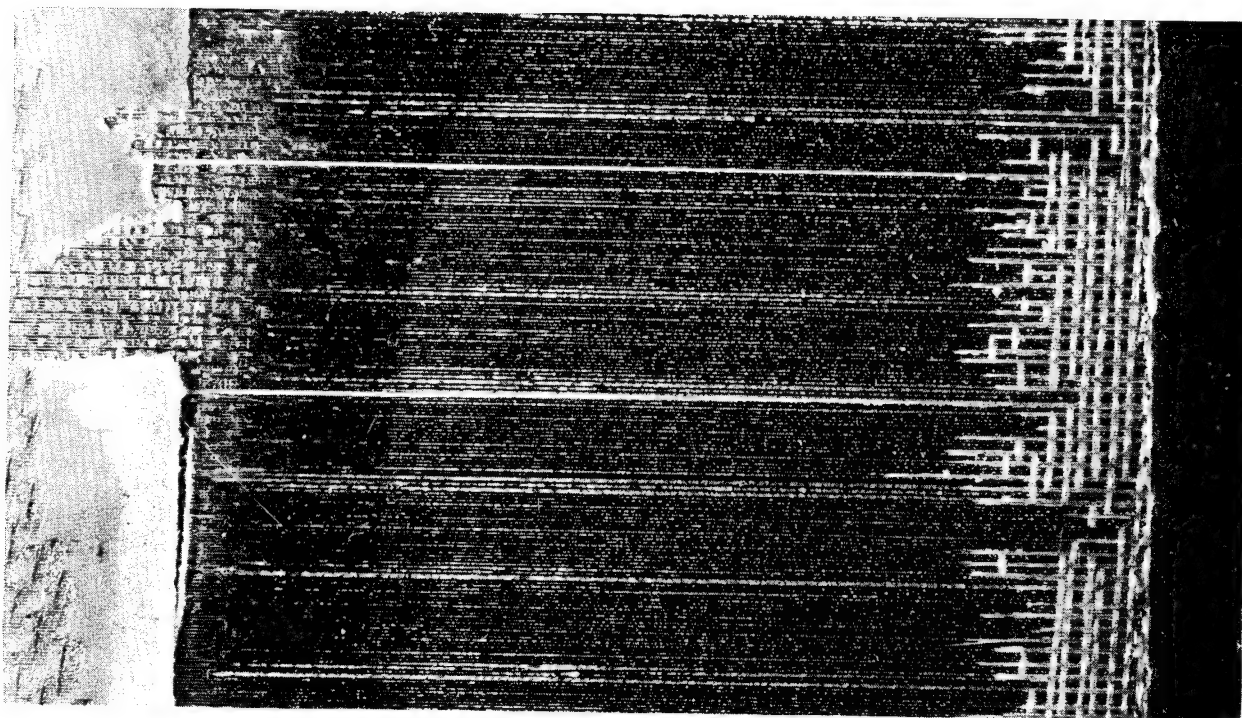


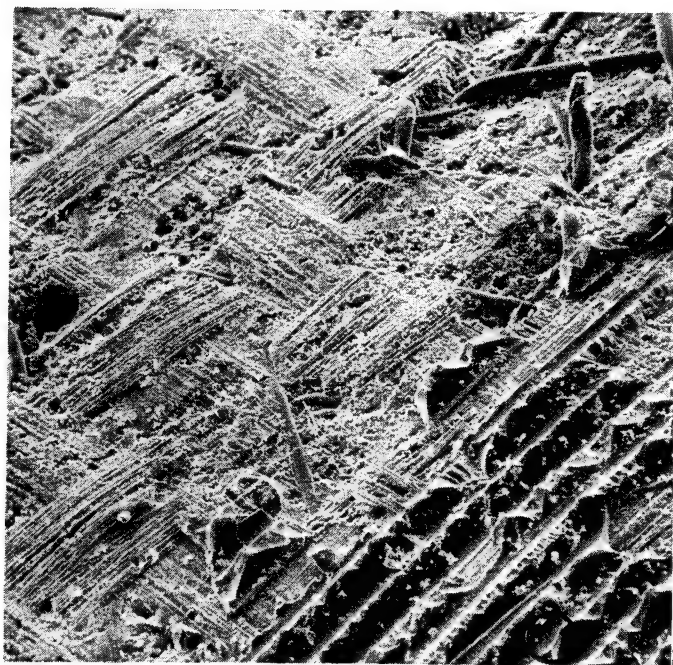
Figure 127 Specimen IC111D03 - Surface "B" - Magnification 4X

3.7 CONCLUSION OF FAILURE MODE STUDIES

Visual observation of specimens containing different design variables and subjected to different loading conditions indicate that there are numerous failure modes associated with boron-epoxy composite joints.

Based on failure mode studies conducted within the scope of this program, specific modes of failure have been defined and related to load condition. These failure modes and related loading conditions are as follows:

- o Shear fatigue failure in resin parallel to fiber regardless of stress level but subjected to a stress ratio of $R = -1.0$ as illustrated in Figure 128.
- o Shear failure in matrix parallel to fiber due to static tension on the joint or tension-tension fatigue $R = +0.1$ as illustrated in Figure 129.
- o Shear failure in matrix parallel to fiber due to static compression or compression-compression fatigue $R = +10.0$ as illustrated in Figures 130 and 131. Also, cohesive shear in the adhesive as illustrated in Section 2, Figure 132.
- o Spalling of boron fibers in 45° plies resulting from a tension-tension fatigue load applied at 0° , as illustrated in Figure 133.
- o Peel mode of failure in the matrix in static tension as illustrated in Figure 134.
- o Shear and flatwise tension or peel in a "T" joint as shown in Figure 135. Striations appear in the transition zone between shear and the final fracture mode.

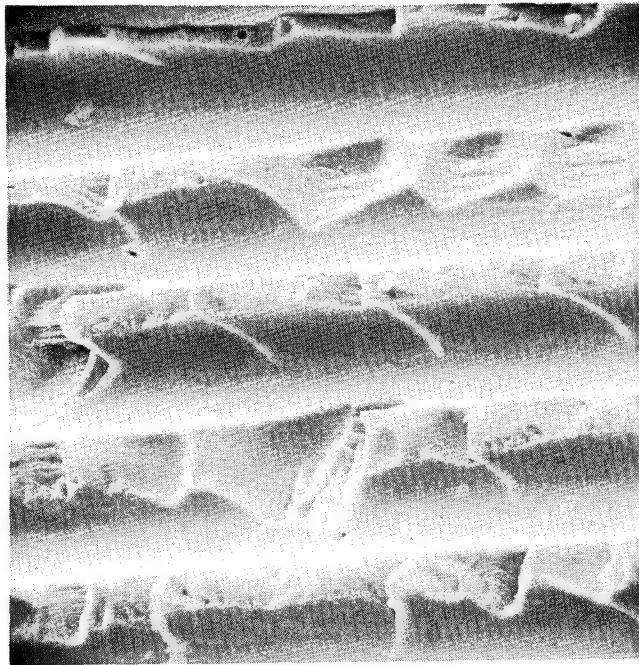


MAG. 52X



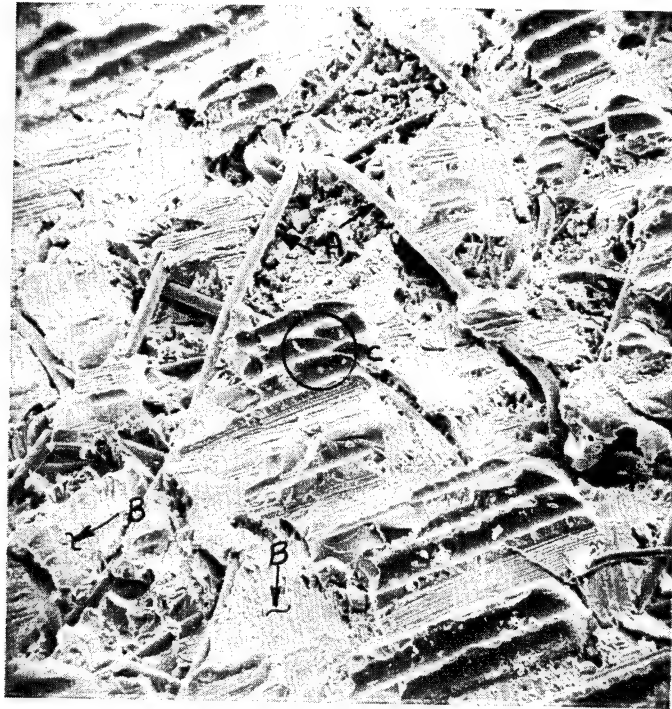
MAG. 575X

Figure 128 Shear Failure in Matrix Subjected to a Stress Ratio of $R = -1.0$



MAG. 200X

Figure 129 Shear Failure in Matrix Subjected to
Tension-Tension Fatigue, $R = +0.1$



MAG. 50X



MAG. 500X

Figure 130 Shear Failure in Matrix Subject to Compression-Compression Fatigue, $R = +10.0$

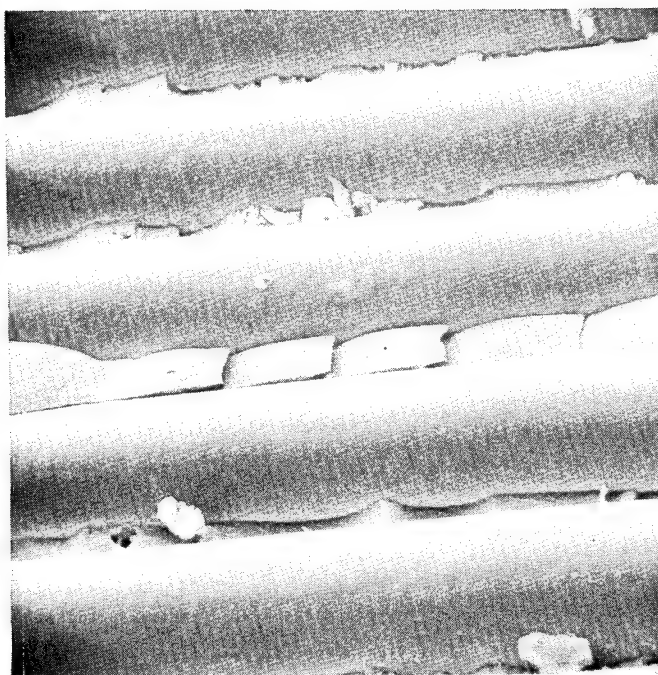


Figure 131 Shear Failure in Matrix Subjected
To Static Compression

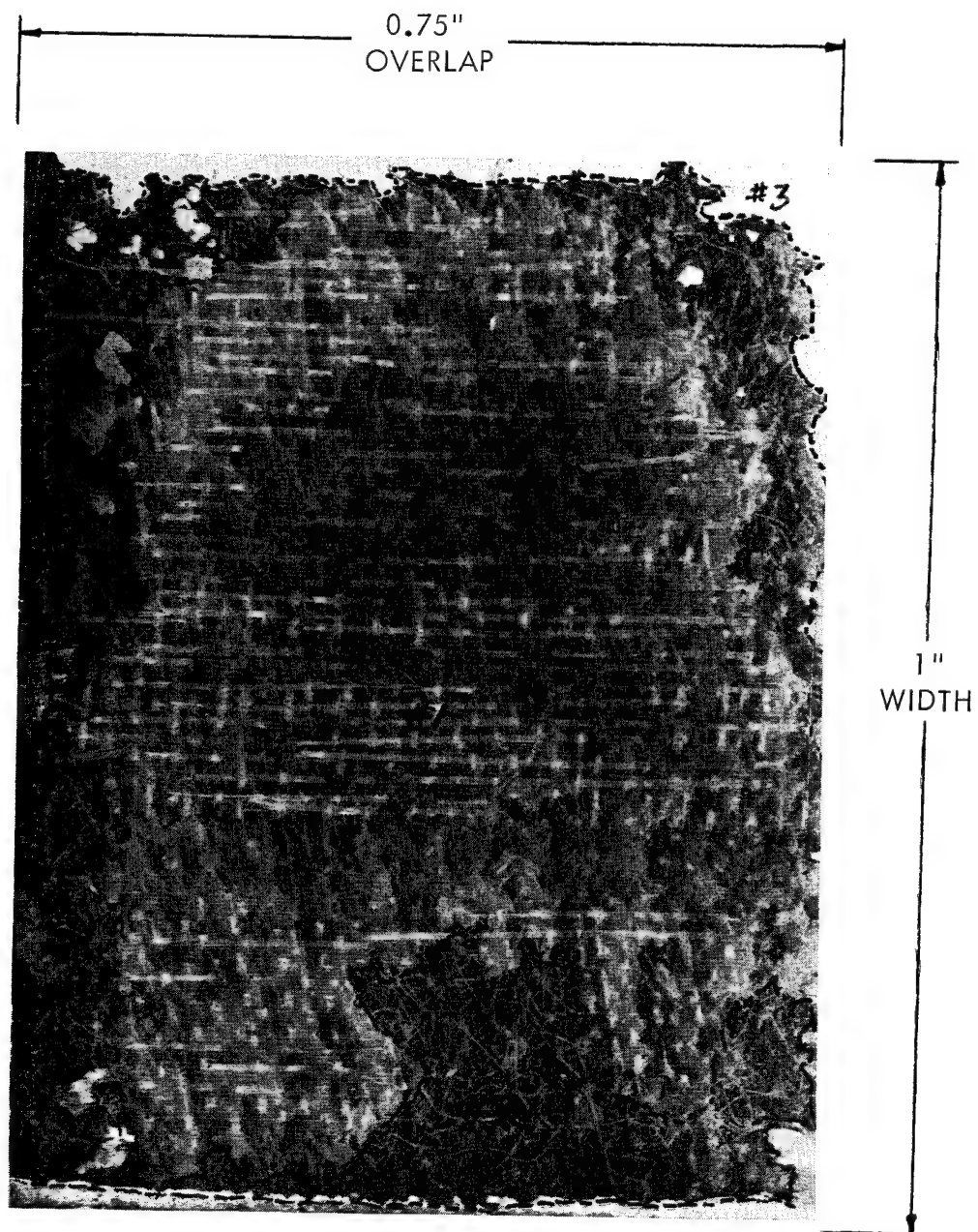
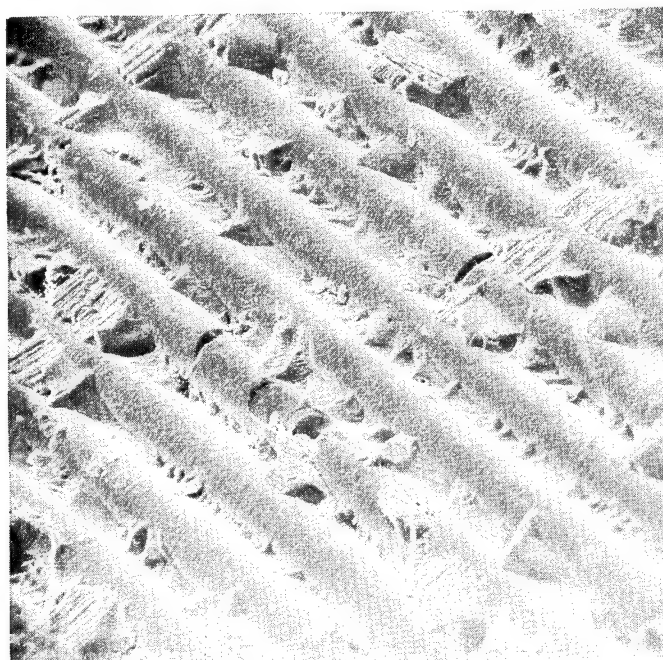
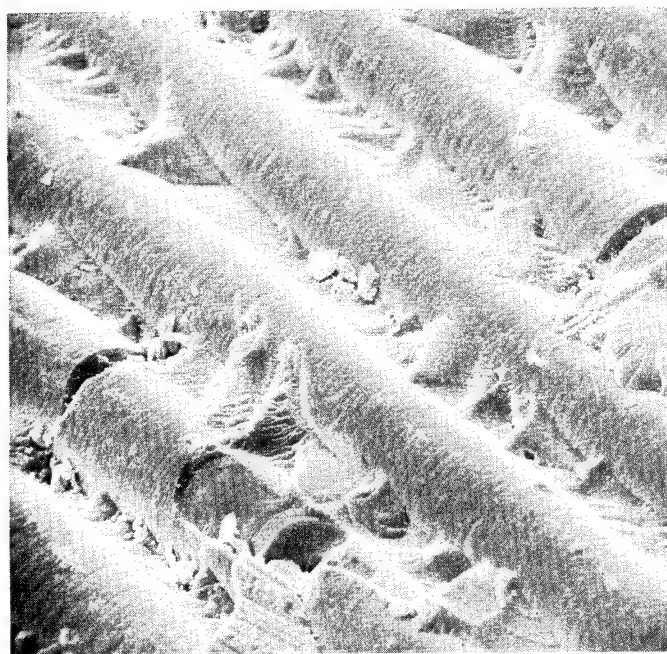


Figure 132 Cohesive Shear in the Adhesive,
Illustrated in Section 2

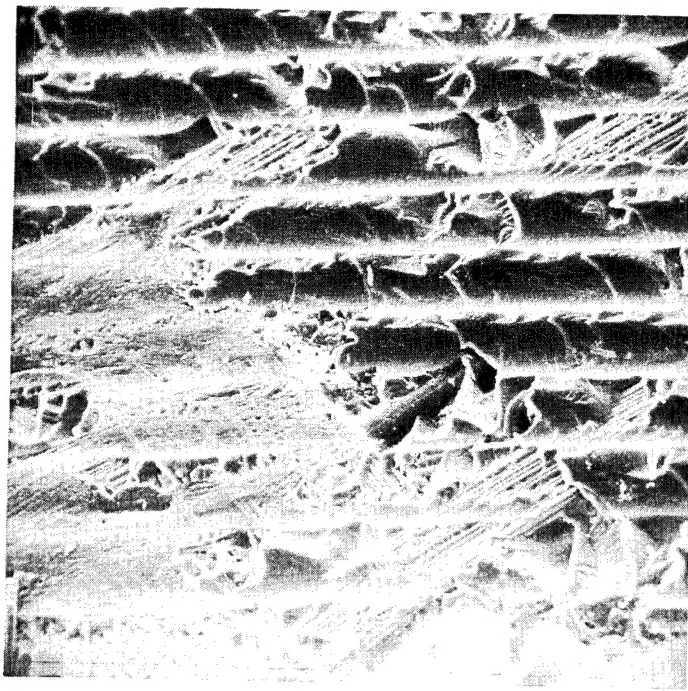


MAG. 117X



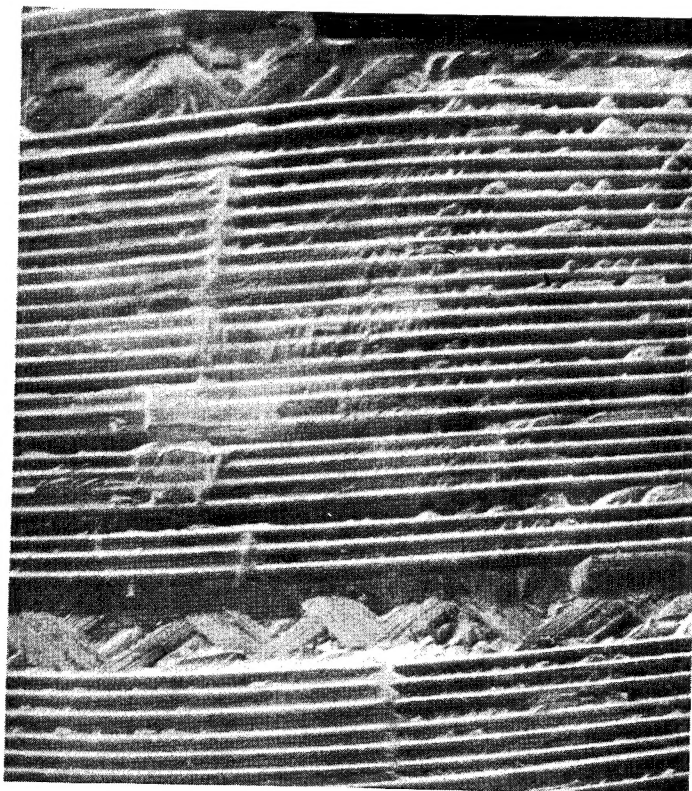
MAG. 235X

Figure 133 Spalling of Boron Fibers in 45° Plies
Subjected to a Tension-Tension Fatigue
Load Applied at 0°



MAG. 112X

Figure 134 Peel Failure in Matrix Subjected to Static Tension



MAG. 20X

Figure 135 Shear and Flatwise Tension or Peel in a Tee Joint

REFERENCES

1. Anon., Military Specification, "Airplane Strength and Rigidity, Reliability Requirements, Repeated Loads, and Fatigue, " MIL-A-8866 (ASG), May 1960.
2. Anon., Military Specification, "Airplane Strength and Rigidity, Flight Loads, " MIL-A-8861, May 1960.
3. Anon., "Air Force Airplane Structural Integrity Program Requirements, " ASD-TR-66-57, January 1968.
4. McManus, N. P., "Combat Load Factor Experiences on the F-5A and F-105D Aircraft, " ASD-TR-68-65, March 1969.
5. Anon., "Development of F-111 Mission Composite Fatigue Spectrum and Fatigue Test Programming, " General Dynamics, Ft. Worth Division, FW69-257, July 1969.
6. Bouton, I., Fisk, M., Trent, D. J., "Quantitative Structural Design Criteria by Statistical Methods, " AFFDL-TR-67-107, Vol. II, June 1968.
7. Fehrle, A. C., et. al., "Advanced Composites Joints and Attachments, " ACDAP Report 4, September 1971.
8. McKinney, J. M., "Fatigue of Composites, " ACDAP Report 3, August 1971.
9. Shockey, P. D., et. al., "Structural Airframe Application of Advanced Composite Materials - Vol. V Mechanical Properties - Fatigue, " AFML-TR-69-101, Vol. V, March 1970.
10. McGowan, P. R., et. al., "Structural Design for Acoustic Fatigue, " ASD-TDR-63-820, October 1963.

UNCLASSIFIED

Security Classification

DOCUMENT CONTROL DATA - R & D

(Security classification of title, body of abstract and indexing annotation must be entered when the overall report is classified)

1. ORIGINATING ACTIVITY (Corporate author) Lockheed-Georgia Company A Division of Lockheed Aircraft Corporation Marietta, Georgia 30060		2a. REPORT SECURITY CLASSIFICATION Unclassified	
		2b. GROUP	
3. REPORT TITLE DEVELOPMENT OF AN UNDERSTANDING OF THE FATIGUE PHENOMENA OF BONDED AND BOLTED JOINTS IN ADVANCED FILAMENTARY COMPOSITE MATERIALS			
4. DESCRIPTIVE NOTES (Type of report and inclusive dates) Final Technical Report August 1970 through April 1972			
5. AUTHOR(S) (First name, middle initial, last name) Albert C. Fehrle, James R. Carroll and Samuel M. Freeman, et al			
6. REPORT DATE June 1972		7a. TOTAL NO. OF PAGES	7b. NO. OF REFS
8a. CONTRACT OR GRANT NO. F33615-70-C-1302		9a. ORIGINATOR'S REPORT NUMBER(S) AFFDL-TR-72-64 Vol III	
b. PROJECT NO. 4364		9b. OTHER REPORT NO(S) (Any other numbers that may be assigned this report) ER-11319	
c.			
d.			
10. DISTRIBUTION STATEMENT Approved for public release; distribution unlimited.			
11. SUPPLEMENTARY NOTES Volume III, Fatigue Analysis and Fatigue Mode Studies		12. SPONSORING MILITARY ACTIVITY Air Force Flight Dynamics Laboratory Air Force Systems Command Wright-Patterson AFB, Ohio	
13. ABSTRACT This is Volume III of a final report presented in three volumes: Vol I - Analysis Methods, Vol II - Fabrication, Inspection and Testing; Volume III - Fatigue Analysis and Failure Mode Studies. This report presents the results of the empirical program undertaken to increase the basic understanding of the fatigue phenomena of advanced composites joints. Four basic design concepts have been evaluated and include both bonded and mechanically fastened joints. A broad spectrum of joint geometry variations and loading conditions are included to identify the significant parameters affecting the fatigue endurance of composite joints. Test data and analyses are included for constant amplitude testing and program fatigue loading. Realistic spectrum and block spectrum data are evaluated using Miners Cumulative Damage Theory. In conjunction with other analyses and evaluations, failure mode studies were conducted on the fracture surface of failed specimens. Scanning electron microscope (SEM) photomicrographs were used for this failure study. Specific failure modes related to specimen configuration, loading conditions and fatigue history were defined. Failure modes that have been identified and related to loading conditions include, shear in the resin versus load direction and stress ratio (R), peel in the laminate due to a cleavage load, peel or tension fracture due to tension-tension fatigue. Some specimens subjected to complex loading exhibited multiple failure modes.			

UNCLASSIFIED

Security Classification

14.	KEY WORDS	LINK A		LINK B		LINK C	
		ROLE	WT	ROLE	WT	ROLE	WT
	bonded joints						
	mechanical joints						
	joint analysis						
	boron composite materials						
	fatigue testing						
	failure modes						
	fatigue endurance						
	fatigue analysis						
	photoelastic stress analysis						
	material properties						
	non-destructive inspection						

UNCLASSIFIED

Security Classification